Manipulation of the Insulin-Like Growth Factor 1 Receptor on the Vascular Endothelium: The Effect on Whole Body and Endothelial Specific Insulin Sensitivity

Dr Victoria Kate Gatenby

Submitted in accordance with the requirements for the degree of Doctor of Philosophy

The University of Leeds

School of Medicine

March 2014

The candidate confirms that the work submitted is her own except where work which has formed part of jointly authored publications has been included. The contribution of the candidate and the other authors to this work has been explicitly indicated below. The candidate confirms that appropriate credit has been given within the thesis where reference has been made to the work of others.

Chapters 1.5, 1.6, 1.7 and 1.8 are based upon the below publication. Figures 1.3-2, 1.6-1 and 1.7-1 are reproduced with permission from the same publication. The manuscript and figures were written and produced entirely by myself with editorial contribution from Dr Imrie and Professor Kearney

Gatenby VK, Imrie H, Kearney M (2013) The IGF-1 receptor and regulation of nitric oxide bioavailability and insulin signalling in the endothelium. Pflugers Arch. 465(8): 1065-74

Acknowledgements

As a clinician, embarking on a pure science PhD was initially daunting and although at times it has been intensely frustrating it has also been enlightening, challenging and predominantly a pleasure. For this I am particularly grateful to my supervisors Professor Mark Kearney and Dr Helen Imrie. To Professor Kearney I am grateful for his enthusiasm, trust and for always having an open door, although I'm slightly less appreciative that he goaded me into doing a triathlon. To Helen, I am grateful for her patience with my intense lack of laboratory skills at the beginning, willingness to discuss even the most mundane problem, and her complete disinterest in goading me into taking part in sporting events.

The work contained within this thesis is entirely my own, except for the invaluable contribution by Dr Simon Futers, who generated the MIGFREO plasmid, Miss Anna Skorma who prepared the fat samples for analysis and Dr Hema Viswambharan who performed the L-citrulline assay. I am indebted to them all.

I have been very lucky to have worked in a very happy and productive laboratory, and would like to thank Dr Steve Wheatcroft, Dr Matt Gage, Dr Nadira Yuldasheva, Dr Paul Cordell and Dr Piruthivi Sukumar.

As a complete laboratory novice the technical support from Mrs Stacey Galloway and Mrs Jessica Smith has been priceless; as are they.

I would also like to thank Mr Kingsley Simpson for lending his expertise in quantitative PCR.

For keeping me sane amongst the scientists, and for making coming to work a pleasure I would like to thank Dr Anshu Sengupta, Dr Ben Mercer, Dr Amir Aziz, Dr Noman Ali, Dr Matt Kahn, Dr Simon Lines and Dr Honey Prasai.

To the British Heart Foundation for generously funding this research.

To my parents, for making everything possible.

Finally, to my wonderful husband Ben and my amazing daughter Freya who both make my world sparkle.

Abstract

Endothelial dysfunction is associated with the onset of atherosclerosis and cardiovascular disease. Whole body and endothelial cell insulin resistance results in reduced nitric oxide (NO) bioavailability; this is a prominent feature of endothelial dysfunction. Recent work published by our group has suggested that expression of insulin like growth factor-1 receptors (IGF-1R) in the endothelium may play a role in determining both endothelial cell insulin sensitivity and NO bioavailability.

We have generated a transgenic mouse which expresses a non-functional mutation of the IGF-1R solely on the vascular endothelium (MIGFREO) under control of the Tie2 promoter. In vivo metabolic tests have shown that MIGFREO mice have enhanced whole body insulin sensitivity and significant reduction in plasma free fatty acid level in keeping with enhanced whole body insulin sensitivity.

In contrast, MIGFREO mice have endothelial cell insulin resistance; measured by significant reduction in the vasodilatory response to insulin, and markedly reduced insulin stimulated NO production in pulmonary endothelial cells (PECs). In addition, the MIGFREO PECs are also resistant to IGF-1 as measured by significantly reduced IGF-1 stimulated NO production.

In order to investigate a potential mechanism we assessed production of the reactive oxygen species H_2O_2, production of which has been demonstrated to enhance insulin signalling. Vascular tissue from the MIGFREO mice has elevated basal levels of H_2O_2 in comparison wt. counterparts; measured by response to catalase in the organ bath, and by direct measurement of H_2O_2 in aortae.

Mutation of the IGF-1R specific to the vascular endothelium has divergent effects on whole body and endothelial cell specific insulin resistance. Furthermore, there is evidence of excess production of H_2O_2 in MIGFREO vascular tissues; this may provide a mechanistic link for observed finding of divergent whole body and endothelial cell insulin sensitivity seen in the MIGFREO mice.

Table of contents

LIST OF FIGURES 11

LIST OF TABLES 14

GLOSSARY 16

1 INTRODUCTION 21

1.1 Atherosclerosis: A historical perspective 22

1.2 Atherogenesis and Endothelial Physiology 24

1.2.1 Endothelial function in health 24

1.2.2 Endothelial dysfunction 24

1.2.3 Endothelial dysfunction and the development of atherosclerosis 25

1.3 Nitric Oxide 28

1.3.1 Nitric oxide synthases 29

1.3.2 Endothelial nitric oxide synthase 30

1.3.3 Reactive Oxygen Species and Endothelial Dysfunction 33

1.3.4 NADPH oxidases 35

1.4 Insulin Resistance 38

1.4.1 Insulin and the insulin receptor 39

1.4.2 Insulin and glucose homeostasis 41

1.5 Insulin like growth factor 1 43

1.5.1 IGF binding proteins 43

1.5.2 Insulin like growth factor-1 and glucose homeostasis 44

1.5.3 The link between IGF-1 and cardiovascular disease 45

1.6 Structure of the IGF-1 Receptor. 50

1.6.1 Genetics 50

1.6.2 Structure of the IGF-1R 50

1.6.3 Ligand binding and activation of TK domain 51

1.7 Insulin, insulin like growth factor-1 and endothelial cell function 54

1.7.1 IGF-1R and IR activation and nitric oxide production 54

1.7.2 Insulin signalling and MAPK 56

1.8 Insulin like growth factor / insulin receptor hybrids 58

1.8.1 IGF-1R, hybrid expression and cardiovascular disease 62

1.9 Insulin and IGF-1 resistance and endothelial dysfunction 64

1.9.1 The development of whole body insulin resistance 64

1.9.2 The development of endothelial cell insulin resistance 65

1.10 Reactive oxygen species and enhanced insulin signalling 71

1.10.1 The effect of hydrogen peroxide on insulin signalling 71

1.10.2 Vascular effects of hydrogen peroxide 73

1.11 The link between endothelial insulin sensitivity and glucose homeostasis 75

1.12 Summary 80

2 HYPOTHESIS AND AIMS 83

3 MATERIALS 86

4 GENERATION OF MOUSE AND VALIDATION OF MODEL 92

4.1 Introduction 93

4.2 Methods 95

4.2.1 Generation of transgenic mouse 95

4.2.2 Genotyping of mice 103

4.2.3 Quantitative PCR 103

4.2.4 Pulmonary endothelial cell isolation 105

4.2.5 Western blotting 107

4.2.6 Statistics 110

4.3 Results 111

4.3.1 Genotyping 111

4.3.2 Quantitative PCR 112

4.3.3 Western blots 114

4.4 Conclusion and Discussion 116

5 ASSESSING ENDOTHELIAL FUNCTION AND ENDOTHELIAL INSULIN SENSITIVITY 121

5.1 Introduction 122

5.2 Methods 124

5.2.1 Organ bath assessment of endothelial function 124

5.2.2 Pulmonary endothelial cell isolation 126

5.2.3 Preparation of cells 126

5.2.4 Western blotting 126

5.2.5 L-citrulline assay of eNOS activity 127

5.2.6 Statistics 129

5.3 Results 130

5.3.1 ACh Relaxation 130

5.3.2 Vasomotor insulin sensitivity 131

5.3.3 Vasomotor IGF-1 sensitivity 134

5.3.4 Sodium Nitroprusside relaxation 135

5.3.5 PE + L-NMMA 137

5.3.6 Western blots 139

5.3.7 eNOS activity (L-citrulline assay) 142

5.4 Conclusion and Discussion 144

6 METABOLIC ASSESSMENT 149

6.1 Introduction 150

6.2 Methods 152

6.2.1 Weight 152

6.2.2 Glucose tolerance test 152

6.2.3 Insulin tolerance test 153

6.2.4 Insulin-like growth factor tolerance test 153

6.2.5 Plasma insulin concentration 153

6.2.6 Plasma insulin-like growth factor type 1 concentration 154

6.2.7 Plasma adiponectin measurement 155

6.2.8 Plasma leptin measurement 156

6.2.9 Plasma Free Fatty Acid measurement 157

6.2.10 Plasma Triglyceride Measurement 159

6.2.11 Blood pressure measurement 160

6.2.12 Statistics 161

6.3 Results 162

6.3.1 Weight 162

6.3.2 Fat cell size 165

6.3.3 Glucose tolerance 166

6.3.4 Insulin Tolerance 170

6.3.5 IGF-1 Tolerance 173

6.3.6 Plasma insulin and IGF-1 level 176

6.3.7 Plasma adiponectin, leptin, free fatty acid and triglyceride 177

6.3.8 Blood pressure 179

6.4 Conclusion and Discussion 181

7 MEASURING REACTIVE OXYGEN SPECIES 190

7.1 Introduction 191

7.2 Methods 192

7.2.1 Assessment of Hydrogen Peroxide levels using the Organ Bath 192

7.2.2 Amplex® Red to detect H_2O_2 from Homogenised Aorta 192

7.2.3 Amplex® Red to measure H_2O_2 in aortic rings 197

7.2.4 Quantitative polymerase chain reaction assessment of potential sources of ROS 199

7.2.5 Statistics 200

7.3 Results 201

7.3.1 ACh + catalase 201

7.3.2 H_2O_2 production in aorta 203

7.3.3 Quantitative PCR of potential sources of ROS 205

7.4 Conclusion and Discussion 206

8 CONCLUSION, DISCUSSION AND FUTURE PLANS 209

8.1 Discussion 210

8.2 Suggested future work 214

8.3 Concluding remarks 216

REFERENCES 217

List of Figures

FIGURE 1.2-1: STAGES IN THE DEVELOPMENT OF AN ATHEROSCLEROTIC PLAQUE: 27
FIGURE 1.3-1: MECHANISM BY WHICH NO CAUSES VASODILATATION. 28
FIGURE 1.3-2: PRODUCTION OF NO BY ENOS. 31
FIGURE 1.3-3: MECHANISMS OF ROS INDUCED ENDOTHELIAL DYSFUNCTION. 35
FIGURE 1.4-1: PLASMA INSULIN AND GLUCOSE LEVELS IN THE PRE-DIABETIC PHASE. 39
FIGURE 1.4-2: INSULIN AND IGF-1 INDUCED GLUCOSE UPTAKE. 40
FIGURE 1.6-1: DIAGRAMMATIC REPRESENTATION OF IGF-1R. 53
FIGURE 1.7-1: INITIATION OF PI3-K / AKT PATHWAY BY LIGAND BINDING TO THE IGF-1R. 57
FIGURE 1.8-1: HYBRID AND HOLO-RECEPTORS. 60
FIGURE 1.9-1: OXIDATIVE STRESS AND THE DEVELOPMENT OF INSULIN RESISTANCE 66
FIGURE 1.9-2: PATHWAY SPECIFIC INSULIN RESISTANCE. 68
FIGURE 1.10-1: REACTIVE OXYGEN SPECIES AND ENHANCED INSULIN SIGNALLING VIA INTERACTION WITH PTP. 72
FIGURE 4.2-1: SCHEMATIC REPRESENTATION OF "QUICK KNOCK-IN™" STRATEGY: 97
FIGURE 4.2-2: SCHEME OF IDENTIFICATION AND BREEDING OF CHIMERIC MICE 100
FIGURE 4.2-3: BREEDING STRATEGY FOR DEVELOPING TRANSGENIC MICE. 101
FIGURE 4.3-1: REPRESENTATIVE GEL OF PCR PRODUCTS. 111
FIGURE 4.3-2: DISTRIBUTION OF GENOTYPES. 112
FIGURE 4.3-3: QUANTITATIVE PCR DEMONSTRATING PRESENCE OF MOUSE IGF-1R MRNA IN VARIOUS TISSUES. 113
FIGURE 4.3-4: QUANTITATIVE PCR DEMONSTRATING PRESENCE OF MUTATED HUMAN IGF-1R MRNA IN LABELLED PEC. 113
FIGURE 4.3-5: AGAROSE GEL OF PRODUCTS FROM QUANTITATIVE PCR USING HUMAN IGF-1R PRIMER 114
FIGURE 4.3-6: QUANTITATIVE PCR DEMONSTRATING PRESENCE OF HUMAN IGF-1R MRNA IN VARIOUS TISSUES. 114
FIGURE 4.3-7: MEAN DENSITOMETRY OF IGF-1R B. 115
FIGURE 4.3-8: REPRESENTATIVE BLOT OF IGF-1R B. 115
FIGURE 5.3-1: ACH RELAXATION. 130
FIGURE 5.3-2: PE CONSTRICTION +/- INSULIN. 132
FIGURE 5.3-3: MAXIMAL PE CONSTRICTION +/- INSULIN. 133
FIGURE 5.3-4: IGF-1 RELAXATION. 135
FIGURE 5.3-5: SNP RELAXATION. 136
FIGURE 5.3-6: PE CONSTRICTION +/- LNMMA. 137
FIGURE 5.3-7: AKT AND PAKT EXPRESSION. 140
FIGURE 5.3-8: ENOS AND PENOS EXPRESSION. 141
FIGURE 5.3-9: ENOS ACTIVITY, INSULIN AND IGF-1 STIMULATED, NORMALISED TO CONTROL. 143

FIGURE 5.3-10: ENOS ACTIVITY: (A) INSULIN STIMULATED (B) IGF-1 STIMULATED 143
FIGURE 6.2-1: STANDARD CURVE GENERATED FROM OPTIMISATION EXPERIMENT. 158
FIGURE 6.2-2: DIAGRAM DEPICTING BASIS BY WHICH VOLUME PRESSURE RECORDING MEASURES BLOOD PRESSURE. 160
FIGURE 6.3-1: BODY WEIGHT. 162
FIGURE 6.3-2: (A) ORGAN WEIGHT; (B) FAT PAD SIZE. 163
FIGURE 6.3-4: FAT CELL SIZE FROM (A) WILD TYPE MOUSE AND (B) MIGFREO MOUSE. 165
FIGURE 6.3-5: (A) FAT CELL SIZE; (B) FAT CELL NUMBER. 166
FIGURE 6.3-6: GLUCOSE TOLERANCE TEST (ABSOLUTE). 167
FIGURE 6.3-7: GLUCOSE TOLERANCE TEST (% BASELINE). 168
FIGURE 6.3-8: AREA UNDER CURVE OF GLUCOSE TOLERANCE TEST. 169
FIGURE 6.3-9: FASTED BLOOD GLUCOSE. 170
FIGURE 6.3-10: INSULIN TOLERANCE TEST (ABSOLUTE). 170
FIGURE 6.3-11: INSULIN TOLERANCE TEST (% BASELINE). 172
FIGURE 6.3-12. CORRELATION BETWEEN INSULIN UNITS GIVEN (AND HENCE WEIGHT) AND BLOOD GLUCOSE. 173
FIGURE 6.3-13: AREA UNDER CURVE OF INSULIN TOLERANCE TEST. 173
FIGURE 6.3-14: IGF-1 TOLERANCE TEST (ABSOLUTE). 174
FIGURE 6.3-15: IGF-1 TOLERANCE TEST (% OF BASELINE). 175
FIGURE 6.3-16: AREA UNDER CURVE OF IGF-1 TOLERANCE TEST. 176
FIGURE 6.3-17: (A) PLASMA INSULIN ELISA (B) PLASMA IGF-1 ELISA. 177
FIGURE 6.3-18: (A) PLASMA ADIPONECTIN ELISA (B) PLASMA LEPTIN ELISA. 178
FIGURE 6.3-19: (A) PLASMA FREE FATTY ACID QUANTIFICATION (B) PLASMA TRIGLYCERIDE QUANTIFICATION. 179
FIGURE 6.3-20: BLOOD PRESSURE. 180
FIGURE 6.4-1: REPRODUCED WITH PERMISSION FROM VICENT *ET AL* 186
FIGURE 7.2-1: STANDARD CURVE GENERATED FROM OPTIMISATION EXPERIMENT. 194
FIGURE 7.2-2: RESULTS OF OPTIMISATION EXPERIMENT. 195
FIGURE 7.2-3: RESULTS FROM PILOT EXPERIMENT 1 196
FIGURE 7.2-4: RESULTS FROM PILOT EXPERIMENT 1 197
FIGURE 7.2-5: RESULTS FROM PILOT EXPERIMENT 2 199
FIGURE 7.3-1: ACH RELAXATION +/- CATALASE (WT.). 202
FIGURE 7.3-2: ACH RELAXATION +/- CATALASE (MIGFREO) 202
FIGURE 7.3-3: MAXIMAL % CHANGE IN RELAXATION +/- CATALASE. 203
FIGURE 7.3-4: PERCENTAGE CHANGE IN RELAXATION WITH CATALASE. 203
FIGURE 7.3-5: TOTAL AND CATALASE INHIBITABLE SIGNAL FROM AMPLEX RED ASSAY 204
FIGURE 7.3-6: CATALASE INHIBITABLE H_2O_2 PRODUCTION IN AORTA AS MEASURED USING AMPLEX® RED. 204

FIGURE 7.3-7: RELATIVE EXPRESSION OF NOX AND SOD IN PEC. 205

List of tables

TABLE 1 : ANTI AND PRO ATHEROGENIC FUNCTIONS OF THE VASCULAR ENDOTHELIUM 25
TABLE 2: ENDOTHELIAL ACTIONS OF NITRIC OXIDE 29
TABLE 3: PRO-ATHEROGENIC EFFECTS OF ROS. 33
TABLE 4: SUMMARY OF ANIMAL MODELS EXAMINING EFFECT OF MANIPULATION OF IR AND IGF-1R ON VARIOUS TISSUES. 81
TABLE 5: COMPOSITION OF LYSIS BUFFER 107
TABLE 6: COMPOSITION OF TRANSFER BUFFER 108
TABLE 7: COMPOSITION OF BLOCKING BUFFER; 109
TABLE 8: PRIMARY ANTIBODIES USED IN WESTERN BLOTTING EXPERIMENTS 109
TABLE 9: COMPOSITION OF 5X TBS TWEEN 109
TABLE 10: GENOTYPE OF MICE. 111
TABLE 11: SUB-TYPES OF IR AND IGF-1R DIMERS POSTULATED TO BE FOUND ON ENDOTHELIUM OF MIGFREO MICE. 119
TABLE 12: COMPONENT OF KREBS HENSELHEIT SOLUTION 124
TABLE 13: PRIMARY ANTIBODIES USED IN WESTERN BLOTTING EXPERIMENTS 127
TABLE 14: COMPOSITION OF HEPES-BSA BUFFER 128
TABLE 15: RELAXATION IN PRESENCE OF ACETYLCHOLINE. 131
TABLE 16: ASSESSMENT OF PE INDUCED CONSTRICTION PRE AND POST INCUBATION WITH INSULIN. 134
TABLE 17: ASSESSMENT OF IGF-1 INDUCED VASO-RELAXATION. 135
TABLE 18: ASSESSMENT OF ENDOTHELIAL INDEPENDENT VASODILATATION WITH SNP 136
TABLE 19: PE INDUCED CONSTRICTION PRE AND POST INCUBATION WITH L-NMMA. 138
TABLE 20: ENOS ACTIVITY IN WT. AND MIGFREO MICE, CONTROL, INSULIN AND IGF-1 STIMULATED. 142
TABLE 21: MEAN TOTAL BODY WEIGHT. 163
TABLE 22: ORGAN WEIGHT. 164
TABLE 23: FAT CELL SIZE AND NUMBER. 165
TABLE 24: BLOOD GLUCOSE (ABSOLUTE). 167
TABLE 25: BLOOD GLUCOSE (PERCENTAGE OF BASELINE). 168
TABLE 26: AREA UNDER CURVE OF TOLERANCE TESTS (CALCULATED FROM PERCENTAGE CHANGE). 169
TABLE 27: INSULIN TOLERANCE TEST (ABSOLUTE BLOOD GLUCOSE). 171
TABLE 28: INSULIN TOLERANCE TEST (% CHANGE IN BLOOD GLUCOSE). 172
TABLE 29: IGF-1 TOLERANCE TEST (ABSOLUTE BLOOD GLUCOSE). 174
TABLE 30: IGF-1 TOLERANCE TEST (% OF BASELINE BLOOD GLUCOSE). 175
TABLE 31: PLASMA INSULIN AND IGF-1 LEVELS. 176

TABLE 32: RANDOM PLASMA LEVELS OF ADIPONECTIN, LEPTIN, FREE FATTY ACID AND TRIGLYCERIDE. 178
TABLE 33: SYSTOLIC AND DIASTOLIC BLOOD PRESSURE MEASUREMENTS. 179
TABLE 34: COMPOSITION OF MODIFIED KREBS-HEPES BUFFER 198
TABLE 35: PRIMERS USED TO ASSESS MRNA IN NOX 1-4 AND SOD 1-3 200
TABLE 36: ACETYLCHOLINE INDUCED VASODILATATION IN PRESENCE AND ABSENCE OF CATALASE. 201

Glossary

ACE	Angiotensin converting enzyme
ACh	Acetylcholine
ADMA	Asymmetric dimethyl-L arginine
AGE	Advanced glycosylated end products
AMPK	AMP activated protein kinase
Akt	Protein kinase B
ATP	Adenosine triphosphate
BH_4	Tetrahydrobiopterin
BP	Blood pressure
BSA	Bovine serum albumin
Ca^{2+}	Calcium
cDNA	Complementary DNA
cGMP	Cyclic guanosine monophosphate
CR	Cystine rich domain
CRP	C-reactive protein
DAG	Diaglycerol
DBP	Diastolic blood pressure
DM	Diabetes mellitus
DNA	Deoxyribonucleic acid
ECIGFRKO	Endothelial specific IGF-1R knock-out transgenic mouse
EDHF	Endothelium derived hyperpolarizing factor
EDTA	Ethylenediaminetetraacetic acid
ELISA	Enzyme linked immunosorbent assay
eNOS	Endothelium derived nitric oxide synthase
EPC	Endothelial progenitor cell
ES	Embryonic stem cell
ESMIRO	Endothelial specific mutant insulin receptor transgenic mouse
ET1	Endothelin-1
FAD	Flavin adenine dinucleotide
FFA	Free fatty acid
FMD	Flow mediated dilation
FMN	Flavin mononucleotide
FnIII	Fibronectin type III

GC	Guanylate cyclase
GH	Growth hormone
GLUT-4	Glucose transporter type 4
HAT media	Hypoxanthine aminopterin thymidine media
HBSS	Hanks balanced salt solution
HCAEC	Human coronary artery endothelial cells
HIGFREO	Human IGF-1 receptor over-expressing transgenic mouse
HMVEC	Human microvascular endothelial cells
HMVEC-C	Human cardiac microvascular endothelial cells
HO	Hydroxyl radical
HOMA	Homeostasis model assessment
HPRT	Hypoxanthine phosphoribosyltransferase
HUVEC	Human umbilical vein endothelial cells
H_2O_2	Hydrogen peroxide
ID	Insert domain
IGF-1	Insulin-like growth factor-1
IGF-1R	Insulin-like growth factor-1 receptor
IGFBP	Insulin-like growth factor binding protein
IGFRKO	Insulin-like growth receptor knock-out
IGT	Impaired glucose tolerance
IKK	Inhibitor κB kinase
IL-6	Interleukin-6
IR	Insulin receptor
IRKO	Insulin receptor knockout
IRS	Insulin receptor substrate
JNK	c-Jun N-terminal kinases
LDL	Low density lipoprotein
L-NAME	NG-nitro-L-arginine methyl ester
L-NMMA	L-NG-monomethyl arginine
MAPK	Mitogen active protein kinase
MIGFREO	Mutant IGF-1R endothelial specific over-expression
MIRKO	Muscle specific insulin receptor knockout
mRNA	Messenger ribonucleic acid
mTOR	Mammalian target of rapamycin

NAC	N-acteyl-cysteine
NADPH	Nicotinamide adenine dinucleotide phosphate
NFκB	Nuclear factor kappa-light-chain-enhancer of activated B cells
NO	Nitric oxide
NOS	Nitric oxide synthase
Nox	NADPH oxidase
NT-proBNP	N-terminal prohormone of brain natriuretic peptide
O_2^-	Superoxide
$ONOO^-$	Peroxynitrite
PBS	Phosphate buffered saline
PCOS	Polycystic ovarian syndrome
PEC	Pulmonary endothelial cell
PCR	Polymerase chain reaction
PDGF	Platelet derived growth factor
PDK-1	Protein dependent kinase-1
PGI-2	Prostacyclin
PIP_2	Phosphatidylinositol 3,4,-bisphosphate
PIP_3	Phosphatidylinositol 3,4,5-trisphosphate
PI3-K	Phosphatidyl inositol 3-kinase
PKC	Protein kinase C
PTEN	Phosphatase and tensin homolog
RNA	Ribonucleic acid
ROS	Reactive oxygen species
SBP	Systolic blood pressure
Ser	Serine
SH2	Src homology domain 2
siRNA	Small interfering RNA
SNP	Sodium Nitroprusside
SOD	Superoxide dismutase
T2DM	Type 2 Diabetes Mellitus
TBA	3,3′,5,5′-tetramethylbenzidine
Thr	Threonine
TK	Tyrosine kinase
TNFα	Tumour necrosis factor α

Tyr	Tyrosine
VEGF	Vascular endothelial growth factor
VENIRKO	Vascular endothelial IR knockout transgenic mouse
VSMC	Vascular smooth muscle cell

Chapter 1: Introduction

1 Introduction

1.1 Atherosclerosis: A historical perspective

The development of atherosclerosis within blood vessels and the subsequent clinical sequelae of myocardial infarction, cerebrovascular disease and peripheral vascular disease continue to be the principal cause of death in Europe, the United States of America and much of Asia, [339] with the world wide figure expected to exceed 23.3 million deaths in 2030 [1].

Early in the 1960s, the landmark mass epidemiological Framingham study [2] began to identify risk factors for the development of premature cardiovascular disease. Once these studies appeared to show an association between hyperlipidaemia and cardiovascular disease, research began in earnest in an attempt to discover therapies that would lower cholesterol and hence mortality.

As early as 1856 the pathologist Rudolph Virchow had hypothesised that blood lipid accumulation in artery walls lead to atherosclerosis. In 1951 Duff and McMillan [3] formulated the lipid hypothesis in its modern form, whereby they believed that "stability of the solution of the cholesterol within the blood rather than hypercholesterolemia *per se* is the general condition responsible for its deposition in the arterial intima." Interestingly they observed that atherosclerotic plaques contained large numbers of macrophages although at that point there was inadequate evidence to suggest that "non-traumatic vascular inflammation" was a factor in the development of atherosclerosis.

The development of lipid lowering therapies which followed, lead to an improvement in both cholesterol levels and mortality. The use of HMG-CoA reductase inhibitors (hereafter referred to as statins), which were first used in the late 1980s and early 1990s appeared to have a marked effect on mortality. A meta-analysis [4], published in 1999 which analysed data from several major trials looking at populations treated with statins (4S, CARE, LIPID, [secondary prevention] and WOSCOPS, AFCAPS/TexCAPS [primary prevention]) showed a 31% reduction in major coronary events and 21% reduction in mortality, associated with a drop in serum cholesterol. More recently the heart protection study [5] showed an 18% proportional reduction in the coronary death rate in patients with known vascular disease or diabetes, irrespective of the level of cholesterol.

Although there is an undoubted association between hypercholesterolemia and the development of atherosclerosis, approximately 50% of patients who have cardiovascular

disease do not have hypercholesterolemia [6]. Therein lies the problem with the “lipid hypothesis” as first postulated in the late 19th century. It is now certain that there are mechanisms other than the deposition of lipid within the vasculature that contribute to the development of atherosclerosis. And it is by understanding these mechanisms that we may be able to formulate additional therapies to aid those suffering with vascular disease.

1.2 Atherogenesis and Endothelial Physiology

It is now recognized that atherosclerosis is a much more complex disease than simply being deposition of lipid into the vasculature. Atherosclerosis is best characterised as an inflammatory disease of the blood vessels, associated with complex cellular and sub-cellular responses [7] . The currently accepted theory suggests that dysfunction of the endothelium, the monocellular lining of blood vessels, plays a critical role in the development of atherogenesis [8].

1.2.1 Endothelial function in health

The endothelium is a thin mono cellular layer of cells which covers the inner surface of blood vessels. Whilst a major role of the endothelium is to act as a protective barrier, it has other effects which are far more complex and dynamic. The endothelial cell has the ability to act both as a receptor and as an effector, sensing both chemical and physical stimuli. In response, it can act either to change the shape of the vessel which encompasses it, or it can release substances to counteract the effects of the stimulus, thereby maintaining homeostasis. The products secreted by an endothelial cell can have an effect on the cell itself, on cells adjacent to the original cell, or more widespread effects and hence the endothelium could be considered to have autocrine, paracrine and endocrine functions.

The endothelial cell secretes, amongst others: vasoconstrictors and vasodilators, anti-inflammatory molecules and pro-inflammatory cytokines, pro-coagulants and anti-coagulants [9]; it is by regulating the production of these compounds that the endothelial cell is able to maintain vessel homeostasis.

1.2.2 Endothelial dysfunction

The term endothelial dysfunction refers to an imbalance of the production of mediators produced by the endothelial with a deleterious result on the blood vessel [10]. This is particularly related to imbalances between the rate of production of nitric oxide (NO) and the rate of breakdown, primarily by reactive oxygen species (ROS). Factors which increase ROS production, increase NO scavenging, or reduce NO production by endothelial nitric oxide synthase (eNOS) (either by reduced eNOS expression or by uncoupling eNOS activity) will hence all lead to endothelial dysfunction. It is now recognised that endothelial dysfunction plays a very early role in the development of atherosclerosis. In experimental animals the presence of endothelial dysfunction has been shown to be associated with the

development of thrombosis, vessel occlusion and a tendency to vessel spasm, and hence is strongly implicated in the pathogenesis of acute coronary syndrome and myocardial infarction [11].

Function	Anti-atherogenic	Pro-atherogenic
Vessel tone	Production vasodilatory compounds; Nitric Oxide (NO), prostacyclin (PGI_2), endothelial derived hyperpolarizing factor (EDHF) [9, 12, 13]	Production of vasoconstrictors: endothelin 1 (ET1) [14]
Cellular proliferation	Production of NO with subsequent anti-proliferative effects [15-19]	MAPK mediated production of growth factors [20]
Inflammation	Production of NO with anti-inflammatory effects [21]	Pro-inflammatory cytokines (IL-6, TNFα)
Thrombosis	Production of compounds which inhibit platelet aggregation; NO, PGI_2 [9, 12, 13]	Secretion of platelet activating factor and von Willebrand factor [22, 23]
Oxidative stress		Production of reactive oxygen species; superoxide (O_2^-); hydroxyl radical (HO); hydrogen peroxide (H_2O_2) [24]

Table 1 : Anti and pro atherogenic functions of the vascular endothelium

Endothelial dysfunction has been demonstrated to be present in patients with traditional cardiovascular risk factors [25, 26], and it is known that endothelial dysfunction itself is an independent predictor for the development of cardiovascular disease [27]. It has therefore been widely accepted that further study of the function of the endothelium, and indeed factors which may cause its dysfunction is of vital importance.

1.2.3 Endothelial dysfunction and the development of atherosclerosis

The stages in the development of an atherosclerotic plaque are now well described [8]. Exposure to cardiovascular risk factors such as hypertension, insulin resistance and smoking lead to the development of endothelial dysfunction and an imbalance in the production of

NO and ROS, which leads to oxidative stress. Low-density lipoprotein (LDL), which is innocuous in a healthy vessel become oxidised under oxidative stress to form ox-LDL, which is highly immunogenic and attacks the vessel intima, leading to the release of phospholipids which cause further endothelial damage. In addition to causing intimal damage, the ox-LDL particles first activate macrophages, which ingest the ox-LDL and become foam cells. Endothelial dysfunction leads to the aggregation of platelets which release platelet derived growth factor (PDGF) inducing vascular smooth muscle cell (VSMC) migration and disruption of the internal elastic lamina. This provides further scope for the foam cells to invade which release ROS during invasion. The ROS further compounds the oxidative environment. Lipids and collagen are able to invade the disrupted matrix of the intima leading to formation of an atherosclerotic plaque. If covered by a thick fibrous cap, the plaque may remain stable and cause symptoms related to relative vessel occlusion such as angina pectoris. If ulceration of the endothelium occurs, platelet aggregation, thrombus formation and vessel occlusion swiftly ensue and may lead to the clinical sequelae of myocardial infarction or cerebral infarction. **Error! Not a valid bookmark self-reference..**

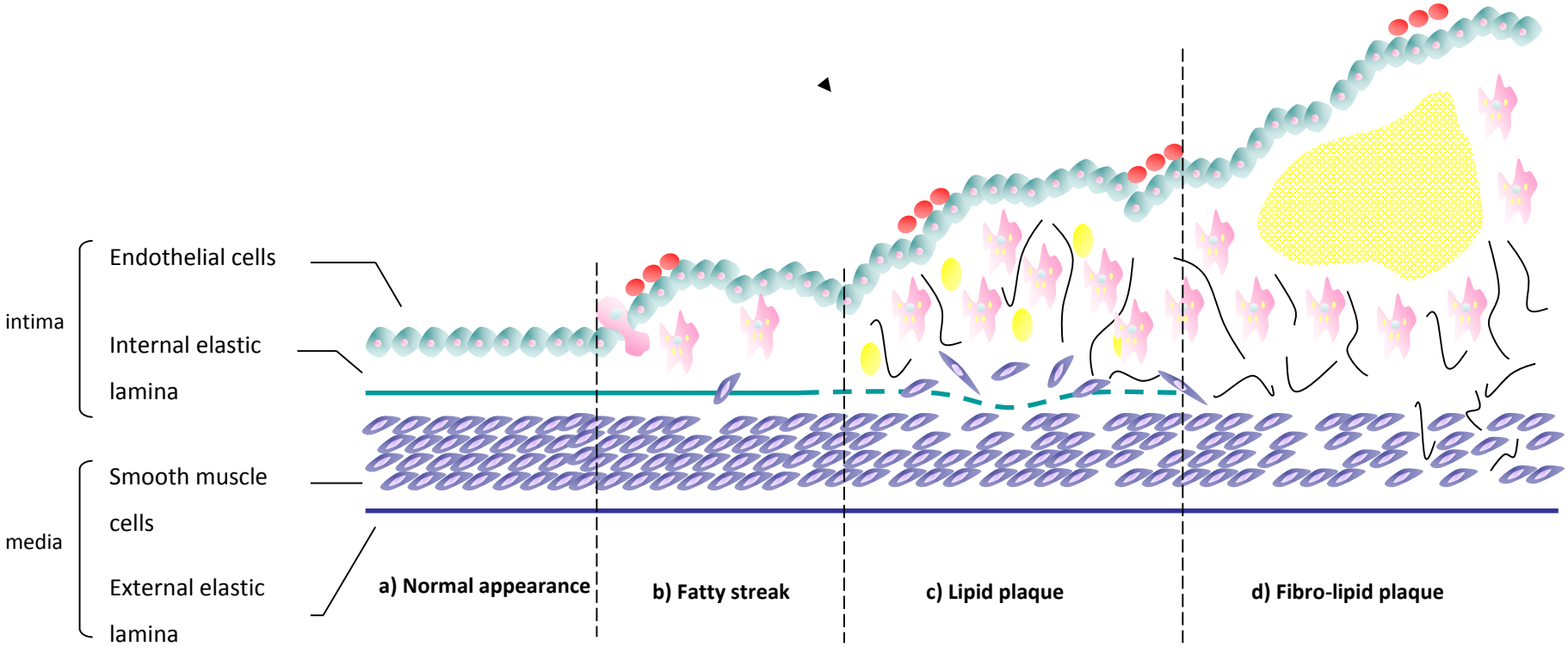

Figure 1.2-1: Stages in the development of an atherosclerotic plaque: a) despite a relatively normal appearance exposure to risk factors such as insulin resistance cause endothelial dysfunction with subsequent release of pro-inflammatory cytokines and an increasing membrane permeability to lipids and LDL; b) the development of the fatty streak can occur as early as infancy and represents invasion of monocytes which take up LDL and become foam cells. Platelets begin to adhere to the dysfunctional endothelium and release growth factors which induce smooth muscle cell migration; c) the development of the lipid plaque – disruption of the internal elastic lamina occurs and allows further smooth muscle migration into the intima. Macrophages continue to infiltrate and release ROS which causes further endothelial damage. Deposition of lipid and collagen within the matrix of the intima; d) complicated plaque – muscle is replaced by collagen and large amount of lipids accumulate. This may be covered by a thick fibrous coating. The endothelium may ulcerate leading to further platelet aggregation and thrombus formation leading to vessel occlusion.

1.3 Nitric Oxide

The function of the endothelium which has been most widely studied is the regulation of vascular tone. The endothelial cell produces a variety of vasoconstrictor agents, primarily ET-1 and thromboxane A_2 and vasodilator substances such as NO [13], prostacyclin and the endothelium derived hyperpolarising factor (EDHF) [28].

Within the coronary and systemic circulation, NO is the major determinant of endothelial dependent vasodilatation [29].

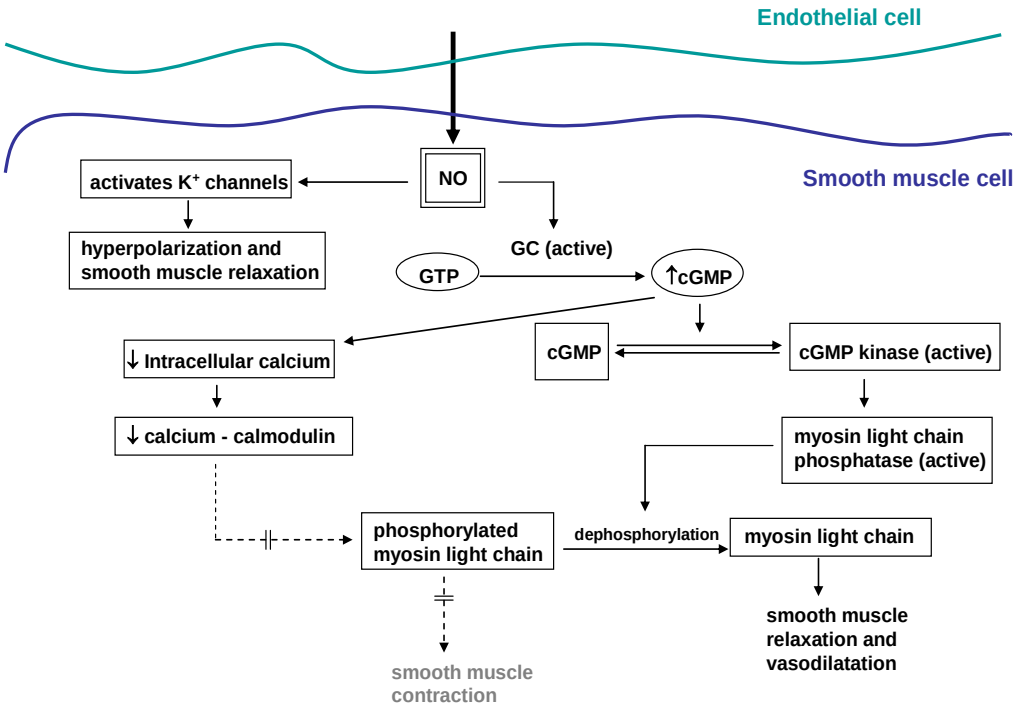

Figure 1.3-1: Mechanism by which NO causes vasodilatation. Following diffusion into smooth muscle cells, NO has dual effects to cause vasodilatation: a) via activation of K+ channels leading to direct hyperpolarization and smooth muscle relaxation; b) promotion of guanylate-cyclase (GC) mediated conversion of guanosine triphosphate (GTP) to cyclic guanosine monophosphate (cGMP), causing dephosphorylation and hence activation of the myosin light chain with subsequent smooth muscle relaxation.

NO exerts its effect via guanylate-cyclase (GC) mediated increases in cyclic guanosine monophosphate (cGMP) which in turn regulates cytosolic calcium and also causes the de-

phosphorylation of myosin light chain thereby causing smooth muscle relaxation and vasodilatation [30]. Figure 1.3-1

Effect	Physiology	References
Vasodilatation	Direct vasodilatory effect Indirect effect by antagonising vasoconstrictive factors (angiotensin II and sympathetic vasoconstriction)	[13] [31, 32]
Anti-thrombotic	Inhibition of platelet aggregation Inhibits thrombin induced platelet adhesion to vascular endothelium	[33-35] [36-38]
Anti-inflammation	Reduction of leucocyte adhesion	[21]
Anti-proliferation	Inhibition of vascular smooth muscle cell (VSMC) proliferation Inhibition of endothelial cell growth	[15-17] [18, 19]
Pro- Angiogenic	Post ischaemic angiogenesis and collateral formation	[39]

Table 2: Endothelial actions of nitric oxide

The overall bioavailability of nitric oxide is dependent upon the rate of production via nitric oxide synthase (NOS) and the rate of breakdown by combination with reactive oxygen species (ROS), particularly superoxide (O^-). Following phosphorylation of NOS, NO itself is formed from L-arginine, oxygen and NAPDH requiring the presence of tetrahydrobiopterin (BH_4) as an essential co-factor [40].

1.3.1 Nitric oxide synthases

There are 3 distinct iso-enzymatic forms of nitric oxide synthase (NOS) described in mammals; neuronal “n” NOS (NOS I), inducible “i” NOS (NOS II) and endothelial “e” NOS (NOS III) [41]. They differ in the primary site in which they are found, and also by the stimuli which cause them to produce nitric oxide [42].

Constitutive NOS (including NOS-I from neurological tissue and NOS III from endothelial tissue) respond to agonists that exert an effect by raising intracellular calcium (Ca2+). The effect of this is that eNOS produces NO for short periods when exposed to vasodilator

substances such as acetylcholine and bradykinin [41]. Inducible NOS (NOS-II) is expressed in endothelial cells and also in macrophages in response to stimulus from proinflammatory cytokines like tumour necrosis factor α (TNFα). The effect of inducible NOS is to produce NO levels several levels of magnitude larger than the constitutive NOS and also increased levels are sustained for a more constant, longer period of time. Inducible NOS is responsible, at least in part for the profound circulatory effects seen in endo-toxic shock [43].

The NOS enzymes are formed as monomers, but require dimerisation at a heme binding site [44]. Dimerisation occurs between the C terminal reductase site (also binding site for nicotinamide adenine dinucleotide phosphate [NADPH], flavin mononucleotide [FMN] and flavin adenine dinucleotide [FAD]) of one monomer to the N terminal oxygenase site (which carries the heme group, binds tetrahydrobiopterin [BH4], molecular oxygen and L-arginine) of the second monomer [41]. Electron transfer from NADPH on the C terminus to the heme group (a process mediated by flavin) results in the reduction and activation of O_2. Cycling through this process twice results in the production of NO. In the first cycle, L-arginine is hydroxylated to N-hydroxy-L-arginine; in the second N-hydroxy-L-arginine is oxidised to L-citrulline and NO [45]. Figure 1.3-2

1.3.2 Endothelial nitric oxide synthase

The predominant form of NOS found within the vasculature is eNOS, and it is eNOS that is responsible for the majority of the NO found within the vasculature. Activation of eNOS follows either in response to increased levels of intracellular calcium, or alternatively, eNOS becomes activated following phosphorylation. Phosphorylation of threonine 495 (Thr495) residues occurs constitutively, whereas serine phosphorylation (Ser1177) occurs following direct stimulus. Phosphorylation of Ser1177 follows stimulation by: vascular endothelial growth factor (VGEF) and oestrogen (mediated by protein kinase B [Akt]); by bradykinin (modulated by calcium calmodulin); by fluid shear stress (modulated by protein kinase A); by insulin (modulated by both Akt and AMP activated protein kinase [AMPK]) [41].

As is described above, eNOS generates NO from the substrate L-arginine, in a process which is tightly controlled. When disturbed, electron transfer fluxes through an alternative pathway, leading to the generation of the ROS superoxide (O_2^-) instead of NO. This is referred to as eNOS uncoupling.

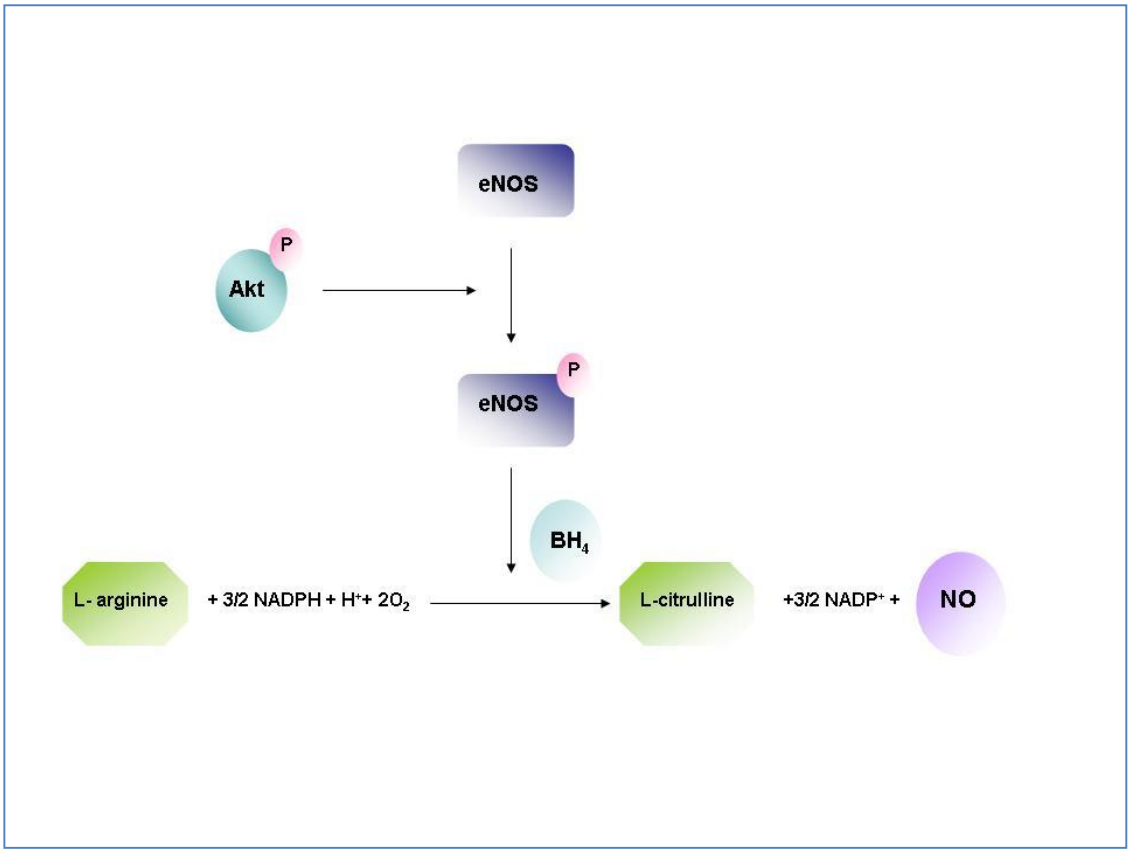

Figure 1.3-2: Production of NO by eNOS. The reaction requires tetrahydrobiopterin (BH4) which binds to the oxygenase domain of eNOS. L-arginine and O2 also bind to the oxygenase of eNOS; NADPH and flavin mononucleotide (FMN) and flavin adenine dinucleotide (FAD) bind to the reductase domain of eNOS. Reproduced with permission from Gatenby et al [46]

Contrary to what might be expected, and in spite of reduced bioavailability of NO, the level of eNOS expression seen in patients with risk factors for cardiovascular disease (hypertension [47], diabetes [48] and hyperlipidaemia [49]) appear to be increased or unchanged; eNOS expression levels appear to be reduced in later stages of the disease when atherosclerosis is evident [50, 51]. The elevated level of eNOS expression seen early on in the disease is likely to reflect a compensatory mechanism. Therefore it seems increasingly likely that eNOS function, particularly eNOS uncoupling is of particular importance in determining endothelial function.

Uncoupling of eNOS activity has been demonstrated in patients with endothelial dysfunction and diabetes [52], hypertension [53], hyperlipidaemia [54] and smokers [55]. Enhanced oxidative stress, well established as a feature of many traditional risk factors for

the development of cardiovascular disease, has been found to be of critical importance in modulating eNOS uncoupling [56]. Molecular mechanisms shown to potentiate eNOS uncoupling include: S-glutathionylation of eNOS [57]; L-arginine depletion [58-60]; BH_4 oxidation [56]; and excess asymmetric dimethyl-L-arginine (ADMA) [61].

Oxidative stress appears to promote S-glutathionylation (a reversible protein modification) of eNOS at the critical cysteine residues; which leads to eNOS uncoupling, enhanced O_2^- production, and is associated with impaired endothelial dependent vasodilatation [57]. In hypertensive vessels thiol specific reducing agents, which reverse S-glutathionylation, restored endothelial dependent vasodilatation, suggesting rescue of eNOS function [57].

BH_4 is a powerful reducing agent which is a critical co-factor in the production of NO [44]. In hyperlipidaemic APOE deficient mice BH_4 levels are depleted, and eNOS production is uncoupled [56]. It is recognised that BH_4 supplementation is able to partially restore NOS function and endothelial dependent vasodilatation in smokers [55] and in patients with diabetes [52], hyperlipidaemia [54] and hypertension [53] . In environments of elevated oxidative stress BH_4 is oxidised (particularly by $ONOO^-$) to BH_3 which renders it inactive [62]; hence causing eNOS uncoupling. Supplementation with ascorbic acid has been shown to reverse this process [62].

ADMA is an endogenous inhibitor of eNOS [63] , and is associated with endothelial dysfunction and cardiovascular mortality [64-66]. In addition to direct eNOS inhibition, ADMA appears to have an effect on eNOS uncoupling [61] and importantly, oxidative stress is associated with an imbalance of ADMA production and degradation [67, 68], likely to trigger increased ADMA levels.

Relative L-arginine deficiency also appears to lead to uncoupling of eNOS activity. Intracellular reserves of L-arginine make absolute deficiency unlikely to play a role in endothelial dysfunction however relative deficiency, associated with higher activity of arginases which compete with eNOS for substrate is a possible factor. Endothelial specific elevation of arginase 2 induces hypertension and atherosclerosis in mice [59]; in aged mice, arginase 2 levels are increased and are associated with eNOS uncoupling and endothelial dysfunction [60]. When compared with normal corpus cavernosum, tissue from patients with erectile dysfunction and diabetes were shown to have significantly higher levels of arginase 2; inhibition of arginase 2 in these patients was associated with restoration of

eNOS function. Similar increased levels of arginase 2 and reduction in NO production has been found in patients with pulmonary arterial hypertension [58].

Irrespective of the mechanism, uncoupling of eNOS enhances oxidative stress by producing ROS [41] , particularly O_2^-, which scavenges NO to form peroxynitrite ($ONOO^-$): this enhances oxidative stress and a vicious cycle, culminating in reduced NO bioavailability and subsequent endothelial dysfunction is set in motion.

1.3.3 Reactive Oxygen Species and Endothelial Dysfunction

The reactive oxygen species which are of particular importance when considering endothelial dysfunction and cardiovascular disease are the hydroxyl radical (OH), superoxide (O_2^-), hydrogen peroxide (H_2O_2) and $ONOO^-$. O_2^- is relatively short-lived and readily converted to H_2O_2 by superoxide dismutase (SOD). Although O_2^- is unable to cross the cell wall, H_2O_2 is relatively stable and diffuses across cell membranes through channels known as aquaporins [69].

Physiologically ROS are produced at low levels and act as signalling molecules however at higher concentrations they play important roles in the development of many diseases including atherosclerosis (Table 3) and cancer.

Action of ROS	Consequence	Reference
Oxidation of BH_4 → BH_2	eNOS uncoupling → O_2^- production	[70]
NO scavenging by superoxide	Formation of $ONOO^-$ → eNOS uncoupling	[71]
NFκB activation by H_2O_2	Enhanced transcription of pro-atherogenic genes (particularly proinflammatory cytokines, adhesion molecules)	[72]
Reduction in endothelial barrier function	Enhanced permeability to fluids, solutes, inflammatory cells	[73]

Table 3: Pro-atherogenic effects of ROS.

Stated simply, NO bioavailability is related to the rate of production via eNOS and the rate of breakdown by ROS. The molecular mechanisms which lead to eNOS uncoupling, with the subsequent sequelae of reduced NO and increased ROS production are discussed above.

There are several specific ways by which ROS act to promote endothelial dysfunction, although the common end point is the reduction in bioavailability of NO coupled with enhanced production of adhesion molecules, proinflammatory cytokines and increased expression of the important vasoconstrictor molecule ET-1, thereby switching the environment within the blood vessel lumen towards a pro-atherogenic one.

The bioavailability of NO is affected by ROS in several ways (Figure 1.3-3):

1) Direct scavenging of NO + O_2^- to form $ONOO^-$
2) Oxidation of BH_4 to the inactive BH_2 leads to eNOS uncoupling and production of O_2^- instead of NO
3) ROS leads to reduced activity of SOD, which leads to enhanced ROS within the vessel wall.

Levels of oxidative stress are increased in humans with hypertension, smoking, obesity, insulin resistance, hyperlipidaemia and diabetes, all of which are independently associated with endothelial dysfunction, and lower bioavailability of NO. Biologically important sources of ROS include: eNOS uncoupling (discussed in detail above); the mitochondrial respiratory chain; xanthine oxidase; and the NADPH oxidases.

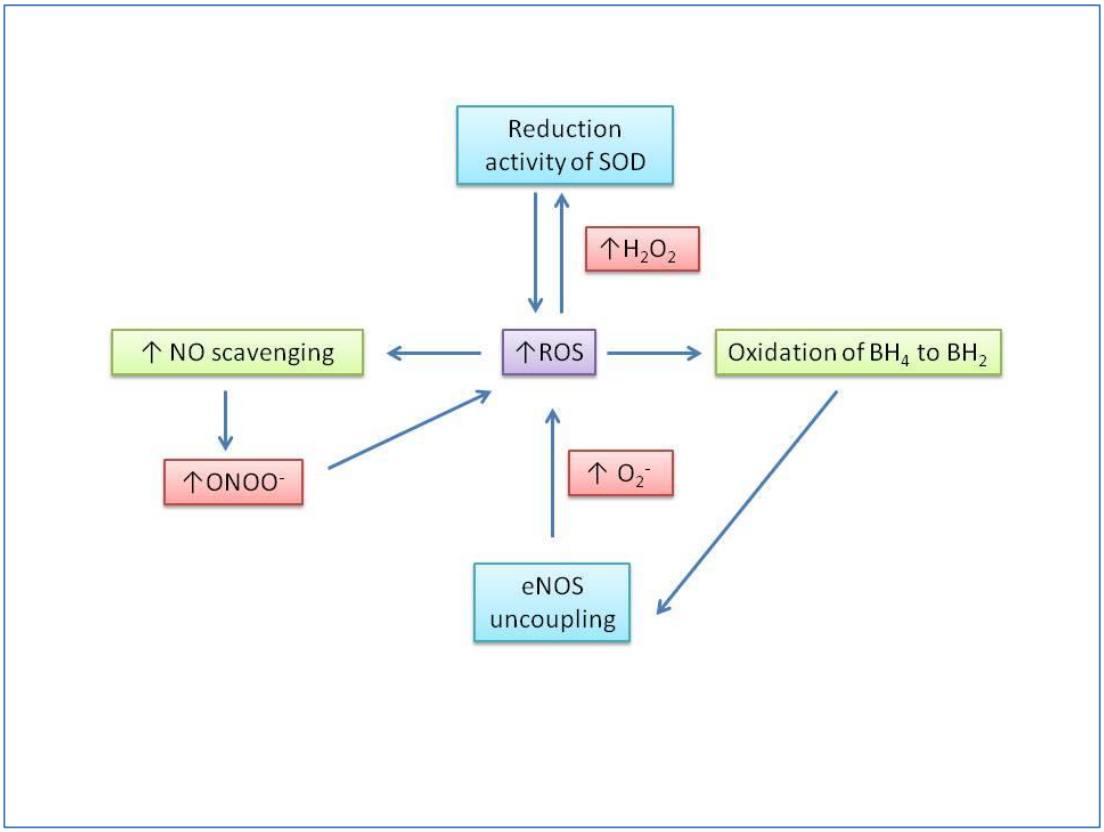

Figure 1.3-3: Mechanisms of ROS induced endothelial dysfunction. Schematic representation of the development of ROS induced endothelial dysfunction and reduced NO bioavailability. ROS: reactive oxygen species; SOD: superoxide dismutase; BH4 tetrahydrobiopterin; eNOS; endothelial nitric oxide synthase; NO: nitric oxide; ONOO-: peroxynitrate; H2O2: hydrogen peroxide

1.3.4 NADPH oxidases

The major biological source of ROS is the nicotinamide adenine dinucleotide phosphate oxidase (Nox) family of enzymes, and the primary function of this family of enzymes is the production of ROS. Originally thought to be solely expressed in phagocytic cells, where bursts of O_2^- are of importance in host defence, the Nox enzymes are now known to be present in non-phagocytic cells. The family are homologues of the catalytic subunit gp91phox. Irrespective of isoform, the Nox family of enzymes are transmembrane proteins; the predominant function is to support the transport of electrons, culminating in the reduction of O_2 to O_2^-.

There are 7 members of the Nox family found in mammals, although only 4 (Nox1, Nox2, Nox4 and Nox5) have been shown to be present in endothelial cells.

1.3.4.1 Nox1

Nox1 is expressed in relatively low levels, and in common with Nox2 produces O_2^- in a stimulus dependent manner. In culture, Nox1 has been shown to be up-regulated by factors including shear stress and angiotensin II [74]. There is evidence that Nox1 may be up-regulated in human atherosclerotic vessels [75], although extensive data is lacking.

1.3.4.2 Nox2

Nox2 is the typical gp91phox containing enzyme, and as such is expressed in phagocytes where it plays a significant role in host defence, but it is also expressed in endothelial cells. As with Nox1 Nox2 is not constitutively active but produces ROS in response to stimuli such as shear stress [76] and angiotensin II [74]. Mice with endothelial specific over expression of Nox2 exposed to angiotensin II demonstrate exaggerated endothelial dysfunction, hypertension and reduced acetylcholine dependent vasodilatation compared with wild type littermates [77]. This suggests a role for Nox 2 in the development of hypertension.

In humans there is good evidence that Nox2 is associated with endothelial function. In subjects with the X-linked immunodeficiency chronic granulomatous disease (CGD) (associated with mutation of gp91phox and hence also Nox2), Violi *et al* [78] demonstrated enhanced flow mediated vasodilatation (FMD) in the forearm, associated with enhanced NO production in those with CGD – suggesting that Nox2 plays a role in maintaining blood vessel tone, and modulating NO bioavailability.

1.3.4.3 Nox4

Unlike Nox1 and Nox2, Nox4 is constitutively active, and predominantly produces H_2O_2 rather than O_2^- [79]. Although there is evidence that Nox4 may play a role in cell senescence [80], in adverse remodelling of the pulmonary vasculature following hypoxia [81], the role which Nox4 plays in atherosclerosis and hypertension is less clear. Indeed there is some data which suggests that Nox4 expression, probably by virtue of the fact that it produces H_2O_2 as opposed to O_2^-, may be protective against the development of endothelial dysfunction. In mice with endothelial specific over expression of Nox4 Ray *et al* [82] demonstrated a reduction in blood pressure, and enhanced acetylcholine dependent vasodilatation when compared to wild type litter mates. This was associated with an increase in H_2O_2 production without a significant change in O_2^- levels. Furthermore, over expression of Nox4 on the endothelium of mice has also been shown to promote

angiogenesis and improve recovery from hypoxia by increased eNOS expression and activation [83]. Pulmonary endothelial cells taken from mice with tamoxifen inducible Nox4-/- have reduced eNOS activity and NO bioavailability in comparison with wild type counterparts, and aortas from the same mice have increased endothelial dysfunction and inflammation induced by angiotensin II [84] supporting the potentially beneficial role of Nox4, most likely in relation to the production of H_2O_2. This will be discussed in greater detail later (see chapter 1.10)

1.3.4.4 Nox5

Less is known about Nox5, the most recently discovered Nox to be found in endothelial cells, although it does produce both O_2^- and H_2O_2. The biological significance has not been entirely elucidated, but like Nox4, there is some evidence that Nox5 can also activate eNOS, although this was associated with reduced, rather than enhanced NO bioavailability, postulated to be due to scavenging of NO by the concomitantly produced O_2^-.

As has been discussed, endothelial function is determined by the balance between the rate of production, and the rate of breakdown of NO. One of the most important inducers of eNOS activity, and hence NO production is insulin, and sensitivity to the effect of insulin both on a whole body, and endothelial level is of critical importance in determining the development of endothelial dysfunction, atherosclerosis and the subsequent clinical sequelae. The relationship between insulin, the endothelium and endothelial function will be considered in greater detail.

1.4 Insulin Resistance

There is now unequivocal evidence that the condition of type 2 diabetes mellitus plays a role in the development of premature cardiovascular disease. In contrast to type 1 diabetes mellitus where autoimmune destruction of the β cells of the pancreas leads to an absolute deficiency of insulin, the hallmark of type 2 diabetes mellitus is resistance to the effects of insulin, particularly in skeletal muscle and adipose tissue.

In the last few decades there has been a significant improvement in the mortality attributable to cardiovascular disease, however this does not extend to those with type 2 diabetes, in whom mortality rates from cardiovascular disease remain stubbornly high [85]. Furthermore, in addition to the poor response to treatment once vascular disease has developed, the inherent risk of developing *de novo* vascular disease in someone with diabetes is significantly elevated with the risk of suffering a myocardial infarction 2 fold higher than the general population [86].

It is known that in patients with type 2 diabetes mellitus there is likely to have been many years of resistance to the effects of insulin preceding the development of hyperglycaemia, with normal glucose levels being achieved by compensatory hyperinsulinaemia [87] Figure 1.4-1**.** It is only when peripheral insulin insensitivity is accompanied by pancreatic β cell failure that abnormal glucose homeostasis develops.

There is a significant overlap between insulin resistance and the clinical condition known as the metabolic syndrome; a constellation of metabolic abnormalities associated with obesity, dyslipidaemia, hypertension, high levels of oxidative stress, a tendency towards pro-coagulation, insulin resistance and diabetes itself [88].

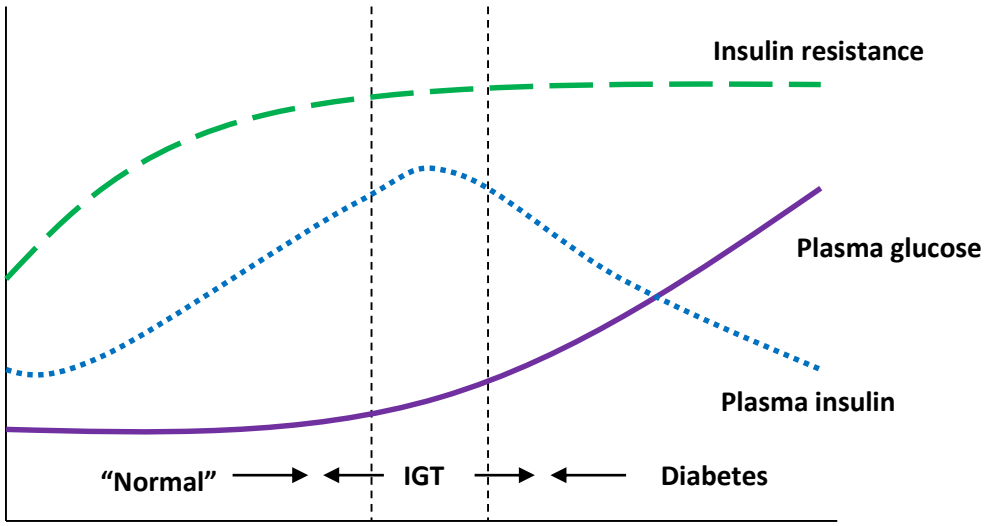

Figure 1.4-1: Plasma insulin and glucose levels in the pre-diabetic phase. Schematic representation of plasma insulin and glucose levels and associated insulin resistance during the transformation from insulin resistance and impaired glucose tolerance (IGT) to overt diabetes. Adapted from Wheatcroft et al [9].

Given the association between insulin resistance and this wide range of factors known to be associated with the development of premature vascular disease it is not surprising that individuals with insulin resistance do themselves have an increased risk of developing premature cardiovascular disease and stroke. Furthermore it has been demonstrated that insulin resistance is itself an independent risk factor for the development of premature cardiovascular disease [89-91], and that in turn insulin resistance is associated with endothelial dysfunction [92]. Given that significant numbers of patients with type 2 diabetes have advanced vascular disease at presentation, and that clinical diabetes is preceded by a prolonged period of insulin resistance, further understanding of the ways in which insulin resistance, and signalling through the insulin axis contribute to endothelial dysfunction may provide potential therapeutic targets to lessen the burden of vascular disease in those with type 2 diabetes.

1.4.1 Insulin and the insulin receptor

Insulin is a protein which is synthesised by the β cells of the pancreas. The structure of insulin was first described by British molecular biologist Frank Sanger, who subsequently won the 1958 Nobel Prize for chemistry in recognition of this work. Insulin is comprised of 2 peptide chains linked together by disulphide bonds. In the peripheral blood these monomers have a tendency to form dimers and in the presence of zinc, the dimers

combine to form hexamers. The β cells, via insulin mRNA, initially form the pro-peptide proinsulin. This is subsequently cleaved into insulin and the biologically inactive C-peptide by the action of endopeptidases [93, 94].

When the β cells are exposed to glucose, transport of glucose into the cell is mediated by a glucose transporter. Hence increased concentrations of extracellular glucose within the pancreas lead to increased intracellular glucose within the β cells. Elevated glucose levels within the β cells lead to membrane depolarization and subsequent calcium flux into the cells, promoting insulin secretion via exocytosis. In addition to promoting the secretion of insulin, elevated intracellular glucose levels also stimulate insulin synthesis [95].

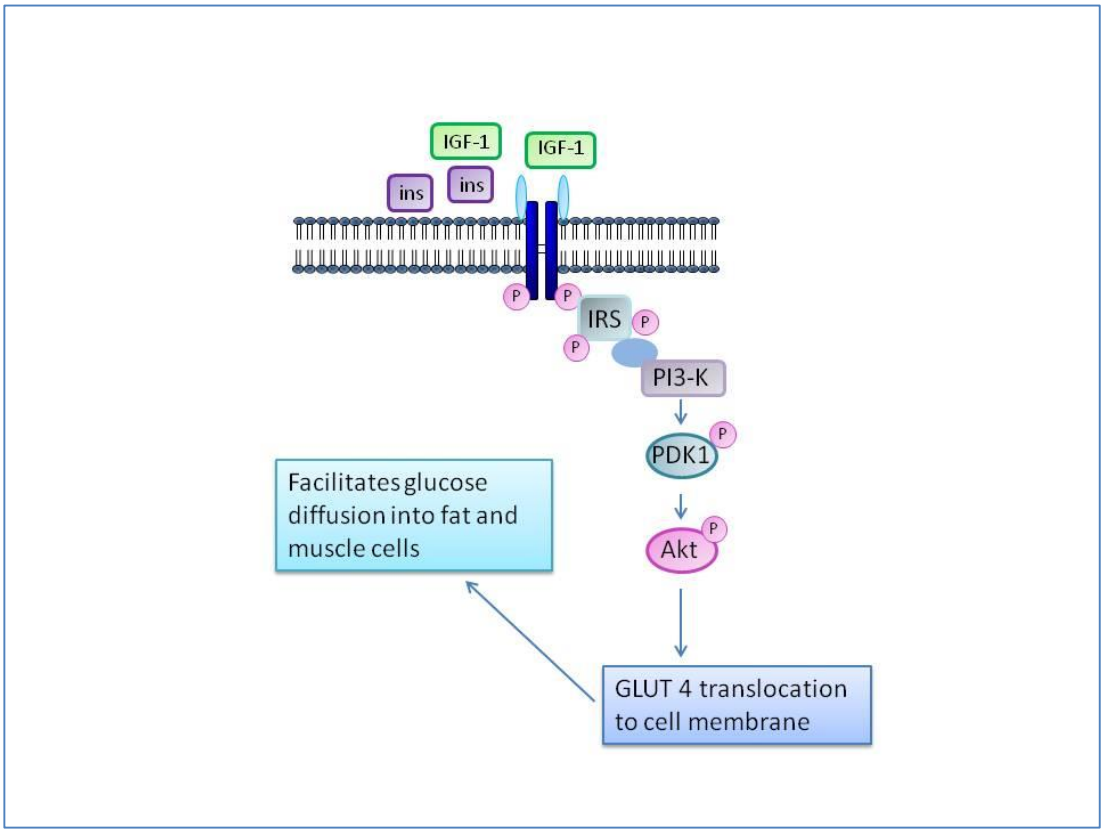

Figure 1.4-2: Insulin and IGF-1 induced glucose uptake. Binding of the ligand to the receptor stimulates a series of intracellular reactions, dependent on the PI3-K Akt pathway. This culminates in translocation of GLUT-4 to the cell membrane where it facilitates glucose uptake into tissues. IRS-1: insulin receptor substrate-1; PI3-K: phosphatidylinositol 3-kinase; PDK-1: protein dependent kinase-1; Akt: Protein kinase B; GLUT-4: glucose transporter - 4. The pink circle with P represents the process of phosphorylation.

Insulin primarily acts upon cells by the interaction with the insulin receptor (IR), although as will be discussed in detail, insulin also interacts with the insulin like growth factor-1 receptor (IGF-1R). The insulin receptor itself is comprised of 2 α subunits and 2 β subunits. The subunits are combined to form the whole receptor with disulphide bonds. The α subunit is located on the surface of the cell, whereas the β subunit penetrates the cell membrane, and hence the insulin receptor has both extracellular and intracellular components. When insulin binds to the hydrophobic area on the α subunit it causes a conformational change within the receptor leading to transfer of signal to the β subunit [96].

Insulin signalling through the IR could be described as a three stage process:

1. Activation of the IR leading to phosphorylation of tyrosine kinase
2. Subsequent tyrosine phosphorylation of various molecules
3. Biological effects caused by a cascade of reactions

The biological effects of insulin are legion. Insulin is responsible for glucose homeostasis; the regulation of fatty acid synthesis and lipolysis; involved in modulating genetic expression and cell growth; has effects on vascular smooth muscle tone and the function of the endothelium. The latter will be discussed in more detail below.

1.4.2 Insulin and glucose homeostasis

Insulin acts to control glucose homeostasis in several ways.

In skeletal muscle and adipose tissue (uptake of glucose into liver and brain cells is insulin independent), insulin initiates uptake of glucose from the extracellular space via activation of glucose transporter type 4 (GLUT-4) [97]. In the basal state GLUT-4 is present within cytoplasmic vesicles, where they have no ability to act upon glucose. Following activation of the insulin receptor GLUT-4 receptors (facilitated by phosphorylation of insulin receptor substrate [IRS] and phosphoinositide-3 kinase [PI3-K] [98]) are released from vesicles and are incorporated into the cell membrane where they allow the cell to efficiently take up glucose. Figure 1.4-2

In hepatocytes insulin leads to glycogen storage by the production of glycogen synthase which is also promoted by activation of PI3-K and phosphorylation of IRS. Conversely, in the

absence of insulin the liver begins to breakdown glycogen hence releasing glucose in to the bloodstream.

1.5 Insulin like growth factor 1

Insulin like growth factor – 1 (IGF-1) is a protein which has a similar structure to that of insulin [99]. It is produced primarily by the liver in response to the action of growth hormone (GH) [100], but unlike insulin, it is also synthesised within peripheral tissues, having autocrine, paracrine and endocrine functions. IGF-1 has many effects, both on a whole organism and a cellular level. It is accepted that IGF-1 is of critical importance in regulating cell and tissue growth [100], and therefore there is a great deal of interest in the study of the manipulation of IGF-1 in the fields of longevity and cancer research. Within the last decade there has also been an increasing interest in the role that IGF-1 plays in interacting with the endothelium, and hence the effect that IGF-1 may have upon the development of atherosclerosis. Whilst a clear link has been established between insulin resistance and atherosclerosis the contribution that alterations in signalling through the IGF-1 axis may play in the development of premature cardiovascular disease is less clear and requires further discussion.

1.5.1 IGF binding proteins

The significant majority of IGF-1 in plasma is bound to one of six IGF binding proteins (IGFBP) [101]. In normal states, less than 1% of IGF-1 is found in the free form, and when in the free form it degrades quickly. Although the binding capacity of IGF-1 for its receptor is high, the affinity towards the IGFBPs is higher. Indeed the binding proteins may modulate IGF-1 IGF-1R interactions [102]. More recently actions of the IGFBP which are independent of IGF-1 have been described, and indeed the IGFBPs may have specific actions controlling cell differentiation, apoptosis and growth [102].

Although there are 6 described IGFBP specific consideration will be given to IGFBP-1 which appears to play a significant role in IGF-1 receptor activity and cardiovascular disease.

Both IGF-1 and IGFBP-1 levels are affected by insulin sensitivity, and low levels of both also appear to predict adverse cardiovascular outcome [103]. Evidence taken from the Rancho Bernado study cohort [104] demonstrated that low levels of both IGF-1 and IGFBP-1 predicted the development of fatal ischaemic heart disease, independent of other risk factors.

There is evidence that over-expression of IGFBP-1 is associated with down regulation of the insulin signalling pathway, possibly by higher levels of IGF-1 sequestration. Conversely,

Wheatcroft *et al* [105], using a mouse which over-expressed IGFBP-1 showed enhanced basal NO production in association with elevated eNOS phosphorylation in the aorta. Further evidence from Rajwani *et al* [106] seems to support the role for IGFBP-1 as a vascular protective factor particularly in an insulin resistant setting: over-expression of IGFBP-1 in obese mice was associated with improved insulin sensitivity and enhanced insulin stimulated NO production; in IR +/- mice, enhanced IGFBP-1 was associated with improved insulin stimulated NO release; in the ApoE model, over-expression of IGFBP-1 was associated with reduced atherosclerosis.

1.5.2 Insulin like growth factor-1 and glucose homeostasis

Although insulin is the most important biological mediator of glucose homeostasis, IGF-1 is also able to promote glucose uptake via activation of the PI3-K / Akt pathway culminating in GLUT-4 translocation to the cell membrane [107] and increased glucose uptake, particularly from skeletal muscle [108, 109].

As is shown in Figure 1.4-2 activation of the PI3-K pathway by IGF-1 [110] leads to translocation of GLUT-4 and increased glucose uptake in skeletal muscle. In humans it has been found that infusion of supra-normal levels of IGF-1 leads to decreased blood glucose [111], but the same is not true for physiological levels of IGF-1 *in vivo* [112].

Several studies have shown that treatment with recombinant IGF-1 improves insulin sensitivity, primarily by improving hepatic and muscle insulin sensitivity [113]. In addition to improving peripheral insulin sensitivity, infusion of IGF-1 also leads to a reduction in circulating levels of GH with the result of reducing hepatic gluconeogenesis [114, 115].

In both diabetic and non-diabetic patients, IGF-1 levels were found to be independently negatively associated with markers of the insulin resistance syndrome, particularly BMI, waist to hip ratio, systolic and diastolic blood pressure, and also independently correlated with varying degrees of glucose intolerance [116]. Given the apparent association between IGF-1 levels and the insulin resistance syndrome, and the well documented association between insulin resistance and the development of premature atherosclerosis it is pertinent to consider the association between IGF-1 and cardiovascular disease.

1.5.3 The link between IGF-1 and cardiovascular disease

1.5.3.1 Clinical studies

Although there remains some degree of controversy the breadth of evidence currently seems to suggest that there is a relationship between reduced IGF-1 bioavailability and increased risk of developing atherosclerosis. There are however, some studies which suggest the contrary.

Elevated fasting serum IGF-1 levels have been noted to be correlated with an increased carotid intima media thickness, a potential marker for the early development of atherosclerosis [117, 118], and high IGF-1 levels have been shown to be positively associated with atherosclerosis in a relatively young population [119, 120]. Andreassen *et al* [121] showed a U shaped relationship between levels of IGF-1 and all-cause mortality in an older population, and a possible association of high levels of IGF-1 with the development of left ventricular systolic dysfunction, as measured by elevated NT-proBNP level, but in common with Botker *et al* [122] did not demonstrate a link between atherosclerotic disease and elevated IGF-1 levels.

Locally, there is evidence that increased IGF-1 levels are found in VSMC at the site of balloon initiated vascular injury [123], suggesting a possible pathogenic role for IGF-1 in the development of restenosis following angioplasty. Although initial data suggested that IGF-1 inhibition may be a useful therapeutic target to reduce restenosis, placebo controlled trials of IGF-1 inhibition with angiopeptin [124, 125] and octreotide [126] in humans were unable to replicate this.

As has been discussed, the general consensus is that there is an association between low levels of IGF-1 and either the presence of cardiovascular disease or worse outcome from cardiovascular disease [103, 104, 127-131]. One probable explanation for the differing findings could relate to the varying assays used to assess serum IGF-1 levels. Generally speaking , many of the studies used total IGF-1 levels as a surrogate marker for IGF-1 activity, however given that a significant proportion of IGF-1 is held in the plasma bound to IGF1BP, and is hence inactive this may not be an accurate reflection of IGF-1 bioavailability. When IGF-1 bioavailability rather than IGF-1 levels, was measured by its ability to activate the IGF-1R, as was done by Brugts *et al* [129] there was a significant association with high

IGF-1 bioavailability and reduction in cardiovascular disease; the same relationship was not found when free and total levels of IGF-1 were assessed.

1.5.3.2 Pro-atherosclerotic effects of IGF-1

Although there is a consensus that there is an association between low plasma IGF-1 and increased risk of cardiovascular disease, there is certainly some evidence that IGF-1 has some pro-atherogenic activity.

IGF-1 induces VSMC migration and proliferation via activation of the mitogen activated protein kinase (MAPK) pathway. In coronary artery specimens taken from patients with cardiovascular disease had significantly higher levels of IGF-1 when compared with normal controls [132], furthermore higher levels of IGF-1 mRNA are found in unstable rather than stable coronary plaques [133]

The role of VSMC is important, not only in the development of atherosclerosis, but is critical in the initiation of restenosis of coronary vessels following angioplasty: vascular injury enhances IGF-1 production[134]; IGF-1 in early restenotic lesions is significantly higher than in normal coronary artery samples [133]; IGF-1 inhibition inhibits VSMC proliferation following balloon injury in rats [135]; IGF-1 inhibition using a somatostatin analogue reduces human VSMC proliferation [123]. Unfortunately, systemic treatment with somatostatin analogues have not shown any significant association with reduced restenosis or reduction in cardiovascular endpoints [124, 126]. Taken together this data suggests that IGF-1 plays a vital role in initiating smooth muscle cell hyperplasia leading to restenosis.

In addition to the effect on VSMC there is some evidence showing a link between IGF-1 and platelet activation [136-138] an effect which was particularly marked in diabetic rats [136]

1.5.3.3 Pathophysiological basis of IGF-1 and atheroprotection

As will be discussed in detail later the most important way in which IGF-1 acts as an athero-protective factor may be by inducing NO production by endothelial cells, via a PI3-K dependent mechanism [139]. The vascular protective effects associated with NO bioavailability have been discussed in detail above. Interestingly, obesity is associated with vascular IGF-1 resistance [140] which may explain some of the associated increased cardiovascular risk.

In addition to the effect on NO bioavailability, IGF-1, as has already discussed, has a beneficial effect on insulin sensitivity; in itself improved insulin sensitivity is associated with reduced atherosclerosis.

1.5.3.4 Lessons from growth hormone deficiency, Laron syndrome and acromegaly

A useful way of looking at the cardiovascular effects of IGF-1 is to study people who have either IGF-1 deficiency or IGF-1 excess. Congenital IGF-1 deficiency is known as Laron syndrome and is associated with insensitivity to growth hormone and presents with dwarfism, marked obesity and hypoglycaemia [141] . Although patients with Laron syndrome are obese, there appears to be a lower than expected rate of co-existing diabetes [142], which is interesting given than laboratory animals with GH deficiency are protected from developing insulin resistance. Adults with Laron syndrome appear to be to protected against the development of cancer [141](which is unsurprising given the known mitogenic actions of IGF-1), and although there is a suspicion that cardiovascular disease accounts for a significant number of deaths in this cohort, the numbers are relatively small and data on a larger scale is lacking.

Patients with acquired adult growth hormone deficiency have increased cardiovascular risk [143] associated with increased oxidative stress [144] and abnormal endothelial dysfunction, measured by reduction in vasodilatation associated with acetylcholine [144] (ACh) and reduction in FMD [145].

The clinical condition of acromegaly caused by a growth hormone secreting tumour in the pituitary gland is associated with excessive IGF-1 production. The excess growth hormone secretion seen in acromegaly leads to gluconeogenesis and lipolysis leading to hyperglycaemia, elevated free fatty acids, hyperinsulinaemia and insulin resistance. Insulin resistance is a major feature of acromegaly, and patients frequently develop type 2 diabetes mellitus. Cardiovascular disease is frequently seen in patients with acromegaly. The development of acromegalic cardiomyopathy (left ventricular hypertrophy, diastolic dysfunction and eventually left ventricular systolic dysfunction) relates to the growth promoting effects of IGF-1 and GH, and regresses following appropriate treatment [146]. Interestingly, the elevated levels of IGF-1 seen do not appear to confer any protection against the development of atherosclerotic disease, indeed this risk is significantly elevated in those with acromegaly. Patients with acromegaly have endothelial dysfunction, reduced

NO levels and higher carotid intima thickness than age and sex matched counterparts [147, 148] and have also been demonstrated to have higher levels of oxidative stress [149]. It is likely that the excess atherosclerotic disease seen is accounted for by the concurrent insulin resistance, and any anti-atherosclerotic effects of IGF-1 are overwhelmed.

The clinical features seen in those with IGF-1 excess and deficiency serve to illustrate the complicated relationship between IGF-1, insulin, endothelial function and atherosclerosis.

1.5.3.5 IGF-1 and longevity

Further evidence of the complicated relationship between the IGF-1 signalling axis and cardiovascular disease exists when one considers the seemingly paradoxical evidence linking reduced IGF-1 signalling with longevity.

There is evidence which links reduced signalling through the insulin / IGF-1 axis with longevity, although it remains contentious. Holzenberger *et al* [150] demonstrated that mice with haploinsufficiency of the IGF-1R have a lifespan 26% longer than wild type counterparts. In contrast, Bokov *et al [151]* who also examined mice with whole body haploinsufficiency of the IGF-1R were unable to replicate this finding. Studies in old humans also demonstrate an association between longevity and genetic polymorphisms which are associated with reduced signalling through the insulin/IGF-1 axis [152-154]. Whether this is a causal relationship is not known, and no studies to date have looked at the distribution of IGR-1 / insulin hybrid receptors (see chapter 1.8) in old age.

Human centenarians tend to have reduced body mass index, increased insulin sensitivity [153] and reduced circulating levels of IGF-1 [155, 156]. This combination of factors hints that reduction in calorie intake, possibly through reduced levels of oxidative stress plays a significant role in the modification of the insulin/ IGF-1 axis, and may be responsible for the alterations in this axis seen in long lived humans. Although many studies certainly demonstrate an association between restricted calorie intake, longevity and delayed onset of old age associated diseases [157], the publication of a recent study in primates contests this [158]. In this most recent publication, calorie restriction in young primates did delay onset of old age associated diseases, but was not associated with improved mortality rates. When calorie restriction was commenced later in life, there was an improvement in several aspects of metabolic function but again, no increase in longevity was seen. This suggests a more complex relationship between calorie in-take and longevity than was first thought.

Given the paradoxical observation that low IGF-1 can be associated with both longevity and increased cardiovascular risk, further examination of the IGF-1 and insulin signalling pathways is required.

1.6 Structure of the IGF-1 Receptor.

The IGF-1 receptor (IGF-1R) is part of the same family of tyrosine kinase receptors as the IR, with which it shares significant structural homology. The IGF-1R preferentially binds IGF-1, although it also has affinity for IGF-2. The IGF-1R was recognised as distinct from the IR in 1974 [159], although probably the two receptors emerged as distinct identities at the time of transition from prochordates to vertebrates [160].

1.6.1 Genetics

The genetic code for the IGF-1R, located on chromosome 15q26, consists of 4989 nucleotides coding a 1367 amino acid precursor [161]. The IGF-1R and IR are remarkably similar, both in terms of exon distribution and size of the two genes, and indeed they share around 70% DNA sequence identity [162, 163]. The receptor is initially formed as a pre-pro receptor and prior to transportation to the Golgi apparatus undergoes cleavage, glycosylation and folding. In the Golgi apparatus the receptor is cleaved into α and β subunits at a tetrabasic protease cleavage site Arg-Lys-Arg-Arg [161, 164], and then transported to the cell membrane. The mature receptor takes the form of a homodimer comprised of two α subunits and two β subunits held together by disulphide bonds [165]. The homodimer is both intra and extracellular: the ligand binding site is located on the extracellular α subunit; the β subunit contains the tyrosine kinase domain and comprises extracellular, trans-membrane and intracellular components.

1.6.2 Structure of the IGF-1R

The N-terminal of the α subunit comprises the cystine rich (CR) domain flanked by two homologous domains (L1 and L2) [166]. The C terminal of the α subunit contains two fibronectin type III (FnIII) domains, which are common to many trans-membrane receptors and facilitate protein binding [167]. Contained within the second FnIII there is a large insert domain (ID) containing the Arg-Lys-Arg-Arg protease cleavage site [168].

Two further FnIII domains are located on the N terminal of the β subunit, which is both extracellular and trans-membrane. The tyrosine kinase (TK) domain, which spans residues 973-1229 is located on the intracellular portion of the β subunit [162]. Phosphorylated tyrosine residues within the TK domain function as docking sites for critical intracellular signalling molecules; of particular relevance to both glucose homeostasis and endothelial function are the insulin receptor substrates 1-4 (IRS 1-4) and the Src-homology domain 2

(SH2) of the Shc adaptor protein. The C tail domain of the β subunit is 108 residues in length and contains phosphotyrosine binding sites. These are potentially important in modulating TK activity, particularly at the ATP binding site [169] although the full physiological role of the C tail is not yet fully understood.

The mature IGF-1R comprises two α subunits and two β subunits, held together by the presence of disulphide bonds. Inter α-chain bonds occur at two locations; a single bond in the Fn-III-1 and a triplet in the ID [166]. α and β subunits are held together by a single disulphide bond between the first FnIII repeat on the α subunit and the second FnIII repeat on the β subunit [170]. Figure 1.6-1

1.6.3 Ligand binding and activation of TK domain

In common with the IR, the interaction between IGF-1 and the IGF-1R is complex.

Analysis of data obtained from Scatchard plots suggest that there are both low and high affinity binding sites on the IGF-1R and furthermore, that dissociation of bound IGF-1 to the IGF-1R is accelerated when the concentration of IGF-1 is increased [163, 171-173]. Taken together this suggests negative co-operativity between the binding sites, which, in contrast with the relationship between insulin and the IR is not lost at high concentrations of IGF-1 [174].

In common with the IR, there are two binding sites on the IGF-1R, both located on the subunit. The first binding site (site 1) comprises three components: the N terminal of the L1 domain, the C terminal of the FnIII-2 domain and a third area within the CR domain [175-179] . This is distinct from the IR, which has only two components of the first binding sites. The location of the second binding site (site 2) is not yet fully elucidated, although is thought to contain part of the FnIII-1 domain [163].

High affinity binding of IGF-1 to the IGF-1R is created by binding to site 1 on one monomer and site 2 on the second monomer. This causes crosslinking, dimerisation and moves the monomers into closer proximity [163, 180]. Binding to the two receptor halves is essential to create a high affinity binding site.

Ligand binding to the α subunit of the IGF-1R initiates trans-auto phosphorylation in the tyrosine residues Tyr 1131, Tyr 1135 and Tyr1136 of the activation loop (A loop) of the TK

domain. In the non-phosphorylated state these tyrosine residues block the active ATP site; autophosphorylation of Tyr1131 and Tyr 1135 leads to the destabilisation of the auto-inhibitory A-loop formation; autophosphorylation of Tyr1136 stabilises the catalytically active A-loop formation [181, 182]. This leads to a conformational change in the A-loop, allowing protein substrates and ATP unrestricted access to the active kinase site [182, 183].

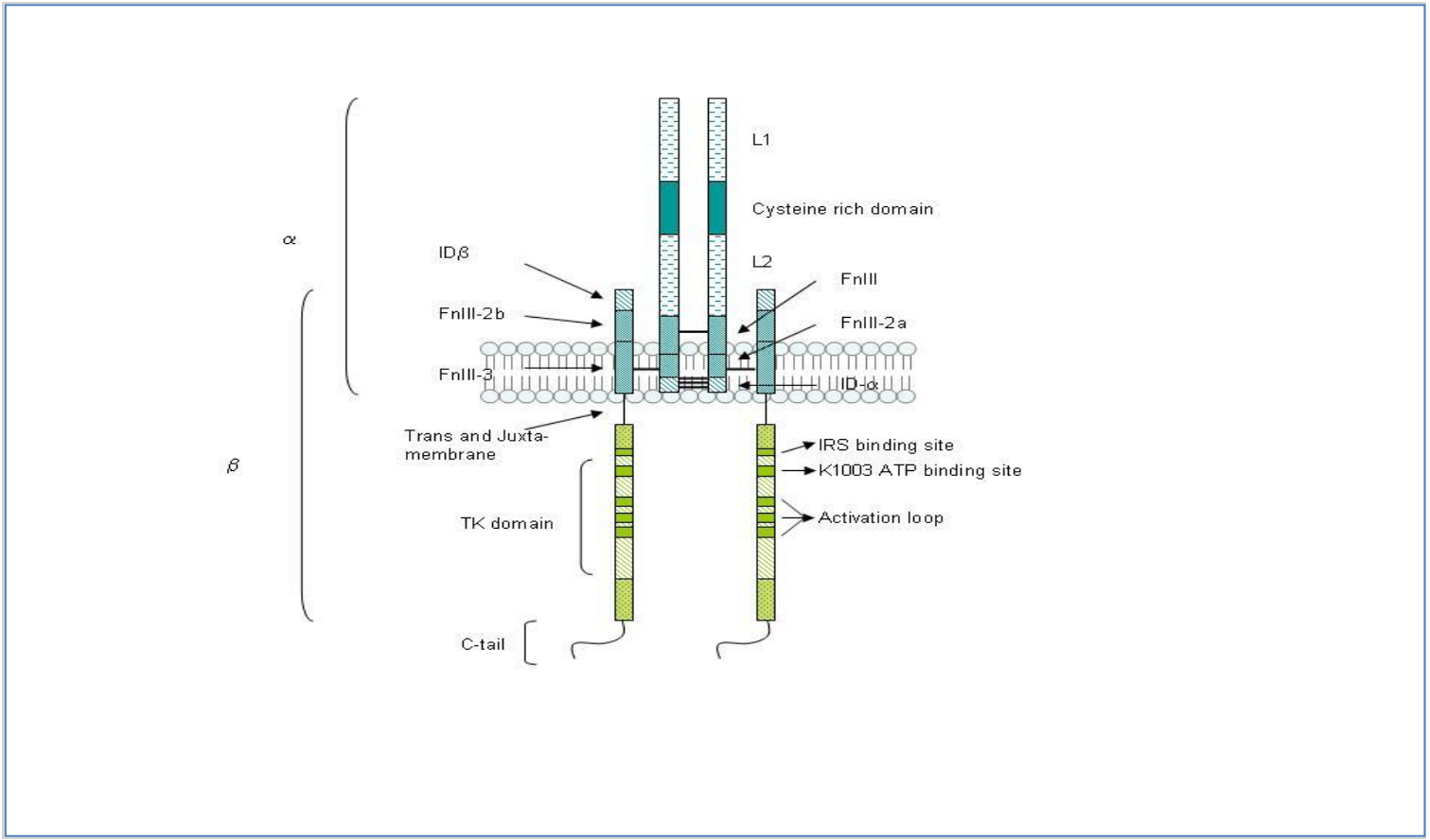

Figure 1.6-1: Diagrammatic representation of IGF-1R. FnIII: fibronectin type III domains. ID: Insert domain. TK domain: tyrosine kinase catalytic domain (residues 973-1229). Trans and juxta-membrane region (residues 930-972). C tail (residues 1230-1337). Adapted from Adams et al (2) and Sehat et al (92). Reproduced with permission from Gatenby et al [46]

1.7 Insulin, insulin like growth factor-1 and endothelial cell function

The role which insulin resistance plays in the development of type 2 diabetes mellitus is well established [9], and it is now accepted that insulin resistance is an independent risk factor for the development of atherosclerosis and its subsequent clinical manifestations[184, 185] . Previous work from our laboratory has demonstrated the relationship between insulin resistance and endothelial cell dysfunction in seemingly healthy south Asian young men [186, 187]. Several other studies in humans have shown a significant correlation between reduced bioavailability of NO and insulin resistance [188-191]. In corroboration with these findings, previous work from our group has shown a strong inverse relationship between endothelial dysfunction (as assessed by NO bioavailability) and whole body insulin sensitivity [192-194]. Critically, there is now emerging evidence that expression of the IR on the vasculature modulates both endothelial cell insulin sensitivity and endothelial function. Mice with endothelial specific mutation of the IR (ESMIRO) are sensitive to insulin on a whole body level, but have endothelial specific insulin resistance and reduced NO bioavailability[195].

Although the link between insulin resistance and the endothelium is relatively well established, the particular role of IGF-1 and the IGF-1R is less clear and requires further consideration.

1.7.1 IGF-1R and IR activation and nitric oxide production

There is little doubt that endothelial dysfunction plays a significant role in the initiation and development of atherosclerosis [7]. The endothelial cell acts not only as a barrier, but as has been discussed above, as a complex paracrine, autocrine and endocrine organ which, by the release of a portfolio of mediators maintains intra-vascular homeostasis [196]. One of the critical aspects of vessel homeostasis is the regulation of blood vessel tone; achieved by the release of the opposing compounds NO and endothelin-1 (ET-1). This is of particular significance when considering the relationship between insulin, IGF-1 and endothelial cell function.

Data suggests that both IGF and insulin are able to induce NO production primarily by interaction with the IGF-1R and IR, respectively. Stimulation of rat renal inter-lobar artery endothelial cells with IGF-1 has been shown to induce NO production; this was blocked by

both the NOS inhibitor L-NAME (thereby confirming that NO production was NOS dependent) and an IGF-1 inhibitor [197]. Both insulin and IGF-1 stimulation induce NO production in HUVECS; incubation with αIR3 (an IGF-1R blocking antibody) has been shown to completely abolish NO production in response to insulin, but reduces NO production in response to insulin by half: strongly suggesting that insulin is able to signal through the IGF-1R [139]. The same group demonstrated that insulin induced NO production was ameliorated by the PI3-K inhibitor, wortmannin [139].

Although both IGF-1 and insulin are able to induce NO production, there is little doubt that insulin is the more potent stimulator; maximal IGF-1 stimulation in human umbilical vein endothelial cells (HUVECs) produced 40% of the NO seen with maximal insulin stimulation [139]. As has been discussed, there is certainly evidence of cross-reactivity between insulin, IGF-1, the IR and IGF-1R it would appear that at physiological levels (100-500pM), insulin only stimulates the IR and not the IGF-1R. Li *et al* showed that in bovine aortic endothelial cells, a physiological dose of insulin did not lead to phosphorylation of the IGF-1Rβ subunit, although phosphorylation of eNOS, Akt1 and IRβ was noted [198]. At the supra-physiological level (1-5nM) insulin stimulation was associated with phosphorylation of the IGF-1Rβ; this effect was blocked by an IGF-1R neutralizing antibody.

Following ligand binding to the IGF-1R or IR a cascade of intracellular reactions occurs, ultimately culminating in, amongst others, the production of NO. Autophosphorylation of tyrosine residues on the β subunit of either receptor allows, as has been discussed above, a conformational change in the A-loop allowing proteins such as IRS-1 access to the active kinase domain. Phosphorylation of IRS-1 at specific tyrosine residues occurs [98, 199]and the phosphorylated IRS-1 binds PI-3K by the SH2 domain of the p85 α regulatory subunit. This initiates increased activity of the catalytic p110 subunit of PI3-K leading to conversion of plasma lipid phosphatidylinositol 3,4,-bisphosphate (PIP_2) to phosphatidylinositol 3,4,5-trisphosphate (PIP_3). Activated PIP_3 has the effect of encouraging proteins containing plekstrin homology (PH) domains to congregate at the cell membrane, of which the most important with regard to IGF-1 and insulin stimulated NO production are the seronine-threonine kinases Akt and 3-phosphoinositide dependent protein kinase-1 (PDK-1) [200]. Accumulation of these proteins at the cell membrane leads to PDK-1 dependent phosphorylation of Akt-1. Figure 1.7-1

Once phosphorylated, Akt-1 induces phosphorylation and activation of eNOS at serine 1177 [201], which, as has been described above stimulates the transfer of electrons from NADPH culminating in the conversion of L-arginine to L-citrulline and the formation of NO [196].

1.7.2 Insulin signalling and MAPK

As well as initiating the PI3-K / Akt dependent pathway binding of insulin or IGF-1 also instigates signalling through the mitogen-activated protein kinase (MAPK) pathway, in a cascade of reactions dependent on Ras interaction with the Src-homology domain 2 (SH2) of the Shc adaptor protein [202]. Activation of this pathway, as well as causing production of the vasoconstrictor peptide ET-1, induces vascular smooth muscle cell (VSMC) proliferation, and migration, and may therefore be of importance in sustaining atherosclerotic plaque stability [203, 204]. Flux of signalling down the MAPK pathway, rather than the PI3-K pathway is of importance in regulating the cell sensitivity to the effects of insulin and will be discussed in detail later.

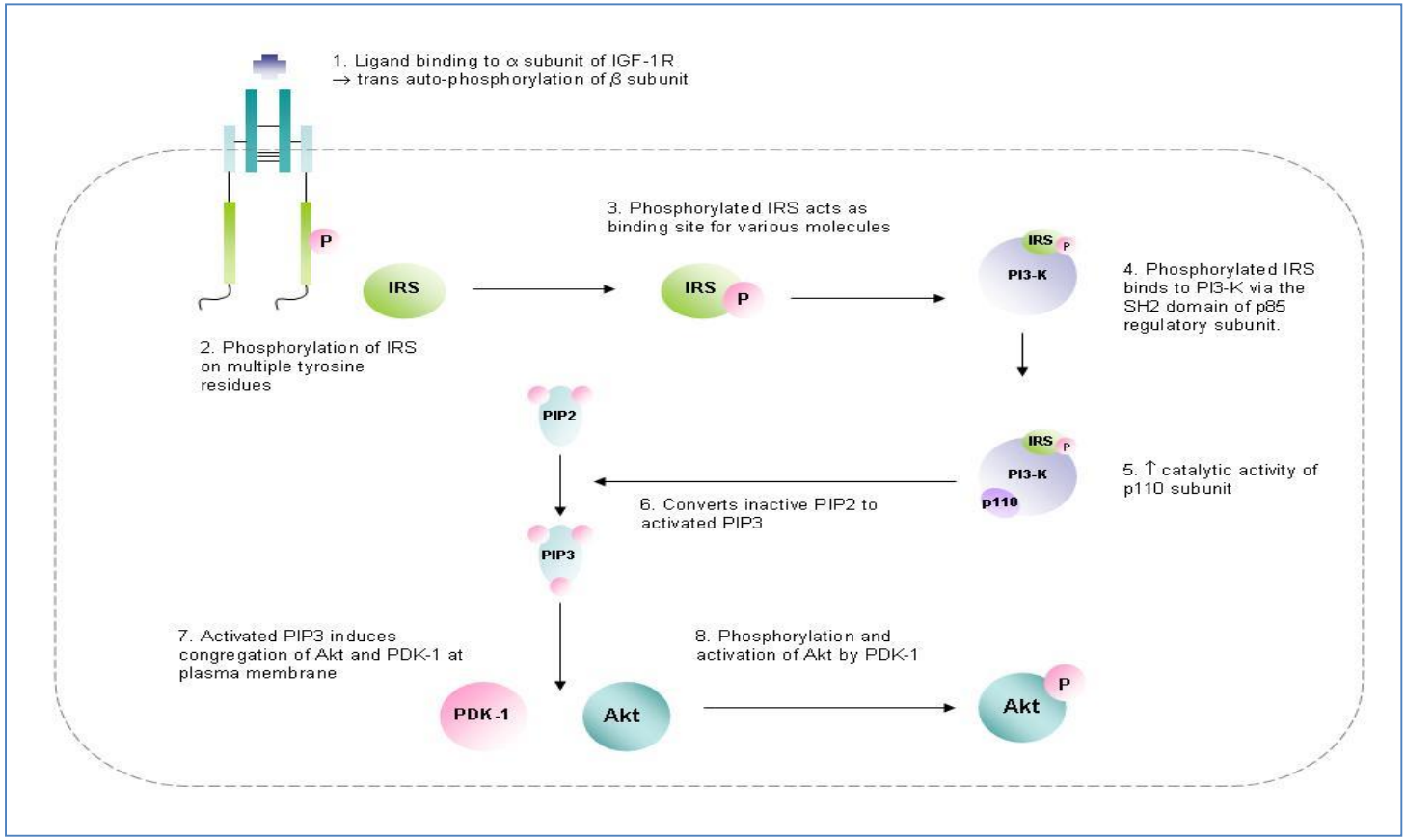

Figure 1.7-1: Initiation of PI3-K / Akt pathway by ligand binding to the IGF-1R. The same applies for binding to the insulin or the IGF-1R/IR hybrid. Reproduced with permission from Gatenby et al [46]. IRS: insulin receptor substrate; PI3-K: phosphatidylinositol 3-kinase; PIP2: Phosphatidylinositol 3,4-bisphhosphate; PIP3: Phosphatidylinositol 3,4,5-trisphosphate; PDK-1: protein dependent kinase – 1; Akt: Protein kinase B. The pink circle with P represents the process of phosphorylation.

1.8 Insulin like growth factor / insulin receptor hybrids

As has been discussed, the IR and IGF-1R share significant genetic and structural homology; both are formed of two heterodimers comprised of α and β sub-units, joined by disulphide bonds to form a homodimer. It is now recognised that the heterodimers of the two receptors are able to combine to form a hybrid receptor (see Figure 1.8-1), consisting of an IR $\alpha\beta$ heterodimer and an IGF-1R $\alpha\beta$ heterodimer [205, 206]. Although the physiological role of these hybrid receptors has yet to be confirmed, it is beginning to become apparent that the formation of the IR/IGF-1R heterodimer has a significant role in determining insulin sensitivity in the cell [207, 208]. Our group has recently published work demonstrating that manipulation of the IR and IGF-1R stoichiometry is able to affect both hybrid receptor formation and cellular insulin sensitivity [209, 210].

Although comprised of both IR and IGF-1R, hybrid receptors behave very much like an IGF-1R homodimer; IGF-1 binds to the hybrid receptor with an affinity 20 times higher than insulin [211-213]. The mechanism of higher affinity IGF-1 binding to the hybrid is unclear, although theories suggest that the ability of the ligand to successfully bind with site 2 on the opposing α subunit is of critical importance. With regards to binding to the hybrid receptor, it appears likely that IGF-1 binds to site 1 on the IGF-1αβ heterodimer, and site 2 of the IRαβ heterodimer, causing cross-linking and receptor activation. The same is true of the interaction between insulin and the IRαβ heterodimer. Two theories would explain the hybrid receptor's higher affinity for IGF-1 than insulin; either binding to both sites is less important in determining high affinity binding for IGF-1, or IGF-1 is able to bind to site 2 of the IRαβ heterodimer with an efficacy equal to that of the IRαβ heterodimer [174, 211]. Recently, research has suggested that the L2/Fn domain of the IGF-1αβ heterodimer plays a critical role in determining the hybrid receptor's affinity for insulin. Insertion of the L2/Fn domain from the IR into the corresponding domain on the IGF-1Rαβ heterodimer within a hybrid receptor renders the hybrid receptor as equally sensitive to insulin as the IR homodimer [211].

Although ligand binding is initiated by binding to site 1 on a single α subunit, *trans* binding to site 2 ensures that autophosphorylation occurs of both β subunit, culminating in activation of the TK domain, as is described above [214]. Signal propagation requires that both subunits are functional; formation of a hybrid receptor comprising a wild type active

IGF-1Rαβ heterodimer and a kinase inactive IRαβ heterodimer results in transdominant inhibition of kinase activity [215].

Although there are 2 isoforms of the insulin receptor, it is not clear if the isoform incorporated into the hybrid affects ligand binding. Although preliminary studies suggested that hybrids comprised of an IR-A isoform have an affinity for insulin higher than those comprised of an IR-B isoform [216] , subsequent studies were unable to demonstrate this [211, 217].

Although there is robust evidence to suggest that the hybrid receptor behaves as an IGF-1 receptor with respect to its binding properties, there are no data proving that the hybrid receptor acts in the same way as the IR or the IGF-1R following autophosphorylation. Though it is reasonable to suspect that following autophosphorylation the hybrid interacts with IRS-1 and initiates the PI3-K / Akt pathway, there is no direct experimental evidence to support this. Of particular note, there is a lack of data directly linking the hybrid receptor with glucose uptake or NO production, although there is a wealth of circumstantial evidence to support the theory that the hybrid receptors initiate signalling through the PI3-K / Akt pathway in the same way as the IR and the IGF-1R.

Although the factors which control hybrid expression are not completely understood, the proportion of receptors expressed as hybrids within various tissue types seem to be associated with a relatively random mode of construction [218]. Although aspects of this process appear arbitrary, there is data to support the theory that the configuration of hybrid receptors found is associated with the molar concentrations of each receptor type. [219]. Furthermore, it has been shown that manipulation of the numbers of heterodimers in various cells has the ability to significantly alter hybrid receptor expression. Increasing the number of IGF-1R drives IR to be incorporated into hybrid receptors, a finding which has been demonstrated in fibroblasts [214] and endothelial cells [210]. The converse also appears to be true, and we have shown that knockout of the IGF-1R on vascular endothelium, and heterozygous knockout on a whole body level is associated with reduced hybrid receptor expression [209].

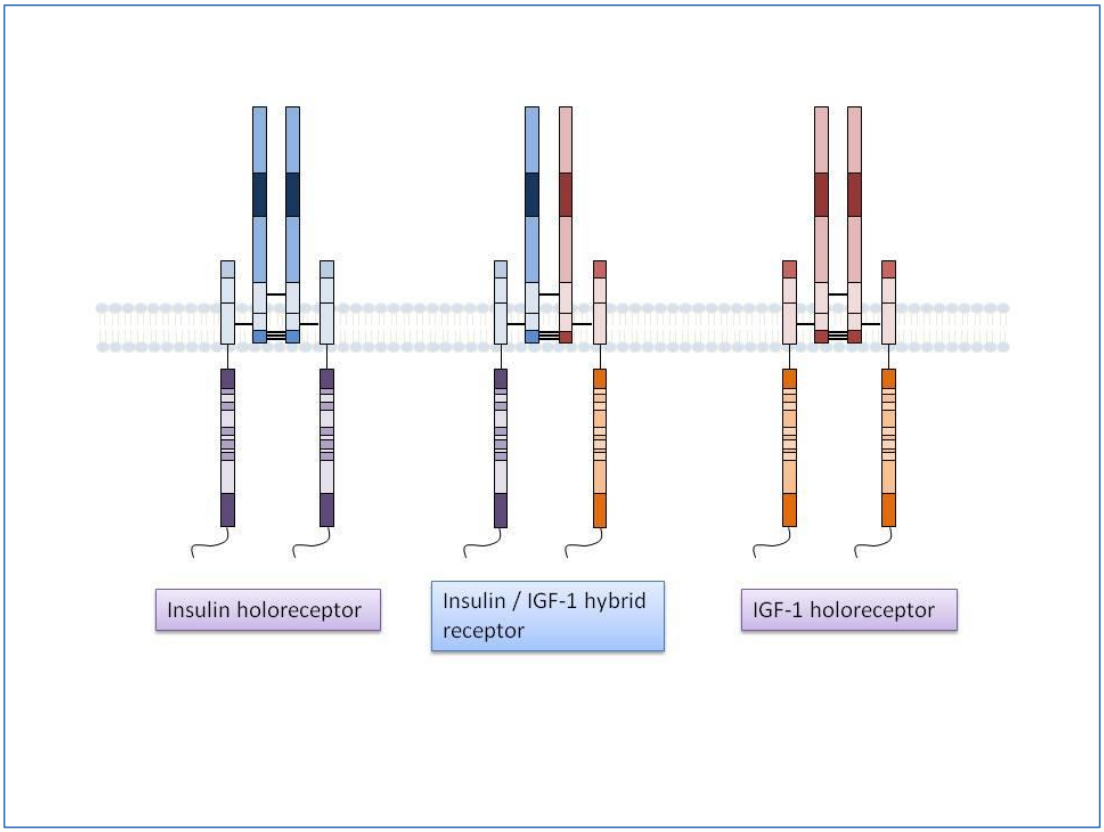

Figure 1.8-1: Hybrid and holo-receptors. This is a schematic representation of the composition of the IGF-1R, IR and hybrid receptor. The IGF-1R and IR have significant structural homology; they both are formed by the combination of 2 heterodimers, consisting of α and β subunits joined by disulphide bonds. The IGF-1R / IR hybrid receptor, as is shown consists of an IGF-1R heterodimer, joined by disulphide bonds to an IR heterodimer.

Hybrid receptors appear to be ubiquitously expressed, and in mammalian tissues a significant proportion of IGF-1 binding sites appear to be incorporated within hybrid receptors, as opposed to the IGF-1R itself. Looking at tissue homogenates, rather than specific cell types, Bailyes *et al* determined that 74% of IGF-1 binding sites in skeletal muscle were found in hybrid receptors, with similar proportions in kidney (70%), fat (68%), heart (87%), placental tissue (72%) and spleen (53%) [219]. Slightly different methodology was used by Federici *et al,* however results still suggested that in the region of a third to a half of IGF-1 binding sites were located within hybrid receptors, although this proportion varied depending on tissue type[220].

Data from HUVECs, [221], human coronary artery endothelial cells (HCAEC) [222] and human cardiac microvascular endothelial cells (HMVEC-C) [223] derived by using

immunoblotting and immunoprecipitation has yielded similar results. All of the endothelial cells examined were shown to express hybrid receptors, and in each cell type IGF-1R mRNA was expressed at a significantly higher level than IR mRNA (8 fold higher in HCAEC [222] ; 7 fold higher in freshly isolated HUVEC [221]; and 120 fold higher in HMVEC-C) [223]). In view of the fact that these cells express higher numbers of IGF-1R than IR it would seem likely that a significant numbers of IR are sequestered into the relatively insulin resistant hybrid receptors, rendering these endothelial cells relatively resistant to the effects of insulin. Indeed data supports this. Phosphorylation of Akt in human microvascular endothelial cells (HMVEC) has been shown to occur at 10^{-7}M, and at between 10^{-8} and 10^{-7}M in response to IGF-1 [224]. Taken together, this data strongly supports the view that IGF-1R outnumbers IR on endothelial cells, driving IR into hybrid receptors with the result that the vascular endothelium is a relatively insulin resistant tissue.

Intriguingly, work from our group, shows that it would appear that manipulation of IR and IGF1-R stoichiometry may not only be able to determine hybrid formation but may also be a useful way of manipulating the sensitivity of a cell to insulin.

Transgenic mice with endothelial specific over-expression of the IGF-1R (HIGFREO) have increased levels of hybrid receptors compared with wild type counterparts, coupled with endothelial insulin insensitivity (as measured by reduced insulin stimulated NO production) [210]. Studies performed on a model which crossed the IRKO mouse mice (whole body haplo-insufficiency of in the insulin receptor; which have both whole body and vascular insulin resistance and endothelial dysfunction) with an endothelial specific knockdown of the IGF-1R (ECIGFRKO) support our hypothesis that manipulation of hybrid numbers may have an effect on insulin sensitivity [209]. The resultant model demonstrated that reducing IGF-1R in IRKO mice restored insulin-mediated vasorelaxation, enhanced insulin-stimulated eNOS activation, and enhanced insulin-stimulated NO release in endothelial cells [46].

These data suggest that manipulation of IGF-1 to insulin receptor stoichiometry may be able to restore insulin sensitivity in insulin resistant states.

Interestingly, there is an association between increased hybrid receptor expression and insulin resistance [225] obesity [226] hyperinsulinaemia [227], hyperglycaemia [228] and type 2 diabetes mellitus [229, 230]. It is unclear if the increased expression of hybrids results from the changes in insulin sensitivity seen in these disease states, or indeed if

hybrid receptors are in part responsible for the altered insulin sensitivity, although treatment of hyperglycaemia in diabetic rats completely restores hybrid receptor expression to a level comparable with non-diabetic rats [228].

It appears that there may be further factors involved in the regulation of hybrid receptor expression. Exposure of VSMCs to the mineralocorticoid aldosterone resulted in a 2 fold increase in the expression of hybrid receptors and a 3 fold increase in the expression of IGF-1R [231]; an effect which was abrogated by the co-administration of the aldosterone antagonist eplerenone. Using in vivo studies, the same group showed that combined treatment with aldosterone and salt, as would be expected rendered mice hypertensive, but was also associated with blunted insulin signalling in the aorta and increased expression of hybrid and IGF-1R [231] . Importantly, treatment with the antihypertensive hydralazine (which does not directly affect the renin angiotensin system) restored normotension in these mice, but did not favourably affect hybrid receptor expression [231], suggesting that the effects seen were related specifically to aldosterone expression, rather than the effect on systemic blood pressure.

In addition to being altered in some disease states, there is evidence to suggest that hybrid receptor expression may, to a degree be developmentally related although studies are conflicting. Hybrid receptor expression appears to increase in murine mammary epithelial cells towards later pregnancy [232], but contrary to this hybrid receptor expression seems to decrease in skeletal muscle of suckling pigs with early development [233]. Clearly it is difficult to draw any firm conclusions about hybrid regulation with regards to development from these data, particularly given the disparate tissue used, but it would appear that hybrid receptor expression may well change in different tissues, during different developmental stages. There is evidence to suggest a link between reduced signal transduction via the IGF-1 axis and longevity [150, 152, 154] , although there is as yet no data looking at whether hybrids play any role in this.

1.8.1 IGF-1R, hybrid expression and cardiovascular disease

Although it seems likely that hybrid receptors play a role in modulating a cell's sensitivity to insulin, it is currently unclear if altered expression of either hybrid or IGF-1R plays a role in the development of cardiovascular disease.

In patients with the traditional risk factors for cardiovascular disease, namely type 2 diabetes, systemic insulin resistance and obesity there appears to be increased expression of hybrid receptors when compared with subjects without these risk factors [225, 226, 229, 230]; the degree of insulin sensitivity is inversely proportional with hybrid receptor expression. As has been discussed it is not entirely clear whether increased hybrid receptor expression is responsible for, or occurs as a result of altered insulin sensitivity, however studies by Federici *et al* [227, 228] would suggest that the former is more likely to be the case, particularly given that treatment of hyperglycaemia resulted in normalisation of hybrid receptor numbers. The implication of these findings is that hybrid receptor expression may play a central role in the propagation of the vicious cycle of insulin resistance culminating in the development of type 2 diabetes mellitus where altered insulin sensitivity is associated with increased hybrid receptor expression, leading to a subsequent reduction in sensitivity to insulin coupled with compensatory hyperinsulinaemia.

Human studies to date have not yet assessed endothelial expression of hybrid receptors particularly in those with diabetes, systemic insulin resistance and hyperglycaemia. However given the ubiquitous expression of hybrids, it is not unreasonable to suspect that similar changes as have been demonstrated in placental, skeletal muscle and adipose tissue factors [225, 226, 229, 230] may exist in the endothelium, and could provide a partial explanation for vascular insulin insensitivity seen in those with the metabolic syndrome.

It is unclear if correction of hyperinsulinaemia is sufficient to reduce hybrid expression in tissues. In women with polycystic ovarian syndrome (PCOS), which is associated with insulin resistance and endothelial cell dysfunction, treatment with the oral biguanide metformin, generally used as an oral hypoglycaemic agent, leads to improvement in endothelial function [234]. Interestingly this study showed that the improvement in endothelial function was achieved independent of a change in insulin sensitivity. Although the above study did not assess insulin levels, metformin has previously been shown to reduce hyperinsulinaemia in patients with PCOS [235]. It is not known if metformin has an effect on expression and distribution of hybrids, but this may be an important question for further research.

1.9 Insulin and IGF-1 resistance and endothelial dysfunction

1.9.1 The development of whole body insulin resistance

The development of insulin resistance on a whole body level is complex, and not yet entirely fully understood. Insulin resistance develops as interplay between genetic and environmental factors, and unsurprisingly many of the molecular and cellular mechanisms which have been shown to contribute to the development of whole body insulin resistance, are also involved in the development of endothelial cell insulin resistance.

In addition to the actions on the endothelial cell described above, the major targets of insulin are: skeletal muscle where, as is described above, insulin stimulates glucose transportation; adipose tissue, where the major action is the inhibition of lipolysis (the process by which triglycerides are broken down to form free fatty acids [FFA]) [236, 237]; and the liver, where insulin inhibits hepatic glucose production from the breakdown of glycogen [238]. There is little doubt that the most important (in population terms) risk factors for the development of insulin resistance are obesity, a sedentary lifestyle and aging, and in these circumstances it would appear that adipose tissue plays a major role in the initiation of insulin resistance.

Nutrient excess and subsequent weight gain leads to the expansion of adipose tissue which has the effect of increasing FFA in the circulation. In addition to this, expanded adipose tissue is prone to developing areas of micro-hypoxia and stress of the endoplasmic reticulum [239, 240]. This causes inflammation. Release of inflammatory cytokines and recruitment of macrophages leads to release of further cytokines such as interleukin-6 (IL-6) and tumour necrosis factor α (TNF-α), both of which are elevated in people with obesity related insulin resistance [241]. The inflammatory markers themselves activate the JNK, mTOR and nuclear factor κB (NFκB) signalling cascades leading to serine/threonine phosphorylation of IRS and inhibition of insulin signalling through the PI3-K / Akt cascade [242-244]. In addition to release of cytokines, hypoxic adipose tissue releases an imbalance of substances known as adipokines, some of which have the effect of enhancing insulin sensitivity; others which inhibit insulin signalling: the net effect of the adipokines released under these circumstances tends to promote insulin resistance [245].

The accumulation of proinflammatory cytokines, adipokines and activated macrophages has a paracrine effect upon adipose tissue, but also leads to the accumulation of

triglyceride in the liver [246] and adipose tissue accumulation in skeletal muscle [247]. This leads to resistance to the effects of insulin within these tissues, with the release of further FFA and cytokines to propagate the cycle. Increased FFA flux leads to an accumulation of intermediary components of lipid metabolism which active serine/ threonine kinases subsequently leading to inhibition of tyrosine phosphorylation of IRS and consequent down regulation of the PI3-K cascade [248, 249].

Interestingly nutrient excess also appears to have direct effects on the p85 regulatory subunit of PI3-K. Effective insulin signalling requires the activity of both the regulatory subunit p85 and the catalytic subunit p110 to form a heterodimer. Changes in calorie availability have been demonstrated to preferentially activate p85, but not p110 [250]. This leads to relatively less heterodimerization, and inhibition of insulin signalling. Interestingly these changes take place after a positive energy balance of only 3 days.

1.9.2 The development of endothelial cell insulin resistance

Whilst it is clearly important to consider the pathways which lead to whole body insulin resistance it is necessary to consider the pathophysiological factors which have been shown to have a specific effect on endothelial cell insulin sensitivity. As has been alluded to, there is considerable cross over between factors which lead to insulin resistance on a whole body level, and those which may promote insulin resistance and dysfunction of the endothelial cell. Although we will look at the factors of hyperglycaemia, hyperinsulinaemia and lipotoxicity separately, themes of inflammation and oxidative stress predominate.

1.9.2.1 Oxidative stress and inflammation

There is significant overlap between the ways which ROS causes or contributes towards the development of endothelial dysfunction, and the ways which ROS might contribute towards endothelial insulin insensitivity (Figure 1.9-1). There is a plethora of research examining the effects of ROS on insulin signalling in various tissues, although the exact mechanism is any one tissue is yet to be elucidated. This section will therefore focus on the general principles by which ROS might contribute towards endothelial specific insulin resistance.

ROS appears to have a negative impact towards insulin signalling, primarily by interaction between a series of mitogen activated protein kinases, particularly c-Jun N-terminal (JNK) and IκB kinase (IKK), both of which induce serine phosphorylation of IRS-1, therefore

interrupting PI3-K dependent insulin signalling. ROS has been demonstrated to inactivate the MAPK phosphatases, which would usually inactive JNK by de-phosphorylation [251]

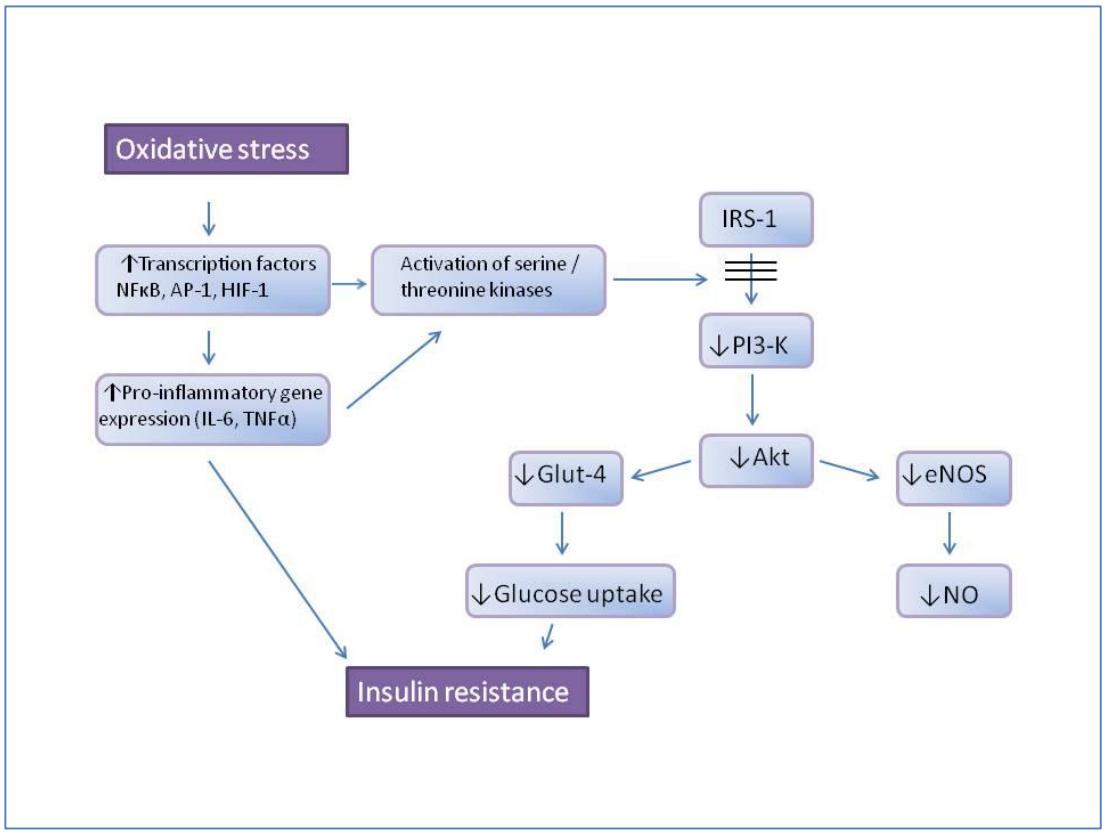

Figure 1.9-1: Oxidative stress and the development of insulin resistance. Schematic representation of the way which oxidative stress contributes to the development of insulin resistance. Enhanced oxidative stress leads to enhanced activation of serine threonine kinases which inhibit signalling through the PI3-K / Akt pathway. In addition enhanced expression of pro-inflammatory cytokines have a direct effect on the development of insulin resistance.IRS-1: insulin receptor substrate 1; PI3-K: phosphatidylinositol -3 kinase; Akt: protein kinase B; eNOS: endothelial nitric oxide synthase; NO: nitric oxide; Glut-4; glucose transporter 4; NFκB: nuclear factor kappa-light-chain enhancer of activated B cells; TNFα: tumour necrosis factor α; Il-6: interleukin 6

ROS also appears to be able to activate IKK, which forms part of the NFκB kinase signalling pathway, by causing Src dependent protein kinase D activation [252, 253], with the subsequent activation of IKK.

Following ROS induced activation of JNK or IKK, serine phosphorylation of IRS-1 occurs, leading to failure of insulin signalling transduction via PI3-K Akt pathway [199].

Although these pathways undoubtedly contribute to the development of insulin resistance, it is not clear, firstly how relevant ROS might be in the initiation of insulin resistance, and indeed the specific mechanisms by which ROS may worsen insulin resistance in the endothelium.

1.9.2.2 Hyperinsulinaemia

Hyperinsulinaemia largely occurs as part of the metabolic syndrome as a consequence of insulin resistance, with compensatory levels of insulin released from the pancreas to maintain glucose homeostasis in the face of increased tissue insulin resistance. It is somewhat artificial to therefore consider the effects of hyperinsulinaemia without factors also associated with the metabolic syndrome, particularly obesity, lipotoxicity and enhanced oxidative stress. Nevertheless, there is evidence that hyperinsulinaemia itself contributes to the development of endothelial cell insulin resistance and endothelial dysfunction.

Arcaro *et al* [254] demonstrated that in normal subjects infusion of insulin at both low and high doses (euglycaemia was maintained by the clamping technique) was associated with reduction in endothelial dependent forearm vasodilatation, an effect which was abrogated by the antioxidant vitamin C, suggesting that the effect was mediated by higher levels of ROS associated with insulin infusion.

There is good evidence to support the theory that hyperinsulinaemia may be involved in the development of pathway specific insulin resistance. The term pathway specific insulin resistance refers to states where insulin stimulated PI3-K pathway activity is reduced and insulin stimulated MAPK pathway activity is enhanced (Figure 1.9-2). In both diabetic humans and obese rats, insulin was found to stimulate MAPK activity, with reduced, or in some cases virtually abolished insulin stimulated PI3-K activity [255, 256]. In endothelial cells inhibition of the PI3-K pathway using wortmannin abolished insulin stimulated eNOS phosphorylation, but was associated with enhanced MAPK signalling [257], suggesting that in situations where PI3-K signalling is reduced, MAPK signalling is not only maintained, but possibly enhanced.

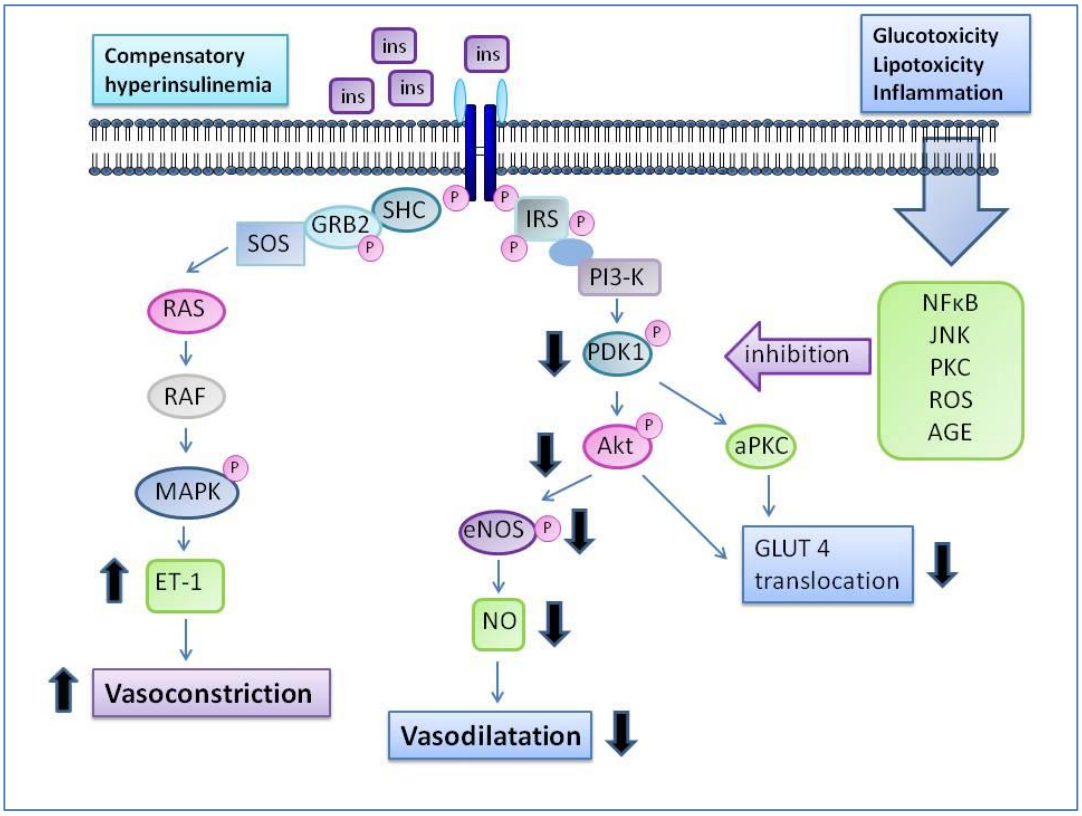

Figure 1.9-2: Pathway specific insulin resistance. Adapted from Muniyappa and Quon [258]. The combination of glucotoxicity, lipotoxicity and inflammation lead to the production of compounds which inhibit signalling through the PI3-K / Akt pathway by inhibiting tyrosine phosphorylation of IRS-1 with the effect of reduced GLUT-4 translocation and reduced insulin mediated glucose disposal. This is ultimately associated with compensatory hyperinsulinaemia and the development of "pathway specific insulin resistance" where the excess insulin is unable to activate the PI3-K pathway, and overstimulates the MAPK pathway. Ins: insulin; IRS: insulin receptor substrate; PI3-K: phosphatidylinositol-3 kinase; PDK-1: protein dependent kinase -1; Akt: protein kinase B; eNOS: endothelial nitric oxide synthase; NO: nitric oxide; GLUT-4: glucose transporter-4; aPKC: activated protein kinase C; NFκB: nuclear factor kappa-light-chain-enhancer of activated B cells; JNK: c-Jun N-terminal kinases; PKC: protein kinase C; ROS; reactive oxygen species; AGE; advanced glycosylated end products; SHC: src homology-2 domain-containing; GRB2: growth factor receptor bound protein-2; SOS: son of sevenless; RAS: Ras protein; Raf: Raf protein; MAPK: mitogen activated protein kinase; ET-1: enodthelin-1; pink circle with P: phosphorylation

In the liver and muscle of rats treated with hyperinsulinaemia Ueno and colleagues [259] observed an associated increase in serine phosphorylation of IRS1/2 (as opposed to tyrosine phosphorylation induced by normal insulin signalling) with subsequent impairment of signalling through the PI3-K pathway, and up regulation of the mTOR pathway. Taken together it would seem that this data support the theory that hyperinsulinaemia may induce pathway specific insulin resistance.

In endothelial cells taken from spontaneously hypertensive rats, insulin stimulation of the MAPK pathway leads to up regulation of ET-1 expression [260], and in endothelial cells treated with wortmannin, there is increased expression of adhesion molecules due to enhanced MAPK signalling [257].

The net effect of pathway specific insulin resistance on the endothelial cell, would therefore lead to enhanced insulin stimulation of the MAPK pathway, with the result of the formation of a pro-atherogenic environment within the vessel.

It has been discussed in detail that endothelial cells express a higher proportion of IGF-1R than IR [221-223], and that insulin at supra-physiological concentrations can autophosphorylate the IGF-1R [139, 197, 198]. In this situation hyperinsulinaemia may lead to the combined effects of enhanced MAPK activation due to pathways specific insulin resistance, and further MAPK activation caused by IGF-1R autophosphorylation.

1.9.2.3 Lipotoxicity

It is well documented that patients with the insulin resistance syndrome have an abnormal lipid profile, with elevated triglyceride and free fatty acid (FFA) levels and an unfavourable low density to high density cholesterol profile.

Although there are several cellular mechanisms behind the association between lipotoxicity and endothelial cell insulin resistance, the mechanisms seem to converge around increased production of ROS with activation of inflammatory pathways. It has been known since the early part of the millennium that treatment of endothelial cells with FFA is able to stimulate production of ROS via protein kinase C mediated activation of NADPH oxidases [261]. More recently, work on bovine aortic endothelial cells has demonstrated that the FFA palmitic acid inhibits insulin mediated tyrosine phosphorylation of IRS-1, with subsequent reduction of eNOS phosphorylation and NO production [262]. Over-expression of an inactive IKK

abolished this, showing that palmitic acid can cause endothelial insulin resistance by an IKK dependent mechanism [262].

In addition to the action on IKK, palmitic acid also up regulates phosphatase and tensin homologue (PTEN) which is a negative regulator of insulin signalling and in contrast, linoleic acid inhibits insulin stimulated, Akt mediated eNOS activation [263].

1.9.2.4 Hyperglycaemia

In the early stages of the development of whole body insulin resistance, maintenance of normoglycaemia is achieved by hyperinsulinaemia; hyperglycaemia only develops following pancreatic β cell failure. Hyperglycaemia itself has an effect on the development of endothelial cell insulin resistance [264] and it is useful to consider the postulated mechanisms for this.

As has been discussed with regards to other factors which can lead to the development of endothelial cell insulin resistance, hyperglycaemia leads to a pro-inflammatory state with increased levels of oxidative stress. In addition to causing endothelial dysfunction itself, excess production of ROS, and activation of pro-inflammatory pathways leads to activation of serine/threonine kinases with the subsequent effect of reduction in signalling through the anti-atherogenic PI3-K pathway, and enhances flux down the pro-atherogenic MAPK pathway.

In addition to causing direct inhibition of eNOS with subsequent reduced bioavailability of NO [265], hyperglycaemia has been demonstrated to induce NFκB activation in endothelial cells. Activation of NFκB and the associated upstream signalling complex inhibitor κB kinase (IKK) have been shown to lead to serine phosphorylation of IRS-1 [266] and insulin resistance in hepatocytes [267] and skeletal muscle [268]. It would seem reasonable to suspect that activation of NFκB in endothelial cells would therefore also be associated with insulin resistance, although specific evidence of this is currently lacking.

The primary way by which hyperglycaemia has an effect on endothelial dysfunction is by enhanced production of reactive oxygen species, mediated either by enhanced direct glucose oxidation; mitochondrial superoxide production; eNOS uncoupling; or enhanced production of advanced glycation end products (AGE).

1.10 Reactive oxygen species and enhanced insulin signalling

There is undoubtedly a link between ROS and the development of endothelial dysfunction; in view of this interest turned towards the potential role which antioxidants might have to play in the prevention of cardiovascular disease. Interestingly, however, several large scale trials failed to show an improvement in the risk of developing cardiovascular disease when subjects with diabetes were treated with antioxidants [269, 270]; indeed the antioxidant vitamin E has been demonstrated to be associated with an increased risk of the development of left ventricular systolic dysfunction following myocardial infarction [271]. Attention has therefore turned to the role which reactive oxygen species may have to play in the modulation of the insulin signalling pathway. Of particular importance is the role of H_2O_2.

1.10.1 The effect of hydrogen peroxide on insulin signalling

It is now appreciated that ROS play a critical role as intracellular second messengers, and are of particular importance in the insulin signalling cascade, via interaction with the protein tyrosine phosphatases (PTPs). The PTPs are a family of proteins including the phosphatase and tensin homologue (PTEN) and PTP-1B. PTEN and PTP-1B, in particular have been shown to be negative regulators of the insulin pathway. PTEN catalyses the conversion of PIP_3 to PIP_2, therefore attenuating the insulin signalling cascade[272]. Transgenic mice with knockout of PTP-1B show enhanced glucose tolerance and enhanced insulin sensitivity, in combination with reduced adiposity and resistance to weight gain [273, 274]. The activity of the PTP family is dependent on reduction of the thiol side chain on the cystine residue; H_2O_2 readily oxidises this side chain leading to progressive and eventual irreversible inactivation of PTP. See Figure 1.10-1.

3T3-L1 adipocytes have been shown to generate H_2O_2 in response to stimulation with insulin, which is associated with oxidative inactivation of PTP-1B, and enhanced insulin signalling. Administration of catalase or the NADPH oxidase inhibitor diphenyleneiodonium abolished the oxidation of PTP-1B and was associated with reduced insulin stimulated autophosphorylation of the IR [275, 276]. In H4IIEC hepatocytes low concentrations of H_2O_2 (5-10μM) were shown to enhance insulin stimulated Akt activity, and suppress PTP-1B activity; higher concentrations (25-50μM) reduced insulin stimulated Akt phosphorylation [277]; suggesting a dose-dependent effect on insulin signal propagation.

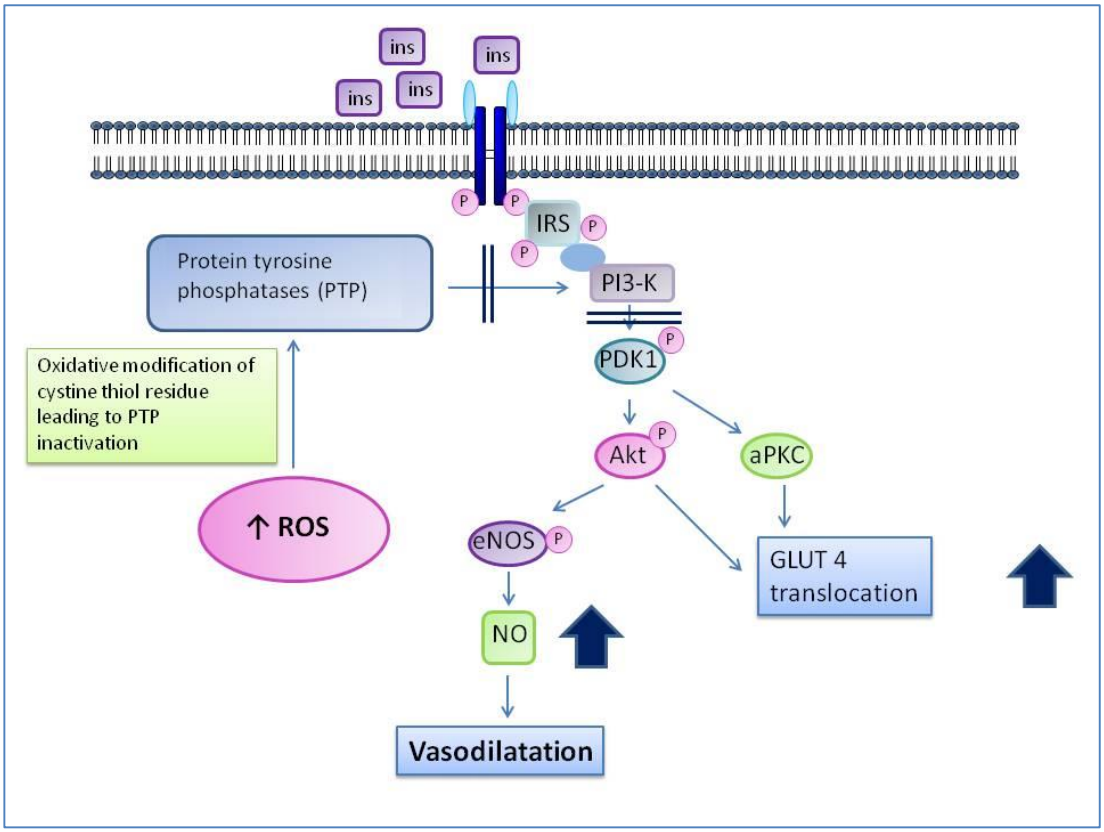

Figure 1.10-1: Reactive oxygen species and enhanced insulin signalling via interaction with PTP. Increased production of H2O2 is associated with oxidative modification of the cysteine thiol residue on protein tyrosine phosphatases, particularly PTP-1B. This renders the PTP inactive and unable to inactivate signalling via the PI3-K / Akt pathway. Although not shown in the diagram, H2O2 is also able to enhance insulin signalling by enhancing oxidation of cysteine residues on the IR itself. Ins: insulin; IRS: insulin receptor substrate; PI3-K: phosphatidylinositol – 3 kinase; PDK-1: protein dependent kinase – 1; Akt: protein kinase B; aPKC: activated protein kinase C; GLUT-4: glucose transporter 4; NO: nitric oxide; eNOS: endothelial nitric oxide synthase; ROS: reactive oxygen species; PTP: protein tyrosine phosphate; pink circle with P: phosphorylation

In addition to the effect on modification of PTPs, H_2O_2 is, at high concentrations, recognised to be to be associated with an insulin-like action. Administration of H_2O_2 to rat adipocytes is associated with increased IR phosphorylation [278], an effect independent of insulin, strongly suggesting that the insulin-mimetic effect of H_2O_2 is mediated through the insulin signalling pathway. Indeed administration of H_2O_2 has been demonstrated to be associated with the same downstream effects on cellular metabolic action as insulin itself [279]. This of course as discussed above could be partly due to the increased oxidation of the thiol side chain of the PTP with subsequent propagation of the insulin signalling cascade, but although this would explain the cellular effect of H_2O_2 it does not explain the increased

phosphorylation of the IR as noted by Hayes *et al* [278]. Interestingly, although stimulation with H_2O_2 was associated with increased IR phosphorylation, this did not appear to be as a direct result of H_2O_2 itself. Subsequent work has demonstrated that H_2O_2, acts to oxidase cystine residues within the kinase domain of the IRβ, and this in turn allows spontaneous autophosphorylation within the activation loop of the IR [280]. This is termed "priming" of the IR.

Interestingly, work by the same group has shown that low doses of H_2O_2 have the opposite effect in the IGF-1R: in T-47D breast cancer cells the administration of low levels of H_2O_2 is associated with inhibition of the IGF-1R receptor kinase [281]. Schmitt *et al* who demonstrated this, hypothesised that this difference might arise due to differences in the position of cystine residues in the tyrosine kinase domain between the IR and the IGF-1R. It is unknown what effect low doses of H_2O_2 might have on the IR/IGF-1R hybrid receptor. Cross talk between the two halves of the receptor is critical for receptor functioning; low dose H_2O_2 would possibly have opposite effects on the 2 halves of the receptor, although this is postulation.

In addition to cellular studies, the principle that increased level of ROS may enhance insulin signalling has been demonstrated on a whole body level. The enzyme glutathione peroxidise 1 (Gpx1) eliminates physiological ROS; transgenic mice lacking Gpx1 are resistant to high fat diet induced insulin resistance and have enhanced insulin stimulated Akt phosphorylation coupled with increased glucose uptake in muscle [282]. This effect was abrogated by administration of the anti-oxidant N-acetyl cystine. Furthermore on a cellular level Gpx1 -/- fibroblasts showed enhanced insulin sensitivity, and oxidation of PTEN.

Taken together this data suggests that insulin stimulated H_2O_2 production is associated with inactivation of PTP-1B and subsequently enhanced transduction of the insulin signalling cascade.

1.10.2 Vascular effects of hydrogen peroxide

In addition to the beneficial effect of H_2O_2 on modulating insulin signalling, there are emerging data to suggest that Nox4 derived H_2O_2 may play a role in modulating blood vessel tone. Mice with endothelial specific Nox4 over-expression have reduced systemic blood pressure and enhanced vasodilatation in response to acetylcholine than wt. counterparts. This was in association with marked increases in H_2O_2, but was independent

of eNOS [82]. The enhanced vasodilatation seen in the Nox4 over-expressing mice was, however blocked by treatment with high levels of potassium and K_{Ca} channel inhibitors, strongly suggesting that H_2O_2 was acting as an endothelial derived hyperpolarizing factor (EDHF).

By acting as an EDHF H_2O_2 has been shown to be important in affecting blood vessel tone in an NO independent manner. Recent evidence suggests that endothelial derived H_2O_2 induces vasodilatation by diffusing to the smooth muscle cells and acting directly on Ca^{2+} activated K^+ channels [283] rather than inducing another substance to cause vasodilatation. EDHF has been shown to be a contributor to vasodilatation in many vessels, and appears to be of particular importance in the micro-vasculature [283-285] . In contrast to endothelial dependent vasodilatation, the vasodilator responses to EDHF are relatively preserved in patients with atherosclerosis, and therefore H_2O_2 may be of significance in maintaining vascular tone in these patients [285].

Further supporting the notion that Nox4 derived H_2O_2 may have a vascular-protective role: inducible Nox4 deficiency is associated with endothelial dysfunction in the aorta, reduced angiogenesis and attenuated ability of pulmonary endothelial cells to form tubes [84]; over-expression of Nox4 is associated with improved angiogenesis and resistance to hypoxia [84].

1.11 The link between endothelial insulin sensitivity and glucose homeostasis

Insulin delivery to the interstitium of skeletal muscle, the principle site of insulin mediated glucose disposal, is of critical importance in determining the rate of glucose disposal by skeletal muscle. There is now good evidence to suggest that insulin is able to regulate its own passage to the muscle interstitium via actions on the vasculature, perhaps in 3 distinct ways: by an action on whole limb blood flow; by increased capillary recruitment; or by enhanced passage across the endothelium itself.

The next section will discuss the evidence to support this theory, particularly with regards to insulin resistance, before considering the potential role of endothelial cell insulin sensitivity in determining glucose homeostasis.

It has been recognised since the mid-1980s that there is a difference in the time period between which insulin enters the plasma, and lymphatic fluid (known to correspond closely with whole body glucose mediated insulin disposal), with a corresponding disparity between the time taken for insulin to suppress hepatic gluconeogenesis and the onset of insulin mediated glucose disposal. In accordance with this observation, tyrosine kinase activation of the IR swiftly follows increases in interstitial insulin levels, with a time lag between increased plasma insulin and receptor activation [286-288]. Taken together this suggests that insulin delivery to skeletal muscle, via the interstitium is of importance in determining insulin mediated glucose disposal, and hence is likely to play a role in influencing whole body insulin sensitivity.

In the early 1990s, Baron and colleagues [289-291] suggested that the hemodynamic effect of insulin (i.e. vasodilatation initiated by insulin stimulated nitric oxide production) was associated with an increase in blood flow to skeletal muscle, an effect that was blunted in conditions associated with insulin resistance. Exogenous insulin infusion was shown to have the effect of increasing whole leg blood flow and associated glucose uptake, an effect that was abolished with the concomitant infusion of the NOS inhibitor L-NMMA. Interestingly in obese and diabetic subjects, there was markedly impaired insulin stimulated increases in skeletal muscle blood flow, with corresponding reduction in glucose uptake. Whether the effect of insulin on whole limb blood flow has a physiological role is unclear; it appears that although physiological levels of insulin can mediate an increase in whole limb blood flow, it occurs relatively slowly, which is contrary to the rapid onset of insulin mediated glucose

disposal seen in healthy humans. Moreover, there is no convincing evidence that the impaired insulin mediated vasodilatation and associated blood flow seen in insulin resistant individuals contributes to derangements in whole body glucose homeostasis.

1.11.1.1 Effect of insulin on micro-vascular perfusion

Although the effect of insulin on increasing whole limb blood flow, with a resultant increase in insulin mediated glucose disposal may not be important physiologically, there is now evidence that insulin plays a role in increasing microvasculature perfusion to skeletal muscle. This has the effect of increasing the endothelial surface available for insulin delivery. Using contrast enhanced ultrasound Barrett and colleagues demonstrated that insulin stimulates rapid microvascular recruitment via eNOS dependent mechanisms [292, 293], a process which was blocked by inhibition of NOS. Furthermore, the ability of insulin to enhance microperfusion to skeletal muscle is blunted in subjects with diabetes [294] and obesity [295].

Interestingly, in humans, hyperinsulinaemia has been shown to cause rapid increases in skeletal muscle microvascular volume, although muscle insulin clearance decreased with increased hyperinsulinaemia, suggesting the presence of a saturable process allowing the transportation of insulin across the endothelium [296].

1.11.1.2 Trans-endothelial insulin transportation

The endothelium is not homogenous throughout the body; the structure varies across different tissues. The integrity of the blood brain barrier is maintained by an endothelial layer with very few junctions between cells, accounting for the fact that few macromolecules traverse the blood brain barrier. Conversely the liver has a discontinuous endothelial layer, which allows relatively easy passage to macromolecules such as insulin. Indeed it is likely that the discontinuity of the hepatic endothelium, coupled with the large blood flow which accounts for the rapid clearance of insulin by the liver, and the rapid suppression of hepatic gluconeogenesis which follows. Skeletal muscle endothelium is continuous, but unlike the endothelium of the blood brain barrier has multiple caveolae and junctional structures.

There are several theories as to how macromolecules might traverse the endothelium:

1. In discontinuous or fenestrated endothelium, transit might occur between cellular junctions, although this would seem unlikely in skeletal muscle where the endothelial junctions are tight.
2. The process could involve random inclusion of macromolecules into caveolae, although if the macromolecule is not abundant then this event would be infrequent.
3. Binding of a ligand to a receptor could lead to receptor-ligand internalisation, with diffusion of ligand through the endothelial cell and release to the interstitium.
4. Localisation of receptors within caveolae to "trap" the macromolecule efficiently.

As will now be discussed, it appears that for insulin, the 4th theory is the most likely, and that furthermore not only is the IR involved in the capture of insulin, IR activation stimulates transendothelial insulin transportation.

The process of transendothelial transportation of macromolecules was suggested by studies which demonstrated the presence of radio-labelled albumin in caveolae within endothelial cells rather than in the inter-cellular space [297]. This effect was abrogated in mice with knockout of caveloin-1 [298] (a critical protein involved in the formation and integrity of caveolae).

In the 1980s King and Johnson [299] observed that radio-labelled insulin moved across the endothelium in a process which was blocked by both antibodies to the IR, and higher concentrations of insulin itself, suggesting a saturable and receptor mediated process. Fluorescent tagging of insulin allowed Barrett and colleagues [300] to localise tagged insulin within the endothelial cells of skeletal muscle following an insulin infusion; intriguingly there was a distinct lack of stained insulin seen to enter the muscle interstitium via the junctions between endothelial cells. Immunohistological staining demonstrated that IR, IGF-1R and caveloin-1 were also found in the muscle cells, and that there was significant co-localisation between the fluorescently tagged insulin and the IR or IGF-1R. To a lesser degree there was also some relationship between the fluorescently tagged insulin, the IR or IGF-1R and caveolin-1. Co-administration of the fluorescently tagged insulin with either supraphysiological doses of unlabelled insulin, IGF-1 or an antibody to the IGF-1R inhibited transendothelial transportation of insulin. Taken together, this data seem to give credence

to the theory that insulin enters the muscle interstitium via trans-endothelial transportation, a process which involves caveolae and localisation with either the IR or the IGF-1R. It is perhaps unsurprising that the IGF-1R might be implicated in transendothelial transportation of insulin, given the structural homology between the IGF-1R and the IR, and the previously discussed evidence that at elevated levels of insulin, both the IR and the IGF-1R are phosphorylated [198].

Although there appears to be a role for the IGF-1R in modulating transendothelial insulin transportation at supraphysiological doses, at physiological levels it appears that only the IR itself is implicated in transendothelial transportation of insulin [301]. Whether hybrid receptors have a role to play is unknown, but it is reasonable to speculate that sequestration of IR into hybrid receptors may also have a role in modulating transendothelial insulin transportation.

1.11.1.3 Does insulin sensitivity regulate transendothelial insulin transportation?

Clearly, whether the process of transendothelial transportation is an active or a passive process is of interest when considering insulin sensitivity. Using cultured bovine aortic endothelial cells, Barrett and colleagues demonstrated that an intact insulin signalling pathway is critical to the uptake of insulin into endothelial cells [302]. The process of transendothelial transportation was inhibited by the PI3-K inhibitor wortmannin; the MAPK inhibitor PD 98059 and the proinflammatory cytokine TNF-α. Intriguingly, inhibition of the protein tyrosine phosphatase PTP-1B enhanced insulin signalling.

There appears to be good evidence to support the theory that insulin delivery to the muscle interstitium plays a major rate limiting step in insulin mediated glucose disposal; that insulin enhances microvascular recruitment; and that delivery to the muscle interstitium is via transendothelial transportation, a process which requires intact insulin signalling. It is perhaps surprising then, that a mouse with endothelial specific knockout of the IR (VENIRKO) was reported to have normal whole body glucose homeostasis under normal dietary conditions [303], albeit with marked endothelial insulin resistance. Contrary to this the transgenic endothelial specific IRS-2 knockdown mouse, was associated with impaired insulin signalling, impaired insulin induced microvascular recruitment, reduced interstitial insulin concentrations and a reduction in glucose uptake by skeletal muscle [304] . Restoration of the insulin signalling cascade in endothelial cells from these mice reversed this phenotype.

It appears that interference to the insulin signalling cascade at various points (inhibition of PI3-K and MAPK inhibition) plays a role in diminishing transendothelial insulin transportation [302]; whether interruption to this signalling cascade by reactive oxygen species would have the same effect is currently unknown.

1.12 Summary

In spite of a significant body of research, patient with diabetes continue to have a significant cardiovascular morbidity and mortality burden, and have failed to benefit from advances in treatment for cardiovascular disease in the same way as insulin sensitive individuals [85]. It is now appreciated that insulin resistance precedes the development of overt diabetes and is itself a risk factor for developing endothelial dysfunction, the precursor of atherosclerosis [92]. Further study has shown that insulin signalling lays at the crossroads of vascular and metabolic homeostasis with insulin playing a significant role in modulating not only glucose homeostasis, but vascular tone via pathways dependent on PI3-K and Akt. Importantly, various animal models (Table 4) have demonstrated that adaptation of these pathways in various tissues can have an effect on tissue specific, and whole body insulin sensitivity.

The IGF-1R shares significant structural and functional homology with the IR, and also plays a role in glucose and vascular homeostasis. Mice with muscle specific IR knockout (dominant negative IR) show only mild metabolic disorder and moderate insulin resistance [305], whereas mice with functional inactivation of the IGF-1R targeted specifically to skeletal muscle, develop severe insulin resistance and Type 2 diabetes at an early age [306]. This finding illustrates that manipulation of the IGF-1R itself may be a more profound way of manipulating insulin sensitivity, an effect which most likely relates to the formation of IGF-1R/IR hybrid receptors. The intriguing relationship between the IGF-1R / IR and the effect on vascular and metabolic function merits further study.

Mouse Type	Phenotype	Glucose handling	Endothelial function
IR (-/-)	Neonatal death from ketoacidosis [307]		
IGF-1R (-/-)	Neonatal death from respiratory failure. 45% of normal size [308]		
IR (-/+) "IRKO" mouse (whole body)	Hypertensive	Comparable baseline blood glucose, FFA and triglyceride level. Insulin levels higher in IRKO in response to glucose load.	Progressive endothelial dysfunction; reduced basal NO production; reduced insulin stimulated eNOS phosphorylation; increased endothelial derived superoxide production [309]
Muscle specific insulin receptor knockout. "MIRKO" mouse	Elevated fat mass, elevated serum triglycerides,	Normal blood glucose, normal serum insulin, normal glucose tolerance test [305]	Not examined
Vascular endothelium specific IR knockout. "VENIRKO" mouse	Fertile, undistinguishable from litter mates.	Glucose homeostasis comparable with wild type mice.	Endothelial function not specifically studied but noted reduced eNOS and Endothelin-1 levels. [303]
Dominant mutant human IR specific to endothelium. "ESMIRO" mouse	Normotensive	Preserved glucose homeostasis.	Blunted aortic vasorelaxation to ACh. Blunted insulin stimulated eNOS phosphorylation. Increased superoxide production. [195]
Homozygous mutant human IGF-1R specific to skeletal muscle. "MKR" mice	Modest growth retardation	Reduction in insulin and IGF-1 mediated glucose uptake into skeletal muscle. Whole body insulin resistance and development of type 2 diabetes.	Not studied [306]
Hemizygous knockout of IGF-1R (+/-). "IGF1RKO"	Reduced numbers of hybrid receptors compared with wild type	Impaired glucose tolerance. Increased insulin sensitivity.	Increased basal NO production. [209]
Endothelial specific hemizygous knockout of IGF-1R (+/-) "ECIGF1RKO" mice	Reduced numbers of hybrid receptors compared with wild type	Normal glucose handling	Enhanced basal NO production. [209]
IRKO x ECIGF1RKO		Normal glucose handling	Restoration of vascular sensitivity to insulin when compared with IRKO mice (which were resistant to vascular effects of insulin) [209]
Over-expression of human IGF-1R specific to vascular endothelium "HIGFREO"		Normal glucose handling	Reduced basal NO production. Reduced insulin stimulated eNOS phosphorylation. [210]
Endothelial IRS-2 deletion		Reduced glucose uptake by skeletal muscle	Reduced insulin induced capillary recruitment [304]

Table 4: Summary of animal models examining effect of manipulation of IR and IGF-1R on various tissues.

Chapter 2: Hypothesis and Aims

2 Hypothesis and Aims

As has been discussed, it has been established by our group that manipulation of the stoichiometry of the IGF-1R and IR on the vascular endothelium plays a role in determining endothelial insulin sensitivity [209, 210]. Increasing the numbers of IGF-1R on the vascular endothelium leads to increased IGF-1R / IR hybrid expression on the vascular endothelium with subsequent reduction in endothelial insulin sensitivity: reduction of IGF-1R on the vascular endothelium results in reduction in the expression of hybrid receptors with associated enhanced endothelial insulin sensitivity.

The importance of the IGF-1R in modulating insulin sensitivity, and endothelial insulin sensitivity in particular, via the effect on hybrid receptors has been established, and presents an intriguing target for therapeutics. In view of the wide range of effects of the IGF-1R it would be impossible to knockout the IGF-1R as a way of offering some therapeutic benefit in humans, however interruption of receptor signalling by the use of exogenous compounds, may be possible, and it is therefore necessary to consider how the presence of a non-functioning IGF-1R might affect insulin sensitivity and endothelial function.

In particular several observations from previous studies formed the basis of this work:

1. The formation of IGF-1R/IR hybrids is of critical importance in modulating the sensitivity of a tissue to insulin.
2. The IGF-1R can be rendered inactive and unable to become autophosphorylated by substitution of a single base mutation at the ATP binding site, lysine K1003 [310-312].
3. Both halves of the IGF-1R or IGF-1R / IR hybrid need to be functional in order for the receptor to be able to active [215].

I therefore generated the following hypothesis: the presence of a non-functioning IGF-1R expressed solely on the vascular endothelium will be associated with reduction in endothelial insulin sensitivity, and may have a subsequent effect on endothelial function. In keeping with other previously published results examining the effect of changing IGF-1R or IR function solely on the vascular endothelium [195, 209, 303], I also hypothesise that this modification of IGF-1R function on the vascular endothelium will have no effect on whole body insulin sensitivity. I attempted to test this hypothesis by conducting a series of investigations designed to answer the following subjects:

1. Does the incorporation of a non-functioning IGF-1 receptor on the vascular endothelium produce a viable mouse – that is to say, are the mice alive, healthy and are they fertile?
2. Does the proposed method of incorporating a non-functioning IGF-1R onto the endothelium produce what is expected – i.e. is expression of the non-functioning IGF-1R expressed solely on the vascular endothelium?
3. Does the presence of a non-functioning IGF-1R expressed on the vascular endothelium have any effects on whole body glucose homeostasis or insulin and IGF-1 sensitivity? In addition to this, is there any evidence that other aspects of the metabolic phenotype are affected in MIGFREO mice?
4. Does the presence of a non-functioning IGF-1R expressed on the vascular endothelium have any effect on endothelial function or endothelial insulin sensitivity?
5. Depending on the results identified – are we able to demonstrate a potential mechanism? In particular, given the recent evidence that hydrogen peroxide is able to potentiate insulin signalling, is there any evidence that hydrogen peroxide levels, or other reactive oxygen species are altered in MIGFREO mice?

Chapter 3: Materials

3 Materials

General chemicals

• NaOH	Sigma-Aldrich®
• EDTA	Sigma-Aldrich®
• Tris HCl	Fisher Scientific
• Tris Base	Fisher Scientific
• Glacial Acetic Acid	Fisher Scientific
• Ethanol	Fisher Scientific
• Methanol	Fisher Scientific
• NaCl	Fisher Scientific
• Tween ® 20	Sigma-Aldrich®
• KCl	Fisher Scientific
• KH_2PO_4	Fisher Scientific
• $NaHCO_3$	Fisher Scientific
• $MgSO_4.7H_2O$	VWR®
• Glucose	Sigma-Aldrich®
• $CaCl_2$	Fischer Scientific
• Glycerol	Sigma-Aldrich®
• Sodium dodecyl sulphate	Sigma-Aldrich®

General Lab supplies

• Corning® Costar® Microcentrifuge tubes	Sigma-Aldrich®
• SafeSeal microtube	Sarstedt AG & Co
• PIPETMAN® diamond tips	Gilson®
• PIPETMAN® pipette	Gilson®
• MiniSpin® centrifuge	Eppendorf
• 5702R Centrifuge	Eppendorf
• Centrifuge MR 1822	Jouan
• UC152 Heat-Stir	Stuart®
• Dri-Block® Tube heater	TECHNE
• Non-skirted 96 well PCR plate	Thermo Scientific
• 8 domed cap strips for PCR plate	Thermo Scientific
• 96 well clear microplate	Greiner bio-one

- Micro-amp® optical adhesive film — Applied Biosystems®
- Corning® centrifuge tubes — Sigma-Aldrich®
- CELLSTAR® centrifuge tubes — Greiner bio-one
- Corning® Costar® Strippette® — Sigma-Aldrich®
- Fisherbrand™ motorized pipet fillers — Fisher Scientific
- SpectraMax® 190 microplate reader — Molecular Devices
- Dynex® MRX TC microplate reader — Dynex Technologies
- PowerPac™ 3000 — Bio-Rad
- Needles — Terumo®
- Syringes — BD Biosciences
- SA8 vortex mixer — Stuart®
- SRT9 analogue tube roller — Stuart®

Genotyping

- PTC-200 Peltier Thermal Cycler — MJ Research
- AmpliTaq® DNA polymerase with buffer II — Applied Biosystems®
- dNTP — Invitrogen®
- Agarose Molecular Grade — Bioline
- Ethidium bromide — Sigma-Aldrich®
- Horizontal Gel Tank — Anachem Ltd.
- Multiimage light cabinet — Alpha Innotech
- Chemi-imager 4400 low light imaging system — Alpha Innotech
- GeneRuler™ 100bp DNA ladder — Applied Biosystems®

Quantitative PCR

- TissueLyser — Qiagen®
- 6mm stainless steel cone balls — Retsch®
- TRIzol® — Sigma-Aldrich®
- Chloroform — Sigma-Aldrich®
- Isopropanol — Sigma-Aldrich®
- RNAase free H_2O — BDH Biochemical
- NanoDrop® ND 1000 Spectrophotometer — Thermo-Scientific®
- ND-1000 v3.1 software — Thermo-Scientific®
- High capacity cDNA reverse transcription kit — Applied Biosystems®

- 96 well optical reaction plate with barcode — Applied Biosystems®
- Power Sybr® green PCR mastermix — Applied Biosystems®
- 7900 real time PCR system — Applied Biosystems®
- SDS v2.2 software — Applied Biosystems®

Pulmonary Endothelial Cell isolation and culture

- Collagenase — Wothington Biomedical
- MACSmix™ tube rotator — Miltenyi Biotech
- Gibco® Dulbecco's phosphate buffered saline — Invitrogen®
- MACS® CD146 (LSEC) microbeads — Miltenyi Biotech
- OctoMACS® manual separator — Miltenyi Biotech
- MACS® MS cell separation columns — Miltenyi Biotech
- Endothelial cell growth medium MV2 — PromoCell
- Fetal Bovine Serum — Biosera
- Fibronectin coated 6 well plate — BD Biosciences
- Bovine serum albumin — Sigma-Aldrich®
- Gibco ®Trypsin — Invitrogen®
- Penicillin / streptomycin / amphotericin — Invitrogen®

Western blotting

- Phosphatase inhibitors 2 & 3 — Sigma-Aldrich®
- Human IGF-1 Receptor Grade — Gro-Pep
- Insulin solution, human — Sigma -Aldrich®
- Pierce® BCA protein assay kit — Thermo Scientific
- NuPage® Sample Reducing Agent — Invitrogen®
- NuPage® LDS Sample Buffer — Invitrogen®
- NuPage® 4-12% Bis-Tris Gel — Invitrogen®
- Precision Plus Protein™ Western Standard — Bio-Rad
- Novex Mini-Cell gel tank — Invitrogen®
- NuPage® MES SDS Running Buffer — Invitrogen®
- Mini Trans-Blot® Cell — Bio-Rad
- Immobilon®-P transfer membrane — Millpore
- Marvel Skimmed milk powder — Premier Brands Ltd.
- Precision Plus Protein™ Streptactin HRP conjugate — Bio-Rad

- β Actin mouse monoclonal IgG — Santa Cruz Biotechnology
- Purified mouse anti-eNOS — BD Biosciences
- Purified mouse anti-eNOS (pS1177) — BD Biosciences
- Akt monoclonal rabbit Ab — Cell Signalling Technology®
- Akt monoclonal rabbit Ab (pS473) — Cell Signalling Technology®
- IGF-1Rβ rabbit polyclonal IgG — Santa Cruz Biotechnology
- Polyclonal rabbit anti mouse immunoglobulins / HRP — Dako
- Polyclonal goat anti rabbit immunoglobulins / HRP — Dako
- Immobilon® Western Chemiluminescent HRP Substrate — Millipore
- Image Station 2000R — Kodak
- Kodak 1D image analysis software — Kodak
- Restore™ PLUS western blot stripping buffer — Thermo Scientific

Fat sample processing

- BX41 microscope — Olympus
- Qicam Imaging Fast 1394 digital camera — QImaging®
- Image Pro-Plus 7.0 software — MediaCybernetics®
- Semi-enclosed Benchtop Tissue Processor Leica TP1020 — Leica Biosystems
- TES99 tissue embedding system — Medite Medizintechnik
- Eosin Y solution aqueous HT1102128 — Sigma-Aldrich®
- Harris Haematoxylin solution modified, HHS32-1L — Sigma-Aldrich®

Tolerance tests

- Accu-chek® Aviva Plus test strips — Roche Diagnostics
- Accu-chek® Aviva Plus Glucometer — Roche Diagnostics
- Human IGF-1 Receptor Grade — Gro-Pep
- Actrapid® insulin — Novo-Dordisk®

Blood Sampling and assessment of plasma components

- Microvette® CB 300 K2E Di-Kallum EDTA tubes — Sarstedt AG & Co
- Ultra Sensitive Mouse Insulin ELISA kit — Crystal Chem
- Mouse IGF-1 High Sensitivity ELISA — IDS
- Mouse Adiponectin ELISA kit — Millipore
- Mouse Leptin ELISA kit — Millipore

- Free Fatty Acid Quantification Kit — abcam®
- Triglyceride Quantification Kit — abcam®

Blood pressure measurement

- CODA™ Tail Cuff Blood Pressure System — Kent Scientific, Torrington

Organ bath

- 8 chamber organ bath system — Panlab
- LabChart Pro Software — Panlab
- Acetylcholine — Sigma-Aldrich®
- Phenylephrine — Sigma-Aldrich®
- Sodium Nitroprusside — Sigma-Aldrich®
- L-NMMA — Merck Millipore
- Human IGF-1 Receptor Grade — Gro-Pep
- Actrapid® insulin — Novo-Dordisk®
- Catalase from bovine liver — Sigma-Aldrich®

L-citrulline assay

- ^{14}C-arginine — Quotient Bioresearch
- HEPES Sodium salt — Sigma-Aldrich®
- L-arginine — Sigma-Aldrich®
- Savant Speed Vac® SPD111V — Thermo Scientific
- Dowex resin — Sigma-Aldrich®
- Scintillation cocktail — Quotient Bioresearch

H_2O_2 production

- Amplex® Red Hydrogen Peroxide/Peroxidase Assay Kit — Invitrogen™
- N-acetyl-cysteine — Sigma-Aldrich®

Chapter 4: Generation of Mouse and Validation of Model

4 Generation of Mouse and Validation of model

4.1 Introduction

Work by our group has demonstrated that the IGF-1R plays a significant role in regulating endothelial insulin sensitivity, and I have therefore attempted to expand this knowledge by assessing the impact of introducing a non-functional IGF-1R on the vascular endothelium.

Given the complexity of the IGF-1R there are several functional sites which are susceptible to mutation, particularly the ATP binding site, IRS binding site, the activation loop within the kinase domain and the C-terminal domain. Although these are all possible sites which would modulate IGF-1R function it was felt necessary to ensure that we used a mutation which would render the IGF-1R inactive. Sperandio *et al* [312] demonstrated that a single base mutation to arginine (K1003R) at the ATP binding site lysine K1003 rendered the IGF-1R unable to be autophosphorylated, and hence was functionally inactive. Importantly it is known that both halves of the IGF-1R or IGF-1R/IR hybrid need to be functional to allow for signal transduction via the insulin or IGF-1 signalling cascade [215].

Work by Fernandez *et al* [306] used mice with a muscle specific functional inactivation of the IGF-1R using the K1003R mutation. Muscle specific expression of the mutant human IGF-1R was associated with the formation of non-functioning hybrid receptors between the mutant, non-functioning human IGF-1R and the normally functioning mouse IGF-1 and IRs. Expression of the mutant IGF-1R in muscle was associated with a marked reduction in insulin and IGF-1 induced tyrosine phosphorylation of IGF-1R and IRS-1. This was also accompanied by striking reduction in insulin and IGF-1 stimulated glucose uptake in skeletal muscle, insulin resistance and the development of overt diabetes at an early age.

The most well validated method of allowing a gene to be incorporated specifically to the vascular endothelium is by using the Tie2 promoter. *In vivo*, Tie2 is a tyrosine kinase receptor, specific to the vascular endothelium which plays a role in vascular remodelling. Korhonen *et al* [313] first suggested that using the Tie2 promoter would be able to restrict expression of a gene specifically on the vascular endothelium; this has subsequently been validated and the Tie2 has been shown to allow an exogenous mutant gene to be inserted and expressed specifically by vascular endothelial cells in mice through embryogenesis and into adulthood [314].

In view of this evidence we sought to create a transgenic mouse with expression of a mutant non-functioning human IGF-1R with the K1003R mutation, limited to the vascular

endothelium under control of the Tie2 promoter, the MIGFREO mouse (mutant human IGF-1R endothelial over-expression).

I will discuss how the mouse was generated, and the way in which I sought to validate the incorporation of the transgene into the host genome, and demonstrate the endothelial specificity of the transgene.

4.2 Methods

The generation of the transgenic blastocyst was performed within the university by Dr Simon Futers (see chapter 4.2.1.1), for which I am extremely grateful and the transgenic mouse was generated in collaboration with GenOway (Lyon, France).

4.2.1 Generation of transgenic mouse

The MIGRFEO mouse expresses human IGF-1R which has a mutation at the ATP binding site, lysine K1003 (hIGF-1R K1003, hereafter referred to K1003R). An IGF-1R with this particular mutation cannot be autophosphorylated resulting in inactivation of the subsequent cascade of IGF-1 initiated signal transduction [310-312]. It has been previously demonstrated that both halves of the IGF-1 receptor need to be functional in order for the receptor to be able to active [215].

4.2.1.1 Site directed mutagenesis

Site- directed mutagenesis was performed on the Tie2 IGF1R construct (pTie2IGF1R) using Qiagen Quickchange II. The two site-directed mutagenesis primers were 5'-AAACCAGAGTGGCCATTAGAACAGTGAACGAGGC-3' and 5'-GCCTCGTTCACTGTTCTAATGGCCACTCTGGTTT-3'.

These primers change the second A to a G to covert lysine 1130 to arginine.

A positive clone was isolated and checked for the presence of the IGF1R sequence by restriction digest. Initial check for the presence of the mutation was demonstrated by the loss of an Mse I restriction site.

The mutation was confirmed by sequencing using an ABI 310 Genetic Analyzer with ABI BigDye Terminator v3.1 cycle sequencing kit.

As the site-directed mutagenesis process can induce other mutations, a small region around the mutation site was transferred by restriction digest and ligated into the original pTie2IGF1R construct. The whole of the IGF1R insert was the checked by DNA sequencing prior to sending to GenOway.

4.2.1.2 Formation of transgenic blastocyst

The transgenic mouse was produced and developed by GenOway in response to a specific request to generate mice expressing the type 1 human IGF-1 receptor with a mutation at the ATP binding site under the control of the Tie-2 promoter.

The transgene composed of the *Tie2* promoter and the K1003R cDNA was then incorporated into a "transgenic cassette" with the K1003R / *Tie2* construct being inserted at the hypoxanthine phosphoribosyltransferase (HPRT) locus to form a "Quick Knock-in™" targeting vector. This vector was then incorporated into specific E14 embryonic stem cells by electroporation (Figure 4.2-1).

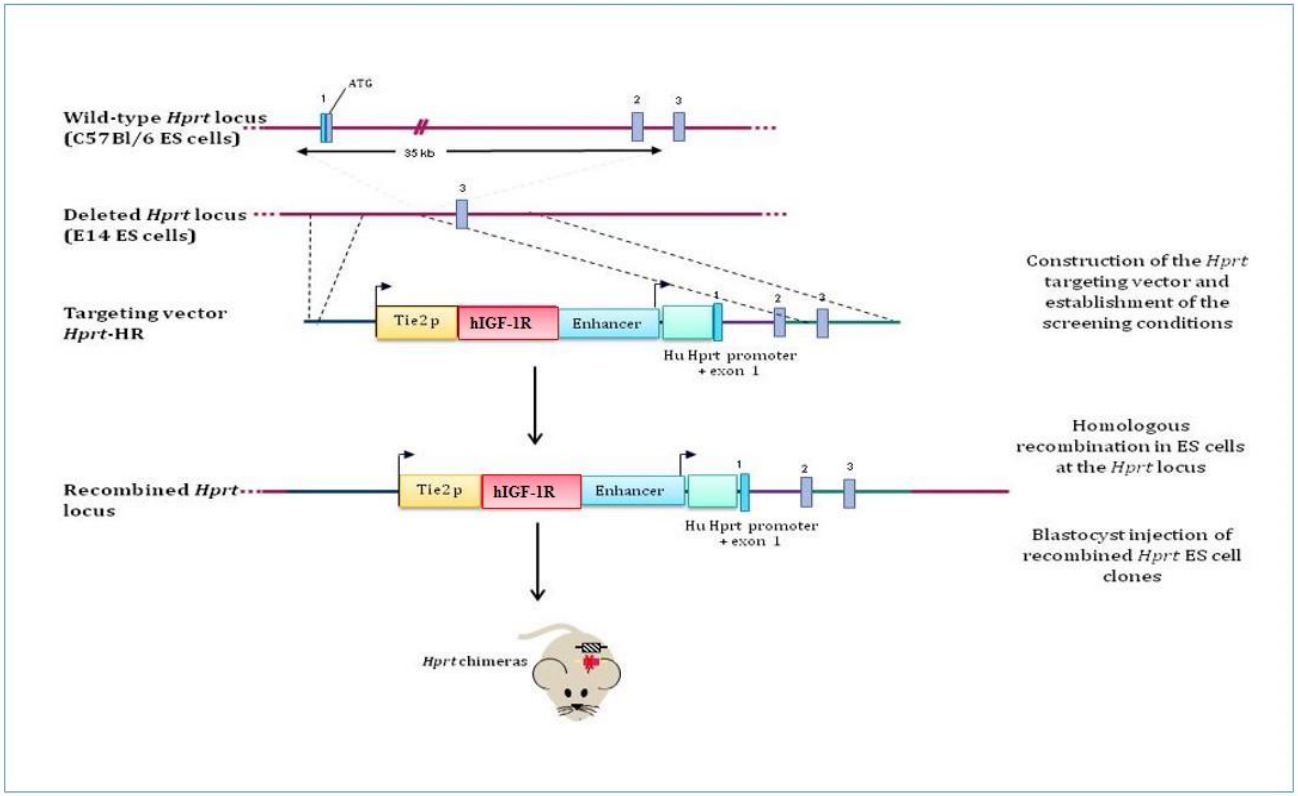

Figure 4.2-1: Schematic representation of "Quick Knock-in™" strategy: Diagram is not to scale. Blue boxes represent HPRT exons; red line represents the reconstituted HPRT locus; red box hIGF-1R K1003 DNA; yellow boxTie2 promoter; light blue box core enhancer.

The HPRT gene in this context is important for 2 reasons. Firstly it has been well validated that insertion of a transgene at the HPRT locus allows for reliable expression of the specific gene in question [315]. Of particular importance to this project, it has also been demonstrated that when inserted at the HPRT locus, under control of the Tie2 promoter a transgene can be reliably expressed specifically in vascular endothelial cells [316].

Secondly, the HPRT gene codes for an enzyme which is constitutively expressed in all cells. This enzyme is involved in the synthesis of purines from the degradation of nucleotide bases. The synthesis of purines in this way can be termed the "salvage pathway", although cells are also able to manufacture purines by the *de novo* pathway. Cells which are depleted of HPRT (and hence lack the ability to synthesise purines by the salvage pathway, but have an intact *de novo* pathway) are generally able to grow in conventional laboratory media. In HAT media (which contains hypoxanthine, aminopterin and thymidine) the *de novo* pathway is blocked, and consequently HPRT depleted cells perish in HAT media [317]. This phenomena was first described by the group led by Oliver Smithies, and comprised part of the work for which he was jointly awarded the 2007 Nobel Prize in Medicine

E14 embryonic stem cells have an inbuilt deletion of the HPRT gene, and they therefore die in HAT media. Following insertion into the E14 cells, the transgenic cassette, containing the GenOway "Quick Knock-in™" targeting vector repaired the HPRT deletion.

Following electroporation, (which uses an electrical current to increase cell membrane permeability allowing the vector to be delivered into the cytoplasm), it was then possible to identify the E14 cells which had successfully taken in the vector by exposing them to HAT media: the cells with the vector survived in HAT media; those without the vector perished. This was therefore a relatively straight forward way of positively selecting and subsequently generating a clone of cells which had the transgenic cassette incorporated into the cytoplasm.

4.2.1.3 Homologous Recombination of Transgene into Embryonic Stem Cells

It was then necessary to assess incorporation of the transgene into the host's genome by the process of homologous recombination

Homologous recombination describes the principle by which genetic material is able to be switched between 2 strands of DNA. The process is utilised within cells to repair breaks

within DNA, but it is also homologous recombination which is responsible for the formation of unique chromosomes during meiosis.

Although the process of homologous recombination has been known for more than half a century it was work done in the 1980s by the group led by Cappechi [318] which identified homologous recombination as a potential target which could be manipulated to introduce exogenous DNA into a host's genome.

In order to ensure that the K100R mutation was present in the embryonic stem cell following homologous recombination the presence of the abnormal gene was confirmed in the host embryonic cell by southern blotting.

4.2.1.4 Breeding of Chimeras

Following confirmation that the transgene had been incorporated into the embryonic stem cell, the stem cell was injected into a blastocyst. In view of the pluripotent nature of stem cells the blastocyst developed as a chimera arising from 2 different cell lines; the embryonic stem cell and the host blastocyst cell. The aim was to produce a chimera in which the germ line cells are derived from the transgenic embryonic stem cells.

In order to breed a population of transgenic mice it was necessary to identify the mice which exhibited high degrees of chimerism, and importantly have a high probability of having germ line cells derived from the genetically manipulated cell line. The genetically manipulated cells were derived from mice which have a greyish coat colour, the recipient blastocysts arose from wild type C57 mice which are black in colour. A mouse born to the foster mother who had a chequered coat was, therefore considered to be chimeric: the dual coat arising from the 2 cell lineages. Figure 4.2-2

After achieving sexual maturation 5 highly chimeric males were generated from the ES cell clone and were mated with wild type C57 females. This resulted in the generation of 4 agouti coated females which were confirmed to be heterozygous for the recombined Hprt allele, and genotypes were confirmed by southern blotting.

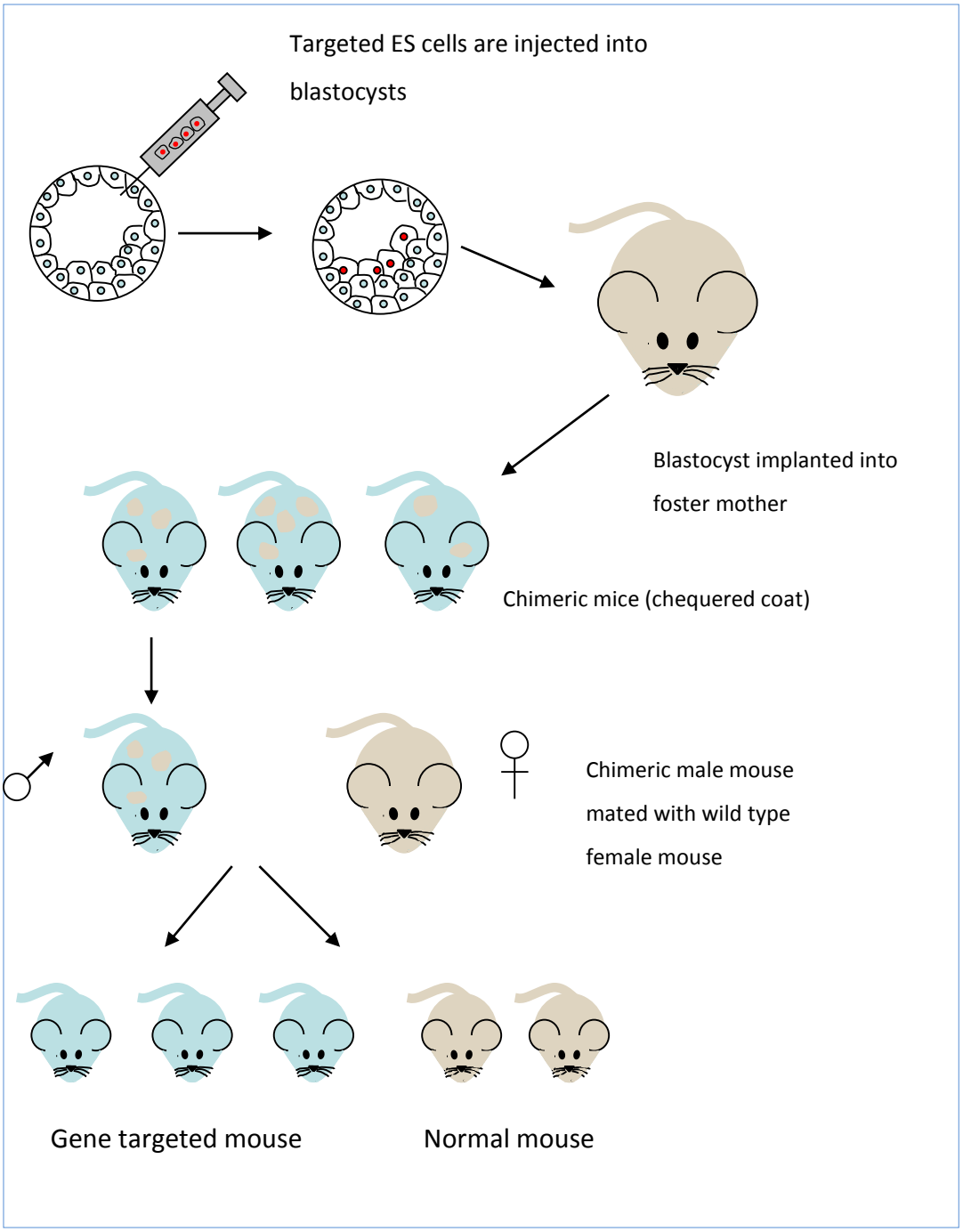

Figure 4.2-2: Scheme of identification and breeding of chimeric mice

4.2.1.5 Breeding of Transgenic Mice

The HPRT gene is located on the X chromosome. When analysing the action of the transgene it is therefore necessary to study either homozygous females ($X^* X^*$) or hemizygous males (X^*Y). Both of these can only be generated following second generation breeding. Figure 4.2-3

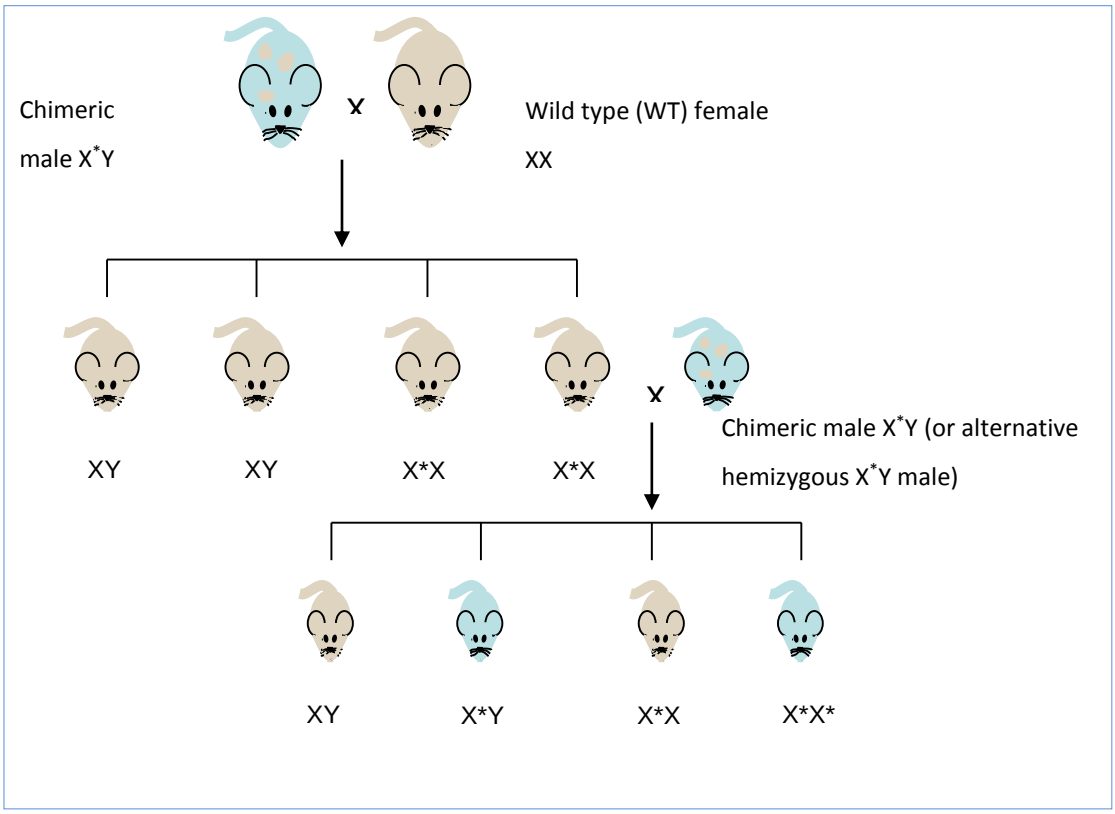

Figure 4.2-3: Breeding strategy for developing transgenic mice. The asterisks represent the X chromosome carrying the transgene. XY – wild type male; XX – wild type female; X*X – heterozygous female; X*Y – hemizygous male; X*X* - homozygous female

4.2.1.6 Terminology

The line of mice was termed MIGFREO (mutant IGF-1 receptor, endothelial specific over-expression). Hence -forth, the expression "MIGFREO" will be used as the terminology to describe male mice, hemizygous for the mutant IGF-1R; the term "wild type" will mean their age and sex matched litter mates used as a control population.

4.2.1.7 Animal Husbandry

4 female heterozygous transgenic animals were transferred to our care. The line was back crossed 10 times with male C57 black 6 mice to produce a population of transgenic mice.

Animals were housed in groups of up to 4 animals with same sex littermates. Animals were housed in appropriate designated rooms with controlled environmental conditions: regular lighting cycle (lights on 0700, lights off at 1900); temperature of 19^{o}C - 23 ^{o}C and humidity of 45-65%. Mice were fed standard laboratory chow diet and normal drinking water. Mice were weaned at 3 weeks of age and ear notched, both as a method of identification but also to provide tissue to genotype.

Only male animals were used in order to exclude the effect of oestrogen on endothelial function.

Animals were weighed between 8-20 weeks of age. Insulin, glucose tolerance and IGF-1 tolerance tests were performed on mice between the ages of 12-14 weeks. Blood pressure was taken between 12-14 weeks of age. Animals were sacrificed for all other experiments between the ages of 12-14 weeks.

Experiments were performed in accordance with UK Home Office Regulations Animals (Scientific Procedures) Act 1986 (PPL No 40/2988).

Sacrifice of animals unless otherwise stated, was performed in accordance with Schedule 1 by exposure to a rising concentration of carbon dioxide and death confirmed by dislocation of the neck.

4.2.2 Genotyping of mice

4.2.2.1 DNA extraction

Using ear notches taken in order to identify the mice, DNA extraction was performed. 100 µl of 25mM NaOH / 0.2mM EDTA solution was added to the ear notch and the samples were heated at 95°C for 20 minutes. After heating 100µl of 40mM Tris-HCl was added to the sample which was then vortexed for 20 seconds. Samples were stored at -20°C.

4.2.2.2 PCR

A mastermix containing 2.5µl of PCR buffer, 1.5µl of MgCl, 2µl of dNTP, 0.4µl of both forward and reverse primers (GAAAAAGGAACTTAACCCTCCCTGTGC and GAACAGCAGCAAGTACTCGGTAATGACC), 0.12µl of Taq enzyme and 17.1µl of distilled H_2O was made. This was added to a PCR tube with 1µl of prepared DNA. The PCR plate was placed into a PTC Pellier Thermal cycler (MJ Research) with cycling conditions as follows : 1. 95°C for 1 minute, 2. 95°C for 15 seconds, 3. 65°C for 30 seconds, 4. repeat steps 2-3 35 times, 5. 72°C for 6 minutes, 6. 4°C for 10 minutes. 7. End.

Products were either stored at -20°C or were identified by electrophoresis on a 1% agarose gel containing 4µl of ethidium bromide (Sigma). Imaging of bands was performed by fluorescent imaging using a 100 base pair reference ladder and commercial software (ChemiImager 5.5).

4.2.3 Quantitative PCR

4.2.3.1 RNA extraction

Samples of RNA from tissue and pulmonary endothelial cells were extracted and analysed. Tissue samples which had previously been stored at -80°C were transferred to appropriately labelled 2ml eppendorf tubes. To each tube was added a tissue lyser bead and 1ml of TRIzol® (Invitrogen). The sample was loaded onto a tissue lyser machine and shaken for 3 cycles of 2 minutes at 30Hz. The liquid left in the tube was transferred into a 1.5ml eppendorf and the solid material and tissue lyser bead were discarded. The above process was not performed for samples from pulmonary endothelial cells, but hereafter the description of the process which follows is identical to both types of sample.

The tube was placed in a centrifuge where it was spun at 10000g for 10 minutes at 4°C. The supernatant was transferred to a clean 1.5ml eppendorf tube, and the substance at the bottom of the tube was discarded. The supernatant was left to air dry for 5 minutes at room temperature. 200µl of chloroform was added. The tube was agitated for 15 seconds and then left at room temperature for 3 minutes, following which it was transferred to the centrifuge and spun for 15 minutes at 12000g at 4°C. The clear supernatant was transferred to a clean 1.5ml eppendorf and the rest discarded. To this 500µl of isopropanol was added. The tube was gently agitated and left at room temperature for 10 minutes.

Following this the tube was spun at 12000g for 10 minutes at 4°C. This caused the collection of a pellet at the bottom of the eppendorf tube. The liquid was discarded leaving the pellet. The pellet was covered with 1ml of 75% ethanol; the sample was then re-spun at 4oC for 5 minutes at 7500g and the ethanol removed, again leaving the pellet. The pellet was left to air dry for 10 minutes at room temperature and then dissolved in 20µl of RNAase free H2O on ice for 20 minutes.

The concentration of RNA (nanograms/microlitre) in each sample was determined by placing a 1µl drop of the solution onto a NanoDrop® machine. Following this, samples were frozen and stored at -80°C.

4.2.3.2 Reverse transcription of RNA

For each sample a master mix was made using components within the High Capacity cDNA Reverse Transcription Kit (Applied Biosystems®). After defrosting slowly on ice, the mastermix was made (as per the manufacturers' instructions), comprising of 2µl PCR buffer; 2µl random primers; 1µl multiscribe; 0.8µl dNTP; 4.2µl ddH_2O. This was added to a PCR plate along with 2µg RNA (volume dependent on concentration as assessed by the NanoDrop® machine) made up to 10µl with ddH2O. The PCR plate was placed into a PTC Pellier Thermal cycler (MJ Research) with cycling conditions as follows: 1. 25°C for 10 minutes, 2. 37°C for 2 hours, 3. 85°C for 5 minutes, 4. 4°C for 30 minutes. 5. End.

Samples were stored at -20°C until required.

4.2.3.3 Quantitative Real-Time PCR

Quantification of RNA expression using cDNA synthesised as described above was performed in a thermal cycler (ABI Prism 7900HT, Applied Biosystems) using SybrGreen

(Applied Biosystems) as the fluorescent dye used to detect PCR products. Samples were analysed in triplicate and an average of the 3 readings used to calculate the relative expression by the comparative Ct method.

25µl volume reactions were used with a typical reaction comprising: 5µl of cDNA (diluted 1:20 with TE buffer), 1.5µl forward primer, 1.5µl reverse primer, 12.5µl of SybrGreen and 4.5µl ddH_2O.

Beta actin was used as a housekeeping gene (TTCTACAATGAGCTGCGTGTG and GGGGTGTTGAAGGTCTCAAA); human IGF-1R (CCAGGCCAAAACAGGA and TCTCTTTCTATGGAAGACGTACAGCAT) and mouse IGF-1R (ACCGTCTAAACCCAGGGAACTAT and CTCATACGTCGTTTTGGCGG) primers were used to identify the presence of human and mouse IGF-1R.

4.2.4 Pulmonary endothelial cell isolation

Isolation of pulmonary endothelial cells was performed by labelling endothelial cells with magnetic CD146 microbeads. CD146 is a transmembrane glycoprotein which is found primarily in mouse liver sinusoidal endothelial cells (LSEC) but the CD146 antibody is also known to bind endothelial cells isolated from pulmonary arteries and pulmonary capillaries (157). Once labelled with magnetic beads the cell suspension is loaded through a column and placed within a magnetic field. The labelled cells are retained within the column; unlabelled cells pass through the column and can be discarded. It is therefore possible to assume that cells that remain within the column are CD146+ve cells, and hence are endothelial cells.

Briefly, lungs collected from mice were transferred in HBSS and finely minced in a solution of 0.01g collagenase (Wothington Biomedical Corporation) reconstituted with 10 ml HBSS. The mixture of minced lungs and collagenase/HBSS was gently rotated for 45 minutes at 37°C. The mixture was sieved and washed to remove solid matter and cellular matter was formed into a pellet by a series of spins in a centrifuge and washes in PBS/BSA. The pellet was re-suspended with 90 µl PBS/BSA and 10 µl CD146 microbeads (MACS ® Miltenyi Biotech) were added. The cells and beads were incubated and gently agitated for 15 minutes at 4°C. After incubation the cellular matter was passed through columns in a magnetic field (MACS® Column and separator). Unlabelled cells were collected in the flow through; CD146+ve cells remained within columns and were forced out by a plunger.

Collected cells were again spun to form pellets and washed several times before plating onto human fibronectin coated 6 well plates (BD Biosciences) with media (PromoCell endothelial cell growth medium MV2) supplemented with fetal calf serum and antibiotics (Invitrogen®) (100units penicillin / 100µg streptomycin / 25µg amphotericin per ml). The medium was changed after 2 hours and every 48 hours after that.

4.2.4.1 Splitting cells

When cells were noted to be confluent they were washed twice with 5ml of PBS and 0.5ml of Gibco® trypsin (Invitrogen®) added. The plate was incubated until cells were seen to lift off from the bottom of the well. Medium (PromoCell endothelial cell growth medium MV2) was added and the cells were removed from the original well and spilt between 3 new wells (human fibronectin coated 6 well plates (BD Biosciences)). The medium was subsequently changed every 48 hours. Cells used in this project were used at either passage 0, 1 or 2 in an attempt to reduce the proliferation of any non-endothelial cells.

4.2.5 Western blotting

4.2.5.1 Preparation of cells

Cells were incubated in medium supplemented with 5% of fetal calf serum (FCS) for 4 hours. Cells were washed twice with 5mls of PBS.

Cells were incubated with a further 3 ml of media supplemented with 5% FCS for 10 minutes at 37°C and then 100 µl of lysis buffer (Table 5) with phosphatase inhibitors (Sigma-Aldrich®) (100µl of phosphatase inhibitor 2 and 3 per 10ml of lysis buffer) was added. Cells and lysis buffer were removed from the plate and stored at -80°C until required.

Component	
Tris-HCl	25ml 500mmol/L
Glycerol	20ml
ddH_2O	43ml
EDTA	2ml 100mmol/l
Sodium dodecyl sulphate	2g

Table 5: Composition of lysis buffer

4.2.5.2 Bicinchoninc Acid (BCA) assay

Pierce® BCA Protein Assay kit (Thermo Scientific) was used to quantify protein concentrations in samples. According to manufacturers' instructions 25µl of previously prepared BSA standard or the sample was added to a 96 well plate in duplicate. For tissue samples the supernatant was pre-diluted (aorta 1 in 5, lung, fat and muscle 1 in 20; liver 1 in 100). To each sample or standard 200 µl of the working reagent was added (50:1 BCA reagent A (sodium carbonate, bicinchoninic acid and sodium tartrate in 0.1M sodium hydroxide): BCA reagent B (4% cupric sulphate). The plate was incubated at 37°C for 30 minutes and absorbance measured at 560nm on a MRX TC microplate reader (Dynex technologies) using Revelation software package (Dynex Technologies).

4.2.5.3 SDS-Page Gel

20 µg of protein was made up to 20 µl with lysis buffer containing inhibitors and added to 5 µl of NuPAGE loading dye (Invitrogen) and 2.5 5 µl of NuPAGE reducing buffer (Invitrogen). This was incubated at 95°C for 10 minutes and briefly spun.

A NuPage (Invitrogen) gel was unpacked and placed in to a Novex Mini-Cell tank with X-Cell surelock (Invitrogen) with 25ml of 20x MES SDS NuPAGE running buffer and 475ml of ddH_2O. Samples were loaded onto the gel, with 8µl of Precison Plus Protein ™ Western C ™ ladder (Bio-Rad). Gel was run at 200v, 120mA for 40-45 minutes.

4.2.5.4 Transfer

The gel was removed from the tank and soaked in ddH_2O for 10 minutes. Appropriate sized pieces of Immobilon® transfer membrane (Millipore) were soaked in methanol for 15 seconds; MilliQ H_2O for 2 minutes; transfer buffer (Table 6) for 2minutes. A transfer cassette was loaded with; a sponge; filter paper; gel; membrane; filter paper; sponge and clamped shut. Cassette was placed in a tank, which was filled with transfer buffer and kept cool with and ice pack. An electrical current of 100V was run through the cassette for 1 hour. After 1 hour the membrane was cut into appropriate sections using the ladder as a guide (typically 75kDa).

		2 litres
Tris	25mM	6.06g
Glycine	192mM	28.84g
Methanol	400ml	400ml
ddH_2O		Up to 2 litres

Table 6: Composition of transfer buffer. pH 8.1-8.4

4.2.5.5 Western blot

After cutting the membrane was placed in blocking solution (Table 7) and gently agitated for 1 hour. After 1 hour of blocking, the membrane was incubated with primary antibody diluted in blocking buffer (Table 8) either for 90 minutes at room temperature, or overnight

at 4°C. After incubating with the primary antibody the samples were washed 3x10 minutes with 1x TBS tween (Table 9)

Following washes the membranes were incubated at room temperature in blocking buffer for 1 hour with: 1:1000 secondary antibody (either polyclonal rabbit anti mouse immunoglobulin HRP (Dako) or polyclonal goat anti rabbit immunoglobulin HRP (Dako)) and 1:25000 Precision Protein™ StrepTactin HRP conjugate (Bio-Rad).

Component		100ml
Dried milk powder	5%	5g
1x TBS tween	0.05%	100ml

Table 7: Composition of blocking buffer; kept at 4°C

Antibody	Concentration	Source	kDa	Company
β Actin	1:1000	Mouse	42	Santa Cruz Biotechnology
IGF-1R β	1:100	Rabbit	90	Santa Cruz Biotechnology

Table 8: Primary antibodies used in western blotting experiments

Component		2 litres
Tris	500Mm	9.7g
Na Cl	5M	292g
Tween 20	0.5%	5ml

Table 9: Composition of 5x TBS tween (made up to 2 litres with ddH_2O); pH adjusted to 7.4)

After incubation with secondary antibody the membrane was washed a further 3 times with 1xTBS tween. Membranes were coated with Immobilon™ Western chemiluminescent HRP substrate (Millipore) (made of a 1:1 solution of HRP substrate peroxide solution and HRP substrate luminal reagent) and left for 5 minutes at most before exposure on a Kodak

image station 2000R for a length of time determined by commercially available software (Kodak 1D image analysis software).

4.2.5.6 Stripping blots

If required, after the membranes were dried, they were stripped and re-probed with further primary antibody. Dried membranes were briefly rehydrated in methanol and washed with ddH_2O. The membranes were incubated at room temperature with Restore™ PLUS Western Blot stripping buffer (Thermo Scientific) for 5-15 minutes and then washed with 1xTBS tween for 3x5 minutes. Membranes were placed in blocking solution for 1 hour and incubated with primary and secondary antibodies as described above.

4.2.5.7 Analysis, densitometry

Developed films were scanned at high resolution and analysed using Kodak 1D image analysis software. Each band was assigned an equal size lane, and band density quantified and background signal subtracted. Densities of the protein of interest were normalised to β actin to correct for any discrepancies in loading.

4.2.6 Statistics

Results are expressed as mean +/- SEM. Comparative analysis within groups was performed using paired Student t test; between groups unpaired Student t test. $P < 0.05$ was considered to be statistically significant.

4.3 Results

4.3.1 Genotyping

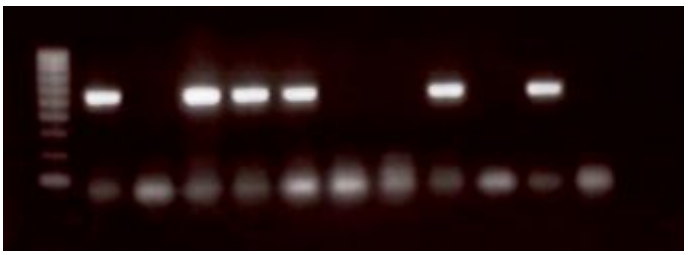

Figure 4.3-1: Representative gel of PCR products. From left to right: 100bp ladder; positive control; negative control; samples 1-9 where samples 1-3, 6, 8 are positive.

Over the course of the project 418 mice were born. The distribution of sex and genotype of animals are shown in Figure 4.3-2 and Table 10. A 4 way chi squared test did not demonstrate any significant variance between observed and expected genotypes. Comparison between wt. and MIGFREO males using the binomial test, again did not demonstrate any significance variance from that expected. It is reasonable to say therefore that the mice displayed normal Mendelian patterns of inheritance for an X linked gene, and there was no evidence of excess intra-uterine loss in MIGFREO mice.

	MIGFREO (%) [expected %]	Wt. (%) [expected]	Significant deviation from expected
Male	119 (28.47) [25]	99 (23.64) [25]	
Female	85 (20.33) [25]	115 (27.51) [25]	No (using 4 way chi squared test p value = 0.07)
Total	204 (48.8)[50]	214 (51.2)[50]	No

Table 10: Genotype of mice. Chart shows absolute numbers of mice shown (% of total mice) with numbers expected shown in square brackets. This was analysed using a chi squared test to assess whether numbers born differed significantly from the numbers expected. Chi squared test did not reveal any significant deviance from the numbers which were expected to be born, hence we concluded that the gene was inherited in a standard Mendelian way.

A sample gel of electrophoresis of PCR products is shown in Figure 4.3-1. A 100 base pair (bp) ladder is seen on the left of the picture, followed left to right by positive and negative controls respectively and unknown samples. The band at 545 bp identified the sample as being DNA from a transgenic mouse.

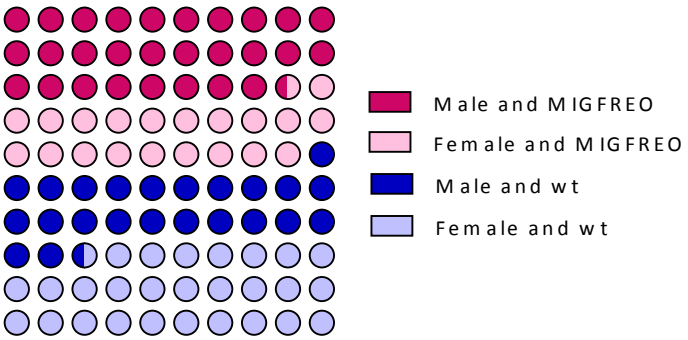

Figure 4.3-2: Distribution of genotypes. As above, this demonstrated the distribution of sex and genotype of mice which were born. There was no variance from that expected.

4.3.2 Quantitative PCR

Quantitative PCR suggests that expression of mouse IGF1-R is similar between the 2 sets of mice, although as expected there is a difference in level of expression displayed in different tissues. See Figure 4.3-3.

Quantitative PCR demonstrates that human IGF-1R mRNA is only found in PEC from the CD146+ve cells isolated from MIGFREO lungs. No discernible human IGF-1R mRNA was found in unlabelled MIGFREO PEC or in any cells from wt. mice. This strongly supports the premise that human (and therefore mutated, functionally inactive) human IGF-1R mRNA is found only on the endothelial cells from the MIGFREO mice. See Figure 4.3-4

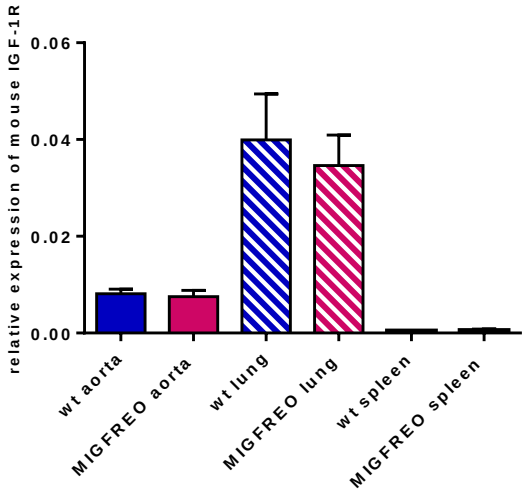

Figure 4.3-3: Quantitative PCR demonstrating presence of mouse IGF-1R mRNA in various tissues. There was no significant difference in expression of mouse IGF-1R between the wt. and MIGFREO mice in any of the tissue examined.

Quantitative PCR performed on RNA extracted from various organs (Figure 4.3-6) demonstrates that the human IGF-1R mRNA is found exclusively in samples from MIGFREO mice. There were no significant differences between levels seen in lung, spleen and aorta within the MIGFREO mice, although the error bars are large.

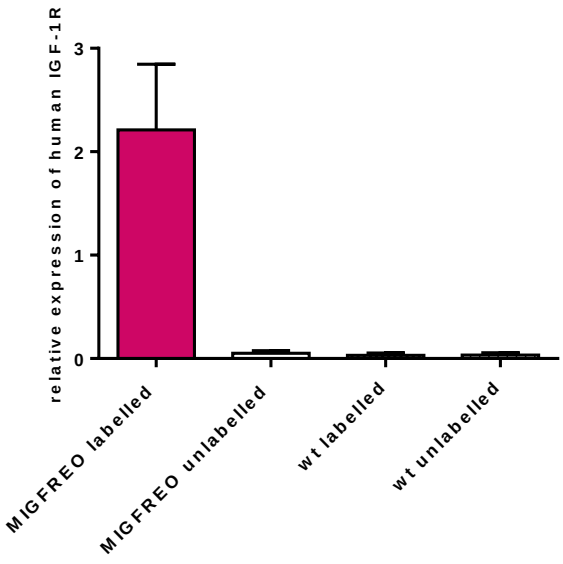

Figure 4.3-4: Quantitative PCR demonstrating presence of mutated human IGF-1R mRNA in labelled PEC. Human IGF-1R is only detected in mRNA extracted from cells from the lungs of MIGFREO mice which were labelled with CD146 microbeads. Given that this antibody is relatively specific for endothelial cells this demonstrates that human IGF-1R was only found in endothelial cells extracted from the lungs of the MIGFREO mice.

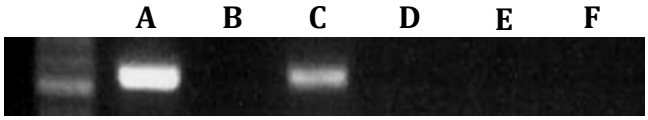

Figure 4.3-5: Agarose gel of products from quantitative PCR using human IGF-1R primer (A) +ve control (B) –ve control (C) MIGFREO "labelled" cells (D) MIGFREO "unlabelled cells" (E) wt. "labelled" cells (F) wt. "unlabelled" cells

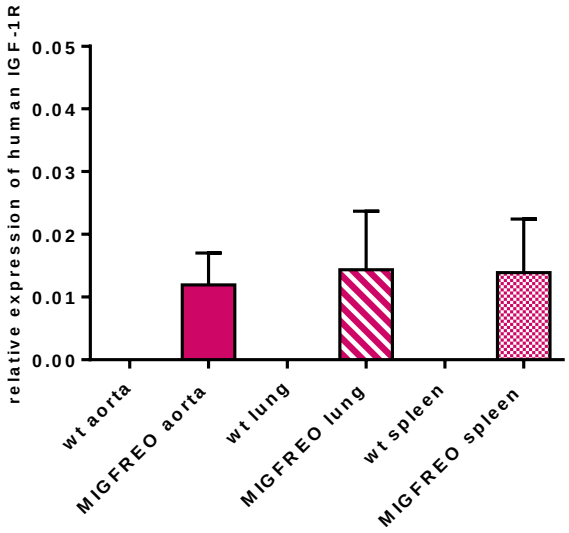

Figure 4.3-6: Quantitative PCR demonstrating presence of human IGF-1R mRNA in various tissues. Human IGF-1R was only found in mRNA extracted from MIGFREO mice. Human IGF-1R mRNA was found in MIGFREO aorta, lung and spleen, although there was no difference in relative expression of human IGF-1R mRNA in these tissues.

4.3.3 Western blots

Analysis of western blots showed a significantly elevated concentration of IGF-1R β subunit protein in PEC from MIGFREO mice (Figure 4.3-7, Figure 4.3-8). This suggests that native IGF-1R is expressed in addition to mutated human IGF-1R in MIGFREO mice.

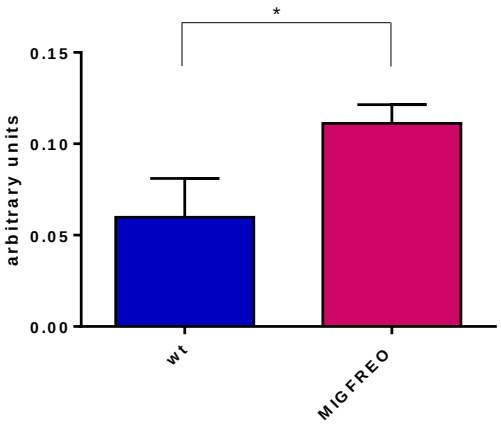

Figure 4.3-7: Mean densitometry of IGF-1R β. This graph demonstrates a clear elevation of IGF-1R β protein found in the PECs of MIGFREO mice when compared with their wt. counterparts. The densitometry of each individual band seen following western blotting experiments was normalised to β actin density. The displayed columns represent densitometry normalised to B actin (+/- SEM) *p=0.05

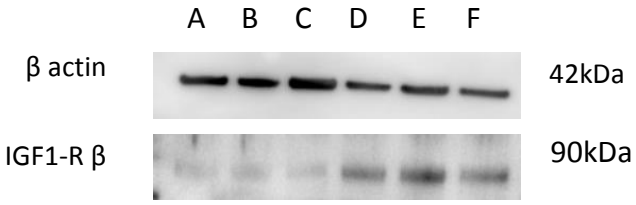

Figure 4.3-8: Representative blot of IGF-1R β. A-C = wild type, D-F = MIGFREO. A clear difference in IGF-1R β protein level is demonstrated between PECs taken from wt. and MIGFREO mice. This strongly supports the supposition that inclusion of the transgene into the MIGFREO endothelial cell is associated with increased total (i.e. both human and mouse) IGF-1R density.

4.4 Conclusion and Discussion

MIGFREO mice are viable and fertile

MIGFREO mice are viable beyond the fetal stage, are fertile and inheritance of the mutated IGF-1R obeys standard laws of Mendelian inheritance.

Validation of the model

Western blot analysis of protein from PECs shows that the IGF-1R β subunit protein is found in significantly higher quantities in PEC from MIGFREO mice than wt. mice. Levels of mouse IGF-1R mRNA are similar between MIGFREO and wt. mice. Taken together this strongly suggests that the insertion of human IGF-1 into the endothelium does not down-regulate numbers of mouse IGF-1R.

Human IGF-1R mRNA is found only on the CD146 “labelled” PECs isolated from the lungs of MIGFREO mice. No human IGF-1R mRNA was identified in pulmonary endothelial cells isolated from wt. mice, or from “non-labelled” cells from either wt. or MIGFREO mice. This shows that expression of the gene is limited to endothelial cells taken from the MIGFREO mice, but also strongly suggests that the method of selecting cells by labelling them with CD146 microbeads and sorting them through a magnetic field is an appropriate one for this project.

CD146 is a transmembrane glycoprotein involved in cell adhesion and expression of CD146 is found on endothelial cells of multiple subtypes; skin, liver, kidney, brain, spleen and lymph nodes. Importantly for this project it is also expressed on blood vessel endothelium, in particular from pulmonary arteries, veins and capillaries. Although expression in humans is also found on T cells and follicular dendritic cells, this is less prominent in murine T cells; only a small proportion of murine natural killer T cells express CD146, hence interaction with non-endothelial cells in mice is likely to be low.

Quantitative PCR demonstrates that the human IGF-1R is found only in MIGFREO mice. See Figure 4.3-6 and expression appears to be restricted to endothelial cells. See Figure 4.3-4. The primers used are specific for the detection of the human IGF-1R in both its non-mutated and mutated forms. The mutation which has been incorporated in to the MIGFREO mouse, is, as has already been discussed, a single base change (lysine K1003) and given the position of restriction enzymes we were unable to design a primer which spanned

the genetic area containing the mutation. The incorporation of the mutation into the genome was confirmed by GenOway with southern blotting, Fernandez et al [306] used a similar strategy; incorporation of the base change in MKR mice (mice with muscle specific inactivation of the IGF-1R using the lysine K1003 mutation) was confirmed with southern blotting; the presence of the human IGF-1R within tissue was accepted as sufficient to confirm that the mouse carried the mutation.

Although human IGF-1R mRNA was only found in tissue taken from MIGFREO mice, there was no significant difference between levels of expression in aorta, lung and spleen. This is somewhat surprising given that the lung, when compared to the aorta is a tissue rich in endothelium. The CD146 antibody is however present on non-vascular endothelial tissue so some of the cells isolated would not have been vascular endothelial cells, but might have been endothelial cells of other subtypes. It is perhaps more accurate to state that in this case I have demonstrated that the human IGF-1R is expressed solely on endothelial cells from the MIGFREO mice, rather than the more specific statement that the human IGF-1R is found only on MIGFREO vascular endothelial cells. Repeated passage of the cells using magnetic separation following labelling with additional antibodies, perhaps towards VE-Cadherin which is involved in vasculogenesis might reduce the amount of non-vascular endothelial cells extracted, although at this stage I am unable to produce any evidence or previously published data that this is a viable experimental technique.

There is a comparatively large standard error for each result which may indicate experimental variability. The quality of the RNA was not reassessed after freezing, and it may be that repeated cycles of freeze-thaw of samples altered the quality of the RNA produced. As has been previously used within our laboratory 2µg of RNA was converted to cDNA, although it is unclear if this was the optimum sample size for analysis of this particular gene; further experiments with varying concentrations of RNA should be considered in future in order to identify optimum experimental conditions.

Given the small quantities of sample involved, pipetting errors may have contributed, but the relative expression of human IGF-1R was assessed simultaneously with the housekeeping gene β actin and results were normalised to β actin expression. Assuming that expression of β actin is ubiquitous, this should have corrected for any differences in absolute quantity of cDNA which was added to the real time PCR plate.

It is possible, however that the choice of β actin as a housekeeping gene may itself have caused results to be skewed. Although β actin is a commonly used housekeeping gene, there is evidence that in mice, there may be variable expression across different tissues, which could perhaps account for the results seen in the MIGFREO mice [319]. In addition, it was assumed that β actin expression was similar between the 2 groups of mice. Although the western blot seen in Figure 4.3-8 seems to demonstrate that there may be a difference in β Actin expression between MIGFREO and wt mice, this was not borne out by subsequent experiments and analysis of β actin expression between wt and MIGFREO mice did not demonstrate any significant difference (analysis of expression of β actin from PEC from 10 wt and 10 MIGFREO mice; in arbitrary units [+/- SEM] wt 721470 [+/- 129498] MIGFREO 623456 [+/- 113040] p=0.57) . Further experiments should be performed using multiple housekeeping genes in order to try and eliminate or reduce potential variability.

It is necessary to consider how the presence of hybrids might be expressed in MIGFREO mice. Human and mouse IGF-1R are able to form hybrids [320]; mutation of the ATP binding site with the single base change lysine K1003 renders the IGF-1 functionally inactive [311, 312, 321]; successful signal transduction via the IR, IGF-1R or hybrid requires both receptor subunits to be functional [215]; mutated and normal IGF-1 monomers form non-functioning hybrid receptors [306]. Taken together this would suggest that there may be 6 configurations of receptors found on the vascular endothelium of MIGFREO mice. These are shown in Table 11 .

Insulin receptors are less numerous than IGF-1 receptors on the endothelium so insulin receptors, as has already been discussed, have a tendency to be incorporated into hybrid receptors [224]. Hybrid receptors have a higher affinity for insulin and hence the endothelium is a relatively insulin resistant tissue [221]. One could postulate that this might be more pronounced in the MIGFREO mouse given the presence of mutated and inactive IGF-1 and hybrid receptors.

Receptor	Functional / non-functional	Affinity for insulin and IGF-1 (if functional)
IR / IR	Functional	Insulin > IGF-1
IGF-1R / IGF-1R	Functional	IGF-1 > insulin
IR / IGF-1R	Functional	IGF-1 > insulin
hIGF-1R / IGF-1R	Non-functional	
hIGF-1R / hIGF-1R	Non-functional	
hIGF-1R / IR	Non-functional	

Table 11: Sub-types of IR and IGF-1R dimers postulated to be found on endothelium of MIGFREO mice. IGF-1R = normally functioning mouse IGF-1R, hIGF-1R = mutant human IGF-1R

Chapter 5: Assessing endothelial function and endothelial insulin sensitivity

5 Assessing endothelial function and endothelial insulin sensitivity

5.1 Introduction

Previous work by our group has demonstrated that manipulation of the IGF-1R on the vascular endothelium plays a critical role in determining endothelial insulin sensitivity: increasing the number of IGF-1R on the endothelium is associated with the generation of increased number of IGF-1R/IR hybrid receptors and reduced endothelial insulin sensitivity; reduction or knockdown of the IGF-1R on the vascular endothelium is associated with the converse [209, 210]. Assessment of endothelial insulin and IGF-1 sensitivity was therefore pivotal to examining the effect of endothelial specific IGF-1R mutation.

Endothelial dysfunction (as determined by no differences in response to acetylcholine induced vasodilatation in the organ bath) *per se* was not a feature of either of these 2 mice, however in the ESMIRO mice (which express a non-functioning endothelial specific IR) there is significant endothelial dysfunction and associated accelerated atherosclerosis [195, 322], and therefore it is important to determine whether endothelial specific manipulation of the IGF-1R is associated with endothelial dysfunction.

In human subjects the function of the endothelium can be assessed in both invasive and non-invasive ways [323].

Assessment of the function of particular blood vessels can be achieved in an invasive manner by assessing the response of the vessel to the administration of substances known to produce endothelial dependent vasodilatation, such as acetylcholine or bradykinin. With a normally functioning endothelium, these substances should cause vasodilatation (and more specifically endothelium dependent vasodilatation, associated with enhanced NO production) and a resultant increase in flow rate. This can be measured by Doppler flow assessment, or by directly measuring luminal diameter. Control measurements are generally obtained by infusing substances known to cause endothelium independent vasodilatation, such as nitro-glycerine or sodium nitroprusside (SNP). Vasodilatation in response to infusion of either of the 2 latter compounds is not impaired in endothelial dysfunction, as they mediate their effects by a direct action on vascular smooth muscle.

Assessing the endothelial function in a non-invasive manner is also possible. It is known that shear stress caused by increased flow velocity of blood leads to an increased NO production and subsequent vasodilatation (flow mediated dilation [FMD]) [324]. Experimentally increased shear stress can be achieved by causing temporary arterial

occlusion, which results in hyperaemia, increased blood flow, and increased NO production and hence vasodilatation. Ultrasound can then be used to assess the size of the brachial artery, which should dilate in response to the stimulus [63].

The comparable method of assessing endothelial function in mice is by using an organ bath. The aorta is excised and mounted on wires in physiological buffer attached to electrical sensors, and vasodilatation and vasoconstriction is assessed in response to a number of stimuli. In common with the way in which endothelial function is assessed in humans, exposure to ACh induces endothelial dependent vasodilatation and exposure to SNP assesses endothelial independent vasodilatation. Given that insulin and IGF-1 induce vasodilatation via production of NO in an eNOS dependent reaction, it is also possible to assess endothelial insulin and IGF-1 sensitivity in the organ bath.

Although assessment of the vasodilatory response to insulin is important, it was also necessary to consider the cellular effects of insulin and IGF-1 on endothelial cells derived from the MIGFREO and wt. mice, and this was performed with western blots examining the expression of proteins in response to stimulation with insulin and IGF-1.

Further assessment of endothelial insulin and IGF-1 sensitivity was made by assessing NO production. Although direct measurement of NO is practically challenging, a useful marker of NO production is the measurement of L-citrulline. The production of NO is determined by the conversion of L-arginine to L-citrulline [45]: if L-arginine is supplied with radio-labelled C^{14}, this carbon atom is included in the formation of L-citrulline, and measurement of the radiolabelled L-citrulline can be used as a surrogate marker for the activity of eNOS and hence NO production. This is a well validated method of assessing NO production [325] and can be used to assess the effect of different stimuli on NO production. Treatment of cells with insulin or IGF-1 before performing this assay is therefore also a method of determining endothelial insulin and IGF-1 sensitivity.

5.2 Methods

5.2.1 Organ bath assessment of endothelial function

Aortas were excised carefully in order to avoid endothelial denudation and transported on ice in chilled Krebs-Henseleit solution (Table 12) which was bubbled for 30 minutes with 95%O_2 / 5% CO_2. Under direct microscopy connective and fatty tissue was cleaned from the aorta and the tissue was divided into 4 rings 3-5mm in length. Rings were subsequently mounted by passing fine wires through the aortic lumen and suspended in a chamber in an organ bath (PanLabs) where it was suspended between a fixed support and a highly sensitive transducer, immersed in Krebs-Henseleit solution and continuously bubbled with 95%O_2 / 5% CO_2 for the duration of the experiment. Over 30 minutes the rings were stretched to a tension of 3g which has been previously shown to be optimum in our laboratory [105, 309] and left to equilibrate for 2 hours.

	Mmol/L
NaCl	119
KCl	4.7
KH_2PO_4	1.18
$NaHCO_3$	25
$MgSO_4.7H_2O$	1.19
CaCl2 $2H_2O$	2.5
Glucose	11

Table 12: Component of Krebs Henseleit solution

5.2.1.1 Measurement of vasoconstrictor response to KCl

Endothelial independent vasoconstriction was assessed by testing maximal response to 100µl KCl (VWR). Any rings failing to contract more than 0.2g were excluded from further analysis. Rings were washed thoroughly with Krebs-Henseleit solution before proceeding.

5.2.1.2 Measurement of calcium dependent vasodilatation using ACh

Rings were partially constricted with 300nM of phenylephrine (Sigma) and rings not constricting more than 0.2g were excluded from further analysis. Calcium dependent endothelial mediated vasodilatation was then assessed by the subsequent relaxation in response to cumulative doses (1nM-10μM) of acetylcholine (Sigma). Rings which relaxed less than 70% were considered to have suffered endothelial denudation during the excision and dissection process and were excluded from further analysis. The presence or absence of endothelial dysfunction was determined by calculating the percentage of relaxation from peak constriction to base ([preconstriction-result]/[preconstriction-base]*100) where relaxation to the baseline would be 100%. Results are expressed as percentage relaxation [309].

5.2.1.3 Measurement of insulin mediated vasodilatation

Rings were either incubated with 100mU/L insulin (Actrapid, NovoNordisk) or control for 2 hours followed by measurement of response to cumulative doses of phenylephrine (1nM-10μM). Rings incubated with insulin were not used for any further experiments. Response to insulin was determined by measuring constriction from baseline, and is expressed in grams [309].

5.2.1.4 Measurement of direct IGF-1 mediated vasodilatation

Rings were pre-constricted as previously described. Receptor grade IGF-1 (GroPep) was reconstituted with 500μl 10mol HCl and 500μl BSA. Vasodilatation in response to cumulative does (1-100nM) of reconstituted IGF-1 was recorded. Rings examined in this way were not used for any further experiments. The presence or absence of vasodilatation in response to IGF-1 was determined by calculating the percentage of relaxation from peak constriction to base ([preconstriction-result]/[preconstriction-base]*100) where relaxation to the baseline would be 100%. Results are expressed as percentage relaxation.

5.2.1.5 Measurement of endothelium independent vasodilatation

Rings not pre-incubated with insulin, or exposed to IGF-1 were pre-constricted as previously described. Endothelium independent vasodilatation was then assessed by the addition of cumulative doses (1nM-10μM) of sodium nitroprusside, which acts as a NO donor. The presence or absence of vasodilatation in response to SNP was determined by calculating the percentage of relaxation from peak constriction to base ([preconstriction-

result]/[preconstriction-base]*100) where relaxation to the baseline would be 100%. Results are expressed as percentage relaxation.

5.2.1.6 Assessment of basal NO production in organ bath using L-NMMA

In order to assess basal level of NO production aortic rings were incubated with the NOS inhibitor L-NMMA. In the presence of L-NMMA NO production will be inhibited and there will be enhanced constriction in the presence of phenylephrine.

10µl of 0.1M L-NMMA (CalBioChem)was added to each chamber and incubated for 1 hour followed by measurement of response to cumulative doses of phenylephrine (1nM-10µM). Rings incubated with L-NMMA were not used for any further experiments.

5.2.2 Pulmonary endothelial cell isolation

Pulmonary endothelial cells were harvested and isolated in the same way as is described above. See chapter 4.2.4 for method.

5.2.3 Preparation of cells

In order to assess protein expression in PECs basally and following stimulation with insulin ad IGF-1 wells were first serum starved in serum free medium for 4 hours. Following serum starvation, medium was removed from the well and the cells were exposed to 1ml of serum free media per well which contained either 150nM of IGF-1 (GroPep) or 100nM of insulin (Sigma-Aldrich®) or had no addition. Cells were incubated for 10 minutes at 37°C and then 100 µl of lysis buffer (Table 5) with phosphatase inhibitors (Sigma-Aldrich®) (100µl of phosphatase inhibitors 2 and 3 per 10 ml of lysis buffer) was added. Cells and lysis buffer were removed from the plate and stored at -80°C until required.

5.2.4 Western blotting

Protein quantification and western blots were performed in the same was as is described above. See chapter 4.2.5.

Primary antibodies used in assessment of endothelial insulin sensitivity are shown in Table 13.

5.2.4.1 Analysis, densitometry

Developed films were scanned at high resolution and analysed using Kodak 1D image analysis software. Each band was assigned an equal size lane, and band density quantified and background signal subtracted. Densities of the protein of interest were normalised to β actin to correct for any discrepancies in loading.

Antibody	Concentration	Source	kDa	Company
β Actin	1:1000	Mouse	42	Santa Cruz Biotechnology
Akt	1:1000	Rabbit	60	Cell Signalling Technology®
p- Akt (Ser 473)	1:1000	Rabbit	60	Cell Signalling Technology®
eNOS	1:1000	Mouse	140	BD Biosciences
p-eNOS (Ser 1177)	1:1000	Mouse	140	BD Biosciences

Table 13: Primary antibodies used in western blotting experiments

5.2.5 L-citrulline assay of eNOS activity

NO is formed by the conversion of L-arginine to L-citrulline in a process catalysed by eNOS [45]. Although direct quantification of NO is possible, the fact that it dissipates rapidly means that there are technical limitations to the direct quantification of NO, whereas measurement of radio-labelled L-citrulline is well established as a way of measuring eNOS activity.

Given that the technique involves radio-labelling, there are limitations on the personnel who are able to perform this technique. The L-citrulline assay was therefore performed in collaboration with Dr Hema Viswambharan, who has optimised this technique to assess eNOS activity in murine pulmonary endothelial cells in our laboratory.

Pulmonary endothelial cells were harvested and isolated in the same way as is described above. See chapter 4.2.4 for method.

They were grown to confluence at P0 to reduce proliferation of non-endothelial cells. When cells were confluent they washed twice with 3mls of PBS and incubated in medium supplemented with 5% FCS overnight. Media was removed and cells were washed a further

2 times with PBS and the cells were incubated for 30 minutes at 37°C with 0.25% HEPES-BSA buffer (Table 14) +/- phosphatase inhibitors. 0.5µCi/ml of radio-labelled ^{14}C-arginine (Quotient Bioresearch) was added to the cells for 5 minutes, followed by either insulin (100nM) or IGF-1 (150nM) for 30 minutes.

	mM
HEPES	10
NaCl	145
KCl	5
$MgSO_4$	1
Glucose	10
$CaCl_2$	1.5
BSA	0.25%

Table 14: Composition of HEPES-BSA buffer

Cells were washed twice with a stopping buffer comprised of ice-cold PBS containing non-radioisotopic 5mM L-arginine (Sigma-Aldrich®) and 4mM EDTA. Cells were incubated 4 ml of 0.025% Trypsin/EDTA for 2 minutes and dislodged from the plate using a cell scraper. Cells were subsequently denatured by repeated pipetting with 95% ethanol and samples were collected into micro-centrifuge tubes. Samples were spun at 600rpm for 5 minutes to form a pellet and the supernatant evaporated in a SpeedVac (Thermo-Scientific) for 25 minutes. Next, the samples were dissolved in 20mM HEPES-Na (pH 5.5) and spun in a centrifuge again to separate the soluble cellular components from waste.

DOWEX resin was equilibrated by adding 100g of Dowex resin (Sigma-Aldrich®) to 100ml of 1M NaOH and mixing for 30 minutes using a magnetic stirrer. The NaOH was changed for fresh 4 times and then the resin was washed with ddH_2O water until the pH was less than 8. The resin was suspended 1:1 with ddH_2O.

The soluble cellular layer collected following centrifuge (apart from 10µl which was used for protein quantification) was added to 2.7ml of equilibrated resin, vortexed and allowed

to settle over approximately 15-20 minutes by gravity. 1ml of the supernatant obtained was removed and added to 12ml of scintillation cocktail (Quotient Bioresearch). Radio-isotopic emission from ^{14}C-citrulline was quantified using a β counter.

Results were normalised to total protein, quantified using the 10µl of reserved cellular supernatant, using the Pierce® BCA Protein Assay kit (Thermo Scientific), as described in section 4.2.5.2.

Isotope controls were normalised to total protein content and control experiments assigned an arbitrary value of 100. Isotope counts were grouped with results of experiments with identical conditions and analysed using a Student's paired 2 tailed t-test to compare control with either insulin or IGF-1.

5.2.6 Statistics

Results are expressed as mean +/- SEM. Comparative analysis within groups was performed using paired Student t test; between groups unpaired Student t test. $P < 0.05$ was considered to be statistically significant.

5.3 Results

5.3.1 ACh Relaxation

There were no significant differences in responses to the vasodilatory effect of ACh between MIGFREO and wt. mice (Figure 5.3-1**,** Table 15).

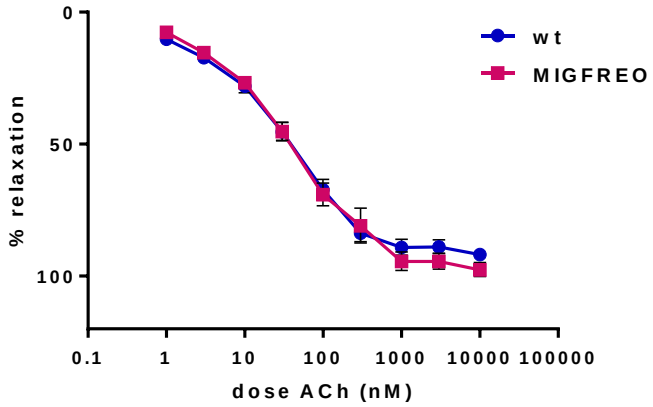

Figure 5.3-1: ACh relaxation. This demonstrates the vasodilatory response to Ach as measured within the organ bath. n > 20 mice for each group with at least 2 rings of aorta for each mouse. Results are expressed as % of relaxation and the mean % of relaxation towards the base is displayed +/SEM. No significant differences between the 2 groups at any point.

ACh dose (nM)	wt. mean % relaxation +/- SEM (n= 22)	MIGFREO mean % relaxation +/- SEM (n=23)	p value
1	10.25 +/- 1.60	7.60 +/- 1.51	0.24
3	17.27 +/- 2.21	15.34 +/- 2.01	0.53
10	28.07 +/- 2.58	26.79 +/- 2.11	0.71
30	45.32 +/- 3.49	45.25 +/- 3.40	0.99
100	67.29 +/- 3.79	69.11 +/- 4.30	0.75
300	83.79 +/- 3.30	80.91 +/- 6.60	0.68
1000	89.17 +/- 3.01	94.41 +/- 3.49	0.26
3000	88.96 +/- 2.57	94.41 +/- 2.99	0.17
10000	91.90 +/- 2.26	97.61 +/- 2.66	0.10

Table 15: Relaxation in presence of acetylcholine. Tabulated results of relaxation in response to increasing doses of Ach within the organ bath. For each group n > 20 with at least 2 rings per mouse. Results are expressed as mean % of relaxation (Where relaxation to the baseline is 100%) +/- SEM. The results are corrected to 2 decimal places. No statistically significant differences noted between the 2 groups for any dose of Ach.

5.3.2 Vasomotor insulin sensitivity

As expected, following incubation with insulin, the response to phenylephrine is significantly blunted in wt. mice (Figure 5.3-2**, Error! Reference source not found.,** Figure 5.3-3**,** Table 16); maximum constriction pre insulin 0.87g +/- 0.05 vs. maximum constriction post insulin 0.54g +/- 0.06 p = 0.0005. The responses to PE diverge significantly in wt. following [log] 300 of PE

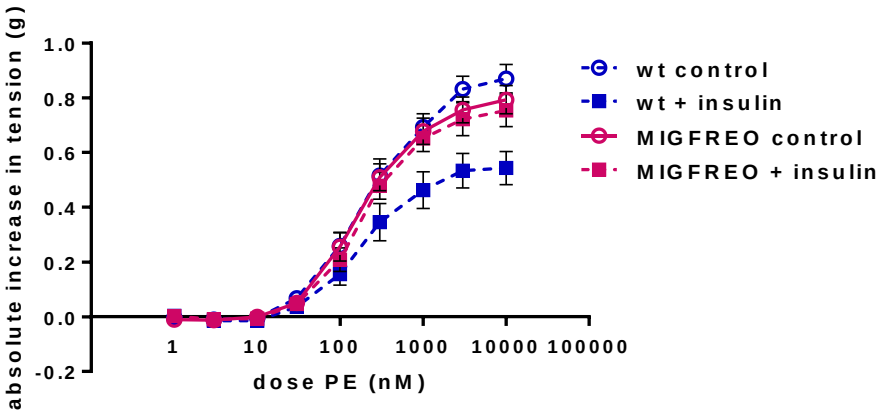

Figure 5.3-2: PE constriction +/- insulin. This demonstrates the absolute increase in tension (g) seen with incremental doses of phenylephrine before and after incubation with insulin. In each group n > 20 with at least 2 rings of aorta per mouse. The graph represents mean increase in absolute tension +/-SEM. In the wt. group incubation with insulin was associated with a significant reduction in response to incremental doses of phenylephrine ($p < 0.001$), an effect which was abolished in the MIGFREO mouse.

In MIGFREO mice, the response to insulin is abolished, and the curves of constriction pre and post insulin dose overlap (Figure 5.3-2, **Error! Reference source not found.**,). This is in marked contrast to the divergence of curves seen beyond 300nM PE in wt. mice (**Error! Reference source not found.**). Maximum constriction pre insulin in MIGFREO mice 0.80g +/- 0.05 vs. maximum constriction post insulin 0.75g +/- 0.06 $p = 0.64$ (Figure 5.3-3**,** Table 16). It should also be noted that whilst there is no difference in maximum constriction pre insulin between the 2 groups, there is a significant difference between the 2 groups post insulin (Figure 5.3-3). Taken together, this data shows that MIGFREO mice are resistant to the vasodilatory effect of insulin which as has been discussed earlier, occurs via an eNOS dependent pathway.

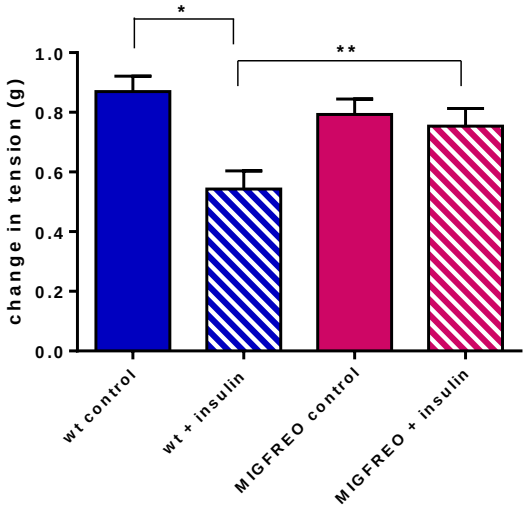

Figure 5.3-3: Maximal PE constriction +/- insulin. This represents maximal change (n>20 per group, bars represent mean +/- SEM) in tension seen following exposure to phenylephrine both before and after incubation with insulin. As is clearly demonstrated there is marked reduction in change in tension following incubation with insulin in the wt. mice (*p=0.0005) although this is abolished in the MIGFREO mice. There is also a striking difference between maximal change in tension seen post insulin incubation between the wt. and MIGFREO mice (**p=0.02)

PE dose (nM)	wt. control +/- SEM	wt. insulin +/- SEM	MIGFREO control +/- SEM	MIGFREO insulin +/- SEM	p value wt. con vs. wt. ins	p value MIG con vs. MIG ins	p value wt. con vs. MIG con	p value wt. ins vs. MIG ins
1	-0.00+/- 0.01	0.00 +/- 0.01	-0.01 +/- 0.017	0.00+/- 0.01	0.62	0.38	0.62	0.96
3	-0.01 +/- 0.01	-0.02 +/- 0.02	-0.01 +/- 0.01	-0.01 +/- 0.01	0.85	0.83	0.91	0.81
10	-0.004 +/- 0.01	-0.01+/- 0.02	-0.01 +/- 0.01	-0.01 +/- 0.01	0.61	0.75	0.80	0.73
30	0.07 +/- 0.02	0.04 +/- 0.02	0.05 +/- 0.02	0.05 +/- 0.02	0.26	0.89	0.55	0.68
100	0.26 +/- 0.05	0.16+/- 0.04	0.26 +/- 0.05	0.21 +/- 0.04	0.13	0.50	0.96	0.38
300	0.52 +/- 0.06	0.35 +/- 0.07	0.51 +/- 0.05	0.48 +/- 0.05	0.08	0.67	0.94	0.12
1000	0.69 +/- 0.05	0.46 +/- 0.07	0.68 +/- 0.05	0.65 +/- 0.05	0.009	0.71	0.84	0.03
3000	0.83 +/- 0.05	0.53 +/- 0.06	0.76 +/- 0.05	0.72 +/- 0.06	0.0008	0.68	0.29	0.04
10000	0.87 +/- 0.05	0.54 +/- 0.06	0.80 +/- 0.05	0.75 +/- 0.06	0.0005	0.64	0.34	0.02

Table 16: Assessment of PE induced constriction pre and post incubation with insulin. Tabulated results of increased tension seen in response to increasing doses of phenylephrine either pre or post incubation with insulin within the organ bath. For each group n > 20 with at least 2 rings per mouse. Results are expressed as mean increase in tension +/- SEM. The results are corrected to 2 decimal places. There is marked reduction of response to phenylephrine seen following incubation with insulin in the wt. mice, although this is abolished in the MIGFREIO mice.

5.3.3 Vasomotor IGF-1 sensitivity

Although there is a marked difference in the way which MIGFREO and wt. mice respond following incubation with insulin, there is no significant difference in the way which the aortas respond to IGF-1 (Figure 5.3-4, Table 17). As expected, in both sets of mice IGF-1 induces vaso-relaxation, and the responses overlap, with no difference in maximal relaxation in the MIGFREO mouse compared to the wt. (98.94% +/- 7.81 vs. 93.86% +/- 7.12 respectively, p=0.64).

IGF-1 dose (nM)	wt. mean % relaxation +/- SEM	MIGFREO mean % relaxation +/- SEM	p value
1	17.28 +/- 4.38	20.89 +/- 3.05	0.52
3	25.16 +/- 5.23	26.62 +/- 4.82	0.83
10	48.17 +/- 8.11	43.46 +/- 7.74	0.66
30	72.43 +/- 7.36	76.24 +/- 7.81	0.73
100	93.86 +/- 7.12	98.94 +/- 7.81	0.64

Table 17: Assessment of IGF-1 induced vaso-relaxation. This demonstrates the direct vasodilatory response to IGF-1 seen within the organ bath. In each group n>10 with at least 2 aortic rings for each mouse. The data is represented as mean % relaxation to base (where baseline represents 100%) +/- SEM. Corrected to 2 decimal places. No significant differences seen between the 2 groups of mice.

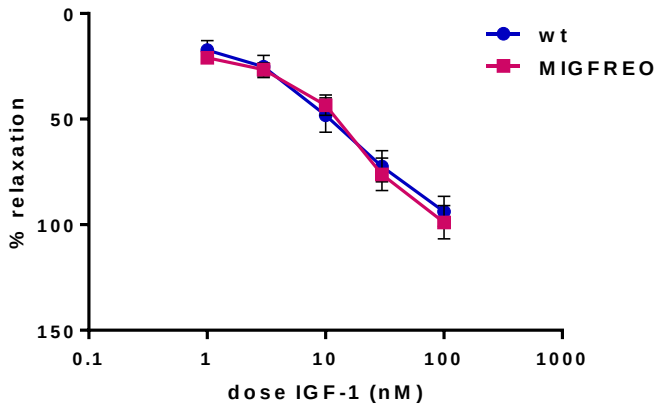

Figure 5.3-4: IGF-1 relaxation. This demonstrates the vasodilatory response to IGF-1 as measured within the organ bath. Each group represents n>10 mice for each group with at least 2 rings of aorta for each mouse. Results are expressed as % of relaxation and the mean % of relaxation towards the base is displayed +/SEM. No significant differences between the 2 groups at any point.

5.3.4 Sodium Nitroprusside relaxation

Measurement of endothelial independent vasodilatation as assessed by quantifying vaso-relaxation in response to SNP was comparable between the groups (Figure 5.3-5, Table 18).

SNP dose (nM)	wt. mean % relaxation +/- SEM	MIGFREO mean % relaxation +/- SEM	p value
1	10.35 +/- 2.88	12.16 +/- 2.48	0.64
3	17.14 +/- 4.72	18.48 +/- 2.26	0.80
10	21.11 +/- 3.62	28.39 +/- 4.12	0.19
30	27.91 +/- 4.08	35.07 +/- 3.83	0.21
100	40.33 +/- 5.63	49.66 +/- 4.99	0.23
300	63.56 +/- 5.62	75.75 +/- 4.41	0.10
1000	88.56 +/- 4.17	97.39 +/- 3.17	0.10
3000	105.12 +/- 3.74	108.62 +/- 4.82	0.57
10000	115.82 +/- 3.44	114.62 +/- 5.88	0.86

Table 18: Assessment of endothelial independent vasodilatation with SNP. This demonstrates the direct vasodilatory response to SNP seen within the organ bath. In each group n>10 with at least 2 aortic rings for each mouse. The data is represented as mean % relaxation to base (where baseline represents 100%) +/- SEM. Corrected to 2 decimal places. No significant differences seen between the 2 groups of mice.

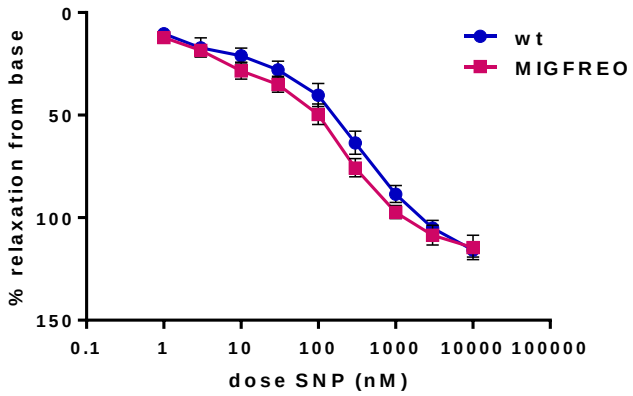

Figure 5.3-5: SNP relaxation. This demonstrates the vasodilatory response to SNP as measured within the organ bath. Each group represents n > 10 mice for each group with at least 2 rings of aorta for each mouse. Results are expressed as % of relaxation and the mean % of relaxation towards the base is displayed +/SEM. No significant differences between the 2 groups at any point.

5.3.5 PE + L-NMMA

As expected, following incubation with the NOS inhibitor L-NMMA, there is enhanced constriction in the presence of phenylephrine in wild type mice: this is also present in MIGFREO mice, and is of the same magnitude (Figure 5.3-6, Table 19). This suggests a comparable basal level of NO in the 2 groups of mice.

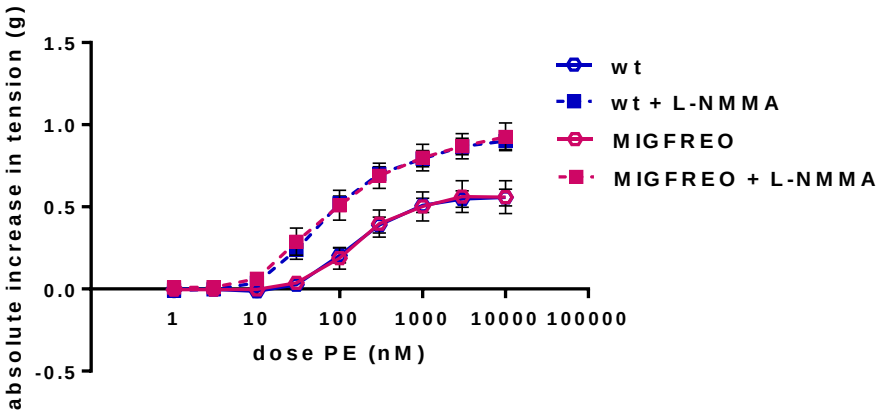

Figure 5.3-6: PE constriction +/- LNMMA. This demonstrates the absolute increase in tension (g) seen with incremental doses of phenylephrine either before or after incubation with L-NMMA. In each group n > 10 with at least 2 rings of aorta per mouse. The graph represents mean increase in absolute tension +/-SEM. In both groups, incubation with the NOS inhibitor L-NMMA was associated with increased response to phenylephrine, however there was no difference seen between wt. and MIGFREO mice.

PE dose (nM)	wt. control +/- SEM	wt. LNMMA +/- SEM	MIGFREO control +/- SEM	MIGFREO LNMMA +/- SEM	p value wt. con vs. wt. LNMMA	p value MIG con vs. MIG LNMMA	p value wt. con vs. MIG con	p value wt. LNMMA vs. MIG LNMMA
1	0.00 +/- 0.01	-0.01 +/- 0.01	-0.01 +/- 0.01	0.01 +/- 0.01	0.13	0.34	0.54	0.12
3	-0.01 +/- 0.01	-0.01 +/- 0.01	-0.01 +/- 0.01	0.01 +/- 0.01	0.94	0.22	0.80	0.26
10	-0.01 +/- 0.15	0.04 +/- 0.02	-0.01 +/- 0.01	0.06 +/- 0.02	0.03	0.01	0.60	0.32
30	0.03 +/- 0.02	0.23 +/- 0.06	0.04 +/- 0.02	0.29 +/- 0.08	0.002	0.01	0.70	0.61
100	0.20 +/- 0.04	0.52 +/- 0.05	0.19 +/- 0.07	0.51 +/- 0.09	9.1E-05	0.01	0.83	0.90
300	0.39 +/- 0.05	0.70 +/- 0.04	0.40 +/- 0.08	0.69 +/- 0.08	0.0002	0.02	0.92	0.90
1000	0.51 +/- 0.04	0.79 +/- 0.05	0.50 +/- 0.09	0.8 +/- 0.08	0.0004	0.03	0.95	0.94
3000	0.55 +/- 0.05	0.87 +/- 0.05	0.56 +/- 0.10	0.87 +/- 0.08	0.0003	0.03	0.89	0.99
10000	0.56 +/- 0.05	0.90 +/- 0.05	0.56 +/- 0.10	0.93 +/- 0.08	0.0002	0.02	0.98	0.79

Table 19: PE induced constriction pre and post incubation with L-NMMA. Tabulated results of increased tension seen in response to increasing doses of phenylephrine either pre or post incubation with L-NMMA within the organ bath. For each group n > 10 with at least 2 rings per mouse. Results are expressed as mean increase in tension +/- SEM. The results are corrected to 2 decimal places. There are no significant differences between the 2 groups at any point.

5.3.6 Western blots

Cells from 10 transgenic and 12 wt. mice were analysed. From each mouse, protein was collected from 3 wells of cells, one unstimulated, one stimulated with insulin and one stimulated with IGF-1 as described above. Gels were loaded in the same way in each experiment; wt control, wt insulin, wt IGF-1, MIGFREO control, MIGFREO insulin, MIGFREO IGF-1.

The results of the western blots to assess protein expression in PEC are shown, along with representative blots in Figure 5.3-7 and Figure 5.3-8. Although measures as discussed in the methods section were taken in an attempt to ensure that the process was robust, as can be clearly seen, there is significant variability between the different results and no difference was detected between wild type PEC and PEC derived from lungs of the MIGFREO mice. The cells from wt. mice appear to show enhanced phosphorylation of eNOS and AKT following stimulation with insulin and IGF-1, which would suggest that the doses of IGF-1 and insulin used were appropriate. There is also enhanced AKT phosphorylation in the MIGFREO mice following stimulation with IGF-1, although there is significant variation between different gels, as seen by the large SEM. Although there are some trends seen, there are no significant differences observed between MIGFREO mice and wt. mice for expression of any of the proteins, and given the large error between gels observed (in spite of repeated experiments) I suspect we are unable to draw any conclusions from the western blots. The potential reasons for this will be discussed later (see conclusion and discussion section 5.4).

As has been previously discussed, there was no difference in β actin expression between MIGFREO and wt mice when this was analysed, although some of the blots do appear to show that there may be a difference in β actin expression.

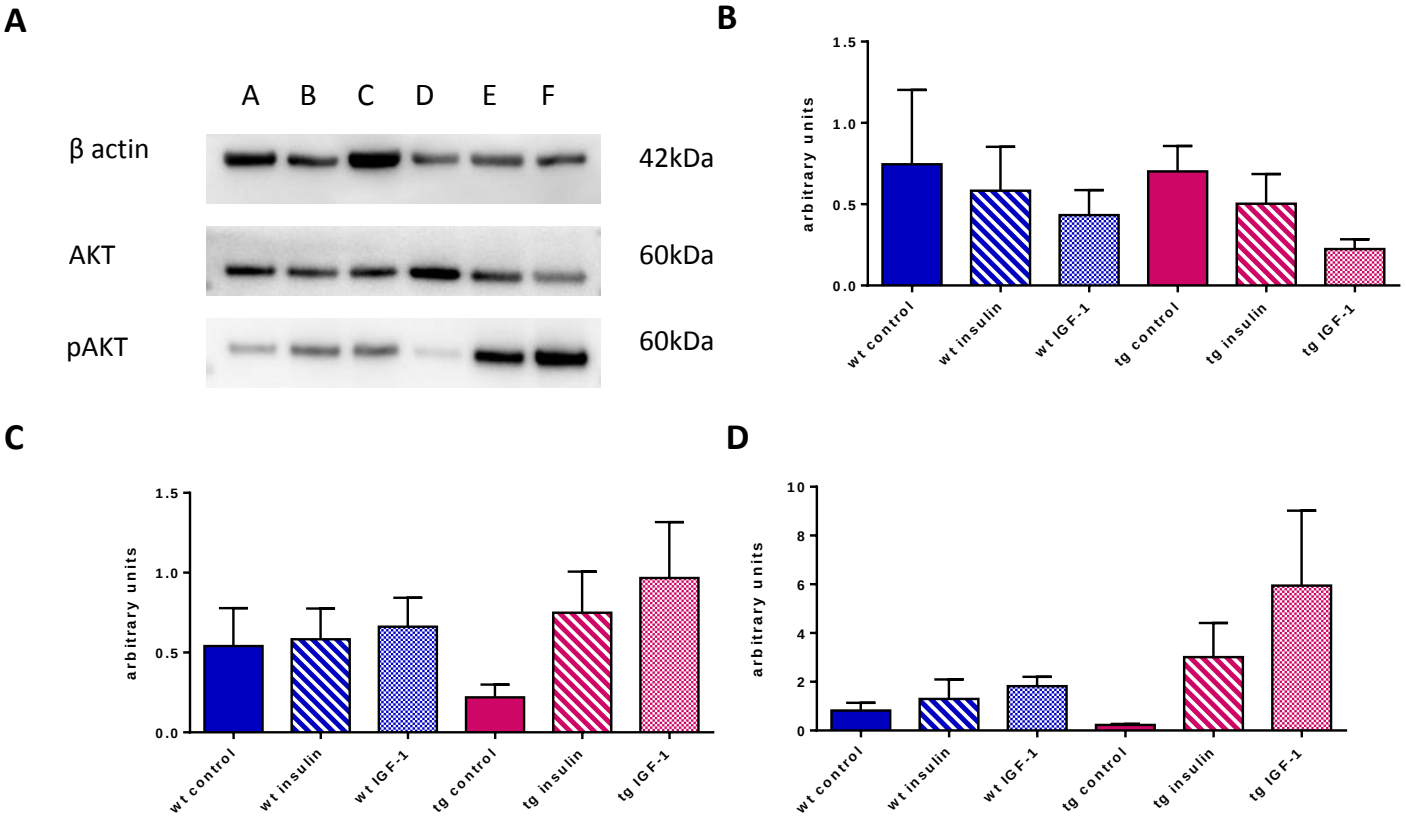

Figure 5.3-7: AKT and pAKT expression. (A) Representative blot of AKT and pAKT A = wt. control, B = wt. insulin, C = wt. IGF-1, D = MIGFREO control, E = MIGFREO insulin, F = MIGFREO IGF-1; (B) Total AKT (mean +/-SEM); (C) Total pAKT (mean +/- SEM); (D) pAKT / AKT (mean +/- SEM). Data analysed includes 10-12 samples per group

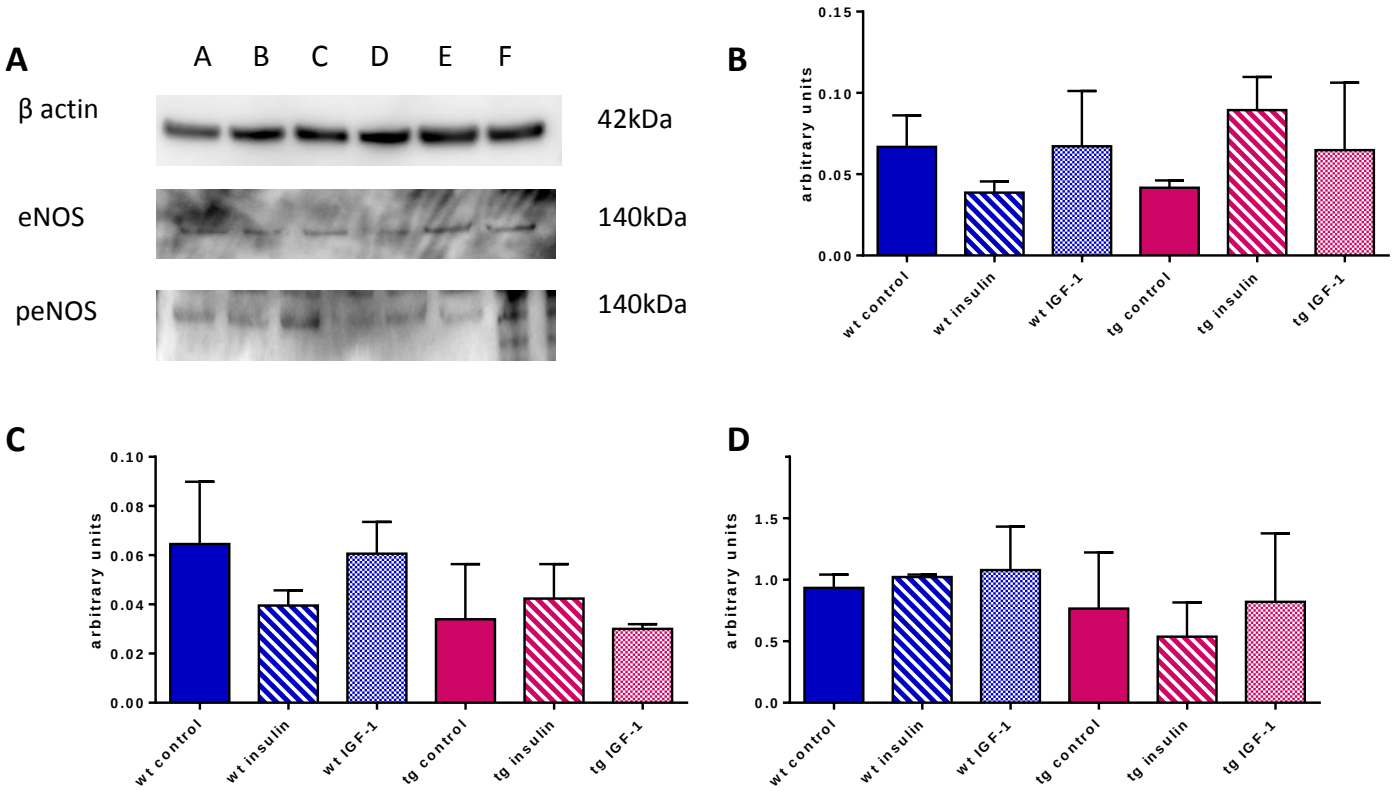

Figure 5.3-8: eNOS and peNOS expression. (A) Representative blot of eNOS and peNOS A = wt. control, B = wt. insulin, C = wt. IGF-1, D = MIGFREO control, E = MIGFREO insulin, F = MIGFREO IGF-1; (B) Total eNOS (mean +/-SEM); (C) Total peNOS (mean +/- SEM); (D) peNOS / eNOS (mean +/- SEM). Data analysed includes 10-12 samples per group.

5.3.7 eNOS activity (L-citrulline assay)

Measurement of eNOS activity demonstrated a significant reduction in insulin and IGF-1 stimulated eNOS activity in the MIGFREO mice (Figure 5.3-9, Figure 5.3-10, Table 20). Control measurements were assigned an arbitrary value of 100, and in the wt. mice insulin stimulation increased eNOS activity to 137.64 +/- 8.06, this was increased to only 104.1 +/- 4.21 in MIGFREO mice (p=0.0025). IGF-1 stimulated eNOS activity increased from 100 to 137.03 +/- 7.90 in wt. mice, this was significantly different from the increase to 105.2 +/- 6.76 (p=0.0179) seen in MIGFREO mice.

	wt. mean	MIGFREO mean	p value
Control	100	100	
Insulin	137.64 +/- 8.06	104.1 +/- 4.21	0.0025
IGF-1	137.03 +/- 7.90	105.2 +/- 6.76	0.0179

Table 20: eNOS activity in wt. and MIGFREO mice, control, insulin and IGF-1 stimulated. This represents eNOS activity in PECs at baseline and in response to insulin or IGF-1 stimuli. In each group n=4. Values shown represent mean +/SEM and are corrected to 2 decimal places. In comparison with wild type mice there is a significant blunting of insulin and IGF-1 stimulated eNOS activity seen in the MIGFREO mice ($p<0.02$ for IGF-1 stimulated eNOS activity, $p<0.01$ for insulin stimulated eNOS activity).

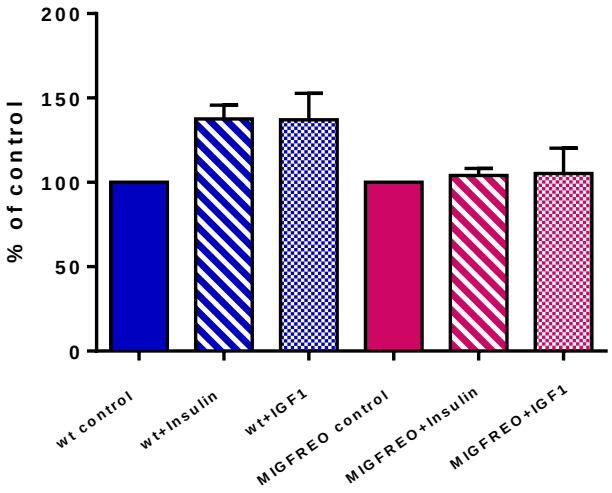

Figure 5.3-9: eNOS activity, insulin and IGF-1 stimulated, normalised to control. Mean +/- SEM. This represents eNOS activity in wt. (blue) and MIGFREO mice (pink) in response to control, insulin and IGF-1. Results are expressed as percentage of baseline activity (where control was assigned 100%). In comparison to wt. mice eNOS activity was significantly blunted in MIGFREO mice in response to stimulation from both insulin ($p < 0.01$) and IGF-1 ($p < 0.02$). N=4 per group

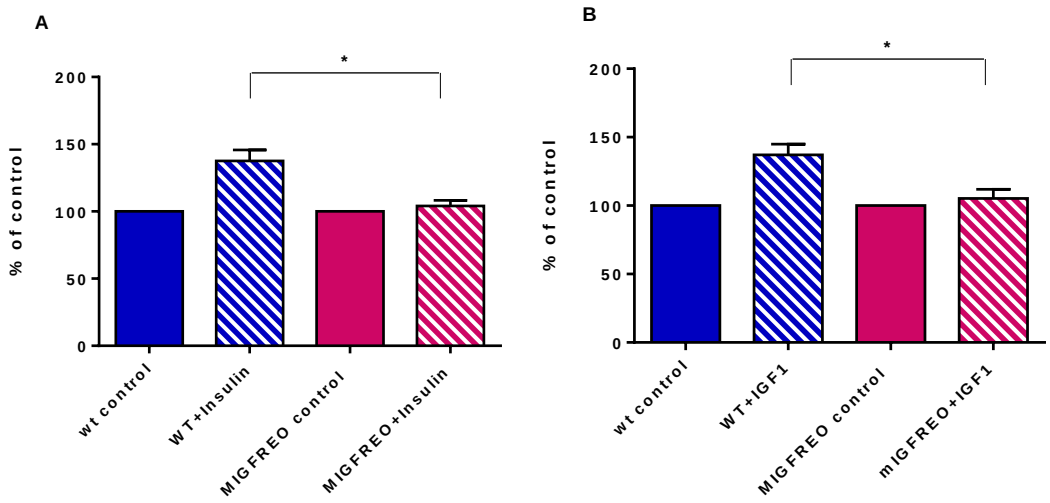

Figure 5.3-10: eNOS activity: (A) insulin stimulated (B) IGF-1 stimulated. Mean +/- SEM *$p < 0.02$. eNOS activity in PEC in both wt. (blue) and MIGFREO (pink) mice in response to insulin (graph A) and IGF-1 (graph B). This again demonstrates that in PEC derived from MIGFREO lungs there is relative resistance to the eNOS stimulating effects of both insulin and IGF-1. N = 4 per group

5.4 Conclusion and Discussion

Assessment of endothelial function

There is no evidence of change in basal NO level in MIGFREO mice as measured by response to PE following incubation with L-NMMA (Figure 5.3-6, Table 19). Following incubation with the NOS inhibitor L-NMMA both wt. and MIGFREO mice had enhanced response to PE. This is in contrast with results seen in mice with over-expression of a human functional IGF-1R on the vascular endothelium, which was associated with a significant reduction in basal NO bioavailability [210].

In addition to this observation there is no evidence of basal endothelial dysfunction as assessed by measuring vasodilatory response to ACh following constriction with PE (Figure 5.3-1, Table 15).

Measurement of endothelial independent vasodilatation as measured by response to the NO donor SNP was similar between the 2 groups (Figure 5.3-5, Table 18).

Although these organ bath experiments do not support significant endothelial dysfunction in the MIGFREO mice it is difficult state that there is normal endothelial function, particularly in view of the marked reduction of endothelial cell insulin sensitivity as will be discussed shortly. Basal NO bioavailability as assessed by response to L-NMMA appears to be comparable between the two groups although assessment of NO production in response to insulin is perhaps more pertinent to consider in these mice. Although response to ACh are also similar between the 2 groups further examination of whether some of the vasodilatory response seen in the MIGFREO mice might, in fact relate to excess production of hydrogen peroxide is necessary and will be considered in chapter 7.

MIGFREO mice have endothelial cell insulin resistance

As was hypothesised, I have demonstrated that over-expression of a non-functioning IGF-1R on the vascular endothelium is associated with endothelial insulin resistance. This is confirmed by the marked reduction in the vasodilatory response to insulin (Figure 5.3-2, Figure 5.3-3, Table 16) and the significant reduction in eNOS activity following stimulation with insulin (Figure 5.3-9, Figure 5.3-10, Table 20). Perhaps surprisingly these results were not replicated when western blots from cell lysates were performed, and although we were able to demonstrate an increase in pAKT and peNOS following stimulation with insulin in

the wt. mice, this was also seen in the MIGFREO mice and there were no significant differences seen between the 2 groups of mice.

There are several potential reasons for this apparent disparity. The PECs used to perform the eNOS activity assay were harvested at P0 in an attempt to ensure that a pure endothelial population was used; this was not possible when harvesting cell lysates for protein quantification, where the cells were used at P1 or P2. Although cells were examined to ensure an endothelial phenotype prior to stimulation with insulin or IGF-1 it is possible that using them at later stages of passage may have allowed proliferation of non-endothelial cells, or change in morphology of the cells which may have affected the results of the western blots. To ensure consistency, I would suggest that the cell lysates in future are all harvested from cells at the same stage of passage, in an attempt to reduce variability between endothelial phenotypes.

Since the detection of the phosphorylated forms of AKT and eNOS is critical to determining endothelial insulin sensitivity it may be that an alternative blocking buffer should have been used. The blocking buffer used contains skimmed milk powder (see Table 7) and it is known that the casein phosphopeptide component of milk can affect detection of phosphorylated forms of protein, and may have affected the level of background interference seen in the blots of peNOS in particular (Figure 5.3-8).

Another possible explanation for the wide variation of results seen in the western blot may be the salt content of the TBS tween used as a washing buffer. The content of salt used in our laboratory is significantly higher than that used in other laboratories, and the high salt content may have been responsible for washing off some of the antibodies with lower affinity, particularly the antibodies for phosphorylated eNOS.

Further consideration should perhaps have been considered to repeating gels on multiple occasions, although the quantity of protein extracted from the lysates may have limited the ability to repeat experiments. Repeating the experiment in triplicate would have helped to ensure that the results were more robust, more reproducible, and may have eliminated the wide confidence intervals seen in the results. Although the results displayed are the results from all gels performed, it may have been appropriate to exclude some of the results; for example if a wt sample did not display enhanced AKT phosphorylation in response to insulin (which should clearly happen) this would suggest a problem with the way in which

the sample was prepared, or the gel run and this results should perhaps have been excluded, or the experiment repeated.

MIGFREO mice show some evidence of endothelial IGF-1 resistance

The results from the eNOS activity assay (Figure 5.3-9, Figure 5.3-10, Table 20) show a significant reduction in eNOS activity stimulated by IGF-1 when comparing MIGREO with wt. littermates, which concurs with the original hypothesis. Certainly the presumed distribution of hybrid receptors on the vascular endothelium would suggest that the MIGFREO mice would have endothelial IGF-1 resistance. However the results from the organ bath and the western blots no not demonstrate any difference in IGF-1 sensitivity between the 2 subsets of mice (Figure 5.3-4, Figure 5.3-7, Figure 5.3-8, Table 17).The disparity between the eNOS activity assay and the western blots may be explained by the same factors as described above, however the absence of resistance to the vasodilatory effect of IGF-1 seen in the organ bath is more surprising, particularly given the marked resistance to insulin induced vasodilatation.

Given that the organ bath is highly likely to be prone to influence by exogenous factors, I hypothesise that this is a less sensitive way of assessing resistance to either insulin or IGF-1 than by measuring eNOS activity directly. This would not only explain why IGF-1 resistance was not demonstrated in the organ bath when it was clearly shown by the eNOS activity assay.

Although there was a difference due to the differing doses of IGF-1 used in the experiments (in organ bath direct IGF-1 relaxation assessed by using doses between 1-100nM in cell lysates the dose used was 150nM), it seems unlikely that this is the explanation. Phosphorylation of the IGF-1Rβ in is known to occur in human cardiac microvascular cells following stimulation with doses of IGF-1 10nM [223], and indeed phosphorylation of the IR occurs following the same level of stimulation with IGF-1, so the doses used in both the experiment should be sufficient to cause activation of the P13-K pathway via interaction with the IGF-1R, IR and hybrid receptor. I would therefore suggest that the dose of IGF-1 used is not an adequate explanation for the differences in results seen.

The development of endothelial insulin and IGF-1 resistance in MIGFREO mice

The presence of endothelial insulin and to a lesser extent IGF-1 resistance, in the MIGFREO mouse concurs with my original hypothesis which was generated in response to the available literature:

- It is known that IGF-1 an insulin receptors form hybrid receptors, which are relatively resistant to activation by insulin [205, 206, 212, 213, 221-223]
- Reduction of numbers of IGF-1R on vascular endothelium is associated with reduction in hybrid formation in combination with enhanced endothelial insulin sensitivity and the converse is true; increased numbers of IGF-1R on the vasculature leads to increased expression of hybrid receptors and reduction in endothelial insulin sensitivity [209, 210].
- Mutation of the IGF-1R at a single base renders the IGF-1R inactive, although IGF-1R with this mutation are able to form hybrid receptors with mouse insulin receptors [306, 311, 312, 321].
- Both halves of the IGF-1R, IR or hybrid receptor need to be active to allow for crosstalk between the two receptor halves, and to allow activity of the kinase domain of the receptors [215].

Using this information we hypothesised that expression of the non-functional IGF-1R on the vascular endothelium of the MIGFREO mice would lead to increased generation of hybrid receptors, a significant proportion of which would be non-functional which would subsequently lead to endothelial resistance to the effects of insulin and IGF-1. If we consider that the endothelium is already comparatively insulin resistant the MIGFREO mice would therefore be expected to have relatively profound endothelial insulin resistance, with less marked IGF-1 resistance. This may well account for the lack of resistance to IGF-1 in the organ bath.

Chapter 6: Metabolic Assessment

6 Metabolic assessment

6.1 Introduction

In addition to any effect on endothelial insulin sensitivity it is crucial to understand whether expression of an endothelial specific non-functioning IGF-1R has an effect on whole body insulin sensitivity.

Fernandez *et al* [306] demonstrated that expression of a human IGF-1R with the same K1003R mutation as the MIGFREO mouse limited to muscle was associated with a profound effect on glucose homeostasis; the mice developed muscle specific and systemic insulin resistance and developed frank diabetes at a young age. Interestingly muscle specific knockout of the IR [305] in the MIRKO mouse exhibited a milder phenotype with only mild insulin resistance, which serves to illustrate the importance of signalling through IGF-1R in determining cellular insulin sensitivity. Skeletal muscle is one of the major sites of insulin mediated glucose disposal, so it is not surprising that manipulation of the IGF-1R on muscle has an effect on whole body insulin sensitivity. The relationship between endothelial and systemic insulin sensitivity is more complex.

As was discussed earlier, endothelial insulin sensitivity has a theoretical role to play in determining whole body insulin sensitivity, primarily by the action of insulin in determining blood flow, and insulin delivery via the interstitium to skeletal muscle (chapter 1.11). Kubota *et al* [304] demonstrated that endothelial cell insulin resistance was associated with impaired insulin stimulated micro-capillary recruitment, reduced insulin mediated glucose disposal and whole body insulin resistance. This strongly supports a role for the endothelium in determining whole body insulin sensitivity.

Changes in endothelial cell insulin sensitivity have also been shown to be associated with changes in fat metabolism [326] and blood pressure regulation [303] and hence in addition to assessing endothelial insulin sensitivity and endothelial function in MIGFREO mice, I will also examine blood pressure, and to a lesser extent fat metabolism.

In addition to assessing plasma insulin and IGF-1 levels I will also briefly examine plasma adipokine profile. Adiponectin is well known to correlate with whole body insulin sensitivity and recently has been demonstrated to enhance insulin sensitivity in hepatocytes via interaction with IRS [341]. Given that there is a strong relationship between adiponectin and whole body insulin sensitivity, we felt that knowing whether there was a significant difference in plasma adiponectin level between the 2 groups of mice would be a useful

experiment, particularly given the previously demonstrated difference in endothelial insulin sensitivity.

There is some evidence (although the exact relationship is not yet determined), that there is interplay between the IGF-1 system and systemic leptin levels, particularly in humans with altered insulin sensitivity [340]. We therefore felt that it was reasonable to ensure that there was no significant difference in plasma leptin levels between the MIGFREO and wt mice. This was done in order to eliminate the possibility that any observed changes in insulin sensitivity were not coupled with significant changes in plasma leptin levels. Any observed differences would have prompted a closer examination of fat metabolism than was originally intended.

6.2 Methods

6.2.1 Weight

Animals were weighed weekly, at 0900h, in an attempt to minimise variation.

Following a Schedule 1 procedure, organs and fad pad were swiftly excised and weighed.

6.2.1.1 Fat cell size

Fat samples were fixed and prepared by Miss Anna Skroma. Slides were examined and analysed by myself.

Adipose tissue was fixed in 4% paraformaldehyde (Sigma-Aldrich®) in PBS with pH corrected to 7.0. Samples were trimmed and placed in cassettes and processed for 17 hours in a Semi-enclosed Benchtop Tissue Processor Leica TP1020 (Leica Biosystems). The following day the samples were embedded into paraffin in TES99 tissue embedding system (Medite Medizintechnik). Once embedded into paraffin the blocks were sectioned into 5 micron slices on the Rotary Microtome Leica RM2235 (Leica Biosystems). Sections were mounted onto slides and dried overnight at 50°C. The following day the samples were stained with Haemotoxylin (Sigma-Aldrich®) and Eosin (Sigma-Aldrich®) stain.

Slides with samples of fat were examined at x20 magnification on a BX41 microscope (Olympus) and images taken using a Qicam Imaging Fast 1394 digital camera (QImaging®). A field of view with minimal blood vessels and limited broken cells was used and cells counted and fat cell size analysed using commercially available Image Pro-Plus 7.0 software (MediaCybernetics®).

6.2.2 Glucose tolerance test

Male mice (both MIGFREO and their wild-type litter mates), between the ages of 10 -14 weeks were fasted overnight. The following morning they were weighed and placed into humane restraint apparatus. To assess baseline blood glucose a drop of blood was taken from a tail vein and analysed using the Accu-Chek® (Aviva) glucose testing strips and glucometer. Next, the mice received an intra-peritoneal injection of 1mg glucose per gram of body weight. Blood glucose was measured at 30, 60, 90 and 120 minutes following the intraperitoneal injection using an identical method to assessing the baseline glucose.

6.2.3 Insulin tolerance test

Male mice were fasted for 4 hours. Baseline glucose was measured as above. Next, the mice received an intra-peritoneal injection of insulin (Actrapid Novo nordisk) at a concentration of 0.75iu per kilogram of body weight. Blood glucose was measured at 30, 60, 90 and 120 minutes as above.

6.2.4 Insulin-like growth factor tolerance test

Male mice were fasted for 4 hours. Baseline glucose was measured as above. Next, the mice received an intra-peritoneal injection of IGF-1 (GroPep) at a concentration of 0.75μg of IGF-1 per gram of body weight. Blood glucose was measured at 30, 60, 90 and 120 minutes as above.

6.2.5 Plasma insulin concentration

6.2.5.1 Plasma collection

Random samples were collected by cardiac puncture following the mouse undergoing a Schedule 1 procedure. Blood was collected into Microvette® CB 300 K2E Di-Kallum EDTA tubes (Sarstedt AG & Co) and was kept on ice and immediately transferred to the laboratory where it was placed in a centrifuge and spun at 6000rpm for 6 minutes. The plasma was transferred to an eppendorf and frozen at -20^{o}C.

6.2.5.2 Insulin ELISA

Assessment of plasma insulin levels was made using the Ultra-Sensitive Mouse Insulin ELISA Kit (Crystal Chem Inc.). In accordance with the manufacturers' instructions insulin standards were prepared to give concentrations of 0.1, 0.2, 0.4, 0.8, 1.6, 3.2 and 6.4ng/ml. Using the supplied "Antibody-coated microplate" (coated with guinea-pig anti-insulin antibody) 95μl of the sample diluent provided by the manufacturer were added to each well of the microplate, in addition to 5μl of either the sample or the insulin standard. Samples were assessed in duplicate. The microplate was covered and incubated at 4^{o}C for 2 hours.

Following the incubation period the contents of the well were aspirated and wells were washed 5 times using 300μl of the wash buffer contained in the kit. 100μl of the supplied horse radish peroxidise conjugated anti-insulin antibody was added to each well, and the microplate covered and incubated for 30 minutes at room temperature.

The well contents were aspirated and washed in the manner described above. 100μl of the provided "enzyme substrate solution" (3,3',5,5'-tetramethylbenzidine (TBA)) was added to each well and the microplate incubated for 40 minutes at room temperature without exposure to light.

The enzyme reaction was stopped by adding 100μl of the "enzyme reaction stop solution" (1N sulphuric acid) to each well and the absorbance was immediately measured using a MRX TC microplate reader (Dynax technologies) at 450/620nm using Revelation software package (Dynax Technologies).

6.2.6 Plasma insulin-like growth factor type 1 concentration

6.2.6.1 Plasma collection

Blood samples were collected and stored as above.

6.2.6.2 Insulin-like growth factor-1 ELISA

Assessment of plasma IGF-1 levels was made using the Mouse IGF-1 High Sensitivity ELISA (Immunodiagnostic Systems Ltd.). Calibration samples were supplied reconstituted, as were 2 control samples. Initially10μl of the sample or the supplied control was placed to an eppendorf to which was added 50μl of the provided "releasing agent" (proprietary reagent for dissociating IGF-1 from binding proteins). Following a brief mix the samples or controls were incubated at 18-25^{o}C for 10 minutes. Following incubation, 1ml of the provided "sample diluent" (phosphate buffer containing protein and 0.09% sodium azide) was added to each eppendorf. 50μl of control, sample or calibration sample were added to a well in the supplied antibody coated 96 well plate. Each sample was assessed in duplicate. 100μl of the supplied "antibody biotin" (PBS with polyclonal goat anti-mouse IGF-1 antibody) was added to all wells. The plate was covered with adhesive plate sealer and incubated on an orbital shaker at room temperature for 1 hour at 500-700rpm.

Following incubation the well contents were aspirated and washed with 250μl of wash solution (PBS with Tween). This was repeated 2 further times. 150μl of the supplied "enzyme conjugate" (PBS containing avidin linked to horseradish peroxidise, protein, enzyme stabilisers and preservative) was added to each well and incubated at room temperature for 30 minutes on the orbital shaker at 500-700rpm.

The wash step was repeated as described above. 150µl of TMB substrate (proprietary aqueous formulation of TBA and hydrogen peroxide) was added to each well. The plate was incubated without exposure to light for 30 minutes at room temperature.

50µl of stop solution (0.5M hydrochloric acid) was added to each well, and absorbance was immediately read using a plate reader. MRX TC microplate reader (Dynax technologies) at 450/620nm using Revelation software package (Dynax Technologies).

6.2.7 Plasma adiponectin measurement

6.2.7.1 Plasma collection

Blood samples were collected and stored as above.

6.2.7.2 Adiponectin ELISA

Assessment of plasma adiponectin levels was made using the Mouse Adiponectin ELISA kit (EMD Millipore). Standards were prepared using the supplied mouse adiponectin standard and sequentially diluted with 1:10 assay buffer (0.05M phosphosaline, pH 7.4 containing 0.025M EDTA, 0.08% sodium azide, 0.05% Triton X100 and 1% BSA) to achieve final dilutions of 1 in 2, 1 in 4, 1 in 8, 1 in 16, 1 in 32, 1 in 62 and 1 in 128.

The supplied 96 well microtitre plate (coated with pre-titered capture antibodies) was washed with 3x300µl of a 1:10 dilution of the supplied HRP wash buffer (50nM Tris Buffered Saline with Tween 20). 60µl of a 1:10 dilution of assay buffer was added to background, standard and quality control wells. A further 20µl of 1:10 assay buffer was added to blank wells; 20µl of either unknown samples, quality control samples or standards (reconstituted mouse adiponectin standard) were added in duplicate to appropriate wells. 20µl of detection antibody (pre tittered biotinylated goat anti-mouse adiponectin polyclonal antibody) was added to all wells and the plate was covered and left at room temperature on an orbital shaker (400-500rpm) for 2 hours.

Contents of the wells were aspirated and the wells were washed with 5x300µl of 1:10 wash buffer. 100µl of enzyme solution (pre tittered streptavidin horseradish peroxidise conjugate in buffer) was added to each well and the plate was sealed and left on an orbital plate shaker (400-500rpm) for 30 minutes. Solutions were decanted and the wells were washed as described above.

100µl of substrate solution (3,3',5,5'-tetramethylbenzidine (TBA)) was added to each well, the plate was covered and placed on an orbital plate shaker for 5-20 minutes, at which point a blue colour had formed in wells. Once colour was deemed to have changed sufficiently, the enzyme reaction was stopped by adding 100µl of the "stop solution" (0.3M HCl) to each well. The absorbance was immediately read using a Spectra Max 190 plate reader (Molecular Devices) at 450/590nm. A standard curve was produced using GraphPad Prism software and concentrations were measured using the standard curve. Quality control was measured by ensuring that the supplied quality control samples fell within the expected range.

6.2.8 Plasma leptin measurement

6.2.8.1 Plasma collection

Blood samples were collected and stored as above.

6.2.8.2 Leptin ELISA

Assessment of plasma leptin levels was made using the Mouse Leptin ELISA Kit (EMD Millipore). The supplied 96 well microtitre plate (coated with pre-titered capture antibodies) was washed with 3x300µl of a 1:10 dilution of the supplied HRP wash buffer (50nM Tris Buffered Saline with Tween 20). 30µl of "Assay buffer" (0.05M phosphosaline, pH 7.4 containing 0.025M EDTA, 0.08% sodium azide, 0.05% Triton X100 and 1% BSA was added to background, standard and quality control wells; 40µl of assay buffer was added to sample wells. 10µl of "matrix solution" (0.08% sodium azide) was added to background, standard and quality control wells. 10µl of "assay buffer" was added to background wells, and 10µl of either leptin standards (0.2, 0.5, 1, 2, 5, 10, 20, 30ng/ml), reconstituted quality control standards (peptides including leptin) or unknown samples were added in duplicate to appropriate wells. 50µl of supplied "antiserum solution" (pre-titered anti-rodent leptin serum) was added to each well. The plate was sealed and incubated at room temperature on a microplate shaker at 400rpm for 2 hours.

Following the incubation period the contents of the well were aspirated and wells were washed 3 times using 300µl of the 1:10 dilution of wash buffer. 100µl of "detection antibody" (pre-titered biotinylated anti-mouse leptin antibody) was added to each well. The plate was sealed, and placed on a microplate shaker at 400rpm for 1 hour.

The well contents were aspirated and washed as above. 100µl of "enzyme solution" (pre-titered streptavidin-horseradish peroxidise conjugate in buffer) was added to each well; the plate was sealed, placed on the microplate shaker as above and was incubated at room temperature for 30minutes.

The well contents were aspirated and washed in the manner described above. 100µl of the provided "substrate solution" (3,3',5,5'-tetramethylbenzidine (TBA)) was added to each well and the microplate incubated for approximately 5-20 minutes. Once colour was deemed to have changed sufficiently, the enzyme reaction was stopped by adding 100µl of the "stop solution" (0.3M HCl) to each well. The absorbance was immediately read using a Spectra Max 190 plate reader (Molecular Devices) at 450/590nm. A standard curve was produced using GraphPad Prism software and concentrations were measured using the standard curve. Quality control was measured by ensuring that the supplied quality control samples fell within the expected range.

6.2.9 Plasma Free Fatty Acid measurement

6.2.9.1 Plasma collection

Blood samples were collected and stored as above.

6.2.9.2 Free Fatty Acid Quantification

Assessment of free fatty acid (FFA) was made using the Free Fatty Acid Quantification Kit (abcam®) in accordance with the manufacturer's instructions.

6.2.9.3 Protocol Optimisation

Although the kit has previously been used to assess mouse plasma FFA levels [327] in published studies, we have not previously used this kit in our laboratory, and therefore the protocol required some optimisation prior to use. Of particular interest was the amount of plasma sample required to fall within the specified standard range.

Plasma samples were diluted in the supplied assay buffer to achieve either 1:1, 1:2, 1:5, 1:10, 1:25 or 1:10 dilution and 50µl of each dilution was added to a 96 well plate in duplicate. Standards and blanks were added to the plate in duplicate to generate 0,2,4,6,8,10 nmol/well of palmitic acid (from the supplied 1nmol/µl palmitic acid standard and the supplied assay buffer).

2µl of ACS reagent (Acyl-CoA) was added to each well, and the plate was incubated at 37°C for 30minutes.

A mastermix containing 44µl of assay buffer, 2µl of supplied fatty acid probe, 2µl of supplied enzyme mix and 2µl of supplied enhancer was added to each well. The reaction was incubated at 37°C for 30 minutes protected from light.

Optical density was measured at 570nm using a Spectra Max 190 plate reader (Molecular Devices). Background readings were subtracted from all standard and sample readings. A standard curve (R^2=0.999) (Figure 6.2-1) was generated using GraphPad Prism software, and the sample readings were used to derive FFA amount per well. Concentration of FFA in nmol/µl = nmol per well / sample volume.

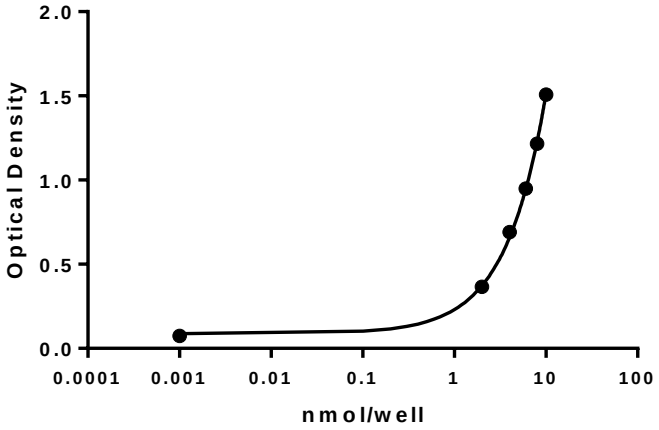

Figure 6.2-1: Standard Curve generated from optimisation experiment. Curve generated by using supplied standards. R2=0.999

6.2.9.4 Experimental protocol

Data from optimisation experiment suggested that 5-10µl per sample would be the optimum sample quantity to use. Experiment was repeated using 10µl sample volume in triplicate. Standard curves were repeated for each individual experiment.

6.2.10 Plasma Triglyceride Measurement

6.2.10.1 Plasma collection

Blood samples were collected and stored as above.

6.2.10.2 Triglyceride Quantification

Plasma triglyceride was measured using the Triglyceride Quantification Kit (abcam®) and was performed in accordance with the manufacturer's instructions. The supplied Triglyceride standard (1mM) was heated in a water bath at 80-100°C for 1 minute and vortexed for 30 seconds; this was repeated once, to ensure that the triglyceride standard retuned to solution. The supplied triglyceride probe (in anhydrous DMSO) was heated to 37°C for 1-5 minutes to melt the DMSO. The supplied triglyceride enzyme mix was dissolved in 200µl of assay buffer. The supplied lipase was dissolved in 220µl of assay buffer.

In order to prepare a standard curve, 40µl of 1mM triglyceride standard was dilute into 160µl of assay buffer, generating 0.2mM triglyceride standard. Either 0, 10, 20, 30, 40 or 50µl of 0.2mM triglyceride standard was added in duplicate to a 96 well plate, the volume was adjusted to 50µl with assay buffer, generating 0, 2, 4, 6, 8, 10nmol/well of triglyceride standard.

The plasma to be analysed was diluted 1 in 2 and 50µl of each diluted plasma sample was added in duplicate to the 96 well plate.

2µl of lipase was added to each standard and sample and the reaction was incubated for 20 minutes at room temperature. 50µl of reaction mix (containing 46µl of assay buffer, 2µl of triglyceride probe and 2µl of triglyceride enzyme mix) was added to each standard and sample. The reaction was incubated for 60 minutes protected from light on an orbital plate shaker at 300rpm.

The absorbance was immediately read using a Spectra Max 190 plate reader (Molecular Devices) at 570nm. A standard curve was produced using GraphPad Prism software and concentrations were measured using the standard curve. The background blank reading was subtracted from all readings. Results were corrected, taking into account the initial 1 in 2 dilution of the plasma.

6.2.11 Blood pressure measurement

Blood pressure was measured non-invasively by determining the tail blood volume with a volume pressure recording sensor and an occlusion tail-cuff (CODA System, Kent Scientific, Torrington) (Figure 6.2-2). Volume pressure recording (VPR) has been shown to provide an accurate assessment of blood pressure when compared with invasive radio-telemetry monitoring (long considered to be the gold standard method of assessing blood pressure in experimental rodents), with the major advantage being that it is non-invasive [310].

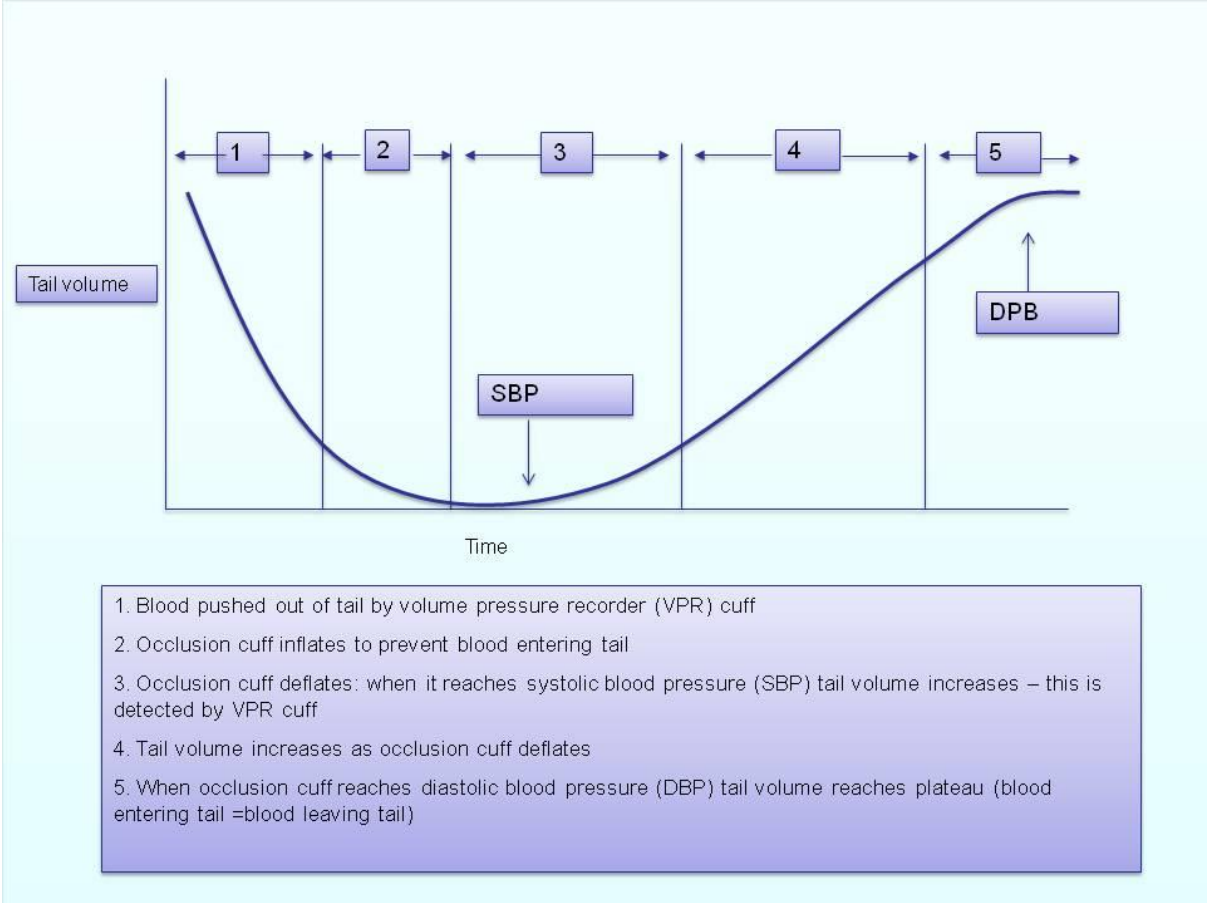

Figure 6.2-2: Diagram depicting basis by which volume pressure recording measures blood pressure. 1) Blood is pushed out of the tail by the VPR cuff; 2) Occlusion cuff inflates to prevent blood from entering it; 3) occlusion cuff deflates, when it reaches systolic blood pressure tail volume increases, which is detected by the cuff; 4) tail volume increases as occlusion cuff deflates; 5) occlusion cuff reaches diastolic blood pressure and tail volume reaches plateau phase.

The animals were acclimatised to the procedure by placing them in the restraining apparatus for 3, 10-20 minute periods on separate days before measurements were taken. When measurements were due to be taken the animals were placed in room heated to 26^{o}C or above for 30 minutes to warm and were placed in the restraining apparatus for a further 15 minutes to acclimatise. This was done in accordance with the manufacturers' instructions. Following 5 acclimatisation inflations, 15 measurements of blood pressure were taken. Measurements were repeated 2 further times within a week period to establish an average blood pressure recording per mouse.

6.2.12 Statistics

Results are expressed as mean +/- SEM. Comparative analysis within groups was performed using paired Student t test; between groups unpaired Student t test. $P < 0.05$ was considered to be statistically significant.

6.3 Results

6.3.1 Weight

There were no significant differences between the total body weight (Figure 6.3-1**,** Table 21) organ weight (Figure 6.3-2**,** Table 22) or fad pad weight (Figure 6.3-2, Table 22) between the MIGFREO mice and the wt. mice, although there was a non-significant trend towards the MIGFREO mice being heavier, this was most marked at 8 weeks and persisted until 18 weeks.

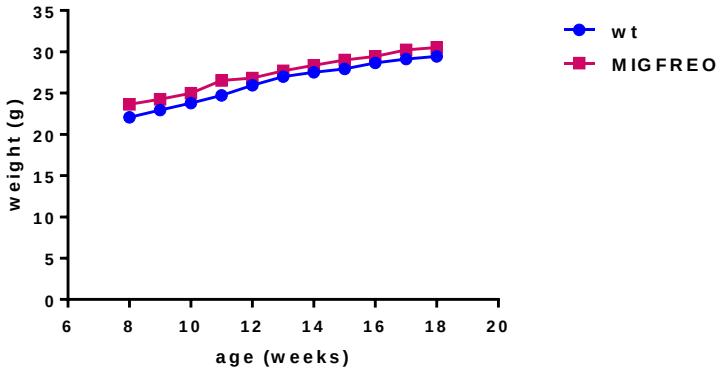

Figure 6.3-1: Body weight. Mean +/- SEM body weight of wt. (blue) and MIGFREO (pink) mice at weeks 8-18. N > 30 in each group. No significant differences between the 2 groups of mice were detected at any stage.

Age (weeks)	wt. mean +/- SEM (n=32)	MIGFREO mean (n=33)	p value
8	22.08 +/- 0.55	23.64 +/- 0.70	0.10
9	22.95 +/- 0.58	24.27 +/- 0.71	0.17
10	23.74 +/- 0.71	24.99 +/- 0.74	0.23
11	24.69 +/- 0.73	26.54 +/- 0.93	0.13
12	25.93 +/- 0.70	26.83 +/- 0.75	0.40
13	26.99 +/- 0.79	27.71 +/- 0.82	0.53
14	27.51 +/- 0.80	28.37 +/- 0.67	0.41
15	27.93 +/- 0.84	29 +/- 0.85	0.38
16	28.61 +/- 0.81	29.45 +/- 0.90	0.49
17	29.13 +/- 0.81	30.23 +/- 0.84	0.35
18	29.44 +/- 0.79	30.53 +/- 0.78	0.33

Table 21: Mean total body weight. Corrected to 2 decimal places. Mean +/- SEM body weight between weeks 8-18. No significant differences were seen between the 2 groups of mice.

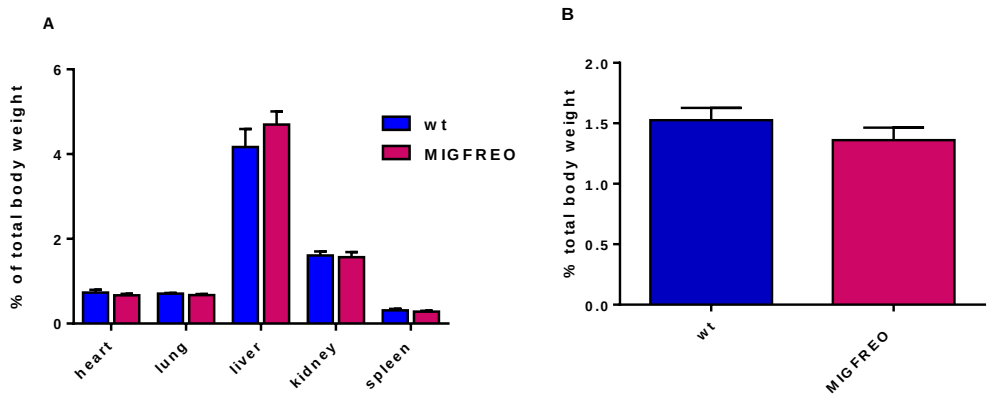

Figure 6.3-2: (A) Organ weight; (B) Fat pad size. Expressed as percentage of total body weight. Mean +/- SEM. No differences between wt. (blue) and MIGFREO (pink) mice for weight of organ or fat pad. N=6

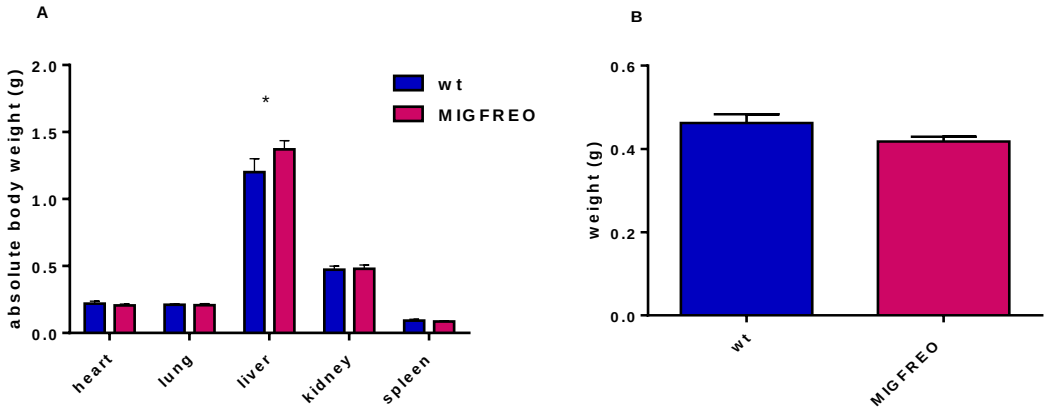

Figure 6.3-3. (A) Organ weight; (B) Fat pad size. Absolute weight. Mean +/- SEM. No differences between wt. (blue) and MIGFREO (pink) mice for weight of organ or fat pad. N=6. *p=0.22

Organ	wt. mean +/- SEM (n=6) (% TBW)	MIGFREO mean +/- SEM (n=6) (% TBW)	p value	wt. mean +/- SEM (n=6) (weight (g))	MIGFREO mean +/- SEM (n=6) (weight (g))	p value
Heart	0.73 +/- 0.06	0.67 +/- 0.03	0.34	0.22 +/- 0.02	0.21 +/- 0.01	0.53
Lung	0.71 +/- 0.02	0.67 +/- 0.03	0.36	0.21 +/- 0.01	0.21 +/- 0.01	0.82
Liver	4.17 +/- 0.43	4.70 +/- 0.31	0.37	1.20 +/- 0.09	1.37 +/- 0.06	0.22
Kidney	1.61 +/- 0.10	1.57+/- 0.12	0.84	0.47 +/- 0.03	0.48 +/- 0.03	0.90
Spleen	0.31 +/- 0.04	0.28 +/- 0.02	0.47	0.09 +/- 0.01	0.09 +/- 0.005	0.55
Epididymal fat pad	1.52 +/- 0.20	1.36 +/- 0.20	0.29	0.46 +/- 0.03	0.41 +/- 0.02	0.11

Table 22: Organ weight. Corrected to 2 decimal places. No differences between wt. and MIGFREO mice for weight of organ or fat pad.

6.3.2 Fat cell size

Analysis of epididymal fat cell size and number does not demonstrate any significant difference between the MIGFREO and wt. mice. There is no clear difference in morphology between the 2 groups.

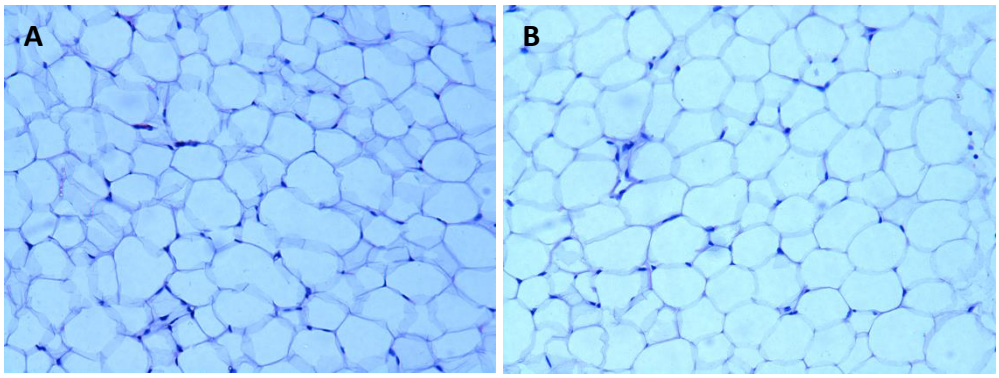

Figure 6.3-4: Fat cell size from (A) wild type mouse and (B) MIGFREO mouse. Comparable pictures taken from direct light microscopy at x 20. Fat cells stained with standard haematoxylin and eosin stain.

	wt. mean +/- SEM (n=4)	MIGFREO mean +/- SEM (n=8)	p value
Fat cell size (arbitrary units)	745126.7 +/- 57501.85	866908.8 +/- 78926.85	0.34
Fat cell number	92 +/- 9.42	80.63 +/- 21.93	0.35

Table 23: Fat cell size and number. Number of cells was determined by examining 3 different fields of view at x 20 with minimal blood vessels per sample. Mean per sample was calculated and then this repeated for the remaining samples. Cell size was determined by examining cells at x20 magnification and using computer software to assess cell size. Again this was done for 3 fields of view per sample and a mean derived for each sample. Cell size is represented by arbitrary units as determined by software. Corrected to 2 decimal places. No significant differences seen in either cell size of cell number between the wt. or MIGFREO mice. N=6 per group

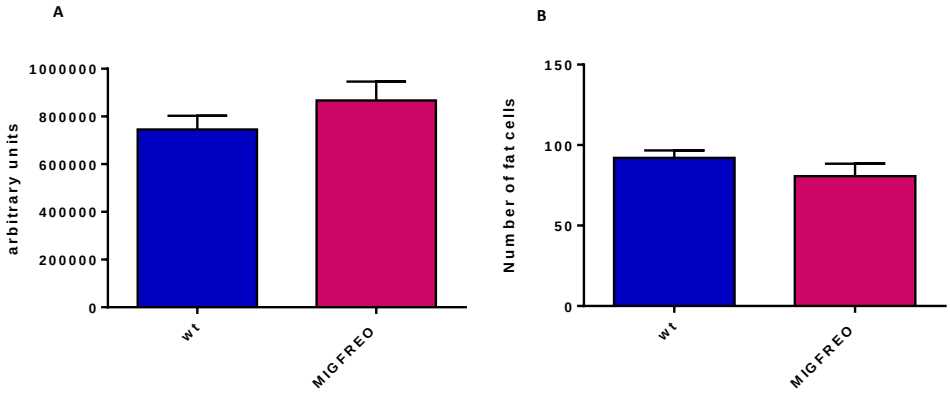

Figure 6.3-5: (A) Fat cell size; (B) Fat cell number. Mean +/- SEM for both cell size (mean cell size) and cell number (per x20 magnification per field of view). No differences seen between the wt. (blue) and MIGFREO (pink) mice.

6.3.3 Glucose tolerance

There were no significant differences between the MIGFREO mice and wt. mice when considering their response to an intra-peritoneal injection of glucose. Both mice were seen to respond to the injection with an initial spike in blood glucose after 30 minutes post injection (as would be expected), with a gradual fall towards baseline blood glucose over the following 90 minutes. This was true for both absolute blood glucose (Figure 6.3-6**,**

Table **24**), and percentage change in blood glucose (Figure 6.3-7**,** Table 25). Unsurprisingly this also equated to no significant difference seen in the area under the curve for the glucose tolerance test (Figure 6.3-8, Table 26).

In addition to the similar responses seen during the glucose tolerance test, there were no significant differences between baseline (fasted) blood glucose between the MIGFREO and wt. littermates (7.11 mmol/l +/- 0.25 vs. 7.08 mmol/l +/- 2.27 respectively). (Figure 6.3-9)

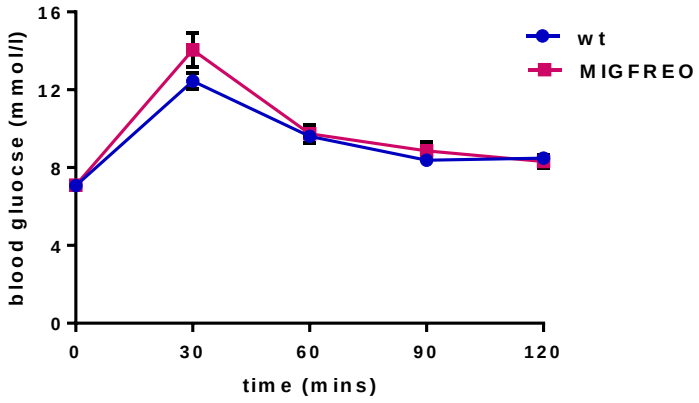

Figure 6.3-6: Glucose tolerance test (absolute). This demonstrates the absolute blood glucose seen during a glucose test at time points following an intra-peritoneal injection of glucose. The lines represent the mean blood glucose +/- SEM for both wt. (blue) and MIGFREO (pink) mice. N=18 per group. No significant differences observed between the 2 groups.

Time (mins)	wt. mean +/- SEM (n=18)	MIGFREO mean +/- SEM (n=18)	p value
0	7.08 +/- 0.27	7.11 +/- 0.25	0.94
30	12.45 +/- 0.43	14.05 +/- 0.86	0.11
60	9.6 +/- 0.29	9.74 +/- 0.47	0.80
90	8.38 +/- 0.27	8.87 +/- 0.46	0.37
120	8.48 +/- 0.30	8.32 +/- 0.35	0.72

Table 24: Blood glucose (absolute). Table of mean +/- SEM blood glucose following an intra-peritoneal injection of glucose in wt. and MIGFREO mice. Corrected to 2 decimal places. No significant differences between the 2 groups.

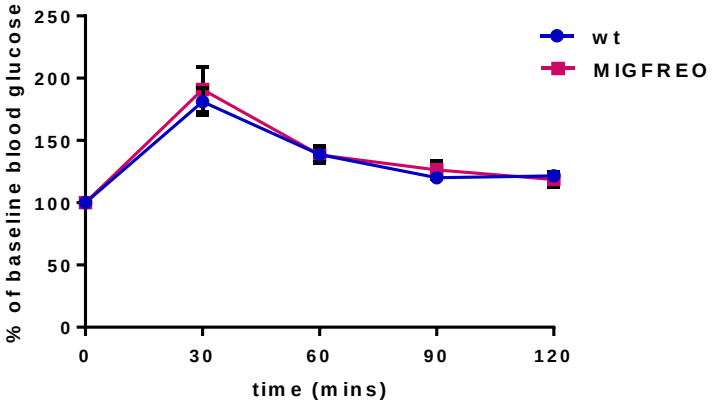

Figure 6.3-7: Glucose tolerance test (% baseline). This demonstrates the blood glucose expressed as a percentage of the baseline blood glucose seen during a glucose test at time points following an intra-peritoneal injection of glucose. The lines represent the mean blood glucose +/- SEM for both wt. (blue) and MIGFREO (pink) mice. N=18 per group. No significant differences observed between the 2 groups.

Time (mins)	wt. mean +/- SEM (n=18)	MIGFREO mean +/- SEM (n=18)	p value
0	100	100	
30	181.22 +/- 10.47	190.97 +/- 17.66	0.64
60	138.58 +/- 5.93	138.50 +/- 6,74	0.99
90	120.05 +/- 4.08	126.28 +/- 7.10	0.45
120	121.55 +/- 4.85	118.70 +/- 5.86	0.71

Table 25: Blood glucose (percentage of baseline). Table of mean +/- SEM blood glucose expressed as a percentage of baseline blood glucose following an intra-peritoneal injection of glucose in wt. and MIGFREO mice. Corrected to 2 decimal places. No significant differences between the 2 groups.

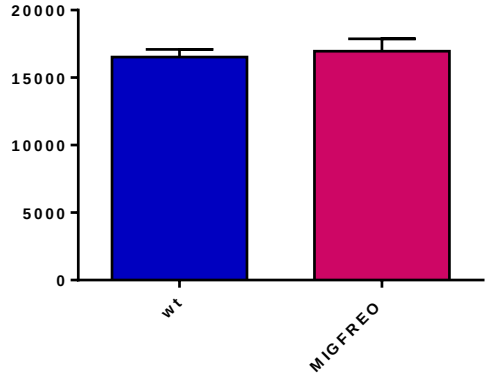

Figure 6.3-8: Area under curve of glucose tolerance test. Using graph pad prism software area under the curve was calculated for each individual glucose tolerance test and the then a mean calculated for wt. (blue) and MIGFREO (pink) mice. The Mean +/- SEM is shown. N=18 for each group. No significant differences between the 2 groups were seen.

	wt. mean +/- SEM	MIGFREO mean +/- SEM	p value
GTT area under curve	16518.78 +/- 571.49	16953.11 +/- 925.13	0.69
ITT area under curve	3743 +/- 250.4	4706 +/- 300.6	0.02
IGF-1T area under curve	2933 +/- 367.7	3837 +/- 300.2	0.07

Table 26: Area under curve of tolerance tests (calculated from percentage change). Using graph pad prism software area under the curve was calculated for each individual tolerance test and then a mean calculated for the wt. and MIGFREO groups. The mean +/-SEM is displayed and this is corrected to 2 decimal places. There was no difference in the AUC for the glucose tolerance test. There was a strong trend to enhanced IGF-1 sensitivity in the MIGFREO mice (p=0.07). The AUC of the ITT demonstrated significantly enhanced insulin sensitivity in the MIGFREO mice when compared to the wt. mice (p=0.02). N=15-24 per group

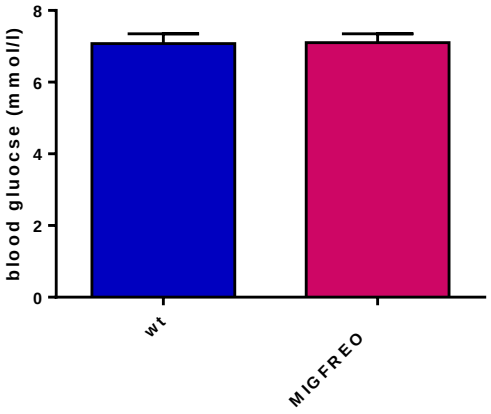

Figure 6.3-9: Fasted blood glucose. Mean fasting glucose +/- SEM in wt. (blue) and MIGFREO (pink) mice. No difference seen between the 2 groups. N=18.

6.3.4 Insulin Tolerance

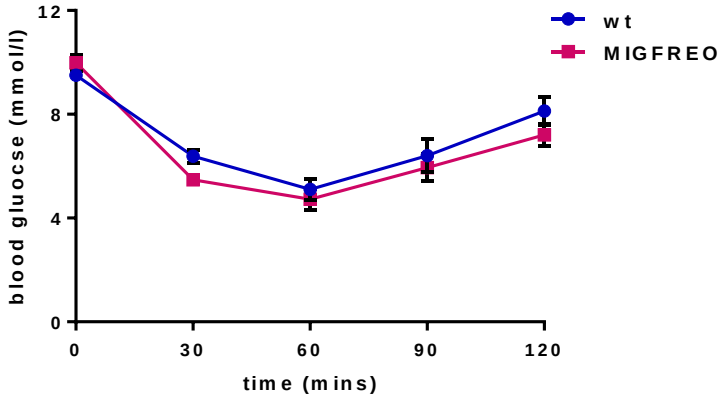

Figure 6.3-10: Insulin tolerance test (absolute). This demonstrates the absolute blood glucose seen during an insulin tolerance test at time points following an intra-peritoneal injection of insulin. The lines represent the mean blood glucose +/- SEM for both wt. (blue) and MIGFREO (pink) mice. N >20 per group. 30 minutes after and intra-peritoneal injection of insulin the MIGFEO mice had significantly lower blood sugar than wt. mice, suggesting enhanced insulin sensitivity (p=0.01).

Although there were no significant differences between MIGFREO mice and wt. mice with respect to their glucose tolerance, there was a difference in the response to an intra-peritoneal injection of insulin. In response to insulin, although both sets of mice as expected experienced a drop in blood glucose, the drop in blood glucose at 30 minutes was more profound in the MIGFREO mice. When considering absolute blood glucose (Figure 6.3-10, Table 27) this was significant at 30 minutes test (5.48 mmol/l +/- 0.23 in MIGFREO

vs. 6.39 mmol/l +/- 0.25 in wt., p = 0.01), although MIGFREO blood glucose had a trend towards being lower throughout the course of the tolerance test.

Time (mins)	wt. mean +/- SEM (n=20)	MIGFREO mean +/- SEM (n=22)	p value
0	9.5 +/- 0.24	9.98 +/- 0.30	0.23
30	6.39 +/- 0.25	5.48 +/- 0.23	0.01
60	5.11 +/- 0.42	4.73 +/- 0.40	0.52
90	6.41 +/- 0.63	5.95 +/- 0.53	0.58
120	8.13 +/- 0.52	7.20 +/- 0.44	0.18

Table 27: Insulin tolerance test (absolute blood glucose). Table of mean +/- SEM blood glucose following an intra-peritoneal injection of insulin in wt. and MIGFREO mice. Corrected to 2 decimal places. Significantly reduced blood sugar seen in MIGFREO mice 30 minutes after intra peritoneal injection of insulin suggesting enhanced insulin sensitivity. N > 20 per group

The difference in response to an intra-peritoneal injection of insulin was more marked when percentage change in blood glucose was calculated (Figure 6.3-11**,** Table 28). 30 minutes following the insulin injection, MIGFREO mice had a blood glucose 56.65% +/- 2.29 of baseline, whilst the wt. mice had a blood glucose 67.51% =/- 2.37 of baseline, which was significantly different, as demonstrated by a p value of less than 0.001. MIGFREO mice display a trend of enhanced insulin sensitivity throughout the tolerance test, and again at 120 minutes post insulin injection the difference is statistically significant (71.91% +/- 4.24 in MIGFREO vs. 85.21% +/- 4.60 in wt., p = 0.04) . Area under the curve of percentage change in blood glucose is statistically different between the 2 sets of mice (Figure 6.3-13) confirming enhanced insulin sensitivity in the MIGFREO mice.

In order to exclude the possibility that the enhanced insulin sensitivity was related to larger doses of insulin given to the slightly heavier MIGFREO mice, a scatter plot was generated demonstrating the relationship between insulin dose (calculated by body weight) and % of baseline blood glucose at 30 minutes. As is clearly shown in Figure 6.3-12 there is no

correlation between these two measurements; R^2 for both MIGFREO and wt mice was less than 0.1.

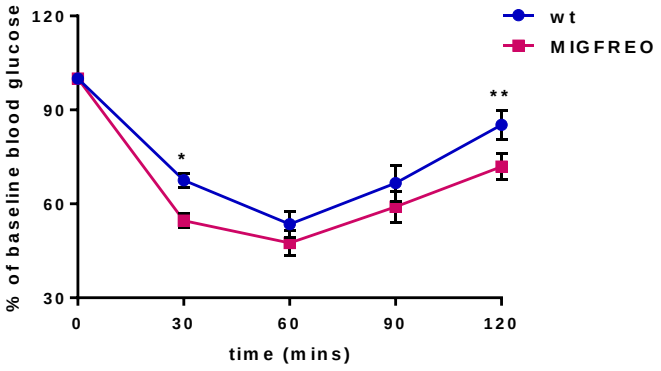

Figure 6.3-11: Insulin tolerance test (% baseline). This demonstrates the blood glucose expressed as a percentage of the baseline blood glucose seen during an insulin tolerance test at time points following an intra-peritoneal injection of insulin. The lines represent the mean blood glucose +/- SEM for both wt. (blue) and MIGFREO (pink) mice. N>20 per group. At 30 minutes and 120 minutes following the intra-peritoneal injection of insulin the MIGFREO mice had significantly enhanced insulin sensitivity; at 30 minutes *p=0.0004, at 120 minutes**p=0.04.

Time (mins)	wt. mean +/- SEM (n=20)	MIGFREO mean +/- SEM (n=22)	p value
0	100	100	
30	67.51 +/- 2.37	54.65 +/- 2.29	0.0004
60	53.49 +/- 4.08	47.51 +/- 4.11	0.31
90	66.65 +/- 5.79	59.09 +/- 4.91	0.32
120	85.21 +/- 4.60	71.91 +/- 4.24	0.04

Table 28: Insulin tolerance test (% change in blood glucose). Table of mean +/- SEM blood glucose expressed as a percentage of baseline blood glucose following an intra-peritoneal injection of insulin in wt. and MIGFREO mice. Corrected to 2 decimal places. Marked enhanced sensitivity to the glucose lowering effects of insulin seen in MIGFREO mice at 30 and 120 minutes in comparison to wt. mice; p=0.0004 and 0.04 respectively. N > 20 per group

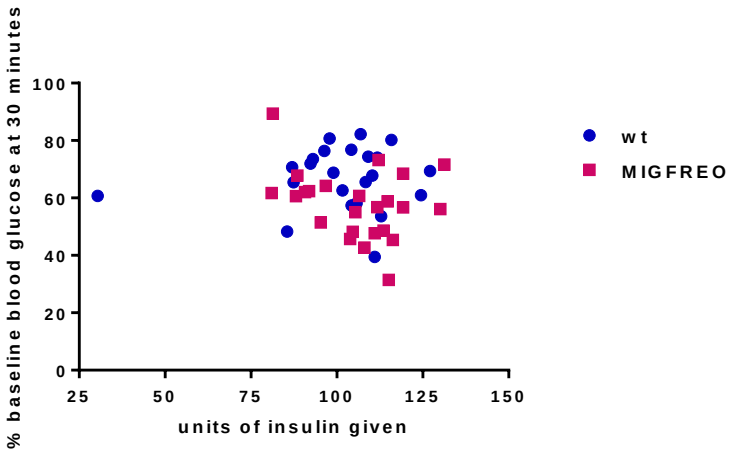

Figure 6.3-12. Correlation between insulin units given (and hence weight) and blood glucose. R^2 shows no correlation with insulin dose given vs. blood glucose at 30 minutes. This is true for MIGFREO and wt mice and suggests that the response to insulin is not solely associated with the dose of insulin give. R^2 0.09 for MIGFREO mice, R^2 0.01 for wt mice.

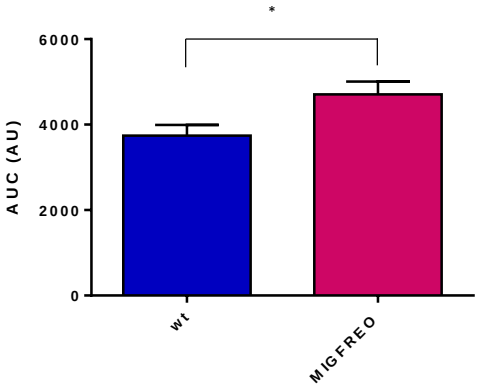

Figure 6.3-13: Area under curve of insulin tolerance test. Using graph pad prism software area under the curve was calculated for each individual insulin tolerance test and the then a mean calculated for wt. (blue) and MIGFREO (pink) mice. The Mean +/- SEM is shown. N > 20 for each group. Area under the curve was significantly elevated in MIGFREO mice (*p=0.02) suggesting significantly enhanced sensitivity to the glucose lowering effects of insulin in MIGFREO mice.

6.3.5 IGF-1 Tolerance

In addition to displaying increased sensitivity to an intra-peritoneal injection of insulin, it appears that MIGFREO mice have enhanced sensitivity to the glucose lowering effects of IGF-1. Absolute blood glucose following IGF-1 is similar between the 2 groups of mice (Figure 6.3-14, Table 29), but when the percentage change in baseline is considered, MIGFREO mice have enhanced sensitivity to IGF-1 after 30 minutes (Figure 6.3-15, Table 30). 30 minutes following the injection of IGF-1 the blood glucose of the MIGFREO mice

was 57.47% +/- 2.77 of baseline, whilst the blood glucose in the wt. mice was 70.64% +/- 4.82 of baseline, p value 0.02 (Figure 6.3-15). Although the trend is sustained throughout the duration of the test it is not statistically significant at 120 minutes. The area under the curve calculation shows a non-statistically significant trend towards enhanced IGF-1 sensitivity throughout the duration of the test (Figure 6.3-16, Table 26)

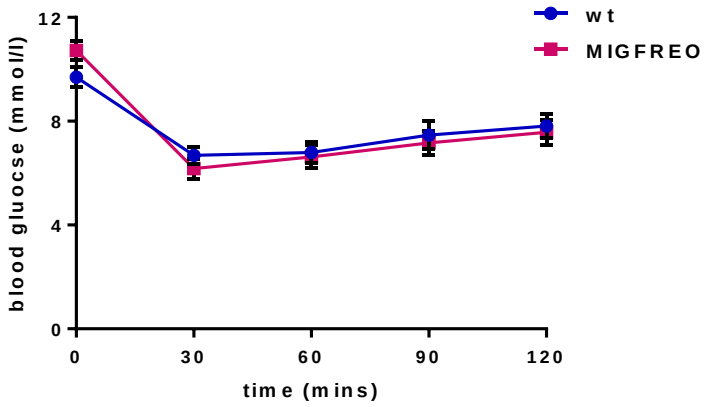

Figure 6.3-14: IGF-1 tolerance test (absolute). This demonstrates the absolute blood glucose seen during an insulin tolerance test at time points following an intra-peritoneal injection of IGF-1. The lines represent the mean blood glucose +/- SEM for both wt. (blue) and MIGFREO (pink) mice. N >15 per group. No differences seen between the 2 groups.

Time (mins)	wt. mean +/- SEM (n=16)	MIGFREO mean +/- SEM (n=17)	p value
0	9.69 +/- 0.39	10.23 +/- 0.37	0.26
30	6.68 +/- 0.33	6.17 +/- 0.38	0.32
60	6.79 +/- 0.42	6.63 +/- 0.45	0.79
90	7.47 +/- 0.54	7.16 +/- 0.47	0.67
120	7.81 +/- 0.48	7.58 +/- 0.48	0.73

Table 29: IGF-1 tolerance test (absolute blood glucose). Table of mean +/- SEM blood glucose following an intra-peritoneal injection of IGF-1 in wt. and MIGFREO mice. Corrected to 2 decimal places. No significant differences between the 2 groups. N > 15 per group

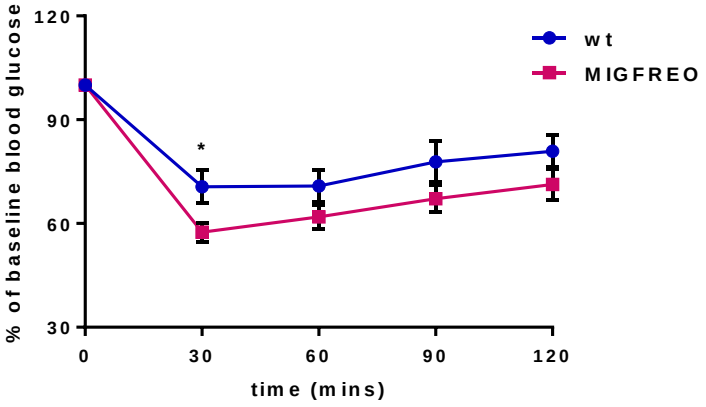

Figure 6.3-15: IGF-1 tolerance test (% of baseline). This demonstrates the blood glucose expressed as a percentage of the baseline blood glucose seen during an IGF-1 tolerance test at time points following an intra-peritoneal injection of glucose. The lines represent the mean blood glucose +/- SEM for both wt. (blue) and MIGFREO (pink) mice. N>15 per group. At 30 minutes following the intra-peritoneal injection of insulin the MIGFREO mice had significantly enhanced insulin sensitivity; at 30 minutes *p=0.02. N > 15 per group

Time (mins)	wt. mean +/- SEM (n=16)	MIGFREO mean +/- SEM (n=17)	p value
0	100	100	
30	70.64 +/- 4.82	57.47 +/- 2.77	0.02
60	70.87 +/- 4.68	61.88 +/- 3.57	0.13
90	77.79 +/- 5.93	67.14 +/- 3.98	0.14
120	80.89 +/- 4.68	71.26 +/- 4.45	0.14

Table 30: IGF-1 tolerance test (% of baseline blood glucose). Table of mean +/- SEM blood glucose expressed as a percentage of baseline blood glucose following an intra-peritoneal injection of IGF-1 in wt. and MIGFREO mice. Corrected to 2 decimal places. Marked enhanced sensitivity to the glucose lowering effects of insulin seen in MIGFREO mice at 30 in comparison to wt. mice; p= 0.02. N > 15 per group

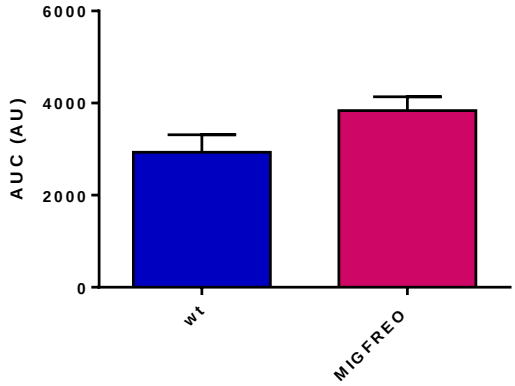

Figure 6.3-16: Area under curve of IGF-1 tolerance test. Using graph pad prism software area under the curve was calculated for each individual IGF-1 tolerance test and the then a mean calculated for wt. (blue) and MIGFREO (pink) mice. The Mean +/- SEM is shown. N > 15 for each group. Trend towards a higher AUC in MIGFREO mice (p=0.07) suggesting a trend towards enhanced IGF-1 sensitivity in MIGFREO mice.

6.3.6 Plasma insulin and IGF-1 level

As shown in Table 31**,** Figure 6.3-17 there is no difference observed between the random plasma insulin or IGF-1 levels seen in MIGFREO and wt. mice.

	wt. mean +/- SEM	MIGFREO mean +/- SEM	p value
Random insulin (ng/ml)	3.53 +/ - 0.45 (n=11)	3.34 +/- 0.59 (n=11)	0.80
Random IGF-1 (ng/ml)	322.03 +/- 10.37 (n=31)	339.29 +/- 13.63 (n=35)	0.33

Table 31: Plasma insulin and IGF-1 levels. The table shows mean +/- SEM plasma insulin (ng/ml) and IGF-1 (ng/ml) in wt. and MIGFREO mice. N=11 for plasma insulin measurements, n > 30 for plasma IGF-1 level. Results are corrected to 2 decimal places. No significant differences seen between wt. and MIGFREO mice.

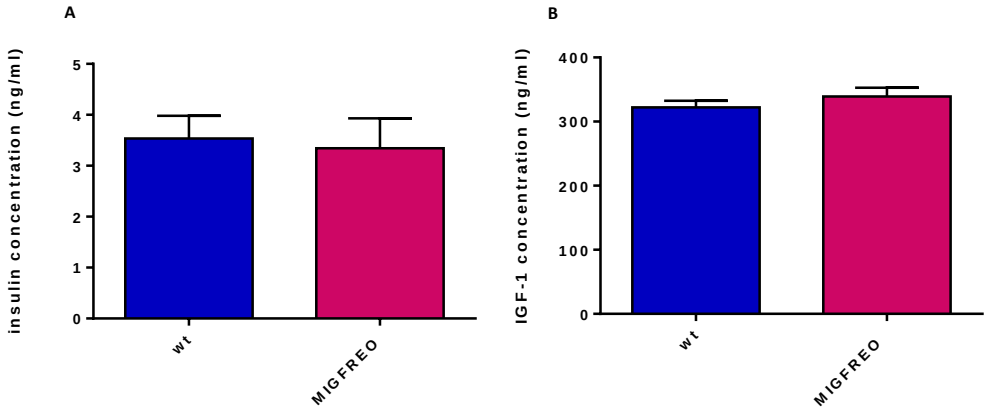

Figure 6.3-17: (A) Plasma insulin ELISA (B) plasma IGF-1 ELISA. Plasma insulin (A) and IGF-1 (B) levels in wt. (blue) and MIGFREO (pink) mice. Columns represent mean +/- SEM and are expressed in ng/ml. N=11 for insulin measurements, n > 30 for plasma IGF-1 level. No difference in random plasma insulin or IGF-1 between wt. and MIGFREO mice.

6.3.7 Plasma adiponectin, leptin, free fatty acid and triglyceride

There is a trend towards elevated levels of plasma adiponectin in MIGFREO mice, (9.29 ng/ml +/- 0.19 vs. 8.70ng/ml +/- 0.25 in MIGFREO vs. wt. respectively) although this does not reach statistical significance (p=0.07) (Figure 6.3-18, Table 32).

Levels of leptin (Figure 6.3-18**,** Table 32) and triglyceride (Figure 6.3-19**,** Table 32) are comparable between the 2 sets of mice.

	wt. mean +/- SEM	MIGFREO mean +/- SEM	p value
Adiponectin (ng/ml)	8.70 +/- 0.25 (n=19)	9.29 +/- 0.19 (n=19)	0.07
Leptin (ng/ml)	8.83 +/- 0.91 (n=18)	8.58 +/- 1.04 (n=18)	0.86
Free fatty acid (nmol/µl)	0.44 +/- 0.07 (n=16)	0.23 +/- 0.03 (n=16)	0.02
Triglyceride (nmol/µl)	6.16 +/- 0.31 (n=12)	5.31 +/- 0.39 (n=19)	0.14

Table 32: Random plasma levels of adiponectin, leptin, free fatty acid and triglyceride. The table shows mean +/- SEM plasma adiponectin (ng/ml), leptin (ng/ml), free fatty acid (nmol/µl) and triglyceride (nmol/µl) in wt. and MIGFREO mice. Results are corrected to 2 decimal places. Numbers of samples are listed within the table. Significantly lower plasma free fatty acid seen in MIGFREO mice (p=0.02). No difference seen in plasma leptin or triglyceride. There was a trend towards higher plasma adiponectin level in the MIGFREO mice (p=0.07). Numbers analysed shown in table.

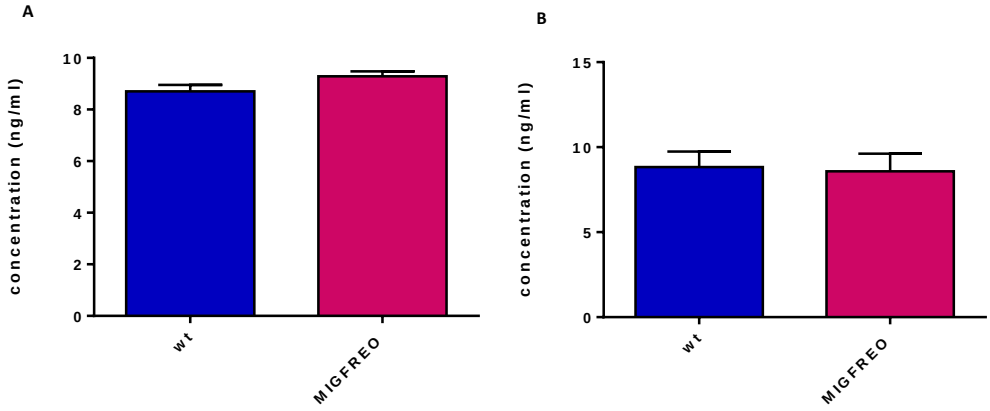

Figure 6.3-18: (A) Plasma adiponectin ELISA (B) plasma leptin ELISA. Plasma adiponectin (A) and leptin (B) levels in wt. (blue) and MIGFREO (pink) mice. Columns represent mean +/- SEM and are expressed in ng/ml. N=19 for adiponectin measurements, n=18 for plasma leptin level. No difference in random plasma adiponectin or leptin between wt. and MIGFREO mice.

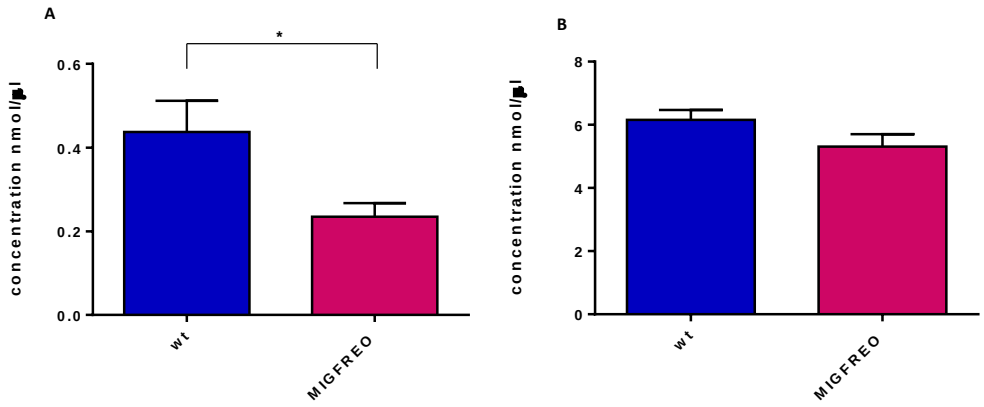

Figure 6.3-19: (A) Plasma free fatty acid quantification (B) plasma triglyceride quantification. Plasma free fatty acid (A) and triglyceride (B) levels in wt. (blue) and MIGFREO (pink) mice. Columns represent mean +/- SEM and are expressed in nmol/µl. N=16 for free fatty acid measurements, n >11 for plasma triglyceride level. Marked reduction in plasma free fatty acid in MIGFREO mice*p=0.02; no difference in plasma triglyceride level.

Interestingly there is a statistically significant difference between plasma levels of free fatty acid between MIGFREO and wt. mice (Figure 6.3-19, Table 32). MIGFREO mice have a plasma free fatty acid level which is 52% that of the level seen in their wt. littermates (0.23nmol/µl +/- 0.03 vs. 0.44nmol/µl +/- 0.07 in MIGFREO vs. wt. respectively, p = 0.02).

6.3.8 Blood pressure

There is no difference in either systolic or diastolic blood pressure between the 2 sets of mice (Figure 6.3-20, Table 33).

	wt. mean +/- SEM (n=10)	MIGFREO mean +/- SEM (n=10)	p value
Systolic mmHg	97.57 +/- 2.15	100.45 +/- 3.90	0.53
Diastolic mmHg	72.89 +/- 2.73	74.72 +/- 3.60	0.69

Table 33: Systolic and diastolic blood pressure measurements. Mean +/SEM. Corrected to 2 decimal places. No difference in systolic or diastolic blood pressure seen between the 2 groups. N =10 per group

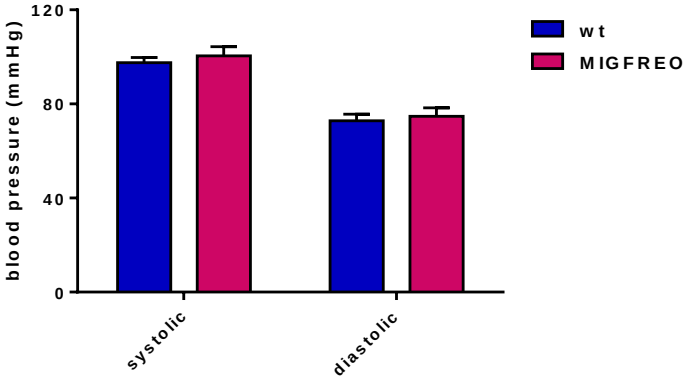

Figure 6.3-20: Blood pressure. Systolic and diastolic blood pressure measurement in wt. (blue) and MIGFREO (pink) mice. Bars represent mean +/- SEM. No significant differences seen in either systolic or diastolic blood pressure between the wt. and MIGFREO mice. N=10 in each group.

6.4 Conclusion and Discussion

MIGFREO mice have enhanced whole body insulin and IGF-1 sensitivity

Contrary to the hypothesis which was generated, MIGFREO mice have enhanced whole body insulin sensitivity, as measured by change in blood glucose following an intra-peritoneal injection of insulin (Figure 6.3-10, Figure 6.3-11, Table 27, Table 28). The differences measured between the 2 populations of mice were small, but statistically significant. A significant difference was seen between the 2 sets of mice 30 minutes after the injection of insulin, with the trend persisting throughout the duration of the test, becoming significant again at 120 minutes post insulin injection. In accordance with this, insulin tolerance throughout the duration of the test as measured by the area under the curve (Figure 6.3-13, Table 26) showed enhanced insulin sensitivity

In common with improved insulin sensitivity the MIGFREO mice have enhanced IGF-1 sensitivity as measured by the increased response to an intra-peritoneal injection of IGF-1 (Figure 6.3-14, Figure 6.3-15, Table 29, Table 30) which is significant at 30 minutes, and shows a trend towards enhanced IGF-1 sensitivity throughout the 120 minutes. There is a strong trend towards enhanced IGF-1 sensitivity in MIGFREO mice as measured by the area under the curve (Figure 6.3-16, Table 26).

Basal blood glucose seen prior to performing the insulin tolerance test was higher in both sets of mice than that seen prior to the glucose tolerance test; this is most likely due to the shorter period of fasting which the mice were subjected to; at least 12 hours prior to the glucose tolerance test and 4 hours prior to the insulin and IGF-1 tolerance tests.

Following the longer period of fasting prior to the glucose tolerance test there was no difference in baseline blood glucose noted between the MIGFREO and the wt mice; however when the mice were exposed to a shorter period of starvation prior to the insulin and IGF-1 tolerance tests, there was noted to be a trend towards a higher basal blood glucose in the MIGFREO mice. Although small, it will have had an effect on the calculation of change in blood glucose from baseline and this should be taken into consideration when contemplating the apparent enhanced insulin sensitivity seen the MIGFREO mice. The MIGFREO mice appear to have marginally larger livers than their wt counterparts, which would perhaps correlate with larger glycogen stores in MIGFREO mice. Given that glycogen breakdown occurs in response to starvation it is possible that this might have had an effect

on fasting blood glucose. If this is the case, then one might expect that the difference in blood glucose would be more marked after a longer period of starvation, whereas the contrary was seen here.

In all cases the tolerance tests were performed in the same order; week 1 glucose tolerance, week 2 insulin tolerance, week 3 IGF-1 tolerance. The mice might therefore have experienced higher stress levels in the later weeks of testing. Signalling through the IGF-1 axis is known to have an effect on cortisol signalling (although the exact mechanism is yet to be entirely elucidated), and release of cortisol is well known to stimulate gluconeogenesis from the liver. It is perhaps the case then, that the MIGFREO mice have exaggerated stress responses and enhanced cortisol secretion in response to starvation. This would be interesting to examine for further experiments.

Further investigation of MIGFREO blood glucose in response to differing periods of starvation and stress would be interesting. I would suggest that blood glucose in the MIGFREO mice should be formally assessed after varying periods of starvation, and that an assessment of plasma cortisol would be an interesting adjunct.

The difference in insulin sensitivity between the 2 groups was admittedly marginal, but reached high statistical significance suggesting that there is a real, but small difference. This is an interesting finding, and irrespective of the magnitude is worthy of some further consideration. The examination of the whole body metabolic phenotype of the mice (as discussed shortly) adds some weight to the finding of marginal insulin sensitivity in MIGFREO mice. The widely acknowledged gold standard assessment of insulin sensitivity in mice would be hyperinsulinaemic euglycaemic clamping which assesses the concentration of glucose required to maintain normoglycaemia in the face of hyperinsulinaemia; enhanced insulin sensitivity is associated with higher rates of insulin mediated glucose disposal, and hence higher concentrations of glucose are required to maintain normoglycaemia. This is not a technique currently available locally, although I would recommend that in order to fully assess the presence, and indeed the magnitude of enhanced insulin sensitivity which the MIGFREO mice appear to demonstrate, this would be a useful addition experiment.

MIGFREO mice have plasma IGF-1 and insulin levels comparable with wt. counterparts

The change in insulin sensitivity seen in the MIGFREO mouse does not appear to be related to changes in plasma insulin levels; there were no differences seen in random plasma insulin or IGF-1 levels between the 2 groups of mice (Figure 6.3-17). As was discussed in the introduction, however, a significant proportion of IGF-1 within the plasma is bound to IGF-1 binding proteins, which themselves play a role in modulating insulin sensitivity. In order to make a robust determination of whether there is a difference in plasma IGF-1 levels between MIGFREO and wt mice an assessment of both total and unbound IGF-1 should be performed. Given that there is good evidence that over-expression of IGFBP-1 in mice has been shown to be associated with down regulation of the insulin signalling pathway and has an effect on NO production it would be necessary to assess IGFBP-1 levels in the MIGFREO mice before concluding that changes in plasma composition are not responsible for any whole body changes demonstrated.

Changes in plasma composition in MIGFREO mice

Interestingly expression of the mutant IGF-1R on the vascular endothelium was also associated with significantly reduced plasma free fatty acid (FFA) level when compared with their wt. littermates (Figure 6.3-19, Table 32). Plasma leptin and triglyceride levels are comparable between the 2 sets of mice, although there is a strong trend, albeit non-significant to elevated plasma adiponectin levels in MIGFREO mice (Figure 6.3-18, Table 32). The reduction in plasma FFA in the MIGFREO mice is consistent with enhanced whole body insulin sensitivity.

The relationship between FFA and insulin sensitivity is somewhat cyclical with elevated free fatty acids not only forming a component of the insulin resistance syndrome, but also being implicated in the development of insulin resistance. Treatment of cells with FFA has been demonstrated to cause insulin resistance via mechanisms involving overproduction of ROS and activation of inflammatory pathways [261-263]. On a whole body level, pharmacological reduction of plasma FFA improves insulin signalling in muscles from subjects with insulin resistance [328] and treatment with the insulin sensitizer metformin is associated with reduction in plasma free fatty acid levels in similar cohorts [329, 330] although the mechanism behind this is not yet completely understood. It is therefore difficult to assess whether the reduction in FFA in MIGFREO mice occurs as a result of

enhanced insulin sensitivity, or whether it might be implicated in the development of enhanced insulin sensitivity.

MIGFREO mice have normal blood pressure, weight and fat morphology

There is no significant difference between MIGFREO mice with regards to blood pressure (Figure 6.3-20, Table 33), weight (Figure 6.3-1**,** Table 21), organ weight, fat pad size (Figure 6.3-2), or on a microscopic level fat cell number or size (Figure 6.3-4, Figure 6.3-5, Table 23).

Although there were no clear statistically significant differences however, the MIGFREO mice certainly had a trend to an enlarged liver which requires further investigation. Microscopic examination of the liver would be useful, as would an assessment of levels of glycogen storage, as clearly both would have an effect on insulin sensitivity and glucose homeostasis.

The assessment of fat cell size and number, could be expanded. Although there were no significant differences between cell size or number between MIGFREO and wt mice the MIGFREO mice appear to have a trend towards larger, less numerous cells in a field of view versus smaller, more numerous cells in the wt mice. In a static area, the number of fat cells will of course be inversely proportional to the size of the cells, so to a certain extent only one of these variables was strictly speaking necessary to measure. Although not statistically significant it is interesting that MIGFREO mice have a trend towards larger, less numerous fat cells in combination with a suggestion of enhanced insulin sensitivity, perhaps suggesting that there is altered insulin signalling within fat cells. Further examination of insulin sensitivity within fat cells (AKT and eNOS phosphorylation in response to insulin stimulation) would be interesting. The first step would be further analysis of fat cell size and number in more samples – only 4 wt fat samples were examined in order to determine if the difference seen was real.

MIGFREO mice display a divergence between whole body and endothelial insulin sensitivity

Contrary to the original hypothesis, MIGFREO mice have enhanced whole body insulin and IGF-1 sensitivity coupled with insulin and IGF-1 endothelial cell insulin resistance. As has been discussed the finding of endothelial cell insulin and IGF-1 resistance can be explained by the distribution of hybrid receptors, and the expression of the mutation on the

endothelial cell of the MIGFREO mice. However, the demonstration of enhanced whole body insulin and IGF-1 sensitivity, irrespective of the magnitude of diversion from the wt. phenotype (which is admittedly small) is interesting and surprising, particularly given that the mutation is expressed, as has been demonstrated, solely on the vascular endothelium.

The ways which the endothelium may theoretically effect whole body insulin sensitivity, via the effect upon insulin mediated glucose disposal have been discussed earlier. There is a good body of evidence to suggest that insulin is able to enhance delivery of insulin to, in particular, skeletal muscle via the interstitium through the processes of augmenting microvascular capillary recruitment [292, 293], enhancing transendothelial insulin transportation [301], and probably less importantly on a physiological level by enhancing whole limb blood flow.

Endothelial specific deletion of IRS-2 has been shown to be associated with the development of whole body insulin resistance, in association with reduced insulin mediated capillary recruitment and reduced insulin mediated glucose disposal [304], so the finding that manipulation of the insulin signalling cascade on the endothelium is associated with changes in whole body glucose sensitivity is not novel. There are however no previous studies demonstrating that manipulation of the IGF-1R specifically on the endothelium has an effect on whole body insulin sensitivity.

That there is a change in insulin sensitivity seen is perhaps then, not unexpected. The direction of this change in insulin sensitivity, is however intriguing. In the above study Kubota *et al* [304] demonstrated endothelial cell insulin resistance in association with whole body insulin resistance. I have demonstrated that the expression of a non-functioning IGF-1R on the vascular endothelium is associated with endothelial cell insulin resistance, yet have demonstrated whole body insulin sensitivity.

Several other mouse models have examined the effect of mutation or knockout of the IR solely on the vascular endothelium. The ESMIRO mouse expresses a dominant negative mutant human IR, which, under control of the Tie2 promoter is expressed solely on the vascular endothelium. The ESMIRO mouse is associated with endothelial insulin resistance, endothelial dysfunction and the accelerated development of atherosclerosis [195, 322] in combination with increased generation of superoxide. Metabolic characterisation of the ESMIRO mouse did not display any marked differences in insulin sensitivity between the

wt. and the transgenic mouse, although intriguingly, there was reported to be a trend towards enhanced whole body insulin sensitivity in the ESMIRO mice.

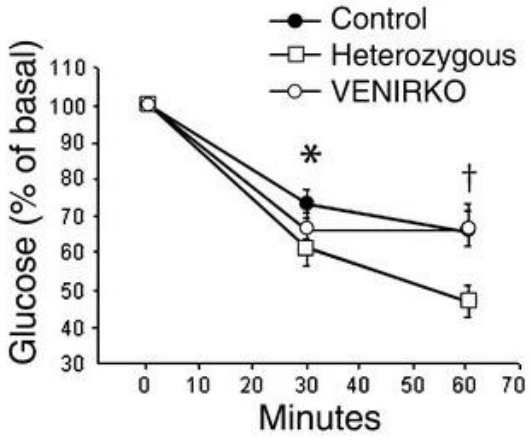

Figure 6.4-1: Reproduced with permission from Vicent *et al* [303] published by American Society for Clinical Investigation. *p <0.05 † p<0.01 for differences between control and VENIRKO mice

Another group looked the effect of knockout of the IR on the vascular endothelium and generated the VENIRKO mouse [303]. This mouse was found to have significant reduction in IR mRNA on the vascular tissues and was associated with the development of endothelial insulin resistance on a low salt diet. Although no metabolic consequences were reported in the text, looking at the results and figures within the paper suggests that at 6 months there was also enhanced insulin sensitivity in the VENIRKO mice in comparison with wt. counterparts.

Although neither of these 2 mouse models specifically state an association with endothelial cell insulin resistance and enhanced whole body insulin sensitivity, in both the ESMIRO and more convincingly in the VENIRKO mouse there is a trend towards enhanced whole body insulin sensitivity which would seem to concur with my findings.

Why this should differ from the results seen in the endothelial specific IRS-2 knockout model is not clear. In both the ESMIRO and VENIRKO mouse, in common with the MIGFREO mouse, manipulation or knockout of the receptor will have an effect on IGF-1R/IR hybrid receptor stoichiometry and function. Conversely, manipulation of the IRS-2 receptor would not affect hybrid formation or function, although has an effect on downstream insulin

signal transduction. Given the emerging importance of hybrid receptors in modulating the signalling of insulin this may be of vital importance.

A similar phenotype to that seen in the MIGFREO mouse has recently been demonstrated in a mouse with endothelial specific knockout of PDK-1 (VEPDK1KO) [326]. These mice have endothelial cell insulin resistance (as measured by reduced threonine 308 phosphorylation of Akt in response to insulin) coupled with loss of insulin stimulated increases in blood flow in VEPDK1KO mice. When fed a normal diet VEPDK1KO mice have enhanced whole body insulin sensitivity coupled with the endothelial cell insulin resistance, and also had smaller epididymal fat pad sizes and inhibition of angiogenesis in white adipose tissue. Following a period of high fat feeding the VEPDK1KO were protected against the development of insulin resistance and weight gain. The authors hypothesised that endothelial cell insulin resistance and inhibition of PDK had led to reduced angiogenesis in white adipose tissue with reduction of age or high fat fed induced adipose tissue hypertrophy. This was associated with modification of the adipokine profile and consequent enhanced whole body insulin sensitivity. Unfortunately, especially given the reduction in plasma FFA seen in the MIGFREO mice, plasma FFA was not measured in this model.

In the VEPDK1KO mice, the authors concluded that the divergence between whole body and endothelial insulin sensitivity was related to differences between angiogenesis in fat in the wild type and transgenic mice. This was associated with smaller epididymal fat pads and smaller fat cell size in transgenic mice and subsequent improvement in the adipokines profile. This would not appear to be the case in MIGFREO mice. In MIGFREO mice fat pad size, fat cell size and fat cell number were comparable with wild type.

Although there is no apparent difference in the macroscopic appearance of fat tissue between the 2 sets of mice, there is a clear reduction in FFA seen in the MIGFREO mice. The relationship between FFA, insulin sensitivity, and adipose tissue mass is complex and not yet fully understood. A recent review of evidence did not find a relationship between adipose tissue mass and plasma FFA level in humans [331], which would appear to support the findings of comparable fat pad mass and cell size, with a significant disparity in plasma FFA between the MIGFREO and wt. mice.

It is possible that the enhanced insulin sensitivity seen in the MIGFREO mice could relate to changes in FFA metabolism and storage, and certainly, further assessment of this should be

considered in this mouse as future work. In view of the findings from the VEPDK1KO mouse, it would be particularly interesting to assess how angiogenesis is affected, if at all, in MIGFREO mice, although this is beyond the scope of this particular project.

Chapter 7: Measuring Reactive Oxygen Species

7 Measuring reactive oxygen species

7.1 Introduction

MIGFREO mice have been demonstrated to display a surprising divergence between whole body and endothelial cell insulin resistance. Compared with their wild type littermates, MIGFREO mice have enhanced whole body insulin and IGF-1 sensitivity and varying degrees of endothelial insulin and IGF-1 resistance. As has been discussed there is emerging evidence that ROS, particularly H_2O_2 plays a role in modulating insulin signalling, and indeed there is good data to support that H_2O_2 can enhance insulin signalling. By oxidising cystine residues on the thiol side chain, H_2O_2 has been shown to inhibit PTP1B signalling, which has the net effect of enhancing insulin signalling [272-274]. H_2O_2 also has an effect directly on the insulin receptor; oxidation of cystine residues within the activation loop of the IR by H_2O_2 leads to "priming" of the IR and enhanced autophosphorylation, and enhanced insulin signalling [278, 280]. As has been discussed the converse is true of the effect on the IGF-1R: stimulation with low doses of H_2O_2 is associated with inhibition of kinase activity of the IGF-1R [281].

It has been previously demonstrated that endothelial insulin resistance is associated with increased production of reactive oxygen species. In addition to endothelial insulin resistance the ESMIRO mouse produces a higher level of vascular superoxide than its wild type litter mates [195] and expresses higher levels of Nox 2 and Nox 4 mRNA. No distinction was made between the various reactive oxygen species, but given that there was an approximate 2 fold increase in aortic Nox 4 mRNA, and also considering that Nox 4 predominantly produces H_2O_2 it would seem possible that the ESMIRO mouse overproduces H_2O_2. Interestingly, as has been alluded to, Duncan *et al* noted that during insulin tolerance tests the ESMIRO mouse had a "trend toward improved insulin sensitivity" [195].

I therefore hypothesised that the improvements in whole body insulin and IGF-1 sensitivity in the MIGFREO mouse were related to overproduction of H_2O_2 in the vasculature.

I made the decision to investigate this in several ways:

1. Assessment of change in endothelial dependent vasodilatation in the organ bath when exposed to catalase
2. Assessment of vascular H_2O_2 production using Amplex® Red
3. Assessment of expression of mRNA from Nox and SOD isoforms in PEC

7.2 Methods

7.2.1 Assessment of Hydrogen Peroxide levels using the Organ Bath

It has been discussed that H_2O_2 has been shown to be an important EDHF, particularly in the micro-vasculature [283-285] . Vasodilatation induced by H_2O_2 is independent from endothelial function; it is independent of eNOS but is blocked by treatment with high levels of K^+ and K_{Ca} channel inhibitors [82]. If present in significant levels, elimination of H_2O_2 by using catalase, in for example the organ bath, is associated with reduced vasodilatation.

The organ bath was set up as is described earlier (see section 5.2.1). Rings were constricted with KCl as described above to ensure viability, and ACh mediated, endothelial dependent vaso-relaxation was measured prior to addition of catalase.

7.2.1.1 Effect of catalase on endothelial dependent vasodilatation

12500 units of catalase from bovine liver (Sigma) was added to each chamber (1250units/ml) and immediately afterwards rings were partially constricted with 300nM of phenylephrine (Sigma). Calcium dependent endothelial mediated vasodilatation was then assessed by the subsequent relaxation in response to cumulative doses (1nM-10μM) of acetylcholine (Sigma). Rings examined in this way were not used for any further experiments. Vaso-relaxation in the presence of catalase was determined by calculating the percentage of relaxation from peak constriction to base ([preconstriction-result]/[preconstriction-base]*100) where relaxation to the baseline would be 100%. Results are expressed as percentage relaxation.

Results of endothelial dependent vaso-relaxation in the presence of catalase were compared with the initial ACh curve.

7.2.2 Amplex® Red to detect H_2O_2 from Homogenised Aorta

Measurement of H_2O_2 in homogenised aorta was performed using the Amplex® Red Hydrogen Peroxide/Peroxidase Assay kit (Invitrogen™, Molecular Probes®). Using horseradish peroxidise as a catalyst, H_2O_2 reacts with colourless Amplex® Red (N-acetyl-3-dihydroxyphenoxazine) in a 1:1 stoichiometry to produce resorufin, which, when excited at 530 nm, emits light at 590nm. Due to the high extinction coefficient measurements of optical density can be made both fluorometrically and spectrophotometrically [332].

7.2.2.1 Optimisation of Protocol: 1

Although previously published [332, 333] this method of assessing H_2O_2 production by aortas has not previously been used in our laboratory, and therefore the method required optimisation.

Stock solutions were prepared in accordance with the manufacturer's instructions:

1. **10mM Amplex® Red stock solution**

A vial of room temperature Amplex® Red (154µg) was reconstituted with 60µl of dimethylsulfoxide (DMSO)

2. **1x Reaction Buffer**

4ml of reaction buffer (28ml of 0.25M sodium phosphate pH 7.4) was added to 16ml of deionized H_2O_2.

3. **10U/ml of Horseradish Peroxidase (HRP) stock solution**

Contents of the supplied horseradish peroxidise (HRP, 10U) were dissolved in 1ml of 1x reaction buffer.

4. **20mM Hydrogen Peroxide (H_2O_2) working solution**

Using the supplied 3% H_2O_2 solution a working solution of 20mM was made by diluting 22.7µl of 3.0% H_2O_2 into 977µl of 1x reaction buffer. Serial dilutions were performed to make solutions of 10µM, 5µM, 1µM, 0.5µM, 0.1µM 0.01µM and 0.001µM. Final concentrations in the plate were 2 fold lower.

5. **Working solution of 100µM of Amplex® Red reagent and 0.2U/ml of HRP**

Working solution of Amplex Red® and HRP was made by adding 50µl of 10nM Amplex® Red stock solution with 100µl of 10U/ml HRP stock solution and 4.85ml of 1x reaction buffer.

To prepare tissue samples, freshly excised aortas were placed into ice cold PBS and cleaned of fat and surrounding connective tissue. Aortas were homogenised in 1ml of PBS using a tissue lyser (Qiagen®) for 30 sec at 30 Hz using a stainless steel cone ball (Retsch®). Following centrifuge for 5 minutes at 8000 rpm the supernatant was removed. In order to

ascertain the optimum dilution of supernatant to use, several dilutions were prepared for the initial experiment: neat; 1:2; 1:5; 1:10; 1:20; 1:50; 1:100. Dilutions were made using the supplied reaction buffer.

Samples were loaded in triplicate onto the plate by adding 50µl of blank, prepared H_2O_2 standards, or diluted samples, with the addition of 50µl of the Amplex® Red working solution. The plate was kept protected from light at room temperature for 30 minutes. Absorbance was read at 560nm on a SpectraMax® 190 microplate reader (Molecular Devices). Baseline OD was subtracted from all standard and sample readings. H_2O_2 concentrations were calculated using an H_2O_2 standard curve (R^2 =0.999) using Graph Pad Prism software and baseline measurements were subtracted.

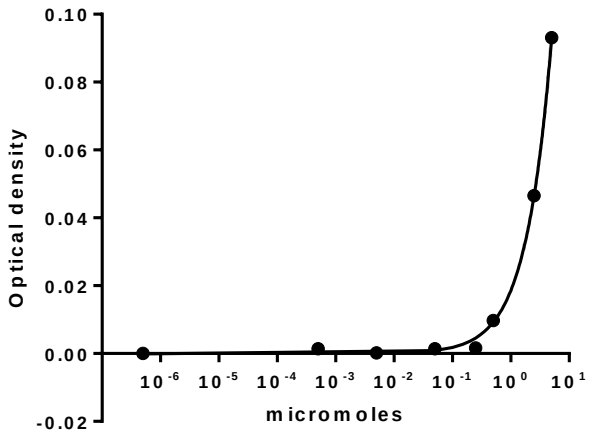

Figure 7.2-1: Standard Curve generated from optimisation experiment. H_2O_2 standard curve obtained from optimisation amplex red experiment. Curve generated using supplied standards. R2 = 0.999

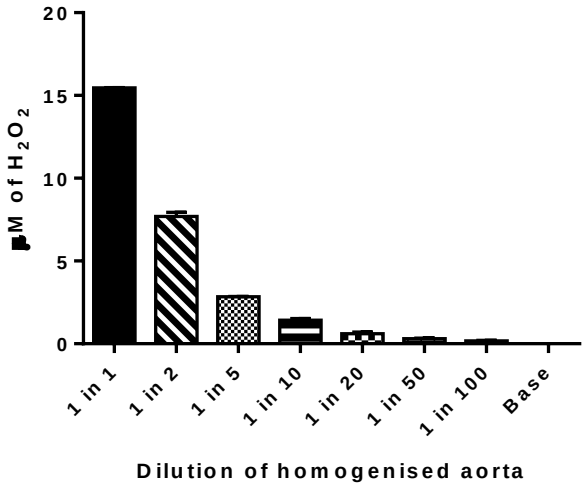

Figure 7.2-2: Results of optimisation experiment. Total H_2O_2 per well using different dilutions of homogenised aorta (n=5). In view of the limits of the assay it was decided to use a dilution of 1:5 of homogenised aorta.

7.2.2.2 Pilot experiment 1

Using the results generated from the optimisation experiment it was decided to use standard concentrations of H_2O_2 of 20µM, 10µM, 5µM, 1µM, 0.5µM, 0.1µM and 0.01µM. Supernatant from homogenised aorta was diluted 1:5 before adding to the plate, and protocol was followed as described above.

Protein concentrations of supernatant were measured using Pierce® BCA Protein Assay kit (Thermo Scientific), as described in section 4.2.5.2, and results are expressed as µM per mg of protein.

Initial results which were obtained from using the above method were promising, and are shown in Figure 7.2-3. The results suggested that the aortas of the male MIGFREO mice had a significantly elevated level of hydrogen peroxide when compared to their wt. counterparts. This concurred with the evidence from adding catalase to the organ bath, and supported our theory that the MIGFREO mice may have elevated levels of H_2O_2, which enhances insulin signalling on a whole body level.

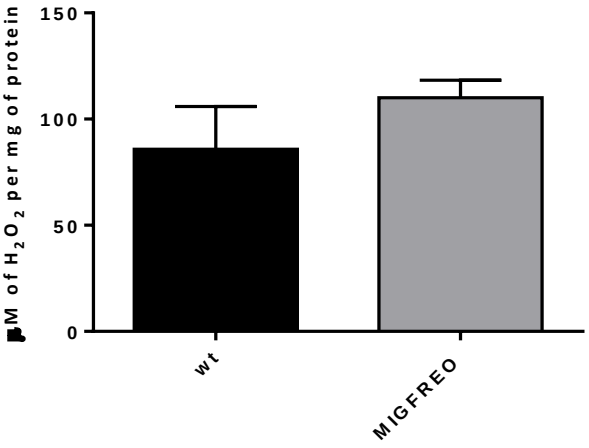

Figure 7.2-3: Results from pilot experiment 1: H2O2 in aorta using amplex® red assay in homogenised aorta. Graph shows mean +/- SEM for wt. (black) and MIGFREO (grey) samples. Following subsequent experiments it was decided that this method was likely to be an inaccurate method of measuring H_2O_2.

During setting up the experiments it was noted that although the aortas had been immersed in fresh PBS and were cleaned of connective tissue, there was some residual pinkish discolouration of the sample. It was noted that the more darkly coloured samples tended to give results suggesting a higher concentration of H_2O_2; it was therefore felt important to ensure that the signal measured from the homogenate was due to amplex® red rather than the inherent discolouration of the sample.

We attempted to ensure that the assay was robust in 2 ways:

1. Absorbance of samples was measured without the addition of amplex® red on the same plate reader (at 560nM)
2. Samples were incubated with catalase for 1 hour to assess whether the signal was inhibitable by catalase (200 units/ml) (as should have been the case if the signal was originating from the formation of resorufin by amplex red combining with H_2O_2).

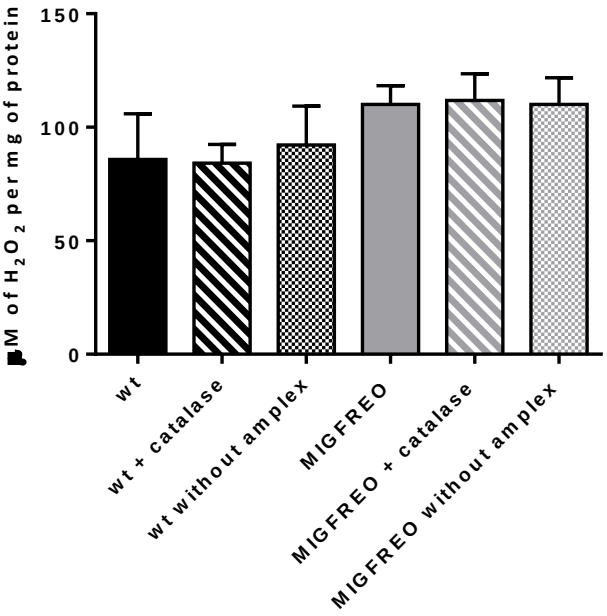

Figure 7.2-4: Results from pilot experiment 1: H_2O_2 in aorta using amplex® red assay in homogenised aorta. These results demonstrate that the initial method of using amplex red to calculate H_2O_2 was inaccurate. There was no demonstrable reduction in signal seen following incubation with catalase and again, no demonstrable reduction in signal seen when the samples were incubated without amplex red.

The results are shown in Figure 7.2-4. In pilot experiments the addition of catalase did not lead to a reduction in measured optical density, and measurements of the homogenate without amplex® red were similar to those measured with amplex® red. This strongly suggests that this method of using amplex® red was not sufficiently robust in our samples to allow for accurate measurement of H_2O_2, and that the inherent discolouration of the sample was the significant contributing factor to the measured optical density. It is unclear from the literature whether the studies using this method encountered similar problems, or whether any attempt to inhibit the signal using catalase was made.

7.2.3 Amplex® Red to measure H_2O_2 in aortic rings

In view of the results obtained from the homogenised aorta it was decided to design a further protocol to assess H_2O_2 production in aorta.

Several other papers have been published using rings of aorta incubated in Krebs solution to assess H_2O_2 production [334-336]; it was decided to follow similar protocols to assess H_2O_2 production.

Stock solutions, H_2O_2 standards and amplex® red working solution were prepared as in section 7.2.2.

	mM	g/litre
HEPES	20	5.206
NaCl	119	6.950
KCl	4.6	0.343
$MgSO_47H_2O$	1	0.246
Na_2HPO_4	0.15	0.021
KH_2PO_4	0.4	0.054
$NaHCO_3$	5	0.420
$CaCl_2$	1.2	0.133
Glucose	5.5	0.991

Table 34: Composition of modified Krebs-HEPES buffer

Freshly excised aortas were collected into modified Krebs-HEPES buffer (pH 7.4) (see Table 34) and cleaned of outer adipose tissue. The aortas were divided into 2 approximately equal segments and each of these divided in to 3 equal rings. 3 x 2mm rings were incubated in 50µl of modified Krebs-HEPES buffer for 1 hour at 37°C. The remaining 3 x2mm rings were incubated with modified Krebs-HEPES buffer with 200 iu/ml of catalase for 1 hour at 37°C. 50µl of 100µM amplex® red working solution was added to the samples and standards and they were incubated for 1 hour protected from light at 37°C. Rings were removed from the samples and the absorbance read at 560nm on a Spectra Max 190 plate reader (Molecular Devices). As detailed before, a standard curve was generated from the H_2O_2 standards using Graph Pad prism software and used to determine H_2O_2 concentration.

Protein concentrations of supernatant were measured using Pierce® BCA Protein Assay kit (Thermo Scientific), as described in section 4.2.5.2, and results are expressed as µM per mg of protein.

In this pilot experiment we were able to demonstrate a reduction in signal in the presence of catalase, albeit of a modest magnitude. Further examination of the literature suggested that a dose of 1250 iu/ml of catalase would be a more appropriate dose and hence this was used in the experimental protocol.

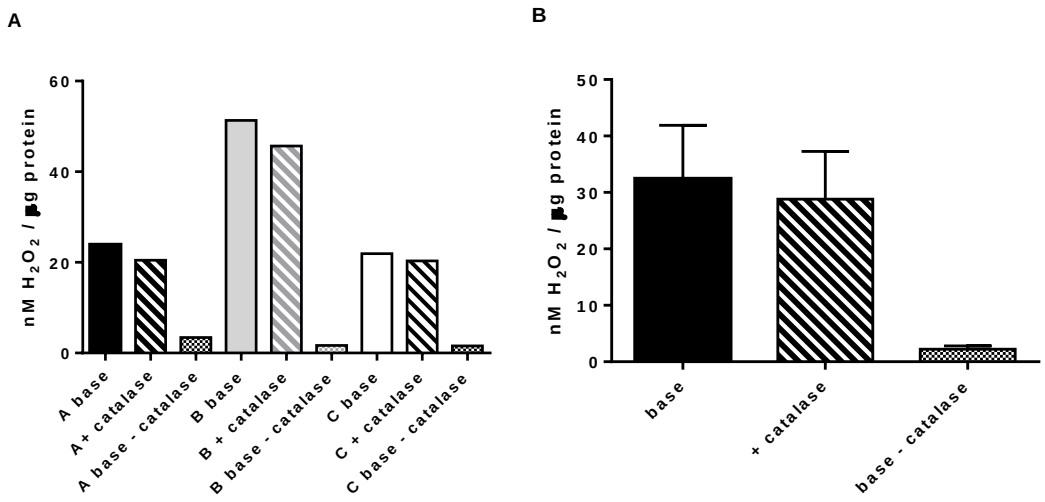

Figure 7.2-5: Results from pilot experiment 2: (A) shows results from 3 samples (A-C) demonstrating a consistent reduction in signal seen when catalase was added (approx. 10% reduction in signal), the bars labelled base – catalase represent the signal inhibitable by catalase. (B) shows the mean +/- SEM of these results.

7.2.4 Quantitative polymerase chain reaction assessment of potential sources of ROS

Quantitative PCR was performed as in chapter 4.2.3. Expression of mRNA of Nox1-4 and SOD1-3 was assessed using primers shown in Table 35.

Gene		Sequence
Nox1	Reverse	TTACACGAGAGAAATTCTGGG
	Forward	TCGACACACAGGAATCAGGA
Nox2	Reverse	GCGGTGTGCAGTGCTATCAT
	Forward	GGTTCCAGTGCGTGTTGCT
Nox3	Reverse	GTCACTCCCTTCGCCTCTCT
	Forward	CCGGCAGATCCAATAGAAGT
Nox4	Reverse	TGTATAACTTAGGGTAATTTCTAGAGTGAATGA
	Forward	GGAGACTGGACAGAACGATTCC
SOD1	Reverse	GGTCTCCAACATGCCTCTCTTC
	Forward	GGACCTCATTTTAATCCTCACTCTAAG
SOD2	Reverse	GGTGGCGTTGAGATTGTTCA
	Forward	CACACATTAACGCGCAGATCA
SOD3	Reverse	ACACCTTAGTTAACCCAGAAATCTTTTC
	Forward	GGGATGGATCTAGAGCATTAAGGA

Table 35: Primers used to assess mRNA in Nox 1-4 and SOD 1-3

7.2.5 Statistics

Results are expressed as mean +/- SEM. Comparative analysis within groups was performed using paired Student t test; between groups unpaired Student t test. $P < 0.05$ was considered to be statistically significant.

7.3 Results

7.3.1 ACh + catalase

Treatment of the aortic rings with catalase before preconstriction with PE and subsequent induction of vasorelaxation with ACh affects acetylcholine induced vasorelaxation in both groups of mice: although the magnitude of the effect is more marked in the MIGFREO mice and the effect in MIGFREO mice is seen immediately and is more sustained. In MIGFREO mice at every dose of ACh, catalase is associated with a significant reduction in vaso-relaxation (Figure 7.3-2, Table 36); a significant change is noted in wt. mice at moderate doses of ACh, but not at low or maximal doses (Figure 7.3-1, Table 36**)**. The difference in maximal relaxation with peak ACh dose achieved pre and post catalase is significantly different in MIGFREO mice (87.27% +/- 2.78 vs. 70.46% +/- 5.40 respectively, p = 0.008) (Figure 7.3-3 and Figure 7.3-4) whilst there is no difference pre and post catalase in wt. mice (89.29% +/- 3.27 vs. 88.50% +/- 8.58 respectively, p = 0.93).

ACh dose (nM)	wt. control +/- SEM	wt. catalase +/- SEM	MIGFREO control +/- SEM	MIGFREO catalase +/- SEM	p value wt. con vs. wt. cat	p value MIG con vs. MIG cat
1	6.74 +/- 2.43	3.817 +/- 2.93	6.97 +/- 1.79	1.62 +/- 0.84	0.44	0.009
3	11.37 +/- 3.20	7.66 +/- 3.30	12.21 +/- 1.80	2.64 +/- 1.45	0.42	0.00011
10	24.09 +/- 3.34	10.50 +/- 4.61	23.68 +/- 2.92	5.68 +/- 2.03	0.02	2.8E-06
30	47.81 +/- 4.86	22.16 +/- 6.25	44.84 +/- 4.58	17.97 +/- 3.04	0.022	8.3E-06
100	69.55 +/- 4.50	40.81 +/- 7.85	69.28 +/- 4.30	37.93 +/- 4.06	0.0025	2.4E-06
300	85.40 +/- 4.09	70.06 +/- 3.36	84.16 +/- 3.68	57.49 +/- 4.96	0.10	6.1E-05
1000	89.29 +/- 3.27	88.50 +/- 8.58	87.27 +/- 2.78	70.46 +/- 5.40	0.93	0.008

Table 36: Acetylcholine induced vasodilatation in presence and absence of catalase. This demonstrates that following incubation with catalase there was reduction in response to Ach in both wt. and MIGFREO mice, although this effect was more marked in MIGFREO mice (peak relaxation in MIGFREO mice was significantly reduced in response to catalase when compared to wt. mice p=0.008) Mean +/- SEM. Corrected to 2 decimal places. N=6.

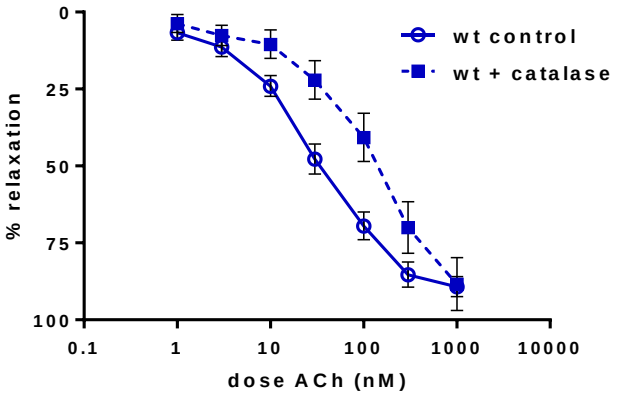

Figure 7.3-1: ACh relaxation +/- catalase (wt.). Relaxation of aorta in the organ bath in response to increasing doses of Ach either with (dotted line) or without (solid line) incubation with catalase. Addition of catalase is associated with reduction of relaxation at lower doses but is not associated with any change in peak relaxation in wt. aorta. N = 6

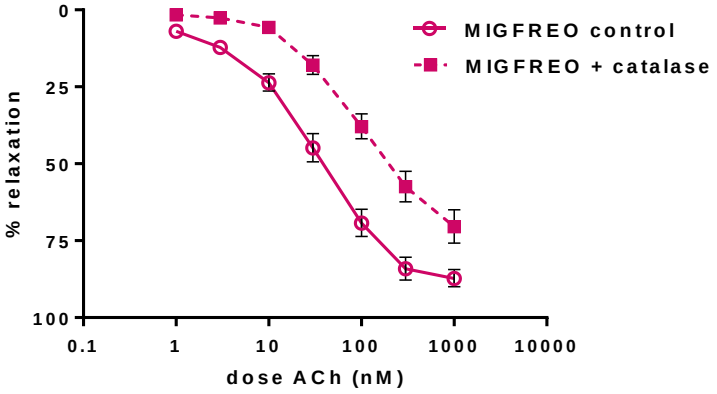

Figure 7.3-2: ACh relaxation +/- catalase (MIGFREO). Relaxation of aorta in the organ bath in response to increasing doses of Ach either with (dotted line) or without (solid line) incubation with catalase. Addition of catalase is associated with significant reduction of maximal relaxation in response to acetylcholine. This suggests that some vasodilatation is due to H_2O_2. N =6

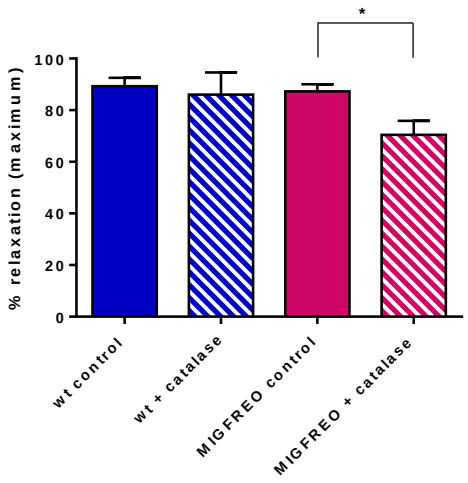

Figure 7.3-3: Maximal % change in relaxation +/- catalase. This shows the percentage of relaxation towards the base in wt. (blue) and MIGFREO (pink) aorta in response to acetylcholine either with (hashed box) or without (solid box) the addition of catalase. Bars represent mean +/- SEM. There is no significant reduction in maximal relaxation in wt. samples following exposure to catalase (p=0.93) although there is a significant reduction in maximal relaxation following exposure to catalase in MIGFREO mice (*p=0.008). N = 6 per group

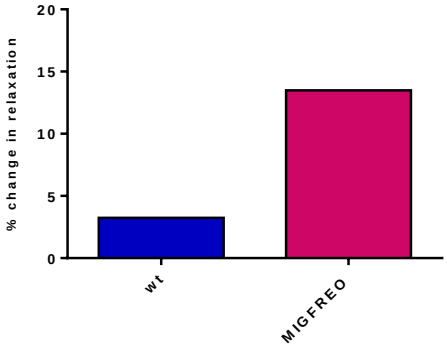

Figure 7.3-4: Percentage change in relaxation with catalase. Percentage change in maximal relaxation following addition of catalase.

7.3.2 H_2O_2 production in aorta

Results from the amplex® red assay are shown below (Figure 7.3-5 Figure 7.3-6). Although the "total" H_2O_2 is plotted this represents the concentration of H_2O_2 normalised to total protein in the sample without catalase added, and given that the concentrations of H_2O_2 seen were relatively small, any contamination of the sample with plasma or red cells would

have significantly skewed the results. I attempted to minimise this by looking at the catalase inhibitable fraction. Use of the catalase inhibitable fraction ensures that the signal obtained is derived solely from resorufin generated from the combination of H_2O_2 and amplex® red, rather than from any inherent discolouration of the sample. There is a clear and statistically significant difference in basal H_2O_2 production between wt. and MIGFREO mice. MIGFREO mice produced significantly more H_2O_2 than wt. mice.

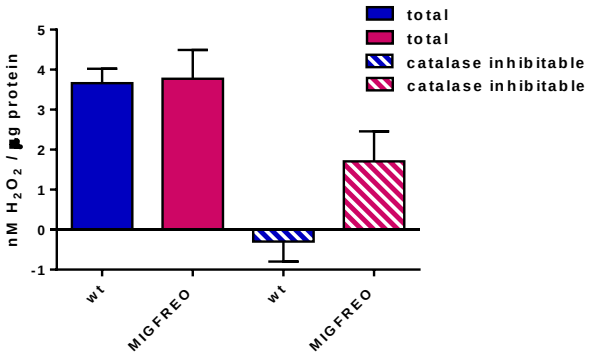

Figure 7.3-5: Total and catalase inhibitable signal from amplex red assay. Total H_2O_2 production (in nMH_2O_2 / µg protein) (solid bars) and catalase inhibitable fraction (hashed bars) in modified krebs solution following incubation with aortic rings. The columns display Mean +/-SEM with wt. (blue) and MIGFREO (pink). When the catalase inhibitable fraction is calculated, there is significantly higher concentration of basal H_2O_2 in the krebs incubated with rings from MIGFREO aortae. N = 10 per group

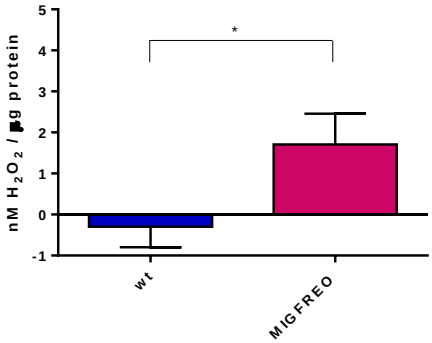

Figure 7.3-6: Catalase inhibitable H_2O_2 production in aorta as measured using amplex® red. The columns display Mean +/-SEM nMH_2O_2 / µg aortic protein taken from wt. (blue) and MIGFREO (pink). When the catalase inhibitable fraction is calculated, there is significantly higher concentration of basal H_2O_2 in the modified krebs incubated with rings from MIGFREO aortae *$p<0.05$. N= 10 per group

7.3.3 Quantitative PCR of potential sources of ROS

Quantitative PCR does not demonstrate any significant differences between MIGFREO and wt. mice with regards to expression of the mRNA of various sources of ROS (Figure 7.3-7). There is a significant variation in results as exhibited by large error bars on almost all data. For each enzyme RNA was obtained from 4 MIGFREO and 4 wt. animals, and it may be that more numbers are required to establish if there is a difference between the 2 sets on animals. As with the quantitative PCR performed to assess expression of human and mouse IGF-1R on the PEC the housekeeping gene used was β actin. Certainly variable expression of β actin may have accounted for differences of apparent expression of human IGF-1R seen between different tissues (Figure 4.3-6) but it seems unlikely that this may explain the large error seen here: the RNA was all derived from PEC. The issue with variation in results may lay more with the quality of the RNA. Although RNA quality was assessed following extraction, the RNA was then frozen at -80°C for in excess of 24 months, and defrosted and re-frozen several times before it underwent the reverse transcription to cDNA prior to the quantitative PCR. In retrospect I suspect that it is possible that the RNA may have degraded in the interim, and the use of fresh samples would have been more appropriate. Certainly it would have been appropriate to reassess quality and concentration of RNA immediately prior to converting it to cDNA.

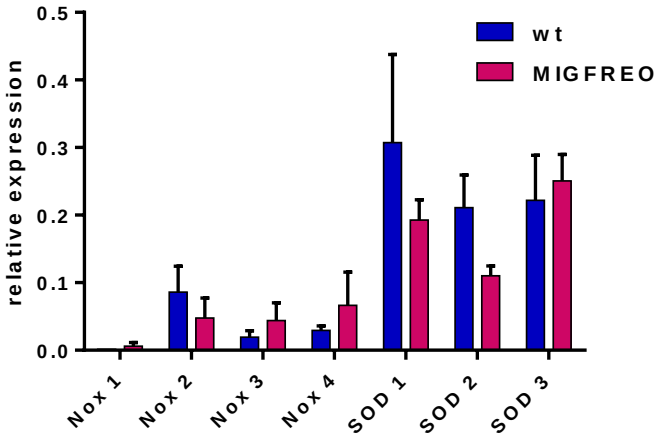

Figure 7.3-7: Relative expression of Nox and SOD in PEC. Mean +/- SEM relative expression of various genes associated with enhanced production of reactive oxygen species in pulmonary endothelial cells derived from wt. (blue) and MIGFREO (pink) lungs. There were no significant differences in gene expression between wt. and MIGFREO. N = 12 per group

7.4 Conclusion and Discussion

MIGFREO mice have elevated basal levels of H_2O_2

The presented data demonstrate enhanced basal H_2O_2 in vascular and endothelial tissue from the MIGFREO mice when compared with wt. counterparts.

The data from the organ bath demonstrates that catalase significantly blunts maximal endothelial dependent vasodilatation in MIGFREO mice; maximal relaxation achieved pre and post catalase (87.27% +/- 2.78 vs. 70.46% +/- 5.40 respectively, p = 0.008) (Figure 7.3-3 and Figure 7.3-4) whilst there is no difference pre and post catalase in wt. mice (89.29% +/- 3.27 vs. 88.50% +/- 8.58 respectively, p = 0.93). This strongly suggests that H_2O_2 is higher in MIGFREO mice; the quenching of H_2O_2 dependent vasodilatation with catalase has a significant impact on maximal endothelial dependent vasodilatation in MIGFREO mice. The same is not true in wt. mice. At modest doses of ACh, catalase does have an effect on endothelial dependent vasodilatation in wt. mice however this is less marked than the change seen in endothelial dependent vasodilatation in MIGFREO mice, and indeed at maximal vasodilatation catalase has no effect on endothelial dependent vasodilatation in wt. mice. Given that H_2O_2 acts as an EDHF [283, 337], it is unsurprising that catalase effects endothelial dependent vasodilatation in wt. mice, although Noronah *et al* [338] using an identical protocol did not demonstrate any effect of catalase on endothelial dependent vasodilatation in wt. chow fed mice.

As a single method of assessing vascular H_2O_2 production, the data from the organ bath is certainly highly suggestive that MIGFREO mice produce higher basal levels of H_2O_2 than their wt. littermates. Whilst this demonstrates an association, further corroboration was sought from alternative methods of assessing H_2O_2 production.

Data from the Amplex® Red assay, which produces resorufin in a 1:1 stoichiometry with H_2O_2 demonstrates a clear and significant difference in basal H_2O_2 production between MIGFREO and wt. mice, with the MIGFREO mice producing significantly elevated levels of H_2O_2 at baseline. This assay measures extracellular H_2O_2: the concentration of H_2O_2 measured is the concentration of H_2O_2 within the Krebs HEPES buffer after a 2 hour incubation period (1 hour with and 1 hour without the amplex® red working solution). Although measurement of the intracellular concentration of H_2O_2 would have been interesting, the measurement of extracellular H_2O_2 was important, given the theory that

endothelial derived H_2O_2 may be responsible for the improved whole body insulin sensitivity seen in the MIGFREO mice.

How could endothelial derived H_2O_2 be responsible for changes in whole body insulin sensitivity? There are several potential possibilities. It has been extensively discussed that H_2O_2 is able to positively regulate insulin signalling, either by directly priming the insulin receptor, or by inhibiting PTP1B. Given that H_2O_2 is relatively stable and diffuses easily through aquaporins [69], it could have a direct effect on insulin signalling, and hence insulin mediated glucose transportation in skeletal muscle, thereby having a paracrine effect. Alternatively, the H_2O_2 could act locally on endothelial cells to enhance local insulin sensitivity, therefore enhancing insulin mediated increases in capillary recruitment and transendothelial insulin transportation. The latter seems less likely given that we have demonstrated reduced endothelial insulin sensitivity.

Chapter 8: Conclusion, Discussion and Future Plans

8 Conclusion, Discussion and Future Plans

8.1 Discussion

The work presented above details the validation of, and investigation into the metabolic and endothelial phenotype of the MIGFREO mouse.

The MIGFREO mouse model has been validated as expressing a mutated form of the human IGF-1R which is expressed solely on the vascular endothelium. Quantitative PCR demonstrates that the human IGF-1R was expressed solely on the endothelial cells derived from the MIGFREO mice. As has been discussed, quantitative PCR used primers specific for the presence of the human IGF-1R, but not specific for the K1003 mutation, which renders the IGF-1R functionally inactive, a strategy employed by Fernandez *et al* [306] who examined the effect of incorporation of a human IGF-1R with the K1003R mutation in the skeletal muscle. The unique presence of human IGF-1R mRNA on the cells labelled with CD146 microbeads strongly supports, not only the method of PEC isolation used in this project, but also that the human, and therefore mutated, IGF-1R is expressed only on endothelial cells. Assessment of protein shows that there is a significantly elevated level of IGF-1Rβ in PEC extracted from MIGFREO lung tissue. This coupled with assessment of levels of mouse IGF-1R mRNA shows that incorporation of the human IGF1-R does not down regulate expression of the native mouse IGF-1R in MIGFREO mice.

The MIGFREO mouse displays normal growth and development and is fertile, producing wild type and transgenic offspring in a characteristic Mendelian pattern of inheritance. There is no discernible difference in weight, organ weight, fat pad size or systemic blood pressure in the MIGFREO mice, and microscopic examination of the epididymal fat pad shows that fat cell size and number are comparable with their wild type litter mates.

As was hypothesised, the MIGFREO mouse has endothelial insulin resistance, as demonstrated by an absent vasodilatory response to insulin (Figure 5.3-2, **Error! Reference source not found.**, **Error! Reference source not found.**, Figure 5.3-3) and significantly reduced insulin stimulated eNOS activity (Figure 5.3-9, Figure 5.3-10). Assessment of protein phosphorylation in response to insulin did not show any significant difference between MIGFREO and wt. mice, although the potential reasons for this have already been discussed. In addition to reduced endothelial insulin sensitivity the MIGFREO mouse also has a degree of endothelial resistance to IGF-1, with marked reduction in IGF-1 stimulated eNOS activity (Figure 5.3-9, Figure 5.3-10), although there was no detectable difference seen between the groups of mice with regards the vasodilatory response to IGF-1. As was

previously discussed I suspect that this disparity related to the relative sensitivities of the 2 methods of detecting response to IGF-1 and insulin.

The cause of endothelial insulin resistance in the MIGFREO mice is, I believe, explained by the postulated distribution of hybrid receptors on the endothelium: the incorporation of the mutant non-functioning IGF-1R drives the production of increased numbers of the hybrid receptors. The functional IGF-1R will continue to be incorporated into hybrid receptors, which by their nature will be less sensitive to insulin; incorporation of the non-functional IGF-1R will render the entire receptor, whatever its composition, entirely inactive. This would be associated with marked endothelial insulin resistance and less marked IGF-1 resistance, as has been shown.

Although this seems a reasonable explanation, it has, of course not been demonstrated. I have not assessed the ratio of hybrid receptors on tissue from either the MIGFREO mouse or wt. mice which is a clear limitation of this project. Using co-immunoprecipitation it is possible to assess the relative density of hybrid receptors in any tissue, and it is possible to assess whether the hybrid are functional or non-functional using either whole body or cell directed stimulation with insulin. Clearly complete characterisation of this model for future should include examination of the density and function of the hybrid receptors.

Whilst the presence of endothelial insulin resistance in the MIGFREO was perhaps predictable, the presence of whole body insulin sensitivity was unexpected and has proven to be very interesting. Although the magnitude of whole body insulin sensitivity in the MIGFREO mice is relatively small it is highly statistically significant and as such merits further consideration. In addition to insulin sensitivity the MIGFREO mouse also has a degree of enhanced IGF-1 sensitivity, and an overall favourable metabolic profile is suggested by lower plasma FFA. As has been discussed the presence of lower FFA is certainly consistent with enhanced insulin sensitivity, although whether lower FFA have any causative role in the development of insulin sensitivity in the MIGFREO mouse is not known. Importantly, plasma IGF-1 and insulin levels are comparable between the groups of mice. Although there are no significant changes in any other plasma component measured, there is a strong trend towards elevated levels of the beneficial adipokine adiponectin in the MIGFREO mouse, which would not be inconsistent with enhancement of whole body insulin sensitivity.

A divergence between whole body and endothelial insulin sensitivity is not a novel finding in the literature. The VEPDK1KO mouse displays endothelial insulin resistance and whole body insulin sensitivity, which appears to be modulated by changes in angiogenesis, particularly in white adipose tissue [326]. I was unable to demonstrate any changes in fat cell size or number in the MIGFREO mice which would suggest that the mechanism may be different, although many of the changes in fat cell number and angiogenesis within adipose tissue in the VEPDK1KO mouse were shown either at 6 months of age or at 3 months of age with a high fat diet. The MIGFREO mice were used at approximately 3 months of age, and further investigation of the adipose tissue of the MIGFREO mouse would be appropriate at an older age, and perhaps after a period of high fat feeding. Given the role of insulin signalling in angiogenesis it is not unreasonable to consider that this too might be affected in MIGFREO mice and could have a role to play in the development of whole body insulin sensitivity. This should certainly be considered as future work.

It seems reasonable at this stage to consider other animal models of endothelial insulin resistance and the effect seen on whole body glucose homeostasis. The ESMIRO mouse [195] expresses a dominant mutant form of the IR expressed on the vascular endothelium, which is associated with endothelial insulin resistance and excess oxidative stress. The ESMIRO mouse displayed a significant trend towards enhanced whole body insulin sensitivity ($p=0.05$), but this was not particularly commented on by the authors. The VENIRKO mouse [303], which has knockout of the IR on the vascular endothelium, also has endothelial insulin resistance and, as shown in Figure 6.4-1 at 6 months also has enhanced insulin sensitivity when compared to the wild type mouse, although again this was not particularly commented on by the authors. In both cases the magnitude of effect was quite small, which may explain why it was not commented on. I wonder if this is related to the degree of endothelial insulin resistance seen.

Although it is difficult to make judgements of the relative degree of endothelial insulin resistance in different models, a useful comparison would be the differences in insulin sensitivity shown when similar strategies are used to affect insulin signalling in skeletal muscle. The MIRKO mouse [305] has a muscle specific deletion of the IR receptor. One might expect, given that muscle is one of the most important sites of insulin mediated glucose disposal that this would have a profound effect on whole body glucose homeostasis. Interestingly, whilst in vitro there was an effect on insulin sensitivity whole body insulin sensitivity in the MIRKO mouse was comparable with wild type. In comparison,

mice with muscle specific K1003R mutation of the IGF-1R receptor [306] have profound insulin resistance and develop type 2 diabetes at an early age. Whilst this is initially somewhat counterintuitive, the explanation is likely to involve the formation of non-functional IGF-1R/IR hybrid receptors in the latter mouse, whilst insulin signalling via native hybrid receptors would not be affected in the former. I suggest that the same might apply in the endothelium: the MIGFREO mouse may be a more profound model of endothelial insulin resistance than either the ESMIRO or the VENIRKO mouse in view of the likely formation of non-functional hybrid receptors.

But how might this be relevant in considering why there is divergence between whole body and endothelial insulin sensitivity seen in the MIGFREO mice?

In view of the increasing body of evidence which supports a role for low levels of H_2O_2 to play a role in enhancing insulin signalling, either by oxidative inactivation of the PTPs, or by directly priming the IR I hypothesised that the endothelial insulin resistance would be associated with higher levels of H_2O_2 which could be associated with whole body insulin sensitivity. It follows that more profound insulin resistance on the endothelium might be associated with higher levels of H_2O_2, which could explain the disparity between degrees of whole body insulin sensitivity seen in ESMIRO and VENIRKO mice, although this of course is purely conjecture.

The data looking at H_2O_2 production in MIGFREO mice appears to support the premise that H_2O_2 may play a role in enhanced whole body insulin sensitivity. Significantly reduced vasodilatation in the MIGFREO mice in the presence of catalase suggests the presence of higher levels of H_2O_2; H_2O_2 production in the aorta assessed by amplex® red is also higher in the MIGFREO mice, substantiating, but not proving the hypothesis. The source of the apparent H_2O_2 is also, as yet undetermined. Qualitative PCR did not demonstrate any significant differences in expression of the various isoforms of Nox, notably Nox4, between the 2 sets of mice, although the limitations of this set of experiments have been previously discussed.

There is a considerable amount of further work which would need to be performed to prove it, but I suggest that in the presence of endothelial insulin resistance, the endothelium acts as a paracrine organ, releasing H_2O_2 which is able to modulate whole body insulin sensitivity.

8.2 Suggested future work

As has been previously discussed, it is necessary to attempt to characterise the distribution of hybrid receptors in MIGFREO mice. It would not be possible to establish whether a particular hybrid receptor actually had the mutation rendering it inactive, but it should be possible to assess the relative density and activity in response insulin and IGF-1 of the hybrid receptors seen on endothelial and non-endothelial cells.

Whilst I feel confident that endothelial insulin resistance has been unequivocally demonstrated in the MIGFREO mice, I was unable to demonstrate any change in protein phosphorylation following insulin and IGF-1 stimulation between the 2 groups of mice. The reasons for this have been discussed, and I would suggest that the western blots should be repeated using endothelial cells at P0, and using milk-free blocking buffer.

The antioxidant N-acetyl-cysteine (NAC) has been widely used in mice to study the effects of reducing ROS on various biological and cellular processes. The hypothesis that elevated levels of H_2O_2 produced by the MIGFREO mouse could be responsible for enhancing whole body insulin sensitivity could be assessed by treating the mice with NAC for 2 weeks and assessing insulin tolerance before and after treatment.

Whole body insulin sensitivity, with particular respect to sensitivity to insulin in muscle and fat could be performed by taking tissue and assessing protein expression and phosphorylation with and without insulin stimulation. A useful further addition would be to see if this changes pre and post treatment with

Further assessment of H_2O_2 is also imperative if a causative association between higher basal levels of H_2O_2 in MIGFREO mice and enhanced insulin sensitivity is to be shown. Assessment of total levels of ROS with lucigenin enhanced chemiluminescence will help to establish if total superoxide levels are elevated. This can be performed in response to a number of stimuli and inhibitors, such as L-NAME, oxypurinol and specific inhibitors of Nox in an attempt to establish the source of ROS. H_2O_2 production from cells can also be established using the amplex® red assay, again this could be performed in response to a number of stimuli and inhibitors. In order to corroborate the results of the amplex® red assay in the aorta further assessment of H_2O_2 production can be performed using the ferrous oxidation-xyenol orange method. This assay is based on the ability of H_2O_2 to convert ferrous into ferric ions which subsequently form a purple complex with xylenol

orange. The resultant colour change can be detected on a plate reader. High performance liquid chromatography can be used to measure the conversion of dihydroethidium to oxyethidium which reflects the rate of intracellular superoxide production and would also be a further useful adjunct to the data already generated.

Given the results seen with the VEPDK1KO mouse [326] It would also be interesting to look more closely at fat composition, metabolism and angiogenesis in the MIGFREO mice to assess whether the endothelial insulin resistance seen in MIGFREO mice is associated with any changes in angiogenesis in fat, with subsequent changes in fat metabolism, particularly in mice at an older age, and following a period of high fat feeding.

Following on from this, further consideration should be given to the way H_2O_2 is affecting insulin signalling in sites of insulin stimulated glucose uptake: is it acting to oxidise PTP1B and therefore enhance insulin signalling; or is the major action at the insulin receptor itself, causing modification of the activation loop and enhancing autophosphorylation? In addition, how is H_2O_2 reaching sites of glucose uptake: is transendothelial insulin transportation or the recruitment of the microvasculature affected or does the H_2O_2 diffuse easily through aquaporins to the sites of glucose disposal?

Arrangements are being made to investigate this further and attempt to understand the mechanism of whole body insulin sensitivity seen in the MIGFREO mouse.

8.3 Concluding remarks

The generation of a mouse with divergent endothelial and whole body insulin sensitivity is an unusual, but not novel finding. However the demonstration that in the MIGFREO mouse this is accompanied by elevated levels of H_2O_2 raises the intriguing possibility that in the face of significant endothelial insulin resistance the endothelium may play a role in modulating, and indeed enhancing whole body insulin sensitivity. If this is confirmed by further work, this would be a novel role of the endothelium, and would potentiality be open to manipulation by pharmacological methods in an attempt to improve treatment for patients with insulin resistance and accelerated atherosclerosis.

References

1. Mathers, C.D. and D. Loncar, *Projections of global mortality and burden of disease from 2002 to 2030.* PLoS Med, 2006. **3**(11): p. e442.
2. Kannel, W.B., et al., *Factors of risk in the development of coronary heart disease--six year follow-up experience. The Framingham Study.* Ann Intern Med, 1961. **55**: p. 33-50.
3. Duff, G.L. and M.G. Mc, *Pathology of atherosclerosis.* Am J Med, 1951. **11**(1): p. 92-108.
4. LaRosa, J.C., J. He, and S. Vupputuri, *Effect of statins on risk of coronary disease: a meta-analysis of randomized controlled trials.* JAMA, 1999. **282**(24): p. 2340-6.
5. *MRC/BHF Heart Protection Study of antioxidant vitamin supplementation in 20,536 high-risk individuals: a randomised placebo-controlled trial.* Lancet, 2002. **360**(9326): p. 23-33.
6. Braunwald, E., *Shattuck lecture--cardiovascular medicine at the turn of the millennium: triumphs, concerns, and opportunities.* N Engl J Med, 1997. **337**(19): p. 1360-9.
7. Ross, R., *Atherosclerosis--an inflammatory disease.* N Engl J Med, 1999. **340**(2): p. 115-26.
8. Ross, R., *The pathogenesis of atherosclerosis: a perspective for the 1990s.* Nature, 1993. **362**(6423): p. 801-9.
9. Wheatcroft, S.B., et al., *Pathophysiological implications of insulin resistance on vascular endothelial function.* Diabet Med, 2003. **20**(4): p. 255-68.
10. Esper, R.J., et al., *Endothelial dysfunction: a comprehensive appraisal.* Cardiovasc Diabetol, 2006. **5**: p. 4.
11. Luscher, T.F., *The endothelium and cardiovascular disease--a complex relation.* N Engl J Med, 1994. **330**(15): p. 1081-3.
12. Mombouli, J.V. and P.M. Vanhoutte, *Endothelial dysfunction: from physiology to therapy.* J Mol Cell Cardiol, 1999. **31**(1): p. 61-74.
13. Palmer, R.M., A.G. Ferrige, and S. Moncada, *Nitric oxide release accounts for the biological activity of endothelium-derived relaxing factor.* Nature, 1987. **327**(6122): p. 524-6.
14. Zeiher, A.M., et al., *Tissue endothelin-1 immunoreactivity in the active coronary atherosclerotic plaque. A clue to the mechanism of increased vasoreactivity of the culprit lesion in unstable angina.* Circulation, 1995. **91**(4): p. 941-7.
15. Garg, U.C. and A. Hassid, *Nitric oxide-generating vasodilators and 8-bromo-cyclic guanosine monophosphate inhibit mitogenesis and proliferation of cultured rat vascular smooth muscle cells.* J Clin Invest, 1989. **83**(5): p. 1774-7.
16. Nakaki, T., M. Nakayama, and R. Kato, *Inhibition by nitric oxide and nitric oxide-producing vasodilators of DNA synthesis in vascular smooth muscle cells.* Eur J Pharmacol, 1990. **189**(6): p. 347-53.

17. Tsihlis, N.D., et al., *Nitric oxide inhibits vascular smooth muscle cell proliferation and neointimal hyperplasia by increasing the ubiquitination and degradation of UbcH10.* Cell Biochem Biophys, 2011. **60**(1-2): p. 89-97.

18. Heller, R., et al., *Nitric oxide inhibits proliferation of human endothelial cells via a mechanism independent of cGMP.* Atherosclerosis, 1999. **144**(1): p. 49-57.

19. Cartwright, J.E., A.P. Johnstone, and G.S. Whitley, *Endogenously produced nitric oxide inhibits endothelial cell growth as demonstrated using novel antisense cell lines.* Br J Pharmacol, 2000. **131**(1): p. 131-7.

20. Marrero, M.B., et al., *Role of Janus kinase/signal transducer and activator of transcription and mitogen-activated protein kinase cascades in angiotensin II- and platelet-derived growth factor-induced vascular smooth muscle cell proliferation.* J Biol Chem, 1997. **272**(39): p. 24684-90.

21. Kubes, P., M. Suzuki, and D.N. Granger, *Nitric oxide: an endogenous modulator of leukocyte adhesion.* Proc Natl Acad Sci U S A, 1991. **88**(11): p. 4651-5.

22. Zimmerman, G.A., et al., *Endothelial cell-associated platelet-activating factor: a novel mechanism for signaling intercellular adhesion.* J Cell Biol, 1990. **110**(2): p. 529-40.

23. Denis, C.V., *Molecular and cellular biology of von Willebrand factor.* Int J Hematol, 2002. **75**(1): p. 3-8.

24. Harrison, D.G., *Cellular and molecular mechanisms of endothelial cell dysfunction.* J Clin Invest, 1997. **100**(9): p. 2153-7.

25. Creager, M.A., et al., *Impaired vasodilation of forearm resistance vessels in hypercholesterolemic humans.* J Clin Invest, 1990. **86**(1): p. 228-34.

26. Zeiher, A.M., et al., *Endothelium-mediated coronary blood flow modulation in humans. Effects of age, atherosclerosis, hypercholesterolemia, and hypertension.* J Clin Invest, 1993. **92**(2): p. 652-62.

27. Schachinger, V., M.B. Britten, and A.M. Zeiher, *Prognostic impact of coronary vasodilator dysfunction on adverse long-term outcome of coronary heart disease.* Circulation, 2000. **101**(16): p. 1899-906.

28. Feletou, M. and P.M. Vanhoutte, *Endothelium-derived hyperpolarizing factor.* Clin Exp Pharmacol Physiol, 1996. **23**(12): p. 1082-90.

29. Kelm, M. and J. Schrader, *Control of coronary vascular tone by nitric oxide.* Circ Res, 1990. **66**(6): p. 1561-75.

30. Williams, I.L., et al., *Obesity, atherosclerosis and the vascular endothelium: mechanisms of reduced nitric oxide bioavailability in obese humans.* Int J Obes Relat Metab Disord, 2002. **26**(6): p. 754-64.

31. Hocher, B., et al., *In-vivo interaction of nitric oxide and endothelin.* J Hypertens, 2004. **22**(1): p. 111-9.

32. Thomas, G.D. and R.G. Victor, *Nitric oxide mediates contraction-induced attenuation of sympathetic vasoconstriction in rat skeletal muscle.* J Physiol, 1998. **506 (Pt 3)**: p. 817-26.

33. Radomski, M.W., R.M. Palmer, and S. Moncada, *An L-arginine/nitric oxide pathway present in human platelets regulates aggregation.* Proc Natl Acad Sci U S A, 1990. **87**(13): p. 5193-7.

34. Hogan, J.C., M.J. Lewis, and A.H. Henderson, *In vivo EDRF activity influences platelet function.* Br J Pharmacol, 1988. **94**(4): p. 1020-2.

35. Bhardwaj, R., et al., *Endothelium-derived relaxing factor inhibits platelet aggregation in human whole blood in vitro and in the rat in vivo.* Eur J Pharmacol, 1988. **157**(1): p. 83-91.

36. Radomski, M.W., R.M. Palmer, and S. Moncada, *The role of nitric oxide and cGMP in platelet adhesion to vascular endothelium.* Biochem Biophys Res Commun, 1987. **148**(3): p. 1482-9.

37. Venturini, C.M., P.J. Del Vecchio, and J.E. Kaplan, *Thrombin induced platelet adhesion to endothelium is modified by endothelial derived relaxing factor (EDRF).* Biochem Biophys Res Commun, 1989. **159**(1): p. 349-54.

38. Sneddon, J.M. and J.R. Vane, *Endothelium-derived relaxing factor reduces platelet adhesion to bovine endothelial cells.* Proc Natl Acad Sci U S A, 1988. **85**(8): p. 2800-4.

39. Murohara, T., et al., *Nitric oxide synthase modulates angiogenesis in response to tissue ischemia.* J Clin Invest, 1998. **101**(11): p. 2567-78.

40. Cosentino, F. and T.F. Luscher, *Tetrahydrobiopterin and endothelial nitric oxide synthase activity.* Cardiovasc Res, 1999. **43**(2): p. 274-8.

41. Forstermann, U. and W.C. Sessa, *Nitric oxide synthases: regulation and function.* Eur Heart J, 2012. **33**(7): p. 829-37, 837a-837d.

42. Alderton, W.K., C.E. Cooper, and R.G. Knowles, *Nitric oxide synthases: structure, function and inhibition.* Biochem J, 2001. **357**(Pt 3): p. 593-615.

43. Schoonover, L.L., A.S. Stewart, and G.D. Clifton, *Hemodynamic and cardiovascular effects of nitric oxide modulation in the therapy of septic shock.* Pharmacotherapy, 2000. **20**(10): p. 1184-97.

44. Forstermann, U. and T. Munzel, *Endothelial nitric oxide synthase in vascular disease: from marvel to menace.* Circulation, 2006. **113**(13): p. 1708-14.

45. Stuehr, D., S. Pou, and G.M. Rosen, *Oxygen reduction by nitric-oxide synthases.* J Biol Chem, 2001. **276**(18): p. 14533-6.

46. Gatenby, V.K., H. Imrie, and M. Kearney, *The IGF-1 receptor and regulation of nitric oxide bioavailability and insulin signalling in the endothelium.* Pflugers Arch, 2013.

47. Vaziri, N.D., Z. Ni, and F. Oveisi, *Upregulation of renal and vascular nitric oxide synthase in young spontaneously hypertensive rats.* Hypertension, 1998. **31**(6): p. 1248-54.

48. Hink, U., et al., *Mechanisms underlying endothelial dysfunction in diabetes mellitus.* Circ Res, 2001. **88**(2): p. E14-22.

49. Kanazawa, K., et al., *Endothelial constitutive nitric oxide synthase protein and mRNA increased in rabbit atherosclerotic aorta despite impaired endothelium-dependent vascular relaxation.* Am J Pathol, 1996. **148**(6): p. 1949-56.

50. Oemar, B.S., et al., *Reduced endothelial nitric oxide synthase expression and production in human atherosclerosis.* Circulation, 1998. **97**(25): p. 2494-8.

51. Wilcox, J.N., et al., *Expression of multiple isoforms of nitric oxide synthase in normal and atherosclerotic vessels.* Arterioscler Thromb Vasc Biol, 1997. **17**(11): p. 2479-88.

52. Heitzer, T., et al., *Tetrahydrobiopterin improves endothelium-dependent vasodilation by increasing nitric oxide activity in patients with Type II diabetes mellitus.* Diabetologia, 2000. **43**(11): p. 1435-8.

53. Higashi, Y., et al., *Tetrahydrobiopterin enhances forearm vascular response to acetylcholine in both normotensive and hypertensive individuals.* Am J Hypertens, 2002. **15**(4 Pt 1): p. 326-32.

54. Stroes, E., et al., *Tetrahydrobiopterin restores endothelial function in hypercholesterolemia.* J Clin Invest, 1997. **99**(1): p. 41-6.

55. Heitzer, T., et al., *Tetrahydrobiopterin improves endothelium-dependent vasodilation in chronic smokers : evidence for a dysfunctional nitric oxide synthase.* Circ Res, 2000. **86**(2): p. E36-41.

56. Laursen, J.B., et al., *Endothelial regulation of vasomotion in apoE-deficient mice: implications for interactions between peroxynitrite and tetrahydrobiopterin.* Circulation, 2001. **103**(9): p. 1282-8.

57. Chen, C.A., et al., *S-glutathionylation uncouples eNOS and regulates its cellular and vascular function.* Nature, 2010. **468**(7327): p. 1115-8.

58. Xu, W., et al., *Increased arginase II and decreased NO synthesis in endothelial cells of patients with pulmonary arterial hypertension.* FASEB J, 2004. **18**(14): p. 1746-8.

59. Vaisman, B.L., et al., *Selective endothelial overexpression of arginase II induces endothelial dysfunction and hypertension and enhances atherosclerosis in mice.* PLoS One, 2012. **7**(7): p. e39487.

60. Shin, W.S., D.E. Berkowitz, and S.W. Ryoo, *Increased arginase II activity contributes to endothelial dysfunction through endothelial nitric oxide synthase uncoupling in aged mice.* Exp Mol Med, 2012. **44**(10): p. 594-602.

61. Antoniades, C., et al., *Association of plasma asymmetrical dimethylarginine (ADMA) with elevated vascular superoxide production and endothelial nitric oxide synthase uncoupling: implications for endothelial function in human atherosclerosis.* Eur Heart J, 2009. **30**(9): p. 1142-50.

62. Kuzkaya, N., et al., *Interactions of peroxynitrite, tetrahydrobiopterin, ascorbic acid, and thiols: implications for uncoupling endothelial nitric-oxide synthase.* J Biol Chem, 2003. **278**(25): p. 22546-54.

63. Corretti, M.C., et al., *Guidelines for the ultrasound assessment of endothelial-dependent flow-mediated vasodilation of the brachial artery: a report of the International Brachial Artery Reactivity Task Force.* J Am Coll Cardiol, 2002. **39**(2): p. 257-65.

64. Boger, R.H., et al., *Plasma asymmetric dimethylarginine and incidence of cardiovascular disease and death in the community.* Circulation, 2009. **119**(12): p. 1592-600.

65. Schnabel, R., et al., *Asymmetric dimethylarginine and the risk of cardiovascular events and death in patients with coronary artery disease: results from the AtheroGene Study.* Circ Res, 2005. **97**(5): p. e53-9.

66. Krempl, T.K., et al., *Elevation of asymmetric dimethylarginine in patients with unstable angina and recurrent cardiovascular events.* Eur Heart J, 2005. **26**(18): p. 1846-51.

67. Boger, R.H., et al., *LDL cholesterol upregulates synthesis of asymmetrical dimethylarginine in human endothelial cells: involvement of S-adenosylmethionine-dependent methyltransferases.* Circ Res, 2000. **87**(2): p. 99-105.

68. Lin, K.Y., et al., *Impaired nitric oxide synthase pathway in diabetes mellitus: role of asymmetric dimethylarginine and dimethylarginine dimethylaminohydrolase.* Circulation, 2002. **106**(8): p. 987-92.

69. Henzler, T. and E. Steudle, *Transport and metabolic degradation of hydrogen peroxide in Chara corallina: model calculations and measurements with the pressure probe suggest transport of H(2)O(2) across water channels.* J Exp Bot, 2000. **51**(353): p. 2053-66.

70. Landmesser, U., et al., *Oxidation of tetrahydrobiopterin leads to uncoupling of endothelial cell nitric oxide synthase in hypertension.* J Clin Invest, 2003. **111**(8): p. 1201-9.

71. Zou, M.H., C. Shi, and R.A. Cohen, *Oxidation of the zinc-thiolate complex and uncoupling of endothelial nitric oxide synthase by peroxynitrite.* J Clin Invest, 2002. **109**(6): p. 817-26.

72. Schreck, R., P. Rieber, and P.A. Baeuerle, *Reactive oxygen intermediates as apparently widely used messengers in the activation of the NF-kappa B transcription factor and HIV-1.* EMBO J, 1991. **10**(8): p. 2247-58.

73. Berman, R.S. and W. Martin, *Arterial endothelial barrier dysfunction: actions of homocysteine and the hypoxanthine-xanthine oxidase free radical generating system.* Br J Pharmacol, 1993. **108**(4): p. 920-6.

74. Tabet, F., et al., *Redox-sensitive signaling by angiotensin II involves oxidative inactivation and blunted phosphorylation of protein tyrosine phosphatase SHP-2 in vascular smooth muscle cells from SHR.* Circ Res, 2008. **103**(2): p. 149-58.

75. Niu, X.L., et al., *Nox activator 1: a potential target for modulation of vascular reactive oxygen species in atherosclerotic arteries.* Circulation, 2010. **121**(4): p. 549-59.

76. White, S.J., et al., *Characterization of the differential response of endothelial cells exposed to normal and elevated laminar shear stress.* J Cell Physiol, 2011. **226**(11): p. 2841-8.

77. Murdoch, C.E., et al., *Role of endothelial Nox2 NADPH oxidase in angiotensin II-induced hypertension and vasomotor dysfunction.* Basic Res Cardiol, 2011. **106**(4): p. 527-38.

78. Violi, F., et al., *Hereditary deficiency of gp91(phox) is associated with enhanced arterial dilatation: results of a multicenter study.* Circulation, 2009. **120**(16): p. 1616-22.

79. Dikalov, S.I., et al., *Distinct roles of Nox1 and Nox4 in basal and angiotensin II-stimulated superoxide and hydrogen peroxide production.* Free Radic Biol Med, 2008. **45**(9): p. 1340-51.

80. Lener, B., et al., *The NADPH oxidase Nox4 restricts the replicative lifespan of human endothelial cells.* Biochem J, 2009. **423**(3): p. 363-74.

81. Ismail, S., et al., *NOX4 mediates hypoxia-induced proliferation of human pulmonary artery smooth muscle cells: the role of autocrine production of transforming growth*

factor-{beta}1 and insulin-like growth factor binding protein-3. Am J Physiol Lung Cell Mol Physiol, 2009. **296**(3): p. L489-99.

82. Ray, R., et al., *Endothelial Nox4 NADPH oxidase enhances vasodilatation and reduces blood pressure in vivo.* Arterioscler Thromb Vasc Biol, 2011. **31**(6): p. 1368-76.

83. Craige, S.M., et al., *NADPH oxidase 4 promotes endothelial angiogenesis through endothelial nitric oxide synthase activation.* Circulation, 2011. **124**(6): p. 731-40.

84. Schroder, K., et al., *Nox4 is a protective reactive oxygen species generating vascular NADPH oxidase.* Circ Res, 2012. **110**(9): p. 1217-25.

85. Cubbon, R.M., et al., *Temporal trends in mortality of patients with diabetes mellitus suffering acute myocardial infarction: a comparison of over 3000 patients between 1995 and 2003.* Eur Heart J, 2007. **28**(5): p. 540-5.

86. Almdal, T., et al., *The independent effect of type 2 diabetes mellitus on ischemic heart disease, stroke, and death: a population-based study of 13,000 men and women with 20 years of follow-up.* Arch Intern Med, 2004. **164**(13): p. 1422-6.

87. Martin, B.C., et al., *Role of glucose and insulin resistance in development of type 2 diabetes mellitus: results of a 25-year follow-up study.* Lancet, 1992. **340**(8825): p. 925-9.

88. Hsueh, W.A., C.J. Lyon, and M.J. Quinones, *Insulin resistance and the endothelium.* Am J Med, 2004. **117**(2): p. 109-17.

89. Despres, J.P., et al., *Hyperinsulinemia as an independent risk factor for ischemic heart disease.* N Engl J Med, 1996. **334**(15): p. 952-7.

90. Pyorala, M., et al., *Plasma insulin and all-cause, cardiovascular, and noncardiovascular mortality: the 22-year follow-up results of the Helsinki Policemen Study.* Diabetes Care, 2000. **23**(8): p. 1097-102.

91. Rundek, T., et al., *Insulin resistance and risk of ischemic stroke among nondiabetic individuals from the northern Manhattan study.* Arch Neurol, 2010. **67**(10): p. 1195-200.

92. Prior, J.O., et al., *Coronary circulatory dysfunction in insulin resistance, impaired glucose tolerance, and type 2 diabetes mellitus.* Circulation, 2005. **111**(18): p. 2291-8.

93. Bell, G.I., et al., *Sequence of the human insulin gene.* Nature, 1980. **284**(5751): p. 26-32.

94. Steiner, D.F., et al., *Proinsulin and the biosynthesis of insulin.* Recent Prog Horm Res, 1969. **25**: p. 207-82.

95. Itoh, N. and H. Okamoto, *Translational control of proinsulin synthesis by glucose.* Nature, 1980. **283**(5742): p. 100-2.

96. Baron, V., et al., *Insulin binding to its receptor induces a conformational change in the receptor C-terminus.* Biochemistry, 1990. **29**(19): p. 4634-41.

97. James, D.E., et al., *Insulin-regulatable tissues express a unique insulin-sensitive glucose transport protein.* Nature, 1988. **333**(6169): p. 183-5.

98. Shepherd, P.R., D.J. Withers, and K. Siddle, *Phosphoinositide 3-kinase: the key switch mechanism in insulin signalling.* Biochem J, 1998. **333 (Pt 3)**: p. 471-90.

99. Delafontaine, P., Y.H. Song, and Y. Li, *Expression, regulation, and function of IGF-1, IGF-1R, and IGF-1 binding proteins in blood vessels.* Arterioscler Thromb Vasc Biol, 2004. **24**(3): p. 435-44.

100. Laron, Z., *Insulin-like growth factor 1 (IGF-1): a growth hormone.* Mol Pathol, 2001. **54**(5): p. 311-6.

101. Janssen, J.A. and S.W. Lamberts, *Is the measurement of free IGF-I more indicative than that of total IGF-I in the evaluation of the biological activity of the GH/IGF-I axis?* J Endocrinol Invest, 1999. **22**(4): p. 313-5.

102. Mohan, S. and D.J. Baylink, *IGF-binding proteins are multifunctional and act via IGF-dependent and -independent mechanisms.* J Endocrinol, 2002. **175**(1): p. 19-31.

103. Juul, A., et al., *Low serum insulin-like growth factor I is associated with increased risk of ischemic heart disease: a population-based case-control study.* Circulation, 2002. **106**(8): p. 939-44.

104. Laughlin, G.A., et al., *The prospective association of serum insulin-like growth factor I (IGF-I) and IGF-binding protein-1 levels with all cause and cardiovascular disease mortality in older adults: the Rancho Bernardo Study.* J Clin Endocrinol Metab, 2004. **89**(1): p. 114-20.

105. Wheatcroft, S.B., et al., *Vascular endothelial function and blood pressure homeostasis in mice overexpressing IGF binding protein-1.* Diabetes, 2003. **52**(8): p. 2075-82.

106. Rajwani, A., et al., *Increasing circulating IGFBP1 levels improves insulin sensitivity, promotes nitric oxide production, lowers blood pressure, and protects against atherosclerosis.* Diabetes, 2012. **61**(4): p. 915-24.

107. Mora, S., et al., *Insulin and insulin-like growth factor I (IGF-I) stimulate GLUT4 glucose transporter translocation in Xenopus oocytes.* Biochem J, 1995. **311 (Pt 1)**: p. 59-65.

108. Dimitriadis, G., et al., *Effects of insulin-like growth factor I on the rates of glucose transport and utilization in rat skeletal muscle in vitro.* Biochem J, 1992. **285 (Pt 1)**: p. 269-74.

109. Dimitriadis, G., et al., *Effects of in-vivo administration of insulin-like growth factor-I on the rate of glucose utilization in the soleus muscle of the rat.* J Endocrinol, 1992. **133**(1): p. 37-43.

110. Dohm, G.L., et al., *IGF-I--stimulated glucose transport in human skeletal muscle and IGF-I resistance in obesity and NIDDM.* Diabetes, 1990. **39**(9): p. 1028-32.

111. Guler, H.P., J. Zapf, and E.R. Froesch, *Short-term metabolic effects of recombinant human insulin-like growth factor I in healthy adults.* N Engl J Med, 1987. **317**(3): p. 137-40.

112. Jones, J.I. and D.R. Clemmons, *Insulin-like growth factors and their binding proteins: biological actions.* Endocr Rev, 1995. **16**(1): p. 3-34.

113. Cusi, K. and R. DeFronzo, *Recombinant human insulin-like growth factor I treatment for 1 week improves metabolic control in type 2 diabetes by ameliorating hepatic and muscle insulin resistance.* J Clin Endocrinol Metab, 2000. **85**(9): p. 3077-84.

114. O'Connell, T. and D.R. Clemmons, *IGF-I/IGF-binding protein-3 combination improves insulin resistance by GH-dependent and independent mechanisms.* J Clin Endocrinol Metab, 2002. **87**(9): p. 4356-60.

115. Holt, R.I., H.L. Simpson, and P.H. Sonksen, *The role of the growth hormone-insulin-like growth factor axis in glucose homeostasis.* Diabet Med, 2003. **20**(1): p. 3-15.

116. Sesti, G., et al., *Plasma concentration of IGF-I is independently associated with insulin sensitivity in subjects with different degrees of glucose tolerance.* Diabetes Care, 2005. **28**(1): p. 120-5.

117. Boquist, S., et al., *Correlation of serum IGF-I and IGFBP-1 and -3 to cardiovascular risk indicators and early carotid atherosclerosis in healthy middle-aged men.* Clin Endocrinol (Oxf), 2008. **68**(1): p. 51-8.

118. Kawachi, S., et al., *Circulating insulin-like growth factor-1 and insulin-like growth factor binding protein-3 are associated with early carotid atherosclerosis.* Arterioscler Thromb Vasc Biol, 2005. **25**(3): p. 617-21.

119. Fischer, F., et al., *Associations of insulin-like growth factors, insulin-like growth factor binding proteins and acid-labile subunit with coronary heart disease.* Clin Endocrinol (Oxf), 2004. **61**(5): p. 595-602.

120. Ruotolo, G., et al., *Serum insulin-like growth factor-I level is independently associated with coronary artery disease progression in young male survivors of myocardial infarction: beneficial effects of bezafibrate treatment.* J Am Coll Cardiol, 2000. **35**(3): p. 647-54.

121. Andreassen, M., et al., *IGF1 as predictor of all cause mortality and cardiovascular disease in an elderly population.* Eur J Endocrinol, 2009. **160**(1): p. 25-31.

122. Botker, H.E., et al., *Insulin-like growth factor-I, insulin, and angina pectoris secondary to coronary atherosclerosis, vasospasm, and syndrome X.* Am J Cardiol, 1997. **79**(7): p. 961-3.

123. Grant, M.B., et al., *Localization of insulin-like growth factor I and inhibition of coronary smooth muscle cell growth by somatostatin analogues in human coronary smooth muscle cells. A potential treatment for restenosis?* Circulation, 1994. **89**(4): p. 1511-7.

124. Eriksen, U.H., et al., *Randomized double-blind Scandinavian trial of angiopeptin versus placebo for the prevention of clinical events and restenosis after coronary balloon angioplasty.* Am Heart J, 1995. **130**(1): p. 1-8.

125. Emanuelsson, H., et al., *Long-term effects of angiopeptin treatment in coronary angioplasty. Reduction of clinical events but not angiographic restenosis. European Angiopeptin Study Group.* Circulation, 1995. **91**(6): p. 1689-96.

126. von Essen, R., et al., *Effects of octreotide treatment on restenosis after coronary angioplasty: results of the VERAS study. VErringerung der Restenoserate nach Angioplastie durch ein Somatostatin-analogon.* Circulation, 1997. **96**(5): p. 1482-7.

127. Conti, E., et al., *Reduced levels of insulin-like growth factor-1 in patients with angina pectoris, positive exercise stress test, and angiographically normal epicardial coronary arteries.* Am J Cardiol, 2002. **89**(8): p. 973-5.

128. van den Beld, A.W., et al., *Endogenous hormones and carotid atherosclerosis in elderly men.* Am J Epidemiol, 2003. **157**(1): p. 25-31.

129. Brugts, M.P., et al., *Low circulating insulin-like growth factor I bioactivity in elderly men is associated with increased mortality.* J Clin Endocrinol Metab, 2008. **93**(7): p. 2515-22.

130. Spallarossa, P., et al., *Insulin-like growth factor-I and angiographically documented coronary artery disease.* Am J Cardiol, 1996. **77**(2): p. 200-2.

131. Conti, E., et al., *Markedly reduced insulin-like growth factor-1 in the acute phase of myocardial infarction.* J Am Coll Cardiol, 2001. **38**(1): p. 26-32.

132. Grant, M.B., et al., *Expression of IGF-I, IGF-I receptor and IGF binding proteins-1, -2, -3, -4 and -5 in human atherectomy specimens.* Regul Pept, 1996. **67**(3): p. 137-44.

133. Wilson, V.J., et al., *Upregulation of IGF-I and collagen I mRNA in human atherosclerotic tissue is not accompanied by changes in type 1 IGF receptor or collagen III mRNA: an in situ hybridization study.* Coron Artery Dis, 1996. **7**(8): p. 569-72.

134. Li, H., et al., *Arterial injury in mice with severe insulin-like growth factor-1 (IGF-1) deficiency.* J Cardiovasc Pharmacol Ther, 2002. **7**(4): p. 227-33.

135. Hayry, P., et al., *Stabile D-peptide analog of insulin-like growth factor-1 inhibits smooth muscle cell proliferation after carotid ballooning injury in the rat.* FASEB J, 1995. **9**(13): p. 1336-44.

136. Stolla, M.C., et al., *Enhanced platelet activity and thrombosis in a murine model of type I diabetes are partially insulin-like growth factor 1-dependent and phosphoinositide 3-kinase-dependent.* J Thromb Haemost, 2013. **11**(5): p. 919-29.

137. Kim, S., et al., *Insulin-like growth factor-1 regulates platelet activation through PI3-Kalpha isoform.* Blood, 2007. **110**(13): p. 4206-13.

138. Hers, I., *Insulin-like growth factor-1 potentiates platelet activation via the IRS/PI3Kalpha pathway.* Blood, 2007. **110**(13): p. 4243-52.

139. Zeng, G. and M.J. Quon, *Insulin-stimulated production of nitric oxide is inhibited by wortmannin. Direct measurement in vascular endothelial cells.* J Clin Invest, 1996. **98**(4): p. 894-8.

140. Imrie, H., et al., *Vascular insulin-like growth factor-I resistance and diet-induced obesity.* Endocrinology, 2009. **150**(10): p. 4575-82.

141. Laron, Z., *The GH-IGF1 axis and longevity. The paradigm of IGF1 deficiency.* Hormones (Athens), 2008. **7**(1): p. 24-7.

142. Guevara-Aguirre, J., et al., *Growth hormone receptor deficiency is associated with a major reduction in pro-aging signaling, cancer, and diabetes in humans.* Sci Transl Med, 2011. **3**(70): p. 70ra13.

143. Colao, A., et al., *The cardiovascular risk of adult GH deficiency (GHD) improved after GH replacement and worsened in untreated GHD: a 12-month prospective study.* J Clin Endocrinol Metab, 2002. **87**(3): p. 1088-93.

144. Gonzalez-Duarte, D., et al., *Measurement of oxidative stress and endothelial dysfunction in patients with hypopituitarism and severe deficiency adult growth hormone deficiency.* Pituitary, 2012. **15**(4): p. 589-97.

145. Elhadd, T.A., et al., *Biochemical and biophysical markers of endothelial dysfunction in adults with hypopituitarism and severe GH deficiency.* J Clin Endocrinol Metab, 2001. **86**(9): p. 4223-32.

146. Colao, A., *Improvement of cardiac parameters in patients with acromegaly treated with medical therapies.* Pituitary, 2012. **15**(1): p. 50-8.

147. Ronconi, V., et al., *Reduced nitric oxide levels in acromegaly: cardiovascular implications.* Blood Press, 2005. **14**(4): p. 227-32.

148. Brevetti, G., et al., *Early vascular alterations in acromegaly.* J Clin Endocrinol Metab, 2002. **87**(7): p. 3174-9.

149. Anagnostis, P., et al., *Oxidative Stress and Reduced Antioxidative Status, along with Endothelial Dysfunction in Acromegaly.* Horm Metab Res, 2012.

150. Holzenberger, M., et al., *IGF-1 receptor regulates lifespan and resistance to oxidative stress in mice.* Nature, 2003. **421**(6919): p. 182-7.

151. Bokov, A.F., et al., *Does reduced IGF-1R signaling in Igf1r+/- mice alter aging?* PLoS One, 2011. **6**(11): p. e26891.

152. Suh, Y., et al., *Functionally significant insulin-like growth factor I receptor mutations in centenarians.* Proc Natl Acad Sci U S A, 2008. **105**(9): p. 3438-42.

153. Bonafe, M., et al., *Polymorphic variants of insulin-like growth factor I (IGF-I) receptor and phosphoinositide 3-kinase genes affect IGF-I plasma levels and human longevity: cues for an evolutionarily conserved mechanism of life span control.* J Clin Endocrinol Metab, 2003. **88**(7): p. 3299-304.

154. van Heemst, D., et al., *Reduced insulin/IGF-1 signalling and human longevity.* Aging Cell, 2005. **4**(2): p. 79-85.

155. Paolisso, G., et al., *Serum levels of insulin-like growth factor-I (IGF-I) and IGF-binding protein-3 in healthy centenarians: relationship with plasma leptin and lipid concentrations, insulin action, and cognitive function.* J Clin Endocrinol Metab, 1997. **82**(7): p. 2204-9.

156. Arai, Y., et al., *Serum insulin-like growth factor-1 in centenarians: implications of IGF-1 as a rapid turnover protein.* J Gerontol A Biol Sci Med Sci, 2001. **56**(2): p. M79-82.

157. Colman, R.J., et al., *Caloric restriction delays disease onset and mortality in rhesus monkeys.* Science, 2009. **325**(5937): p. 201-4.

158. Mattison, J.A., et al., *Impact of caloric restriction on health and survival in rhesus monkeys from the NIA study.* Nature, 2012. **489**(7415): p. 318-21.

159. Megyesi, K., et al., *Insulin and non-suppressible insulin-like activity (NSILA-s): evidence for separate plasma membrane receptor sites.* Biochem Biophys Res Commun, 1974. **57**(1): p. 307-15.

160. Pashmforoush, M., S.J. Chan, and D.F. Steiner, *Structure and expression of the insulin-like peptide receptor from amphioxus.* Mol Endocrinol, 1996. **10**(7): p. 857-66.

161. Ullrich, A., et al., *Insulin-like growth factor I receptor primary structure: comparison with insulin receptor suggests structural determinants that define functional specificity.* EMBO J, 1986. **5**(10): p. 2503-12.

162. Adams, T.E., et al., *Structure and function of the type 1 insulin-like growth factor receptor.* Cell Mol Life Sci, 2000. **57**(7): p. 1050-93.

163. De Meyts, P. and J. Whittaker, *Structural biology of insulin and IGF1 receptors: implications for drug design.* Nat Rev Drug Discov, 2002. **1**(10): p. 769-83.

164. Riedemann, J. and V.M. Macaulay, *IGF1R signalling and its inhibition.* Endocr Relat Cancer, 2006. **13 Suppl 1**: p. S33-43.

165. Massague, J. and M.P. Czech, *The subunit structures of two distinct receptors for insulin-like growth factors I and II and their relationship to the insulin receptor.* J Biol Chem, 1982. **257**(9): p. 5038-45.

166. Ward, C.W. and T.P. Garrett, *Structural relationships between the insulin receptor and epidermal growth factor receptor families and other proteins.* Curr Opin Drug Discov Devel, 2004. **7**(5): p. 630-8.

167. Ward, C.W., *Members of the insulin receptor family contain three fibronectin type III domains.* Growth Factors, 1999. **16**(4): p. 315-22.

168. Lawrence, M.C., N.M. McKern, and C.W. Ward, *Insulin receptor structure and its implications for the IGF-1 receptor.* Curr Opin Struct Biol, 2007. **17**(6): p. 699-705.

169. Mothe, I., et al., *Tyrosine kinase activity of a chimeric insulin-like-growth-factor-1 receptor containing the insulin receptor C-terminal domain. Comparison with the tyrosine kinase activities of the insulin and insulin-like-growth-factor-1 receptors using a cell-free system.* Eur J Biochem, 1995. **228**(3): p. 842-8.

170. Sparrow, L.G., et al., *The disulfide bonds in the C-terminal domains of the human insulin receptor ectodomain.* J Biol Chem, 1997. **272**(47): p. 29460-7.

171. De Meyts, P., *The structural basis of insulin and insulin-like growth factor-I receptor binding and negative co-operativity, and its relevance to mitogenic versus metabolic signalling.* Diabetologia, 1994. **37 Suppl 2**: p. S135-48.

172. de Meyts, P., et al., *Insulin interactions with its receptors: experimental evidence for negative cooperativity.* Biochem Biophys Res Commun, 1973. **55**(1): p. 154-61.

173. Kiselyov, V.V., et al., *Harmonic oscillator model of the insulin and IGF1 receptors' allosteric binding and activation.* Mol Syst Biol, 2009. **5**: p. 243.

174. Christoffersen, C.T., et al., *Negative cooperativity in the insulin-like growth factor-I receptor and a chimeric IGF-I/insulin receptor.* Endocrinology, 1994. **135**(1): p. 472-5.

175. Gauguin, L., et al., *Alanine scanning of a putative receptor binding surface of insulin-like growth factor-I.* J Biol Chem, 2008. **283**(30): p. 20821-9.

176. Gustafson, T.A. and W.J. Rutter, *The cysteine-rich domains of the insulin and insulin-like growth factor I receptors are primary determinants of hormone binding specificity. Evidence from receptor chimeras.* J Biol Chem, 1990. **265**(30): p. 18663-7.

177. Keyhanfar, M., et al., *Precise mapping of an IGF-I-binding site on the IGF-1R.* Biochem J, 2007. **401**(1): p. 269-77.

178. Surinya, K.H., et al., *Role of insulin receptor dimerization domains in ligand binding, cooperativity, and modulation by anti-receptor antibodies.* J Biol Chem, 2002. **277**(19): p. 16718-25.

179. Whittaker, J., et al., *Alanine scanning mutagenesis of a type 1 insulin-like growth factor receptor ligand binding site.* J Biol Chem, 2001. **276**(47): p. 43980-6.

180. Chakravarty, A., et al., *Rescue of ligand binding of a mutant IGF-I receptor by complementation.* Biochem Biophys Res Commun, 2005. **331**(1): p. 74-7.

181. Favelyukis, S., et al., *Structure and autoregulation of the insulin-like growth factor 1 receptor kinase.* Nat Struct Biol, 2001. **8**(12): p. 1058-63.

182. Hubbard, S.R., *Crystal structure of the activated insulin receptor tyrosine kinase in complex with peptide substrate and ATP analog.* EMBO J, 1997. **16**(18): p. 5572-81.

183. Pautsch, A., et al., *Crystal structure of bisphosphorylated IGF-1 receptor kinase: insight into domain movements upon kinase activation.* Structure, 2001. **9**(10): p. 955-65.

184. Pyorala, M., et al., *Insulin resistance syndrome predicts the risk of coronary heart disease and stroke in healthy middle-aged men: the 22-year follow-up results of the Helsinki Policemen Study.* Arterioscler Thromb Vasc Biol, 2000. **20**(2): p. 538-44.

185. Pyorala, M., et al., *Hyperinsulinemia predicts coronary heart disease risk in healthy middle-aged men: the 22-year follow-up results of the Helsinki Policemen Study.* Circulation, 1998. **98**(5): p. 398-404.

186. Murphy, C., et al., *Vascular dysfunction and reduced circulating endothelial progenitor cells in young healthy UK South Asian men.* Arterioscler Thromb Vasc Biol, 2007. **27**(4): p. 936-42.

187. Cubbon, R.M., et al., *Human exercise-induced circulating progenitor cell mobilization is nitric oxide-dependent and is blunted in South Asian men.* Arterioscler Thromb Vasc Biol, 2010. **30**(4): p. 878-84.

188. Laine, H., et al., *Insulin resistance of glucose uptake in skeletal muscle cannot be ameliorated by enhancing endothelium-dependent blood flow in obesity.* J Clin Invest, 1998. **101**(5): p. 1156-62.

189. Steinberg, H.O., et al., *Obesity/insulin resistance is associated with endothelial dysfunction. Implications for the syndrome of insulin resistance.* J Clin Invest, 1996. **97**(11): p. 2601-10.

190. Tack, C.J., et al., *Insulin-induced vasodilatation and endothelial function in obesity/insulin resistance. Effects of troglitazone.* Diabetologia, 1998. **41**(5): p. 569-76.

191. Westerbacka, J., et al., *Marked resistance of the ability of insulin to decrease arterial stiffness characterizes human obesity.* Diabetes, 1999. **48**(4): p. 821-7.

192. Melikian, N., et al., *Determinants of endothelial function in asymptomatic subjects with and without the metabolic syndrome.* Atherosclerosis, 2008. **197**(1): p. 375-82.

193. Williams, I.L., et al., *Effect of fat distribution on endothelial-dependent and endothelial-independent vasodilatation in healthy humans.* Diabetes Obes Metab, 2006. **8**(3): p. 296-301.

194. Williams, I.L., et al., *Endothelial function and weight loss in obese humans.* Obes Surg, 2005. **15**(7): p. 1055-60.

195. Duncan, E.R., et al., *Effect of endothelium-specific insulin resistance on endothelial function in vivo.* Diabetes, 2008. **57**(12): p. 3307-14.

196. Potenza, M.A., F. Addabbo, and M. Montagnani, *Vascular actions of insulin with implications for endothelial dysfunction.* Am J Physiol Endocrinol Metab, 2009. **297**(3): p. E568-77.

197. Tsukahara, H., et al., *Direct demonstration of insulin-like growth factor-I-induced nitric oxide production by endothelial cells.* Kidney Int, 1994. **45**(2): p. 598-604.

198. Li, G., et al., *Insulin at physiological concentrations selectively activates insulin but not insulin-like growth factor I (IGF-I) or insulin/IGF-I hybrid receptors in endothelial cells.* Endocrinology, 2005. **146**(11): p. 4690-6.

199. Gual, P., Y. Le Marchand-Brustel, and J.F. Tanti, *Positive and negative regulation of insulin signaling through IRS-1 phosphorylation.* Biochimie, 2005. **87**(1): p. 99-109.

200. Cantley, L.C., *The phosphoinositide 3-kinase pathway.* Science, 2002. **296**(5573): p. 1655-7.

201. Dimmeler, S., et al., *Activation of nitric oxide synthase in endothelial cells by Akt-dependent phosphorylation.* Nature, 1999. **399**(6736): p. 601-5.

202. Neumann-Haefelin, E., et al., *SHC-1/p52Shc targets the insulin/IGF-1 and JNK signaling pathways to modulate life span and stress response in C. elegans.* Genes Dev, 2008. **22**(19): p. 2721-35.

203. Shai, S.Y., et al., *Low circulating insulin-like growth factor I increases atherosclerosis in ApoE-deficient mice.* Am J Physiol Heart Circ Physiol, 2011. **300**(5): p. H1898-906.

204. Wang, J., et al., *The expression of IGFs and IGF binding proteins in human carotid atherosclerosis, and the possible role of IGF binding protein-1 in the regulation of smooth muscle cell proliferation.* Atherosclerosis, 2012. **220**(1): p. 102-9.

205. Moxham, C.P., V. Duronio, and S. Jacobs, *Insulin-like growth factor I receptor beta-subunit heterogeneity. Evidence for hybrid tetramers composed of insulin-like growth factor I and insulin receptor heterodimers.* J Biol Chem, 1989. **264**(22): p. 13238-44.

206. Soos, M.A. and K. Siddle, *Immunological relationships between receptors for insulin and insulin-like growth factor I. Evidence for structural heterogeneity of insulin-like growth factor I receptors involving hybrids with insulin receptors.* Biochem J, 1989. **263**(2): p. 553-63.

207. Hunter, R.W. and I. Hers, *Insulin/IGF-1 hybrid receptor expression on human platelets: consequences for the effect of insulin on platelet function.* J Thromb Haemost, 2009. **7**(12): p. 2123-30.

208. Chisalita, S.I. and H.J. Arnqvist, *Expression and function of receptors for insulin-like growth factor-I and insulin in human coronary artery smooth muscle cells.* Diabetologia, 2005. **48**(10): p. 2155-61.

209. Abbas, A., et al., *The insulin-like growth factor-1 receptor is a negative regulator of nitric oxide bioavailability and insulin sensitivity in the endothelium.* Diabetes, 2011. **60**(8): p. 2169-78.

210. Imrie, H., et al., *Novel role of the IGF-1 receptor in endothelial function and repair: studies in endothelium-targeted IGF-1 receptor transgenic mice.* Diabetes, 2012. **61**(9): p. 2359-68.

211. Benyoucef, S., et al., *Characterization of insulin/IGF hybrid receptors: contributions of the insulin receptor L2 and Fn1 domains and the alternatively spliced exon 11 sequence to ligand binding and receptor activation.* Biochem J, 2007. **403**(3): p. 603-13.

212. Soos, M.A., C.E. Field, and K. Siddle, *Purified hybrid insulin/insulin-like growth factor-I receptors bind insulin-like growth factor-I, but not insulin, with high affinity.* Biochem J, 1993. **290 (Pt 2)**: p. 419-26.

213. Soos, M.A., et al., *Receptors for insulin and insulin-like growth factor-I can form hybrid dimers. Characterisation of hybrid receptors in transfected cells.* Biochem J, 1990. **270**(2): p. 383-90.

214. Frattali, A.L. and J.E. Pessin, *Relationship between alpha subunit ligand occupancy and beta subunit autophosphorylation in insulin/insulin-like growth factor-1 hybrid receptors.* J Biol Chem, 1993. **268**(10): p. 7393-400.

215. Treadway, J.L., et al., *Transdominant inhibition of tyrosine kinase activity in mutant insulin/insulin-like growth factor I hybrid receptors.* Proc Natl Acad Sci U S A, 1991. **88**(1): p. 214-8.

216. Pandini, G., et al., *Insulin/insulin-like growth factor I hybrid receptors have different biological characteristics depending on the insulin receptor isoform involved.* J Biol Chem, 2002. **277**(42): p. 39684-95.

217. Slaaby, R., et al., *Hybrid receptors formed by insulin receptor (IR) and insulin-like growth factor I receptor (IGF-IR) have low insulin and high IGF-1 affinity irrespective of the IR splice variant.* J Biol Chem, 2006. **281**(36): p. 25869-74.

218. Treadway, J.L., et al., *Assembly of insulin/insulin-like growth factor-1 hybrid receptors in vitro.* J Biol Chem, 1989. **264**(36): p. 21450-3.

219. Bailyes, E.M., et al., *Insulin receptor/IGF-I receptor hybrids are widely distributed in mammalian tissues: quantification of individual receptor species by selective immunoprecipitation and immunoblotting.* Biochem J, 1997. **327 (Pt 1)**: p. 209-15.

220. Federici, M., et al., *Distribution of insulin/insulin-like growth factor-I hybrid receptors in human tissues.* Mol Cell Endocrinol, 1997. **129**(2): p. 121-6.

221. Nitert, M.D., et al., *IGF-I/insulin hybrid receptors in human endothelial cells.* Mol Cell Endocrinol, 2005. **229**(1-2): p. 31-7.

222. Chisalita, S.I., M.D. Nitert, and H.J. Arnqvist, *Characterisation of receptors for IGF-I and insulin; evidence for hybrid insulin/IGF-I receptor in human coronary artery endothelial cells.* Growth Horm IGF Res, 2006. **16**(4): p. 258-66.

223. Back, K., et al., *Insulin and IGF1 receptors in human cardiac microvascular endothelial cells: metabolic, mitogenic and anti-inflammatory effects.* J Endocrinol, 2012. **215**(1): p. 89-96.

224. Johansson, G.S., S.I. Chisalita, and H.J. Arnqvist, *Human microvascular endothelial cells are sensitive to IGF-I but resistant to insulin at the receptor level.* Mol Cell Endocrinol, 2008. **296**(1-2): p. 58-63.

225. Valensise, H., et al., *Increased expression of low-affinity insulin receptor isoform and insulin/insulin-like growth factor-I hybrid receptors in term placenta from insulin-resistant women with gestational hypertension.* Diabetologia, 1996. **39**(8): p. 952-60.

226. Federici, M., et al., *Increased abundance of insulin/insulin-like growth factor-I hybrid receptors in skeletal muscle of obese subjects is correlated with in vivo insulin sensitivity.* J Clin Endocrinol Metab, 1998. **83**(8): p. 2911-5.

227. Federici, M., et al., *Expression of insulin/IGF-I hybrid receptors is increased in skeletal muscle of patients with chronic primary hyperinsulinemia.* Diabetes, 1998. **47**(1): p. 87-92.

228. Federici, M., et al., *Evidence for glucose/hexosamine in vivo regulation of insulin/IGF-I hybrid receptor assembly.* Diabetes, 1999. **48**(12): p. 2277-85.

229. Federici, M., et al., *Increased abundance of insulin/IGF-I hybrid receptors in adipose tissue from NIDDM patients.* Mol Cell Endocrinol, 1997. **135**(1): p. 41-7.

230. Federici, M., et al., *Increased expression of insulin/insulin-like growth factor-I hybrid receptors in skeletal muscle of noninsulin-dependent diabetes mellitus subjects.* J Clin Invest, 1996. **98**(12): p. 2887-93.

231. Sherajee, S.J., et al., *Aldosterone induces vascular insulin resistance by increasing insulin-like growth factor-1 receptor and hybrid receptor.* Arterioscler Thromb Vasc Biol, 2012. **32**(2): p. 257-63.

232. Rowzee, A.M., D.L. Ludwig, and T.L. Wood, *Insulin-like growth factor type 1 receptor and insulin receptor isoform expression and signaling in mammary epithelial cells.* Endocrinology, 2009. **150**(8): p. 3611-9.

233. Suryawan, A., et al., *Insulin/insulin-like growth factor-I hybrid receptor abundance decreases with development in suckling pigs.* J Nutr, 2003. **133**(9): p. 2783-7.

234. Agarwal, N., et al., *Metformin reduces arterial stiffness and improves endothelial function in young women with polycystic ovary syndrome: a randomized, placebo-controlled, crossover trial.* J Clin Endocrinol Metab, 2010. **95**(2): p. 722-30.

235. Velazquez, E.M., et al., *Metformin therapy in polycystic ovary syndrome reduces hyperinsulinemia, insulin resistance, hyperandrogenemia, and systolic blood pressure, while facilitating normal menses and pregnancy.* Metabolism, 1994. **43**(5): p. 647-54.

236. Duncan, R.E., et al., *Regulation of lipolysis in adipocytes.* Annu Rev Nutr, 2007. **27**: p. 79-101.

237. Burns, T.W., et al., *Insulin inhibition of lipolysis of human adipocytes: the role of cyclic adenosine monophosphate.* Diabetes, 1979. **28**(11): p. 957-61.

238. Hartmann, H., et al., *Inhibition of glycogenolysis and glycogen phosphorylase by insulin and proinsulin in rat hepatocyte cultures.* Diabetes, 1987. **36**(5): p. 551-5.

239. Wang, B., I.S. Wood, and P. Trayhurn, *Dysregulation of the expression and secretion of inflammation-related adipokines by hypoxia in human adipocytes.* Pflugers Arch, 2007. **455**(3): p. 479-92.

240. Hosogai, N., et al., *Adipose tissue hypoxia in obesity and its impact on adipocytokine dysregulation.* Diabetes, 2007. **56**(4): p. 901-11.

241. Goyal, R., et al., *Evaluation of TNF-alpha and IL-6 Levels in Obese and Non-obese Diabetics: Pre- and Postinsulin Effects.* N Am J Med Sci, 2012. **4**(4): p. 180-4.

242. Aguirre, V., et al., *Phosphorylation of Ser307 in insulin receptor substrate-1 blocks interactions with the insulin receptor and inhibits insulin action.* J Biol Chem, 2002. **277**(2): p. 1531-7.

243. Hotamisligil, G.S., et al., *IRS-1-mediated inhibition of insulin receptor tyrosine kinase activity in TNF-alpha- and obesity-induced insulin resistance.* Science, 1996. **271**(5249): p. 665-8.

244. Hirosumi, J., et al., *A central role for JNK in obesity and insulin resistance.* Nature, 2002. **420**(6913): p. 333-6.

245. Ye, J., et al., *Hypoxia is a potential risk factor for chronic inflammation and adiponectin reduction in adipose tissue of ob/ob and dietary obese mice.* Am J Physiol Endocrinol Metab, 2007. **293**(4): p. E1118-28.

246. Feldstein, A.E., et al., *Free fatty acids promote hepatic lipotoxicity by stimulating TNF-alpha expression via a lysosomal pathway.* Hepatology, 2004. **40**(1): p. 185-94.

247. Goodpaster, B.H., F.L. Thaete, and D.E. Kelley, *Thigh adipose tissue distribution is associated with insulin resistance in obesity and in type 2 diabetes mellitus.* Am J Clin Nutr, 2000. **71**(4): p. 885-92.

248. Yu, C., et al., *Mechanism by which fatty acids inhibit insulin activation of insulin receptor substrate-1 (IRS-1)-associated phosphatidylinositol 3-kinase activity in muscle.* J Biol Chem, 2002. **277**(52): p. 50230-6.

249. Sathyanarayana, P., et al., *Activation of the Drosophila MLK by ceramide reveals TNF-alpha and ceramide as agonists of mammalian MLK3.* Mol Cell, 2002. **10**(6): p. 1527-33.

250. Anai, M., et al., *Enhanced insulin-stimulated activation of phosphatidylinositol 3-kinase in the liver of high-fat-fed rats.* Diabetes, 1999. **48**(1): p. 158-69.

251. Kamata, H., et al., *Reactive oxygen species promote TNFalpha-induced death and sustained JNK activation by inhibiting MAP kinase phosphatases.* Cell, 2005. **120**(5): p. 649-61.

252. Storz, P. and A. Toker, *Protein kinase D mediates a stress-induced NF-kappaB activation and survival pathway.* EMBO J, 2003. **22**(1): p. 109-20.

253. Kiechl, S., et al., *Blockade of receptor activator of nuclear factor-kappaB (RANKL) signaling improves hepatic insulin resistance and prevents development of diabetes mellitus.* Nat Med, 2013. **19**(3): p. 358-63.

254. Arcaro, G., et al., *Insulin causes endothelial dysfunction in humans: sites and mechanisms.* Circulation, 2002. **105**(5): p. 576-82.

255. Cusi, K., et al., *Insulin resistance differentially affects the PI 3-kinase- and MAP kinase-mediated signaling in human muscle.* J Clin Invest, 2000. **105**(3): p. 311-20.

256. Jiang, Z.Y., et al., *Characterization of selective resistance to insulin signaling in the vasculature of obese Zucker (fa/fa) rats.* J Clin Invest, 1999. **104**(4): p. 447-57.

257. Montagnani, M., et al., *Inhibition of phosphatidylinositol 3-kinase enhances mitogenic actions of insulin in endothelial cells.* J Biol Chem, 2002. **277**(3): p. 1794-9.

258. Muniyappa, R. and M.J. Quon, *Insulin action and insulin resistance in vascular endothelium.* Curr Opin Clin Nutr Metab Care, 2007. **10**(4): p. 523-30.

259. Ueno, M., et al., *Regulation of insulin signalling by hyperinsulinaemia: role of IRS-1/2 serine phosphorylation and the mTOR/p70 S6K pathway.* Diabetologia, 2005. **48**(3): p. 506-18.

260. Potenza, M.A., et al., *Insulin resistance in spontaneously hypertensive rats is associated with endothelial dysfunction characterized by imbalance between NO and ET-1 production.* Am J Physiol Heart Circ Physiol, 2005. **289**(2): p. H813-22.

261. Inoguchi, T., et al., *High glucose level and free fatty acid stimulate reactive oxygen species production through protein kinase C--dependent activation of NAD(P)H oxidase in cultured vascular cells.* Diabetes, 2000. **49**(11): p. 1939-45.

262. Kim, F., et al., *Free fatty acid impairment of nitric oxide production in endothelial cells is mediated by IKKbeta.* Arterioscler Thromb Vasc Biol, 2005. **25**(5): p. 989-94.

263. Wang, X.L., et al., *Free fatty acids inhibit insulin signaling-stimulated endothelial nitric oxide synthase activation through upregulating PTEN or inhibiting Akt kinase.* Diabetes, 2006. **55**(8): p. 2301-10.

264. Tomas, E., et al., *Hyperglycemia and insulin resistance: possible mechanisms.* Ann N Y Acad Sci, 2002. **967**: p. 43-51.

265. Du, X.L., et al., *Hyperglycemia inhibits endothelial nitric oxide synthase activity by posttranslational modification at the Akt site.* J Clin Invest, 2001. **108**(9): p. 1341-8.

266. Gao, Z., et al., *Serine phosphorylation of insulin receptor substrate 1 by inhibitor kappa B kinase complex.* J Biol Chem, 2002. **277**(50): p. 48115-21.

267. Arkan, M.C., et al., *IKK-beta links inflammation to obesity-induced insulin resistance.* Nat Med, 2005. **11**(2): p. 191-8.

268. Choudhary, S., et al., *NF-kappaB-inducing kinase (NIK) mediates skeletal muscle insulin resistance: blockade by adiponectin.* Endocrinology, 2011. **152**(10): p. 3622-7.

269. Kris-Etherton, P.M., et al., *Antioxidant vitamin supplements and cardiovascular disease.* Circulation, 2004. **110**(5): p. 637-41.

270. Golbidi, S., S.A. Ebadi, and I. Laher, *Antioxidants in the treatment of diabetes.* Curr Diabetes Rev, 2011. **7**(2): p. 106-25.

271. Marchioli, R., et al., *Vitamin E increases the risk of developing heart failure after myocardial infarction: Results from the GISSI-Prevenzione trial.* J Cardiovasc Med (Hagerstown), 2006. **7**(5): p. 347-50.

272. Shi, Y., et al., *PTEN at a glance.* J Cell Sci, 2012. **125**(Pt 20): p. 4687-92.

273. Klaman, L.D., et al., *Increased energy expenditure, decreased adiposity, and tissue-specific insulin sensitivity in protein-tyrosine phosphatase 1B-deficient mice.* Mol Cell Biol, 2000. **20**(15): p. 5479-89.

274. Elchebly, M., et al., *Increased insulin sensitivity and obesity resistance in mice lacking the protein tyrosine phosphatase-1B gene.* Science, 1999. **283**(5407): p. 1544-8.

275. Mahadev, K., et al., *Hydrogen peroxide generated during cellular insulin stimulation is integral to activation of the distal insulin signaling cascade in 3T3-L1 adipocytes.* J Biol Chem, 2001. **276**(52): p. 48662-9.

276. Mahadev, K., et al., *Insulin-stimulated hydrogen peroxide reversibly inhibits protein-tyrosine phosphatase 1b in vivo and enhances the early insulin action cascade.* J Biol Chem, 2001. **276**(24): p. 21938-42.

277. Iwakami, S., et al., *Concentration-dependent dual effects of hydrogen peroxide on insulin signal transduction in H4IIEC hepatocytes.* PLoS One, 2011. **6**(11): p. e27401.

278. Hayes, G.R. and D.H. Lockwood, *Role of insulin receptor phosphorylation in the insulinomimetic effects of hydrogen peroxide.* Proc Natl Acad Sci U S A, 1987. **84**(22): p. 8115-9.

279. Higaki, Y., et al., *Oxidative stress stimulates skeletal muscle glucose uptake through a phosphatidylinositol 3-kinase-dependent pathway.* Am J Physiol Endocrinol Metab, 2008. **294**(5): p. E889-97.

280. Schmid, E., et al., *Phosphorylation of the insulin receptor kinase by phosphocreatine in combination with hydrogen peroxide: the structural basis of redox priming.* FASEB J, 1999. **13**(12): p. 1491-500.

281. Schmitt, T.L., H. Klein, and W. Droge, *Hydrogen peroxide inhibits activity of the IGF-1 receptor kinase.* Redox Rep, 2006. **11**(3): p. 105-9.

282. Loh, K., et al., *Reactive oxygen species enhance insulin sensitivity.* Cell Metab, 2009. **10**(4): p. 260-72.

283. Liu, Y., et al., *H2O2 is the transferrable factor mediating flow-induced dilation in human coronary arterioles.* Circ Res, 2011. **108**(5): p. 566-73.

284. Ohashi, J., et al., *Mechanisms for enhanced endothelium-derived hyperpolarizing factor-mediated responses in microvessels in mice.* Circ J, 2012. **76**(7): p. 1768-79.

285. Urakami-Harasawa, L., et al., *Importance of endothelium-derived hyperpolarizing factor in human arteries.* J Clin Invest, 1997. **100**(11): p. 2793-9.

286. DeFronzo, R.A., et al., *Effects of insulin on peripheral and splanchnic glucose metabolism in noninsulin-dependent (type II) diabetes mellitus.* J Clin Invest, 1985. **76**(1): p. 149-55.

287. Yang, Y.J., et al., *Insulin transport across capillaries is rate limiting for insulin action in dogs.* J Clin Invest, 1989. **84**(5): p. 1620-8.

288. Miles, P.D., et al., *Kinetics of insulin action in vivo. Identification of rate-limiting steps.* Diabetes, 1995. **44**(8): p. 947-53.

289. Baron, A.D., et al., *Mechanism of insulin resistance in insulin-dependent diabetes mellitus: a major role for reduced skeletal muscle blood flow.* J Clin Endocrinol Metab, 1991. **73**(3): p. 637-43.

290. Laakso, M., et al., *Decreased effect of insulin to stimulate skeletal muscle blood flow in obese man. A novel mechanism for insulin resistance.* J Clin Invest, 1990. **85**(6): p. 1844-52.

291. Laakso, M., et al., *Impaired insulin-mediated skeletal muscle blood flow in patients with NIDDM.* Diabetes, 1992. **41**(9): p. 1076-83.

292. Vincent, M.A., et al., *Inhibiting NOS blocks microvascular recruitment and blunts muscle glucose uptake in response to insulin.* Am J Physiol Endocrinol Metab, 2003. **285**(1): p. E123-9.

293. Vincent, M.A., et al., *Microvascular recruitment is an early insulin effect that regulates skeletal muscle glucose uptake in vivo.* Diabetes, 2004. **53**(6): p. 1418-23.

294. Clerk, L.H., et al., *Skeletal muscle capillary responses to insulin are abnormal in late-stage diabetes and are restored by angiotensin-converting enzyme inhibition.* Am J Physiol Endocrinol Metab, 2007. **293**(6): p. E1804-9.

295. Clerk, L.H., et al., *Obesity blunts insulin-mediated microvascular recruitment in human forearm muscle.* Diabetes, 2006. **55**(5): p. 1436-42.

296. Eggleston, E.M., L.A. Jahn, and E.J. Barrett, *Hyperinsulinemia rapidly increases human muscle microvascular perfusion but fails to increase muscle insulin clearance: evidence that a saturable process mediates muscle insulin uptake.* Diabetes, 2007. **56**(12): p. 2958-63.

297. Predescu, S.A., D.N. Predescu, and A.B. Malik, *Molecular determinants of endothelial transcytosis and their role in endothelial permeability.* Am J Physiol Lung Cell Mol Physiol, 2007. **293**(4): p. L823-42.

298. Schubert, W., et al., *Caveolae-deficient endothelial cells show defects in the uptake and transport of albumin in vivo.* J Biol Chem, 2001. **276**(52): p. 48619-22.

299. King, G.L. and S.M. Johnson, *Receptor-mediated transport of insulin across endothelial cells.* Science, 1985. **227**(4694): p. 1583-6.

300. Wang, H., et al., *The vascular endothelial cell mediates insulin transport into skeletal muscle.* Am J Physiol Endocrinol Metab, 2006. **291**(2): p. E323-32.

301. Genders, A.J., et al., *Endothelial cells actively concentrate insulin during its transendothelial transport.* Microcirculation, 2013.

302. Wang, H., et al., *Insulin signaling stimulates insulin transport by bovine aortic endothelial cells.* Diabetes, 2008. **57**(3): p. 540-7.

303. Vicent, D., et al., *The role of endothelial insulin signaling in the regulation of vascular tone and insulin resistance.* J Clin Invest, 2003. **111**(9): p. 1373-80.

304. Kubota, T., et al., *Impaired insulin signaling in endothelial cells reduces insulin-induced glucose uptake by skeletal muscle.* Cell Metab, 2011. **13**(3): p. 294-307.

305. Bruning, J.C., et al., *A muscle-specific insulin receptor knockout exhibits features of the metabolic syndrome of NIDDM without altering glucose tolerance.* Mol Cell, 1998. **2**(5): p. 559-69.

306. Fernandez, A.M., et al., *Functional inactivation of the IGF-I and insulin receptors in skeletal muscle causes type 2 diabetes.* Genes Dev, 2001. **15**(15): p. 1926-34.

307. Accili, D., et al., *Early neonatal death in mice homozygous for a null allele of the insulin receptor gene.* Nat Genet, 1996. **12**(1): p. 106-9.

308. Liu, J.P., et al., *Mice carrying null mutations of the genes encoding insulin-like growth factor I (Igf-1) and type 1 IGF receptor (Igf1r).* Cell, 1993. **75**(1): p. 59-72.

309. Wheatcroft, S.B., et al., *Preserved glucoregulation but attenuation of the vascular actions of insulin in mice heterozygous for knockout of the insulin receptor.* Diabetes, 2004. **53**(10): p. 2645-52.

310. Feng, M., et al., *Validation of volume-pressure recording tail-cuff blood pressure measurements.* Am J Hypertens, 2008. **21**(12): p. 1288-91.

311. Sehat, B., et al., *Role of ubiquitination in IGF-1 receptor signaling and degradation.* PLoS One, 2007. **2**(4): p. e340.

312. Sperandio, S., et al., *Paraptosis: mediation by MAP kinases and inhibition by AIP-1/Alix.* Cell Death Differ, 2004. **11**(10): p. 1066-75.

313. Korhonen, J., et al., *Endothelial-specific gene expression directed by the tie gene promoter in vivo.* Blood, 1995. **86**(5): p. 1828-35.

314. Schlaeger, T.M., et al., *Uniform vascular-endothelial-cell-specific gene expression in both embryonic and adult transgenic mice.* Proc Natl Acad Sci U S A, 1997. **94**(7): p. 3058-63.

315. Bronson, S.K., et al., *Single-copy transgenic mice with chosen-site integration.* Proc Natl Acad Sci U S A, 1996. **93**(17): p. 9067-72.

316. Evans, V., et al., *Targeting the Hprt locus in mice reveals differential regulation of Tie2 gene expression in the endothelium.* Physiol Genomics, 2000. **2**(2): p. 67-75.

317. Doetschman, T., et al., *Targetted correction of a mutant HPRT gene in mouse embryonic stem cells.* Nature, 1987. **330**(6148): p. 576-8.

318. Thomas, K.R., K.R. Folger, and M.R. Capecchi, *High frequency targeting of genes to specific sites in the mammalian genome.* Cell, 1986. **44**(3): p. 419-28.

319. de Jonge, H.J., et al., *Evidence based selection of housekeeping genes.* PLoS One, 2007. **2**(9): p. e898.

320. Prager, D., et al., *Human insulin-like growth factor I receptor function in pituitary cells is suppressed by a dominant negative mutant.* J Clin Invest, 1992. **90**(5): p. 2117-22.

321. Kato, H., et al., *Role of tyrosine kinase activity in signal transduction by the insulin-like growth factor-I (IGF-I) receptor. Characterization of kinase-deficient IGF-I receptors and the action of an IGF-I-mimetic antibody (alpha IR-3).* J Biol Chem, 1993. **268**(4): p. 2655-61.

322. Gage, M.C., et al., *Endothelium-specific insulin resistance leads to accelerated atherosclerosis in areas with disturbed flow patterns: A role for reactive oxygen species.* Atherosclerosis, 2013. **230**(1): p. 131-9.

323. Lockhart, C.J., G.E. McVeigh, and J.N. Cohn, *Measuring endothelial function.* Curr Diab Rep, 2006. **6**(4): p. 267-73.

324. Gnasso, A., et al., *Association between wall shear stress and flow-mediated vasodilation in healthy men.* Atherosclerosis, 2001. **156**(1): p. 171-6.

325. Feelisch, M. and J.S. Stamler, *Methods in nitric oxide research*. 1996, Chichester: J. Wiley.

326. Tawaramoto, K., et al., *Ablation of 3-phosphoinositide-dependent protein kinase 1 (PDK1) in vascular endothelial cells enhances insulin sensitivity by reducing visceral fat and suppressing angiogenesis.* Mol Endocrinol, 2012. **26**(1): p. 95-109.

327. Caesar, R., et al., *Gut-derived lipopolysaccharide augments adipose macrophage accumulation but is not essential for impaired glucose or insulin tolerance in mice.* Gut, 2012. **61**(12): p. 1701-7.

328. Liang, H., et al., *Effect of a sustained reduction in plasma free fatty acid concentration on insulin signalling and inflammation in skeletal muscle from human subjects.* J Physiol, 2013. **591**(Pt 11): p. 2897-909.

329. Hollenbeck, C.B., et al., *Effects of metformin on glucose, insulin and lipid metabolism in patients with mild hypertriglyceridaemia and non-insulin dependent diabetes by glucose tolerance test criteria.* Diabete Metab, 1991. **17**(5): p. 483-9.

330. Lund, S.S., et al., *Impact of metformin versus the prandial insulin secretagogue, repaglinide, on fasting and postprandial glucose and lipid responses in non-obese patients with type 2 diabetes.* Eur J Endocrinol, 2008. **158**(1): p. 35-46.

331. Karpe, F., J.R. Dickmann, and K.N. Frayn, *Fatty acids, obesity, and insulin resistance: time for a reevaluation.* Diabetes, 2011. **60**(10): p. 2441-9.

332. Ford, R.J., et al., *Glutathione depletion in vivo enhances contraction and attenuates endothelium-dependent relaxation of isolated rat aorta.* Free Radic Biol Med, 2006. **40**(4): p. 670-8.

333. Rush, J.W., et al., *Chronic resveratrol enhances endothelium-dependent relaxation but does not alter eNOS levels in aorta of spontaneously hypertensive rats.* Exp Biol Med (Maywood), 2007. **232**(6): p. 814-22.

334. Oak, J.H. and H. Cai, *Attenuation of angiotensin II signaling recouples eNOS and inhibits nonendothelial NOX activity in diabetic mice.* Diabetes, 2007. **56**(1): p. 118-26.

335. Oak, J.H., J.Y. Youn, and H. Cai, *Aminoguanidine inhibits aortic hydrogen peroxide production, VSMC NOX activity and hypercontractility in diabetic mice.* Cardiovasc Diabetol, 2009. **8**: p. 65.

336. Szasz, T., J.M. Thompson, and S.W. Watts, *A comparison of reactive oxygen species metabolism in the rat aorta and vena cava: focus on xanthine oxidase.* Am J Physiol Heart Circ Physiol, 2008. **295**(3): p. H1341-H1350.

337. Matoba, T., et al., *Hydrogen peroxide is an endothelium-derived hyperpolarizing factor in mice.* J Clin Invest, 2000. **106**(12): p. 1521-30.

338. Noronha, B.T., et al., *Inducible nitric oxide synthase has divergent effects on vascular and metabolic function in obesity.* Diabetes, 2005. **54**(4): p. 1082-9.

339. World Health Organization, *Factsheet Number 310.* 2013. www.who.int/mediacentre/ factsheets/fs310/en/

340. Zarghani, N., et al., *Relationship between IGF-1 and leptin in type II diabetic patients.* Int J Endocrinol Metab, 2009. **1**: p. 26-34

341. Awazawa M., et al., *Adiponectin enhances insulin sensitivity by increasing hepatic IRS-2 expression via a macrophage-derived IL-6-dependent pathway,* Cell Metab, 2011. **13**(4): p. 401-12